# DYNAMIC ANALYSES OF FLUID-STRUCTURE SYSTEMS

Thesis by

Ahmed Rashed

In Partial Fulfillment of the Requirements

for the Degree of

Doctor of Philosophy

California Institute of Technology

Pasadena, California

1983

(Submitted July 26, 1982)

## ACKNOWLEDGEMENTS

I would like to express my gratitude to my research advisors, Professors W. D. Iwan and G. W. Housner, for their guidance and encouragement during the course of my graduate studies at Caltech. Valuable suggestions were also given by Drs. M. A. Haroun and J. F. Hall.

The financial support of the National Science Foundation and the California Institute of Technology is gratefully acknowledged.

Many thanks are given to Gloria Jackson, Beth McGrath and Sharon Beckenbach for their skillful tying of a rather difficult manuscript.

Finally, I wish to express heartfelt gratitude to the members of my family, especially my wife, Laila, for her steadfast love and support through years of hard work.

# ABSTRACT

Theoretical investigations of the dynamic behavior of some important fluid-structure systems are conducted to seek a better understanding of: 1) the hydrodynamic pressures generated in the fluid as a result of both the rigid body and the vibrational motions of the structure, and 2) the effects of the fluid on the dynamic properties of the structure as well as on its response to earthquake ground motions.

Explicit formulas are presented for the hydrodynamic pressures generated in fluid domains having boundaries which can be approximated by simple geometries. Such domains may be reservoirs behind dams, or around intake towers, water around bridge piers or liquids stored in circular cylindrical tanks. The formulas are used to calculate the hydrodynamic pressures analytically and the results are exhibited in a form showing the pressure dependence on the various parameters of the problem.

The fluid-structure interaction problems of long straight walls, having uniform rectangular sections, and long straight gravity dams, having uniform triangular sections, are investigated. The natural frequencies of vibration and the associated mode shapes are found in the former case, through a fully analytical approach for both the structure and the fluid domains, and in the latter, by discretizing the dam into finite elements and treating the reservoir as a continuum by boundary solution techniques. A method is presented for computing the earthquake

response of both structures, based on superposition of their free vibrational modes.

The problems of limited length dam or wall-reservoir systems are investigated. The natural frequencies of the structure and the corresponding mode shapes are found by the Rayleigh-Ritz method. This method is also used to obtain the frequency domain response of the structure to all three components of the ground motion. The validity of the two dimensional approximation, often made in the analysis of gravity dams, and the effect of the length to height ratio on the dynamic properties and response of the structure are studied.

Time domain responses to arbitrary earthquake ground motions are evaluated by superposing the frequency domain responses, to individual Fourier components of the excitation, through the Fourier Integral. For efficiency of computation, a fast Fourier analysis is used for both the forward transform of the ground excitation and the inverse transform of the Fourier Integral.

# TABLE OF CONTENTS

TABLE OF CONTENTS (CONTINUED)

TABLE OF CONTENTS (CONTINUED)

# CHAPTER I

# INTRODUCTION

## 1.1. Dynamic Analyses of Fluid-Structure Systems

The possible failure of dams retaining large quantities of water presents a hazard for life and property during earthquakes. In addition, the structural damage to the dams themselves may pose a considerable economic loss. The safety of other important structures, such as intake towers and liquid storage tanks, is also of importance. This has focused considerable attention on the dynamic analyses of these fluid-structure systems.

During an earthquake, the shaking of the ground imparts movement to structures which in turn stresses the structural elements. When the structure is in contact with a volume of fluid, it experiences additional forces from the fluid. The horizontal motion of the ground does not impart significant movement to the fluid so the structure must move bodily toward and away from the fluid thus experiencing dynamic fluid pressures. The structure may also experience additional pressures resulting from modifications to its deformational motion. In general, fluid interaction can have a significant effect on the dynamic properties of a structure as well as on its response to earthquake ground motion.

Until recently, most work on fluid-structure systems has been concerned with two uncoupled problems: 1) the hydrodynamic pressures on a structure, assuming it to be rigid, and 2) the response of the

structure, assuming it to be flexible, to the combined action of its internal inertia forces and the pressures as found from problem (1). Thus, the earthquake response of those systems was usually obtained by first assuming the structure to be rigid and finding the pressures generated by its rigid motion, then assuming it to be flexible, applying those pressures together with the inertia forces to it and calculating its dynamic response. But the problem is more complex than this. For example, consider a dam-reservoir system. During an earthquake, both the rigid body and the vibrational motions of the dam generate hydrodynamic pressures in the reservoir and the deformations of the dam are in turn affected by those pressures which act on its upstream face. Thus this is a closed cycle of action and reaction, and to adequately represent this cycle, the formulation of the problem must include the fluid-structure interaction.

To simplify the approach to the complete problem, the fluid-structure system is subdivided into two subsystems, namely the structure domain and the fluid domain. By doing this, it is possible to deal with two separate problems: 1) the response of the structure to known loadings, and 2) the pressures generated in the fluid domain due to known motions of its boundaries. The final step is to couple the solutions of those two problems along the interface boundary.

The problem of the structure response to known loadings is fully understood and any difficulty arising from the geometry of the structure could be overcome by using the finite element method.

Regarding the second problem, the fluid is usually found bounded by irregular boundaries. If the fluid domain is finite, the finite element method can be used. However, this is a relatively expensive approach. If the fluid domain is infinite, a finite element treatment will not be satisfactory unless some sort of non-reflecting boundary is incorporated. On the other hand, an analytical solution for the fluid domain is generally possible only if its boundaries can be approximated as having simple geometries. The second approach is computationally advantageous over the first. In addition, the explicit expressions obtained for the hydrodynamic pressures can be easily studied to throw light on the nature of these earthquake generated loads, which in turn should help engineers achieve better design analyses of the structures.

## 1.2. Outline of the Present Study

The present study develops methods to analyze the dynamic behavior of fluid-structure systems. The study is carried out in three phases: 1) an extensive analysis of the hydrodynamic pressures generated in some simplified fluid domains, 2) a detailed theoretical treatment of long gravity dam-reservoir systems, and 3) a detailed analysis of short dam or wall-reservoir systems.

A necessary first phase is to understand the nature of earthquake generated hydrodynamic pressures. A detailed collection of existing and developed formulas for pressures generated in simplified fluid domains is presented. Emphasis is placed on the case of reservoirs behind gravity dams. The formulas obtained are used to calculate the

hydrodynamic pressures for selected numerical values of the different parameters involved in the problem. These parameters are: 1) the specified motion of the dam, 2) the frequency of vibration, 3) the dam dimensions, and 4) the water compressibility. The results are exhibited in a form that shows the pressure dependence on these various parameters.

The second phase of study is devoted to the analysis of a simplified problem; namely, that of a wall or dam-reservoir system. The problem is reduced to one in two dimensions by assuming the structure to be long compared to its height. Under the assumption of incompressible water, the natural frequencies of vibration and associated mode shapes are found, and the effect of the reservoir on their values is investigated. The structure is modeled by three different theories: 1) pure shear theory, 2) Bernoulli-Euler bending theory, and 3) Timoshenko shear-bending theory. The structure is treated analytically in case of a rectangular section wall, while discretized into finite elements in case of a triangular section gravity dam. In both cases, the water in the reservoir is treated as a continuum and the expressions obtained in phase one are used. In each case, a method is presented to compute the earthquake response of the structure, based on superposition of its free vibrational modes.

The third phase of this study focuses on the effect of the length to height ratio on the dynamic behavior of limited length wall-reservoir systems. The wall is modeled first by a shear plate theory and then by a bending plate theory. Neglecting water compressibility, the natural

frequencies and mode shapes are found using the Rayleigh-Ritz method. The effect of the length to height ratio on the dynamic properties is studied. The Rayleigh-Ritz method is used again to obtain frequency domain responses to harmonic ground motions. The effects of the presence of the reservoir, the water compressibility and the fluid-structure interaction on those responses are illustrated. The frequency domain responses are used to evaluate time domain responses to arbitrary earthquake ground motions through the use of the Fourier Integral. The efficiency of computation is increased by using a fast Fourier analysis for both the forward transform of the ground excitation and the inverse transform of the Fourier Integral.

## 1.3. Organization

This thesis is divided into six chapters. Chapter I has the introduction. Chapters II, III and IV correspond to the three phases of the study, while Chapter V includes numerical examples of time domain responses to some existing earthquake ground motions. The summary and conclusions are given in Chapter VI. Each chapter is further divided into several sections and subsections. Each chapter, and many of the sections, has an individual introduction which gives a brief account of the historical development of the particular subject under investigation. Each chapter is written in a self-contained manner, and may be read more or less independently of the others. The letter symbols are defined where they are first introduced in the text and they are also

summarized in alphabetical order in the "NOTATION" section. Many references have been included so that the reader may obtain a more complete discussion of the various phases of the total subject.

# CHAPTER II

## HYDRODYNAMIC PRESSURES ON VIBRATING STRUCTURES

A necessary first step in analyzing the seismic response of fluid-structure systems is the knowledge of the hydrodynamic pressures generated in the fluid domain due to motions of its boundaries.

In real life systems, the fluid domains usually have irregular boundaries of complicated geometries. Although possible, a finite element treatment of finite fluid domains is relatively expensive because of the large number of elements required. The use of the finite element method for domains of infinite extent requires special techniques. A different approach is sought in which the fluid domain is assumed to have regular boundaries of simplified geometries. In many cases, this approximation is acceptable and may be shown not to introduce considerable errors. This assumption enables the treatment of the fluid domain as a continuum and an analytical solution of the problem may be obtained. This approach has the advantage of drastically reducing the cost of computing. In addition, the explicit expressions derived for the hydrodynamic pressure can be easily studied to throw light on the behavior of these earthquake generated loads.

The purpose of this chapter is to establish the basic equations which govern the dynamic pressure generated in the fluid and to develop analytical solutions to these equations for some simplified fluid domains.

In the first section, the fundamental assumptions regarding the fluid are stated, the equations governing the hydrodynamic pressure are given, and general solutions to those equations are presented. In each of the subsequent sections, the general solution for the pressure is specialized for a particular fluid domain. Each section starts with a brief introduction which gives a historical background about the subject. This is followed by a discussion of the assumptions made about the domain boundaries. Next, the formulas for the pressures generated by specific motions of the boundaries are presented. Finally, each section ends with detailed numerical examples illustrating the pressure dependence on the various parameters. In addition, solutions for the pressures generated in some other simplified fluid domains are listed in the "Appendix" section at the end of the chapter.

## 2.1. Governing Equations and General Solutions

This section contains the basic equations which govern the hydrodynamic pressure, and their general solutions.

### 2.1.1. Fundamental Assumptions

In a consideration of the different factors affecting the motion of the fluid, the following conventional assumptions are made:

i) The fluid is homogeneous, inviscid and linearly compressible.

ii) The flow field is irrotational.

iii) No sources, sinks or cavities are anywhere in the flow field.

iv) The displacements and their spatial derivatives are small.

2.1.2. Governing Equations

According to the assumptions made about the fluid, the hydrodynamic pressure p(x,y,z,t), in excess of the hydrostatic pressure, is governed by:

$$\nabla^2 p = \frac{1}{c^2} \frac{\partial^2 p}{\partial t^2} \tag{2.1}$$

where

$$\nabla^2 = \frac{\partial^2}{\partial x^2} + \frac{\partial^2}{\partial y^2} + \frac{\partial^2}{\partial z^2} \tag{2.2}$$

is the three dimensional Laplace operator in cartesian coordinates $c = \sqrt{k/\rho_\ell}$ is the velocity of sound in the fluid, k is the bulk modulus of elasticity of the fluid, and $\rho_\ell$ its mass density. Equation 2.1 is the three dimensional wave equation governing the hydrodynamic pressure in a linearly compressible fluid.

If the fluid is assumed to be incompressible, one should regard k, and hence c, as infinite. This will change Eq. 2.1 into:

$$\nabla^2 p = 0 \tag{2.3}$$

which is the three dimensional Laplace equation governing the hydrodynamic pressure in an incompressible fluid.

2.1.3. General Solutions

The solution p(x,y,z,t) of the wave equation, Eq. 2.1, can be obtained by the method of separation of variables. Thus a solution is sought of the form:

$$p(x,y,z,t) = X(x) \cdot Y(y) \cdot Z(z) \cdot T(t) \tag{2.4}$$

Two possible solutions of the wave equation can be stated as follows:

$$\begin{aligned} p(x,y,z,t) = {} & [c_1 \exp(\delta x) + c_2 \exp(-\delta x)] \\ & \cdot [c_3 \sin(\beta y) + c_4 \cos(\beta y)] \\ & \cdot [c_5 \sin(\eta z) + c_6 \cos(\eta z)] \\ & \cdot [c_7 \exp(i\tau t) + c_8 \exp(-i\tau t)] \end{aligned} \tag{2.5}$$

in which

$$(\beta^2 + \eta^2) > (\tau/c)^2 \qquad \text{and} \qquad \delta^2 = (\beta^2 + \eta^2) - (\tau/c)^2$$

or

$$\begin{aligned} p(x,y,z,t) = {} & [\bar{c}_1 \exp(i\bar{\delta} x) + \bar{c}_2 \exp(-i\bar{\delta} x)] \\ & \cdot [c_3 \sin(\beta y) + c_4 \cos(\beta y)] \\ & \cdot [c_5 \sin(\eta z) + c_6 \cos(\eta z)] \\ & \cdot [c_7 \exp(i\tau t) + c_8 \exp(-i\tau t)] \end{aligned} \tag{2.6}$$

in which

$$(\beta^2 + \eta^2) < (\tau/c)^2 \qquad \text{and} \qquad \bar{\delta}^2 = (\tau/c)^2 - (\beta^2 + \eta^2).$$

In the above equations, the $c_i$'s and $\bar{c}_i$'s are constant coefficients, $\delta, \bar{\delta}, \beta, \eta$ and $\tau$ are separation constants.

The general solution of the Laplace equation, Eq. 2.3, can be obtained directly from the solutions of the wave equation, given above,

by letting $c \to \infty$. In this case, we have only the form given by Eq. 2.5, with $\delta$ replaced by $\mu$, where $\mu^2 = \beta^2 + \eta^2$, and the time dependent function T(t) is unspecified. Thus:

$$p(x,y,z,t) = [c_1 \exp(\mu x) + c_2 \exp(-\mu x)] \cdot [c_3 \sin(\beta y) + c_4 \cos(\beta y)] \cdot [c_5 \sin(\eta z) + c_6 \cos(\eta z)] \cdot T(t) \qquad (2.7)$$

## 2.2. Infinitely Long Gravity Dams or Walls

H.M. Westergaard [1] was the first to analyze the hydrodynamic pressures generated in reservoirs behind concrete gravity dams. He obtained a solution for the pressure resulting from a harmonic horizontal ground motion. It is based on the following assumptions: 1) the reservoir is of constant depth and of infinite extent in the upstream direction, 2) the effect of waves at the free surface is negligible, 3) the water is linearly compressible, and 4) the dam is rigid, infinitely long, and has a vertical upstream face. The validity of those assumptions has been studied by many investigators and only a brief discussion is given here.

For reservoirs of finite extent, H.A. Brahtz and C.H. Heilbron [2] showed that the effect of length is negligible (the pressure increase is less than 5% as compared to the infinite reservoir case) when the length to depth ratio is greater than two, in the case of a reservoir of fixed far end, and when this ratio is greater than three, in the case where the far end is moving with the ground. These conclusions were supported by the experimental results of L.M. Hoskins and L.S. Jacobsen [3]. The

effect of reservoir length was also investigated by J.I. Bustamante et al. [4], but for a wider range of frequencies of excitation. The conclusion was that the length may be of some importance only in the case of high dams. Thus, the assumption of an infinite reservoir is reasonable, especially since actual reservoirs usually extend to large distances.

The assumption of a constant depth reservoir also seems reasonable since most reservoir bottoms are of small slopes, particularly over a distance, just upstream the dam, extending at least few times the dam height.

J.I. Bustamante et al. [4] give estimates for the error introduced by ignoring the surface waves, as a function of the reservoir depth and the frequency of excitation. Based on this work, one concludes that the effect of those waves can be neglected with little loss of accuracy.

Although H.M. Westergaard [1] included the compressibility of water in his study, S. Kotsubo [5] showed that this solution is valid only for frequencies of excitation less than the fundamental natural frequency of the reservoir. J.I.Bustamante et al. [4] and A.K. Chopra [6] studied the effect of water compressibility, the former in case of harmonic ground motion, the latter in case of earthquake ground motion. They showed that the solution becomes independent of the excitation frequency when compressibility is neglected, and the resulting errors in the time history of the total force acting on the dam may be significant except possibly for reservoirs of depth 100 ft or less.

In practice, gravity dams have upstream faces which are almost vertical over the full height or over the major part of it. Based on the works of C.N. Zangar [7] and A.T. Chwang [8], the pressure distribution for a dam with a vertical upstream face is only slightly different from that of a dam with very steeply sloping face (0 to $5^{o}$ off vertical). Thus, assuming the upstream face to be vertical is a very acceptable assumption.

Earthquake loads cause even the most rigid structures to deform. When the structure is a dam, additional hydrodynamic pressures are generated as a result of this deformation. This was first accounted for by H.A. Brahtz and C.H. Heilbron [2]. They assumed the deformation shape of the upstream face of the dam to be a straight line and calculated the excess in pressure due to this deformation. The ground motion was harmonic with frequency less than the fundamental frequency of the reservoir. Similar results were obtained by J.I. Bustamante et al. [4], for a wider frequency range and for both a linear and a parabolic deformation shape. A.K.Chopra [9] took the deformation shape to be the fundamental mode shape as determined by the finite element method and computed those additional pressures in the case of earthquake ground motion.

The discussion of the assumption that the dam is infinitely long will be deferred to the next section, in which the pressure for the case of limited length dams is investigated.

Under the same assumptions made by H.M. Westergaard [1], except that the effect of surface waves is included, A.K.Chopra [6] gave formulas for the pressure generated by vertical ground motion, both harmonic and earthquake. He showed that, as in the case of horizontal excitation, the wave motion at the free surface may be neglected without introducing significant errors.

In the following, solutions for the pressures generated in reservoirs behind infinitely long gravity dams are given for three types of motions at the reservoir boundaries: 1) vibrational motion of the dam, 2) longitudinal ground motion (normal to the dam), and 3) vertical ground motion. In each case, the boundary conditions are first stated, and then the corresponding expression for the pressure is given and briefly discussed.

2.2.1. Geometry of the Problem

An xyz cartesian coordinate system is chosen such that the xy-plane is horizontal, coinciding with the bottom of the reservoir, and the yz-plane is vertical, coinciding with the undeflected upstream face of the dam. The x-axis points into the reservoir, the y-axis runs along the heel of the dam, while the z-axis points upward, as shown in Fig. 2.1.

The water in the reservoir occupies the domain D where

$$D = \left\{ (x,y,z) \mid 0 \leq x < \infty, -\infty < y < \infty, 0 \leq z \leq H_\ell \right\} .$$

$H_\ell$ is the constant depth of the reservoir.

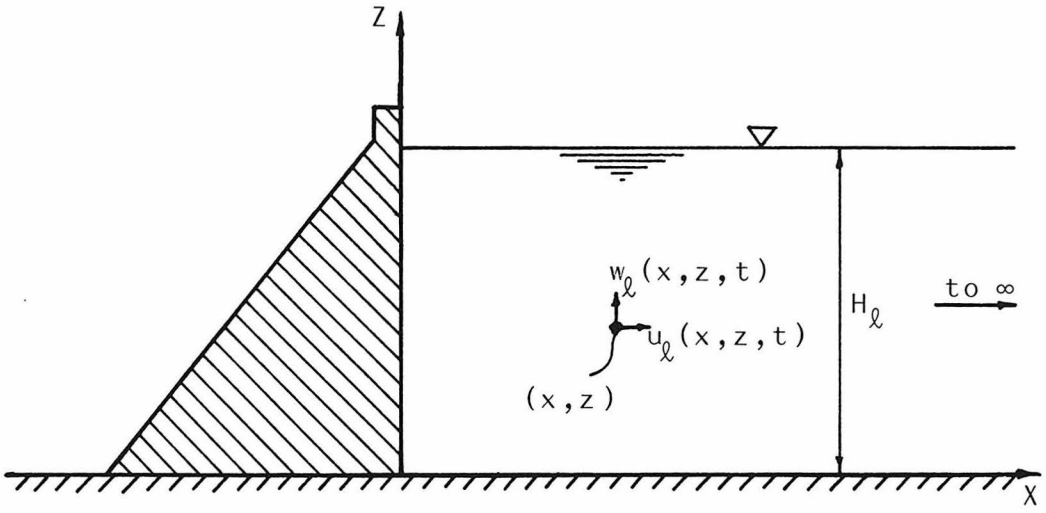


Fig. 2.1 Dam-Reservoir and Coordinate System

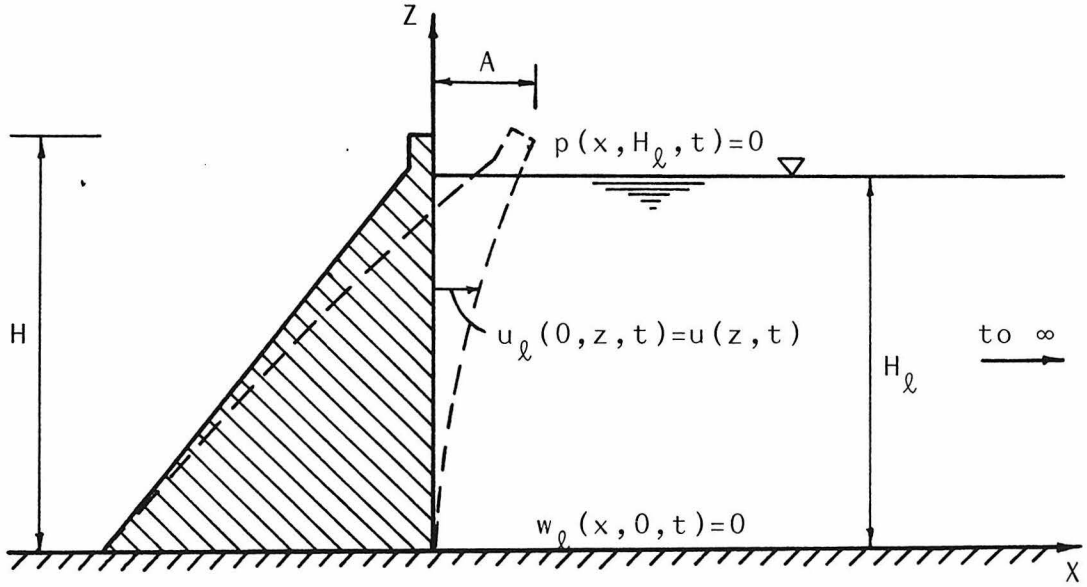


Fig. 2.2 Vibrational Motion

By assuming the dam to be infinitely long in the y-direction, the problem becomes one in two dimensions in which the pressure is independent of the y-coordinate, i.e. $p = p(x,z,t)$.

2.2.2. Vibrational Motion

In this case, the dam is assumed to vibrate harmonically such that the deformation of its upstream face, $u(z,t)$, is given by:

$$u(z,t) = A \cdot \varphi\left(\frac{z}{H}\right) \cdot \exp(i\omega t) \tag{2.8}$$

where A is the maximum amplitude of vibration, $\varphi\left(\frac{z}{H}\right)$ is a given function of z such that $\varphi(1) = 1$, H is the dam height, $i = \sqrt{-1}$ and $\omega$ is the circular frequency of vibration (see Fig. 2.2).

The boundary conditions are as follows:

i) the pressure is bounded as $x \to \infty$, and only waves travelling away from the dam can exist, i.e.,

$$p(\infty,z,t) < \infty \tag{2.9}$$

ii) the effect of waves at the free surface of the reservoir ($z = H_\ell$) is neglected, i.e.,

$$p(x,H_\ell,t) = 0 \tag{2.10}$$

iii) the vertical motion of the water at the bottom of the reservoir ($z = 0$) vanishes, i.e.,

$$w_\ell(x,0,t) = 0 \tag{2.11}$$

iv) the horizontal motion of the water at the upstream face of the dam ($x = 0$) is the same as the deformation of the face, i.e.,

$$u_\ell(0,z,t) = u(z,t) \tag{2.12}$$

Applying these boundary conditions to the general solutions given in Eqs. 2.5 and 2.6, one obtains the following expression for the hydrodynamic pressure:

$$\begin{aligned} p(x,z,t) = & -2\rho_\ell H_\ell A\,\omega^2 \exp(i\omega t) \\ & \cdot \left\{ -i \sum_{m=1}^{m_0-1} \frac{I_{m0}}{\bar{\delta}_{m0}} \cdot \exp\left(-i\bar{\delta}_{m0}\frac{x}{H_\ell}\right) \cdot \cos\left(\eta_m \frac{z}{H_\ell}\right) \right. \\ & \left. + \sum_{m=m_0}^{\infty} \frac{I_{m0}}{\delta_{m0}} \cdot \exp\left(-\delta_{m0}\frac{x}{H_\ell}\right) \cdot \cos\left(\eta_m \frac{z}{H_\ell}\right) \right\} \end{aligned} \tag{2.13}$$

where

$$\eta_m = \frac{(2m-1)\pi}{2} \quad ; \quad m = 1,2,3,\ldots \tag{2.14}$$

$$\left.\begin{aligned} \bar{\delta}_{m0} &= H_\ell \sqrt{(\omega/c)^2 - (\eta_m/H_\ell)^2} \quad ; \quad m = 1,2,\ldots,m_0-1 \\ \delta_{m0} &= H_\ell \sqrt{(\eta_m/H_\ell)^2 - (\omega/c)^2} \quad ; \quad m = m_0, m_0+1,\ldots \end{aligned}\right\} \tag{2.15}$$

$m_0$ = smallest m for which $(\eta_m/H_\ell) > (\omega/c)$

$$I_{m0} = \frac{1}{H_\ell}\int_0^{H_\ell} \varphi\left(\frac{z}{H}\right) \cdot \cos\left(\eta_m \frac{z}{H_\ell}\right) dz \qquad m = 1,2,3,\ldots \tag{2.16}$$

Examination of Eq. 2.13 yields:

i) The hydrodynamic pressure becomes unbounded as the excitation frequency approaches a value that makes $\bar{\delta}_{m0}$ or $\delta_{m0}$ vanish. These particular values define the natural frequencies of the reservoir, and are given by:

$$\omega_i^r = \frac{\eta_i c}{H_\ell} = \frac{(2i-1)\,\pi\, c}{2\, H_\ell} \quad ; \; i = 1,2,3,\ldots \tag{2.17}$$

The fundamental natural frequency of a reservoir of depth $H_\ell$ is then given by:

$$\omega_1^r = \frac{\pi\, c}{2\, H_\ell} \tag{2.18}$$

ii) When the excitation frequency is less than the fundamental frequency of the reservoir, $m_0$ takes the value 1, and the first series in Eq. 2.13 vanishes. When $\omega$ is larger than $\omega_1^r$, $m_0$ will be larger than 1, and both series will be present.

iii) The first series represents a part of the pressure which, for a fixed time, is oscillatory and non-decaying in the x-direction. The second series represents a non-oscillatory decaying part.

iv) The first part of the pressure is a wave travelling in the positive x-direction, while the second is a standing wave.

v) The second part of the pressure is in-phase with the excitation, while the first has, in general, an in-phase and an out-of-phase component.

If the water is assumed to be incompressible, a solution for the pressure can be obtained without requiring the motion of the dam to be harmonic in time as given in Eq. 2.8. In this case, the boundary conditions, Eqs. 2.9 - 2.12, together with the general solution, Eq. 2.7, leads to:

$$p(x,z,t) = 2\,\rho_\ell \left\{ \sum_{m=1}^{\infty} \frac{J_{m0}}{\eta_m} \cdot \exp\left(-\eta_m \frac{x}{H_\ell}\right) \cdot \cos\left(\eta_m \frac{z}{H_\ell}\right) \right\} \qquad (2.19)$$

where

$$J_{m0} = \int_0^{H_\ell} \ddot{u}(z,t) \cdot \cos\left(\eta_m \frac{z}{H_\ell}\right) dz \qquad ; \qquad m\ 1,2,3,... \qquad (2.20)$$

In particular, for harmonic motion as given in Eq. 2.8, Eq. 2.19 becomes:

$$p(x,z,t) = -2\,\rho_\ell H_\ell A\,\omega^2 \left\{ \sum_{m=1}^{\infty} \frac{I_{m0}}{\eta_m} \cdot \exp\left(-\eta_m \frac{x}{H_\ell}\right) \cdot \cos\left(\eta_m \frac{z}{H_\ell}\right) \right\} \exp\ (i\omega t) \qquad (2.21)$$

The above equation is clearly the limit, as $c \to \infty$, of Eq. 2.13. Examination of Eq. 2.21 yields:

i) For a fixed amplitude of crest acceleration, the pressure is independent of the frequency of excitation.

ii) There is no resonance in the reservoir at any frequency.

iii) For a fixed time, the pressure is non-oscillatory and decaying in the positive x-direction.

iv) The generated pressure is in-phase with the excitation.

2.2.3. Longitudinal Ground Motion

In this case, the dam is assumed to be rigid. A harmonic ground motion $u_g(t)$, along the x-axis, is applied to the dam base, such that:

$$u_g(t) = \bar{u}_g \cdot \exp\ (i\omega t) \qquad (2.22)$$

where $\bar{u}_g$ is the amplitude of motion, as shown in Fig. 2.3.

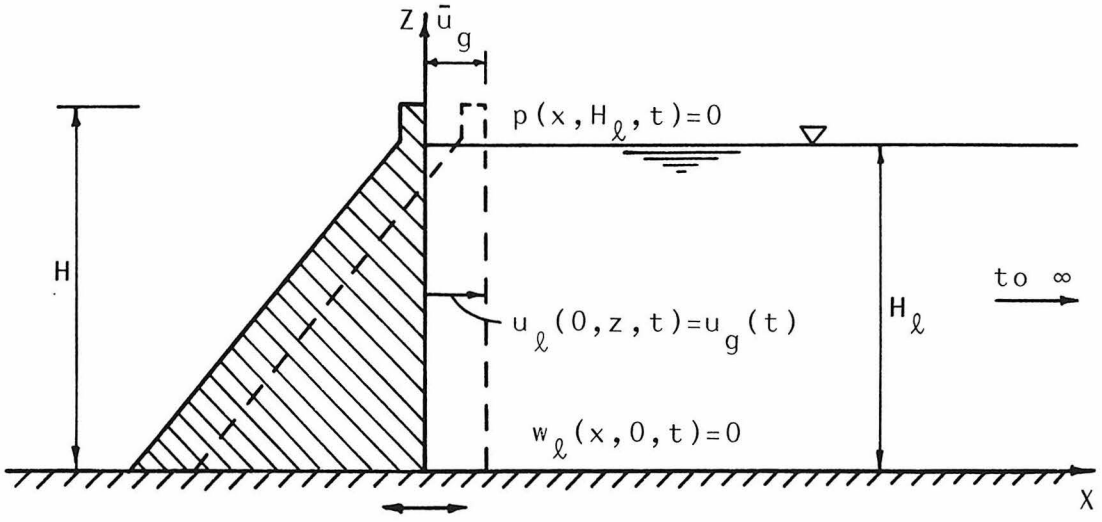


Fig. 2.3 Longitudinal Ground Motion

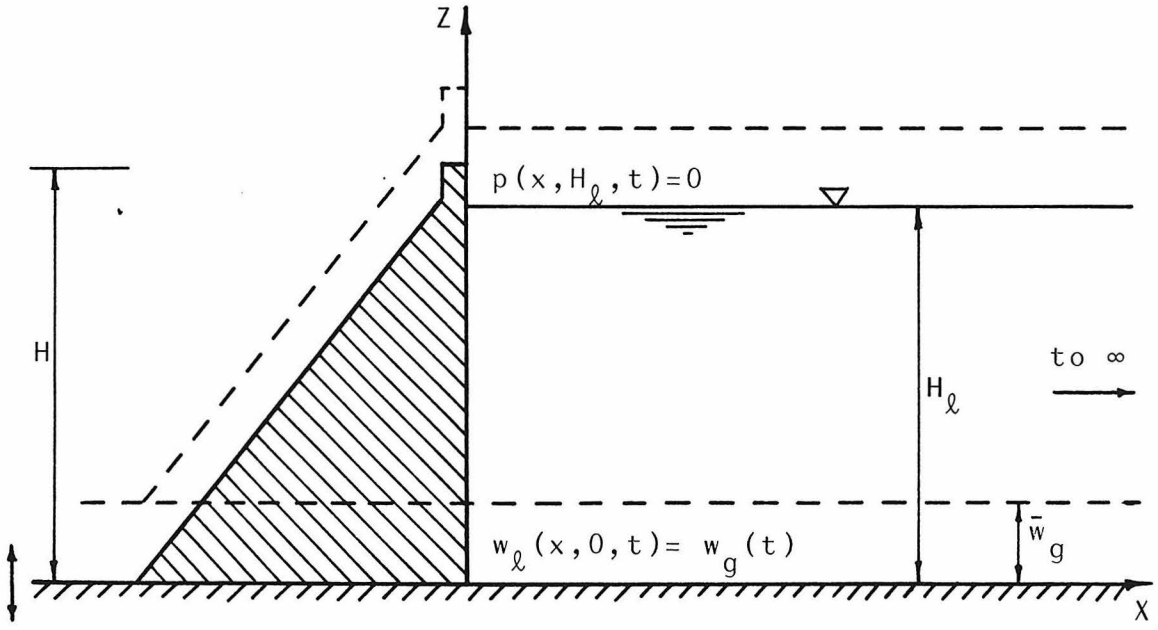


Fig. 2.4 Vertical Ground Motion

The boundary conditions will be the same as those of the previous case, except that the one given by Eq. 2.12 is replaced by:

$$u_\ell(0,z,t) = u_g(t) \tag{2.23}$$

The solution will be a special case of Eq. 2.13, in which A is replaced by $\bar{u}_g$ and $\varphi\left(\frac{z}{H}\right) \equiv 1$. The pressure will be given by:

$$p_{gx}(x,z,t) = -2\,\rho_\ell H_\ell \bar{u}_g\,\omega^2 \exp(i\omega t)$$

$$\cdot\left\{-i \sum_{m=1}^{m_0-1} \frac{(-1)^{m+1}}{\eta_m\,\bar{\delta}_{m0}} \cdot \exp\left(-i\bar{\delta}_{m0}\,\frac{x}{H_\ell}\right) \cdot \cos\left(\eta_m\,\frac{z}{H_\ell}\right)\right.$$

$$\left. + \sum_{m=m_0}^{\infty} \frac{(-1)^{m+1}}{\eta_m\,\delta_{m0}} \exp\left(-\delta_{m0}\,\frac{x}{H_\ell}\right) \cdot \cos\left(\eta_m\,\frac{z}{H_\ell}\right)\right\} \tag{2.24}$$

where $p_{gx}$ is the hydrodynamic pressure generated by a ground motion in the x-direction.

For incompressible water, $\ddot{u}(z,t)$ in Eq. 2.20 is replaced by $\ddot{u}_g(t)$, which reduces Eq. 2.19 to:

$$p_{gx}(x,z,t) = 2\,\rho_\ell H_\ell \ddot{u}_g(t) \left\{ \sum_{m=1}^{\infty} \frac{(-1)^{m+1}}{\eta_m^2} \cdot \exp\left(-\eta_m\,\frac{x}{H_\ell}\right) \cdot \cos\left(\eta_m\,\frac{z}{H_\ell}\right)\right\} \tag{2.25}$$

For a harmonic motion, as given by Eq. 2.22, the above equation becomes:

$$p_{gx}(x,z,t) = -2\ \rho_\ell H_\ell \bar{u}_g\ \omega^2\ \exp(i\omega t)$$

$$\cdot\left\{\sum_{m=1}^{\infty} \frac{(-1)^{m+1}}{\eta_m^2} \cdot \exp\left(-\eta_m \frac{x}{H_\ell}\right) \cdot \cos\left(\eta_m \frac{z}{H_\ell}\right)\right\} \qquad (2.26)$$

which is the limit of Eq. 2.24 as $c \to \infty$.

The conclusions given in page 17, in case of compressible water, and those given in page 19 for incompressible water, are also applicable here.

2.2.4. Vertical Ground Motion

In this case, a harmonic vertical ground motion $w_g(t)$ is applied to the base of the rigid dam, as well as to the reservoir bottom, such that

$$w_g(t) = \bar{w}_g \cdot \exp(i\omega t) \qquad (2.27)$$

where $\bar{w}_g$ is the amplitude of motion, as shown in Fig. 2.4.

The problem in this case is further independent of the x-coordinate, i.e., $p = p(z,t)$. The boundary conditions are:

$$p(H_\ell, t) = 0 \qquad (2.28)$$

$$w_\ell(0,t) = w_g(t) \qquad (2.29)$$

Applying those two conditions to the general solution, one obtains:

$$p_{gz}(z,t) = -\rho_\ell H_\ell \bar{w}_g\ \omega^2 \left\{\frac{\sin\left[\frac{\omega}{c} H_\ell\left(1 - \frac{z}{H_\ell}\right)\right]}{\frac{\omega}{c} H_\ell \cdot \cos\left(\frac{\omega}{c} H_\ell\right)}\right\} \exp(i\omega t) \qquad (2.30)$$

where $p_{gz}$ is the hydrodynamic pressure generated by a ground motion in the z-direction.

Examination of Eq. 2.30 yields:

i) The hydrodynamic pressure becomes unbounded as $\omega$ approaches a value that make $\cos\left(\frac{\omega}{c} H_\ell\right)=0$. These values are given by: $\frac{\omega}{c} H_\ell = \frac{(2i-1)\pi}{2}$ , i = 1,2,3,... , which are the same natural frequencies of the reservoir given by Eq. 2.17.

ii) Since the pressure is independent of the x-coordinate, then for a fixed time, it is non-oscillatory and non-decaying.

iii) Depending on the sign of the denominator, which depends on the value of $\omega$, the pressure may be in-phase or in opposite-phase with the excitation.

For incompressible water, the governing equation for the pressure will be a special case of Eq. 2.3, and is given by:

$$\frac{\partial^2 p}{\partial z^2} = 0 \tag{2.31}$$

which has a general solution of the form:

$$p(z,t) = (\bar{c}_5 z + \bar{c}_6) \cdot T(t) \tag{2.32}$$

where $\bar{c}_5$ and $\bar{c}_6$ are constant coefficients to be determined. The above equation, together with the boundary conditions, Eqs. 2.28 and 2.29, leads to:

$$p_{gz}(z,t) = -\rho_\ell H_\ell \ddot{w}_g(t) \cdot \left(1 - \frac{z}{H_\ell}\right) \tag{2.33}$$

For a harmonic motion as given by Eq. 2.27, Eq. 2.33 becomes:

$$p_{gz}(z,t) = -\rho_\ell H_\ell \bar{w}_g \omega^2 \cdot \left(1 - \frac{z}{H_\ell}\right) \cdot \exp(i\omega t) \qquad (2.34)$$

which again is obtainable from Eq. 2.30 by letting c go to $\infty$.

Examination of Eq. 2.34 reveals that:

i) For a fixed amplitude of ground motion, the generated pressure is frequency independent.

ii) No resonance of pressure occurs.

iii) For a fixed time, the pressure is non-oscillatory and non-decaying.

iv) The pressure is in-phase or in opposite-phase with the excitation.

v) The pressure distribution on the face of the dam is linear.

2.2.5. Numerical Examples

The hydrodynamic pressure, as given by Eq. 2.13 (or Eq. 2.24), depends on several parameters. Excluding the density $\rho_\ell$ and the bulk modulus of elasticity k of the water, which are rather constant, these parametèrs are:

i) The depth of the reservoir, $H_\ell$.

ii) The maximum amplitude of dam acceleration, $A\omega^2$.

iii) The excitation frequency, $\omega$.

iv) The prescribed vibrational shape, $\varphi\left(\frac{z}{H}\right)$.

The hydrodynamic pressure, when normalized by the maximum hydrostatic pressure $p_s = \rho_\ell g H_\ell$, where g is the acceleration of gravity, turns out to be independent of $H_\ell$. Equation 2.13 (or Eq. 2.24) also shows it directly proportional to the amplitude of crest acceleration.

The dependence on the fourth parameter is studied by determining the distribution of the normalized hydrodynamic pressure, acting on the upstream face of the dam, which results from different prescribed vibrational shapes. Equation 2.24 is used for the case of rigid motion, while Eq. 2.13 is used with the following prescribed vibrational shapes:

1) $$\varphi\left(\frac{z}{H}\right) = \sin\left(\eta_j \frac{z}{H}\right) \quad ; \quad j = 1,2$$

where $\eta_j = \dfrac{(2j-1)\pi}{2}$ (2.35)

2) $$\varphi\left(\frac{z}{H}\right) = A_j\left(\frac{z}{H}\right) / A_j(1) \quad ; \quad j = 1,2$$

where

$$A_j\left(\frac{z}{H}\right) = \left[\sin\left(\gamma_j \frac{z}{H}\right) - \sinh\left(\gamma_j \frac{z}{H}\right)\right] - d_j\left[\cos\left(\gamma_j \frac{z}{H}\right) - \cosh\left(\gamma_j \frac{z}{H}\right)\right]$$

in which $\gamma_j$ are roots of:

$$\cos(\gamma_j) \cdot \cosh(\gamma_j) = -1 \quad ,$$

and

$$d_j = \frac{\sin(\gamma_j) + \sinh(\gamma_j)}{\cos(\gamma_j) + \cosh(\gamma_j)}$$

(2.36)

It is observed that these shapes are nothing but the free lateral vibrational shapes of a cantilever shear beam, and a cantilever bending beam, respectively.

Taking the unit weight of water $\rho_\ell g = 62.4$ pcf, its bulk modulus $k = 3 \times 10^5$ psi, and $A\omega^2 = g$, the pressures generated in the reservoir, when the dam is assumed to move rigidly or to deform according to the prescribed shapes given by Eqs. 2.35 and 2.36, are calculated for two values of the normalized forcing frequency of vibration $\bar{\omega} = \omega/\omega_1^r$. The results are normalized by the maximum hydrostatic pressure $p_s$ and plotted in Figs. 2.5 and 2.6, when j in Eqs. 2.35 and 2.36 is 1 and 2, respectively. For $\bar{\omega} = 0.7 < 1.0$, the pressure is in-phase with the excitation, while for $\bar{\omega} = 1.5 > 1.0$, it has an in-phase (real, dashed line) and an out-of-phase (imaginary, solid line) component. In the latter case, the absolute pressure is also plotted (dotted line).

The dependence on the excitation frequency is better shown by calculating the total hydrodynamic force acting on the dam,

$$p_d = \int_0^{H_\ell} p(0,z,t)dz \quad ,$$

for a wide range of frequency. Figure 2.7 shows the real and imaginary components of the hydrodynamic force, normalized by the total hydrostatic force $P_s = 1/2\ \rho_\ell g\ H_\ell^2$, as a function of $\bar{\omega}$, for the case of a rigid motion. The absolute value of the normalized force is shown in Fig. 2.8 for the rigid motion as well as for the first mode of both the shear and bending deformations.

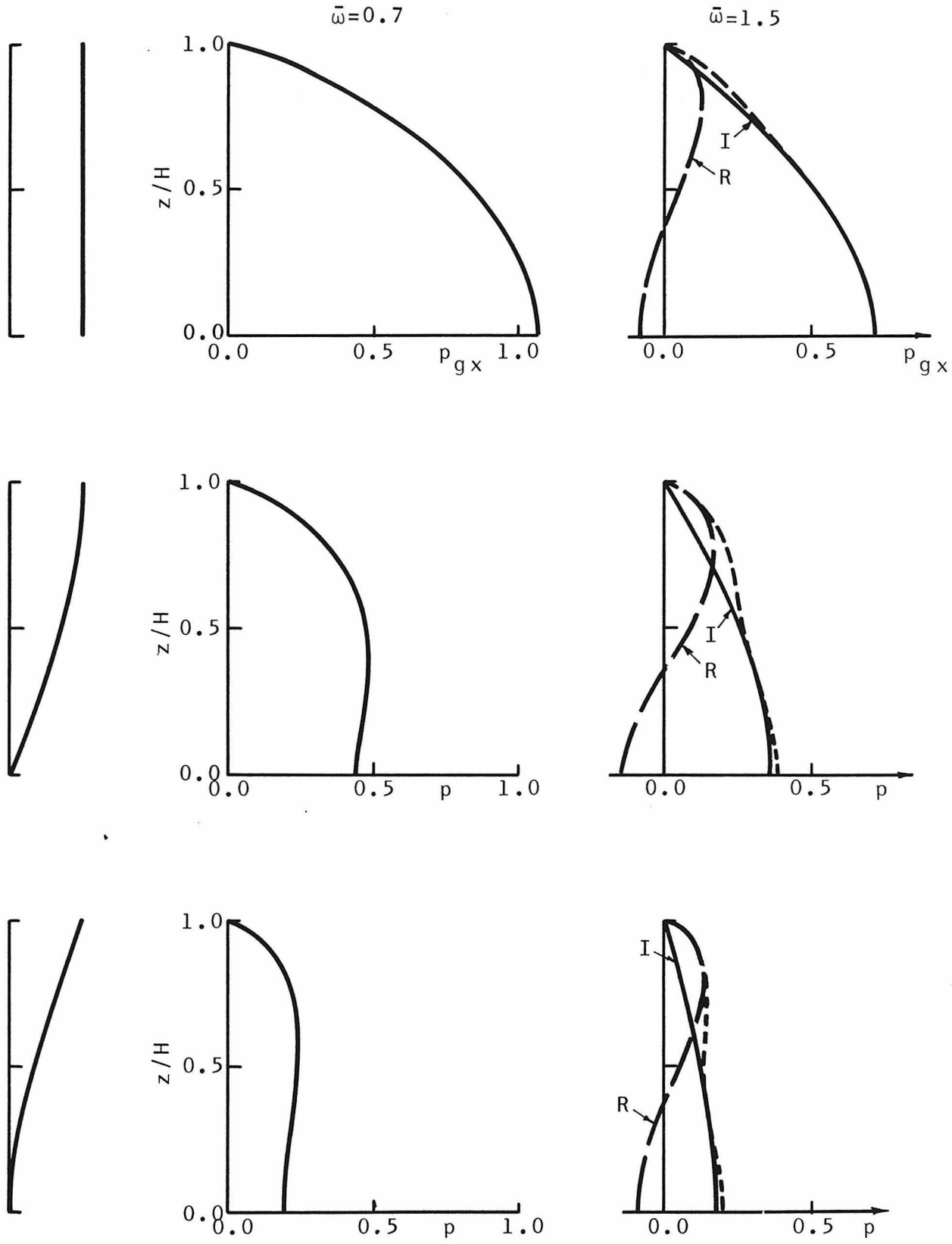


Fig. 2.5 Prescribed Motion and Hydrodynamic Pressure Distribution

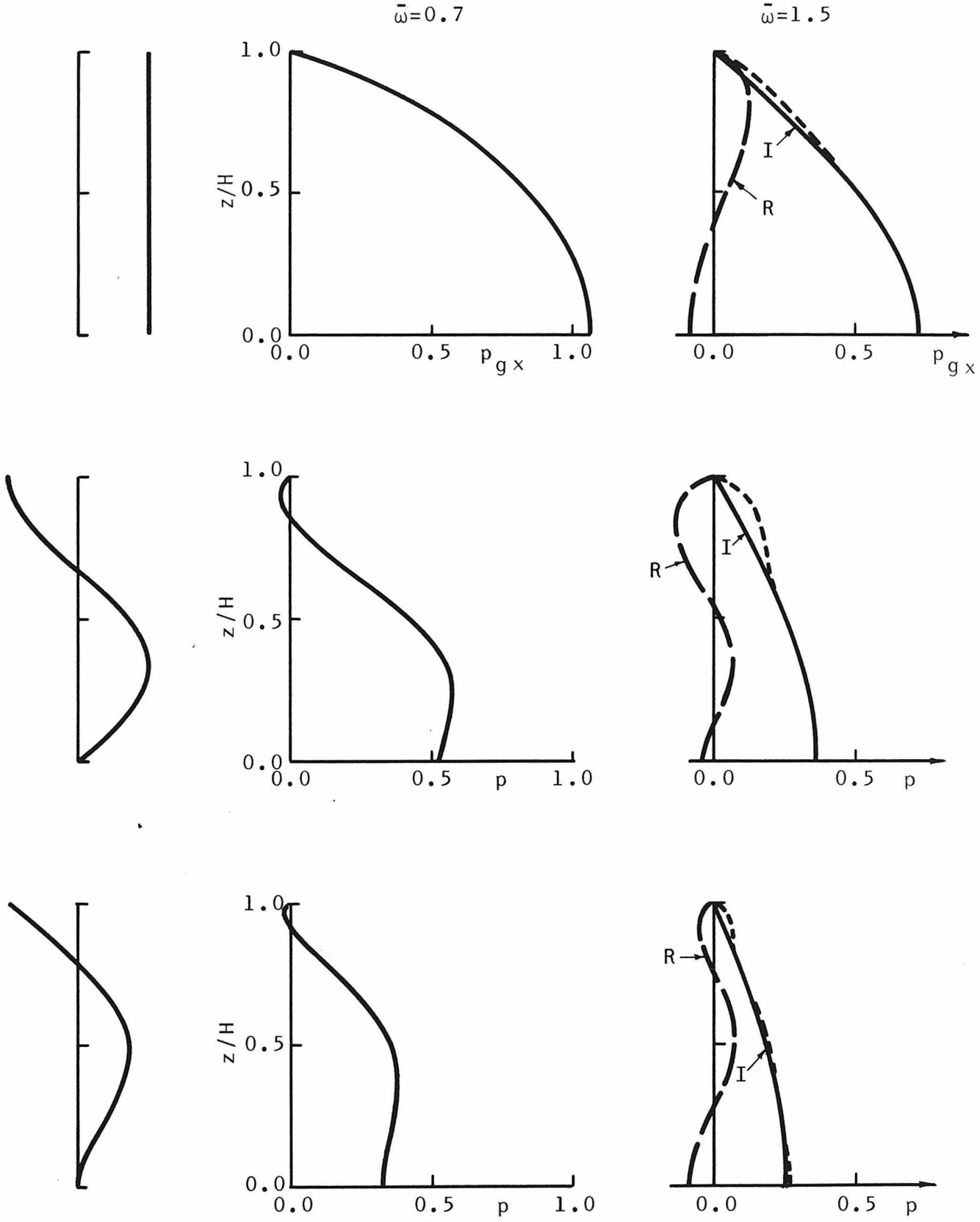


Fig. 2.6 Prescribed Motion and Hydrodynamic Pressure Distribution

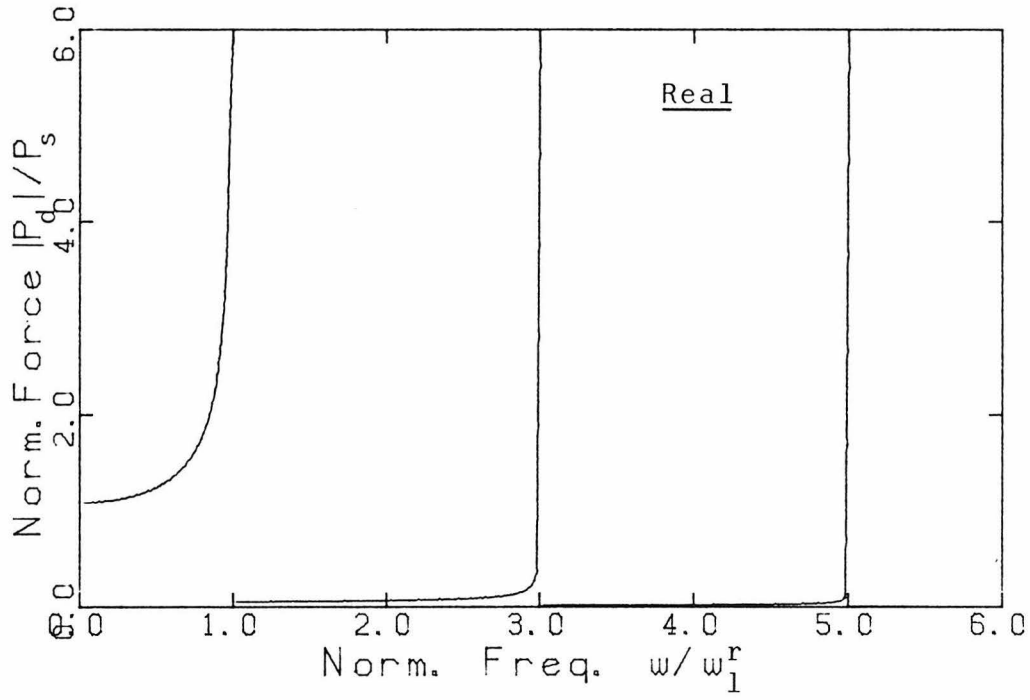


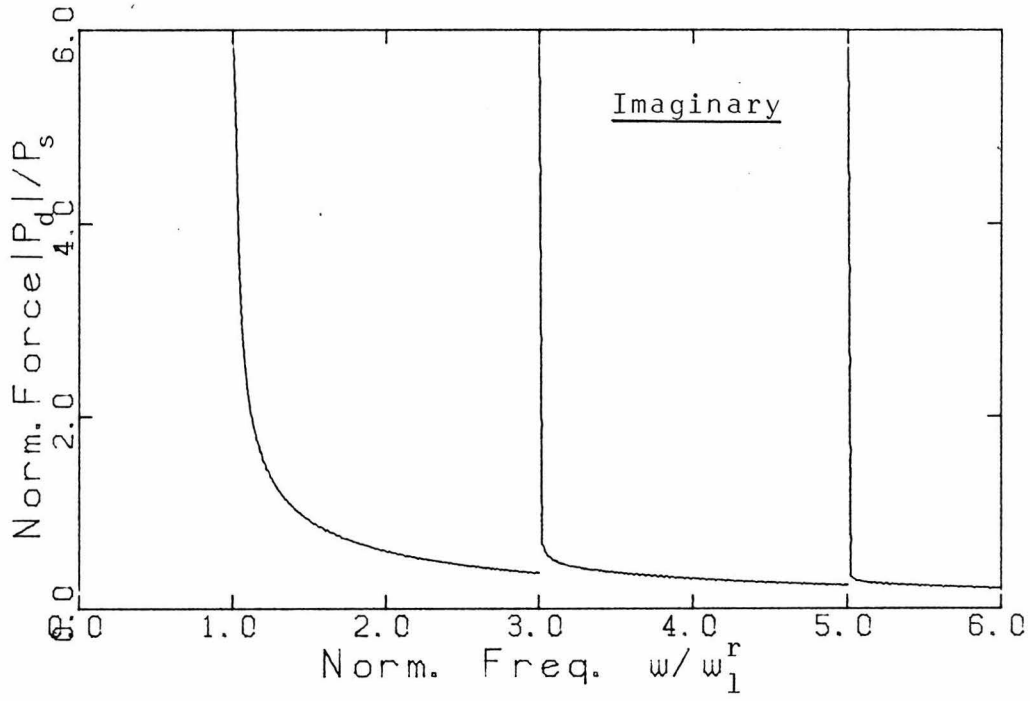


Fig. 2.7 Hydrodynamic Force Response (Rigid Dam)

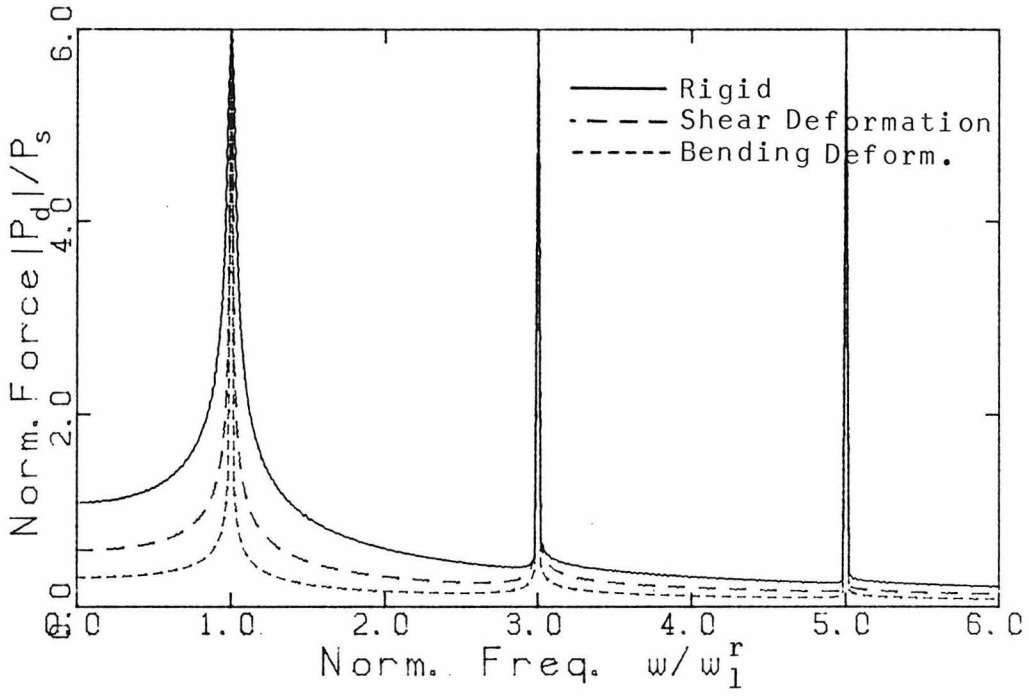


Fig. 2.8 Hydrodynamic Force Response

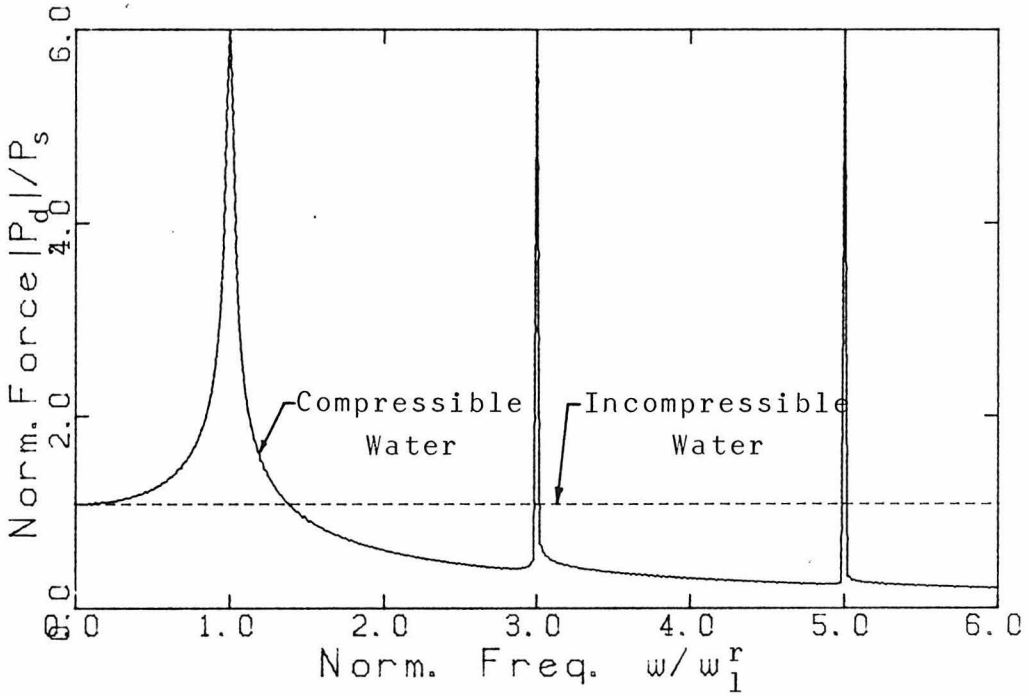


Fig. 2.9 Hydrodynamic Force Response (Rigid Dam)

The compressibility of water was taken into consideration in all the previous calculations. Neglecting water compressibility, Eq. 2.25 is used to compute the pressures resulting from a rigid motion, and the absolute normalized force is plotted in Fig. 2.9 as a horizontal dashed line, indicating the pressure independence of the forcing frequency. The force, for compressible water, is given by a solid line, and a comparison reveals the error committed by neglecting water compressibility.

## 2.3. Limited Length Gravity Dams or Walls

In analyzing the hydrodynamic pressure generated in reservoirs behind gravity dams, most work to date has considered the dam to be infinitely long, an assumption which simplifies the problem to one in two dimensions. This would be expected to be satisfactory for dams of length B, relatively large as compared to the height H. Judgment and intuition would indicate that a two dimensional solution would err considerably for a system with relatively small B/H. This conclusion is supported by the results of a vibration experiment done by A. Selby and R.T. Severn [10] on a wall of B/H = 2, storing a body of water. A quick review of the existing gravity dams in the United States, as given by T.W. Mermel [11], reveals that a considerable number have small B/H ratio. Thus, it is important to develop solutions for the pressure in those cases so that the significance of the B/H ratio could be evaluated.

In the following, a reservoir of width B is considered and expressions for the pressures generated by four different boundary motions are developed. Those formulas are next used to evaluate the pressures for selected numerical values of the different parameters involved.

2.3.1. Geometry of the Problem

In addition to the assumptions made in the previous section, the reservoir is assumed to have uniform rectangular cross-section of width B, i.e., the banks are vertical, parallel and extend to infinity normal to the upstream face of the dam.

As before, an xyz cartesian coordinates system is chosen such that the xy-plane coincides with the horizontal reservoir bottom, the yz-plane coincides with the vertical upstream dam face, and the xz-plane coincides with the vertical left bank of the reservoir. The x-axis points into the reservoir, the y-axis runs along the heel of the dam, and the z-axis points upward, as shown in Fig. 2.10.

The water in the reservoir occupies the domain D, where

$$D = \left\{(x,y,z) \mid 0 \leq x < \infty \, , \, 0 \leq y \leq B \, , \, 0 \leq z \leq H_\ell\right\} \quad .$$

Unlike the case of infinitely long dams, the problem under consideration is a three dimensional one, in which $p = p(x,y,z,t)$.

2.3.2. Vibrational Motion

In this case, the dam is assumed to vibrate harmonically such that the deformation of its upstream face, $u(y,z,t)$, is given by:

$$u(y,z,t) = A \cdot \varphi\left(\frac{y}{B},\frac{z}{H}\right) \cdot \exp(i\omega t) \qquad (2.37)$$

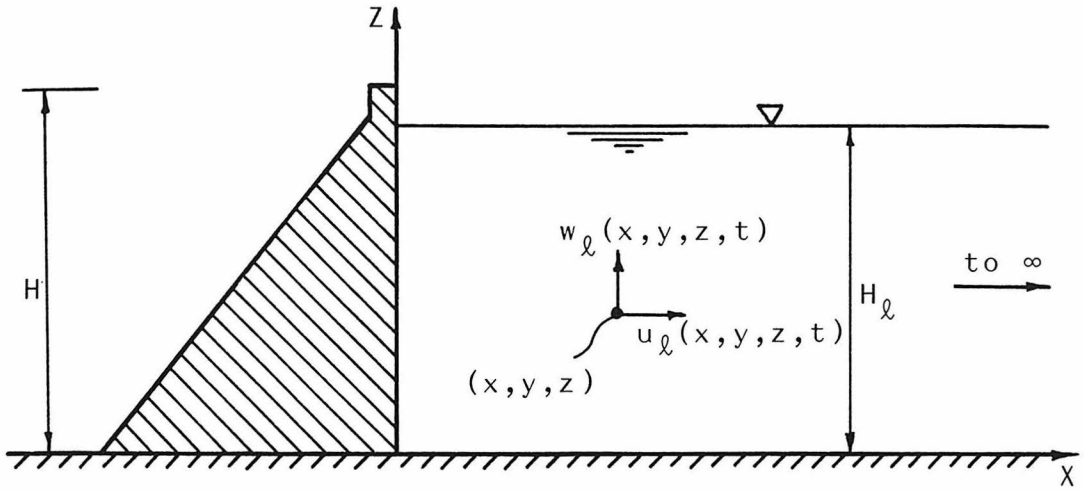


(a) Sectional Elevation

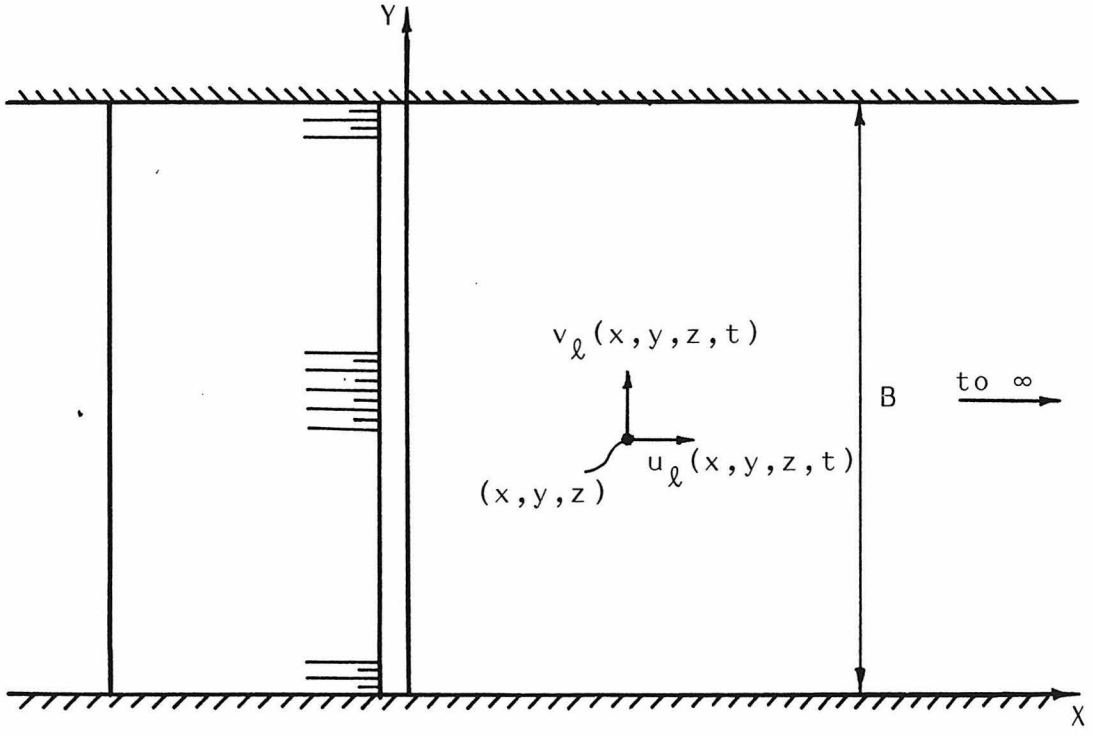


(b) Plan View

Fig. 2.10 Dam-Reservoir and Coordinate System

where here $\varphi\left(\frac{y}{B},\frac{z}{H}\right)$ is a given function of y and z whose maximum equals 1. This is illustrated in Fig. 2.11.

The boundary conditions are as follows:

i) the pressure is bounded as $x \to \infty$, and only waves travelling away from the dam can exist, i.e.,

$$p(\infty,y,z,t) < \infty \tag{2.38}$$

ii) the effect of waves at the free surface of the reservoir ($z = H_\ell$) is neglected, i.e.,

$$p(x,y,H_\ell,t) = 0 \tag{2.39}$$

iii) the vertical motion of the water at the bottom of the reservoir ($z = 0$) vanishes, i.e.,

$$w_\ell(x,y,0,t) = 0 \tag{2.40}$$

iv) the horizontal transverse motion of the water at the left bank of the reservoir ($y = 0$) vanishes, i.e.,

$$v_\ell(x,0,z,t) = 0 \tag{2.41}$$

v) the horizontal transverse motion of the water at the right bank of the reservoir ($y = B$) vanishes, i.e.,

$$v_\ell(x,B,z,t) = 0 \tag{2.42}$$

vi) the horizontal longitudinal motion of the water at the upstream face of the dam ($x = 0$) is the same as the motion of the face, i.e.,

$$u_\ell(0,y,z,t) = u(y,z,t) \tag{2.43}$$

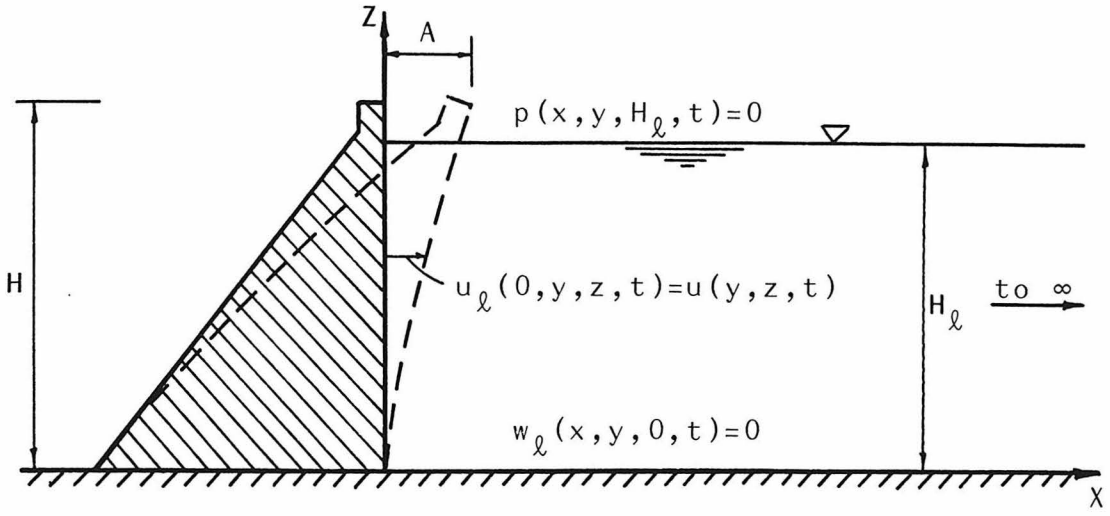


(a) Sectional Elevation

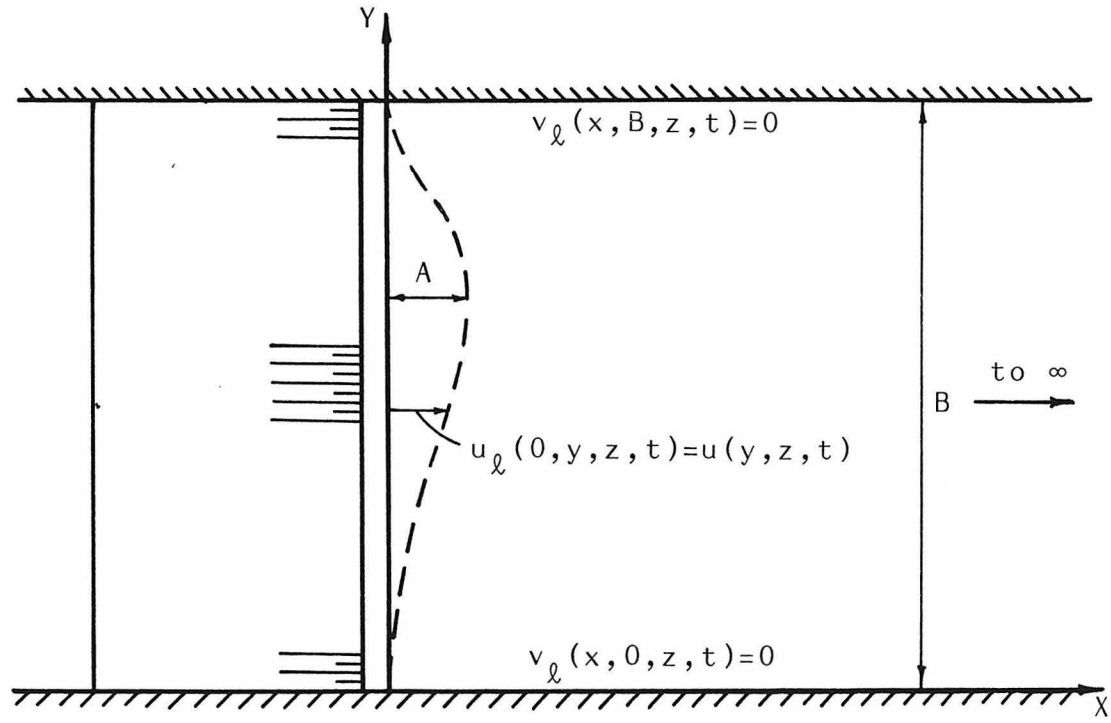


(b) Plan View

Fig. 2.11 Vibrational Motion

Applying these conditions to the general solutions, Eqs. 2.5 and 2.6, one obtains:

$$p(x,y,z,t) = -4\,\rho_\ell H_\ell A\,\omega^2 \exp(i\omega t)$$

$$\cdot\left\{-i\sum_{n=0}^{\infty}\sum_{m=1}^{m_n-1}\frac{I_{mn}}{\varepsilon_n\,\bar{\delta}_{mn}}\exp\left(-i\bar{\delta}_{mn}\frac{x}{H_\ell}\right)\cdot\cos\left(\beta_n\frac{y}{B}\right)\cdot\cos\left(\eta_m\frac{z}{H_\ell}\right)\right.$$

$$\left.+\sum_{n=0}^{\infty}\sum_{m=m_n}^{\infty}\frac{I_{mn}}{\varepsilon_n\,\delta_{mn}}\exp\left(-\delta_{mn}\frac{x}{H_\ell}\right)\cdot\cos\left(\beta_n\frac{y}{B}\right)\cdot\cos\left(\eta_m\frac{z}{H_\ell}\right)\right\} \tag{2.44}$$

where

$$\left.\begin{aligned}
\beta_n &= n\,\pi \quad ; \quad n = 0,1,2,\ldots \\
\eta_m &= \frac{(2m-1)\pi}{2} \quad ; \quad m = 1,2,3,\ldots \\
\varepsilon_n &= \begin{cases} 2 & (n = 0) \\ 1 & (n \neq 0) \end{cases}
\end{aligned}\right\} \tag{2.45}$$

$$\left.\begin{aligned}
\bar{\delta}_{mn} &= H_\ell\sqrt{(\omega/c)^2 - (\beta_n/B)^2 - (\eta_m/H_\ell)^2} \quad ; \quad m = 1,2,\ldots,m_n-1 \\
\delta_{mn} &= H_\ell\sqrt{(\beta_n/B)^2 + (\eta_m/H_\ell)^2 - (\omega/c)^2} \quad ; \quad m = m_n, m_n+1,\ldots
\end{aligned}\right\} \tag{2.46}$$

$m_n$ = smallest m, for a given n, satisfying:

$$\left[\,(\beta_n/B)^2 + (\eta_m/H_\ell)^2\,\right] > (\omega/c)^2$$

$$I_{mn} = \frac{1}{B\,H_\ell}\int_0^{H_\ell}\int_0^{B}\varphi\left(\frac{y}{B},\frac{z}{H}\right)\cdot\cos\left(\beta_n\frac{y}{B}\right)\cdot\cos\left(\eta_m\frac{z}{H_\ell}\right)dy\,dz \tag{2.47}$$

From Eqs. 2.46, it is clear that the natural frequencies of the reservoir are given by:

$$\omega_{ij}^{r} = \frac{\pi\, c}{H_\ell}\sqrt{\left(\frac{i\, H}{B}\right)^2 + \left(\frac{2j-1}{2}\right)^2} \quad ;\ i = 0,1,\ldots \text{ and } j = 1,2,\ldots \tag{2.48}$$

The fundamental frequency of the reservoir, which corresponds to $i = 0$ and $j = 1$, is then $\omega_1^r = \pi c/2H_\ell$, same as that of the two dimensional reservoir. Conclusions, similar to those given on page 17, are applicable here.

For an incompressible fluid, one obtains:

$$p(x,y,z,t) = \frac{4\,\rho_\ell}{B}\left\{\sum_{n=0}^{\infty}\sum_{m=1}^{\infty}\frac{J_{mn}}{\varepsilon_n\,\mu_{mn}}\cdot\exp\left(-\mu_{mn}\frac{x}{H_\ell}\right)\cdot\cos\left(\beta_n\frac{y}{B}\right)\cdot\cos\left(\eta_m\frac{z}{H_\ell}\right)\right\} \tag{2.49}$$

where

$$J_{mn} = \int_0^{H_\ell}\int_0^{B}\ddot{u}\,(y,z,t)\cdot\cos\left(\beta_n\frac{y}{B}\right)\cdot\cos\left(\eta_m\frac{z}{H_\ell}\right)dy\,dz \tag{2.50}$$

$$\mu_{mn} = H_\ell\sqrt{(\beta_n/B)^2 + (\eta_m/H_\ell)^2} \tag{2.51}$$

In particular, for harmonic motion, Eq. 2.49 becomes:

$$p(x,y,z,t) = -4\,\rho_\ell H_\ell A\,\omega^2\exp(i\omega t)\cdot\left\{\sum_{n=0}^{\infty}\sum_{m=1}^{\infty}\frac{I_{mn}}{\varepsilon_n\,\mu_{mn}}\cdot\exp\left(-\mu_{mn}\frac{x}{H_\ell}\right)\cdot\cos\left(\beta_n\frac{y}{B}\right)\cdot\cos\left(\eta_m\frac{z}{H_\ell}\right)\right\} \tag{2.52}$$

Again, the same conclusions given on page 19 are applicable here.

2.3.3. Longitudinal Ground Motion

Here, the dam is assumed to be rigid, and a harmonic ground motion, as given by Eq. 2.22, is applied to its base (see Fig. 2.12).

The boundary conditions being the same as those of the previous case, the solution is obtained from Eq. 2.44 by replacing A by $\bar{u}_g$ and taking $\varphi\left(\frac{Y}{B},\frac{Z}{H}\right) \equiv 1$. In this case, Eq. 2.47 yields

$$\left.\begin{aligned} I_{mn} &= \frac{(-1)^{m+1}}{\eta_m} \qquad (n = 0) \\ &= 0 \qquad\qquad (n \neq 0) \end{aligned}\right\} \tag{2.53}$$

Hence, the expression for the pressure reduces to exactly the one given by Eq. 2.24.

Similarly for an incompressible fluid, the pressure is given by Eq. 2.25.

2.3.4. Transverse Ground Motion

In this case, a harmonic horizontal transverse ground motion is applied to the dam and the reservoir boundaries. The dam is assumed rigid and the banks are assumed to move together, with a motion given by:

$$v_g(t) = \bar{v}_g \cdot \exp(i\omega t) \tag{2.54}$$

where $\bar{v}_g$ is the amplitude of bank motion, as shown in Fig. 2.13.

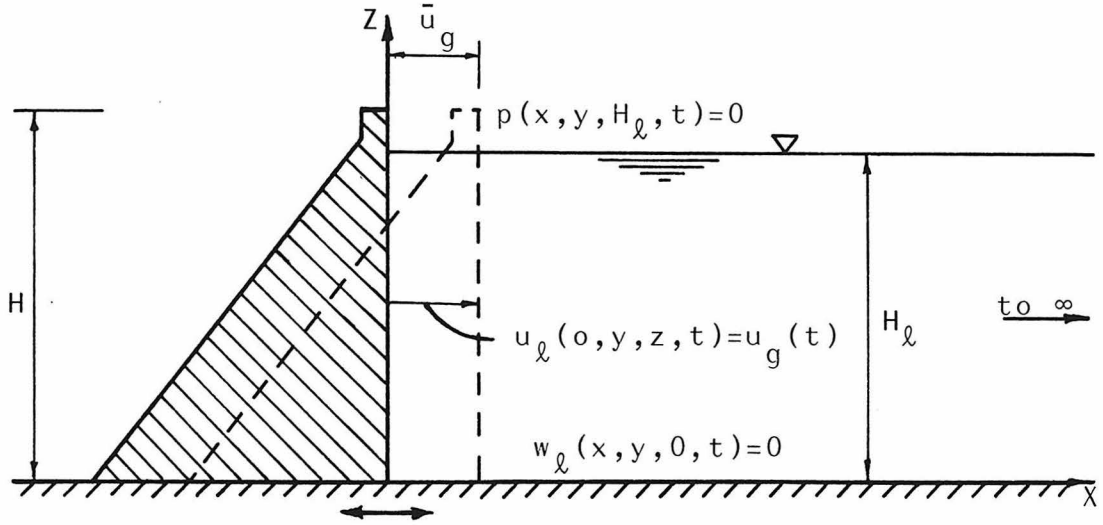


(a) Sectional Elevation

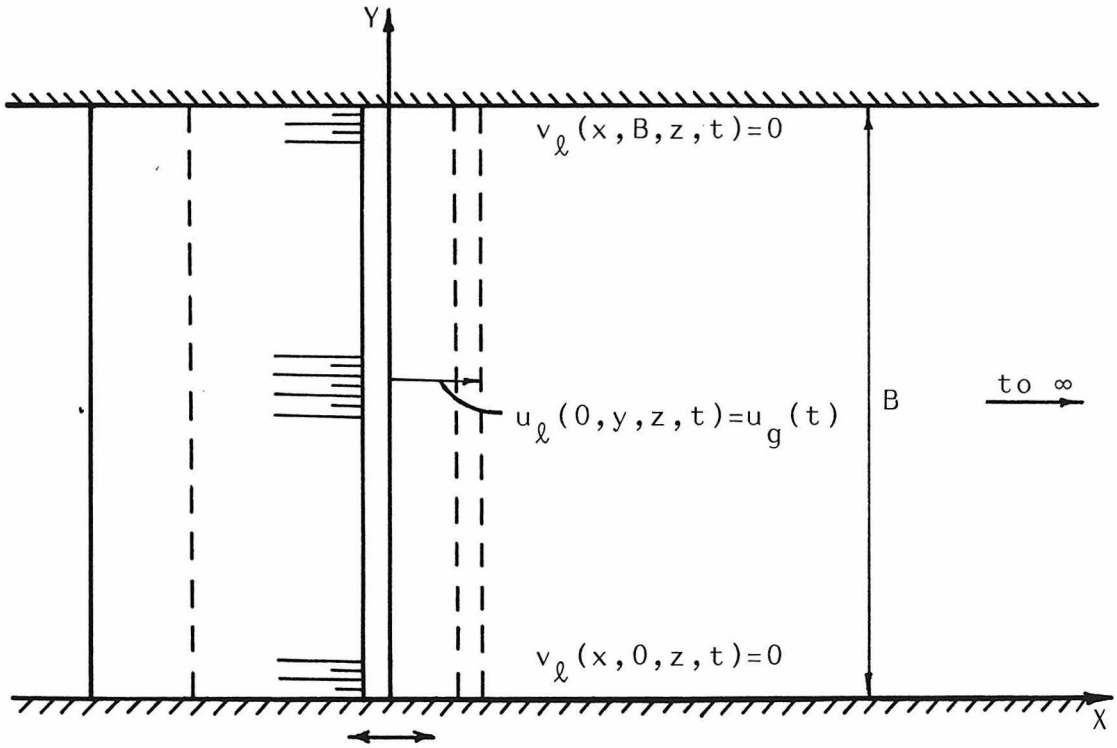


(b) Plan View

Fig. 2.12 Longitudinal Ground Motion

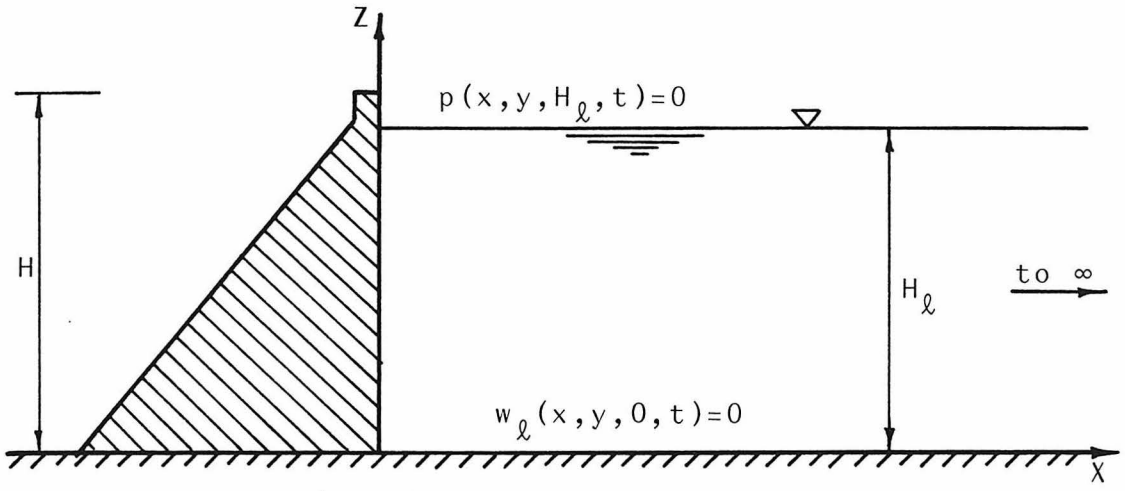


(a) Sectional Elevation

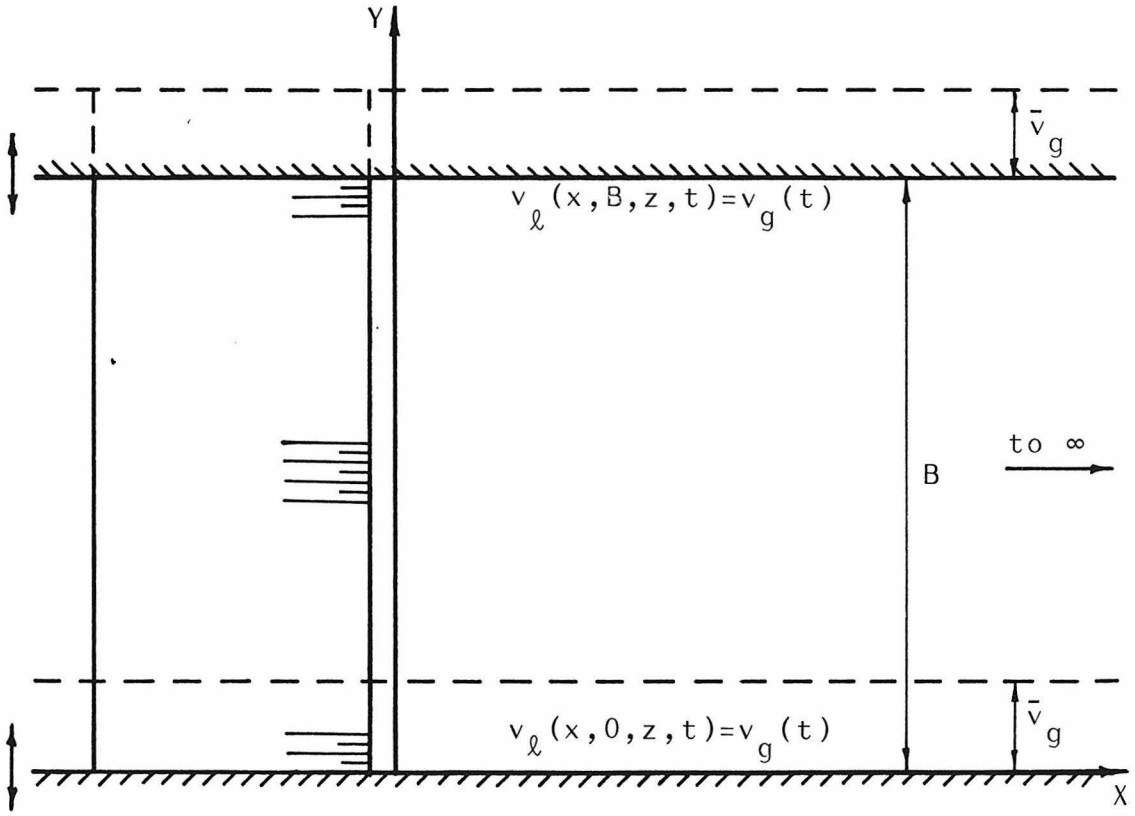


(b) Plan View

Fig. 2.13 Transverse Ground Motion

The problem is independent of the x-coordinate, i.e., $p = p(y,z,t)$. The boundary conditions are:

$$p(y,H_\ell,t) = 0 \tag{2.55}$$

$$w_\ell(y,0,t) = 0 \tag{2.56}$$

$$v_\ell(0,z,t) = v_g(t) \tag{2.57}$$

$$v_\ell(B,z,t) = v_g(t) \tag{2.58}$$

where the last two conditions simply state that the transverse water motion at the reservoir banks is identical to the motion prescribed to the banks.

An expression for the hydrodynamic pressure can be obtained in the form:

$$\begin{aligned} p_{gy}(y,z,t) = -2\,\rho_\ell H_\ell \bar{v}_g\,\omega^2 \exp(i\omega t) \\ \cdot \Bigg\{ \sum_{m=1}^{m_0-1} \frac{(-1)^{m+1}}{\eta_m \bar{\delta}_{m0} \cos(B\bar{\delta}_{m0}/2H_\ell)} \\ \cdot \sin\left[\bar{\delta}_{m0}\left(\frac{B}{2}-y\right)/H_\ell\right] \cdot \cos\left(\eta_m \frac{z}{H_\ell}\right) \\ + \sum_{m=m_0}^{\infty} \frac{(-1)^{m+1}}{\eta_m \delta_{m0} \cosh(B\delta_{m0}/2H_\ell)} \\ \cdot \sinh\left[\delta_{m0}\left(\frac{B}{2}-y\right)/H_\ell\right] \cdot \cos\left(\eta_m \frac{z}{H_\ell}\right) \Bigg\} \end{aligned} \tag{2.59}$$

where all variables are as defined before.

By examining the above equation, it is concluded that:

i) The hydrodynamic pressure remains bounded as the excitation frequency approaches a natural frequency of the reservoir, as defined in Eq. 2.48, with i = 0. This is true because the expression has a limiting value as $\bar{\delta}_{m0}$ or $\delta_{m0} \rightarrow \infty$. In particular, the following limits exist:

$$\left.\begin{aligned} &\lim_{\bar{\delta}_{m0} \rightarrow 0} \frac{\sin\left[\bar{\delta}_{m0}\left(\frac{B}{2}-y\right)/\,H_\ell\right]}{\bar{\delta}_{m0}} = \left(\frac{B}{2}-y\right)/\,H_\ell \\ &\text{and} \\ &\lim_{\delta_{m0} \rightarrow 0} \frac{\sinh\left[\delta_{m0}\left(\frac{B}{2}-y\right)/\,H_\ell\right]}{\delta_{m0}} = \left(\frac{B}{2}-y\right)/\,H_\ell \end{aligned}\right\} \quad (2.60)$$

ii) The pressure, however, becomes infinite as $\omega$ approaches a value which makes $\cos(B\,\bar{\delta}_{m0}\,/\,2\,H_\ell)$, in the denominator of the first series, vanish. Those values are found to be:

$$\omega = c\sqrt{(2\eta_k/B)^2 + (\eta_m/H_\ell)^2} \quad ; \; k,m = 1,2,3 \qquad (2.61)$$

which are the same ones given by Eq. 2.48, with odd values of i.

iii) The first series vanishes for $\omega < \omega_1^r$. Thus no pressure singularity occurs over the range $0 \leq \omega \leq \omega_1^r$.

iv) The pressure is either in-phase or in opposite-phase with the excitation.

For an incompressible fluid, the solution is obtained as the limit of Eq. 2.59 as $c \to \infty$, and is given by:

$$p_{gy}(y,z,t) = 2\,\rho_\ell H_\ell \bar{v}_g\,\omega^2 \exp(i\omega t) \cdot \left\{ \sum_{m=1}^{\infty} \frac{(-1)^{m+1}}{\eta_m^2 \cosh(B\eta_m / 2H_\ell)} \cdot \sinh\left[\eta_m\left(\frac{B}{2} - y\right)/ H_\ell\right] \cdot \cos\left(\eta_m \frac{z}{H_\ell}\right)\right\} \tag{2.62}$$

and it is clear that resonance does not occur in this case.

The problem in case of transverse ground motion is equivalent to that of an infinitely long rigid dam, with finite length reservoir, subject to longitudinal ground motion. The solution was given by P.W. Werner and K.J. Sundquist [12] for compressible fluids, and by L.M. Hoskins and L.S. Jacobsen [3] for incompressible fluids.

2.3.5. Vertical Ground Motion

Although this case has a three dimensional geometry, the pressure turns out to be independent of the x and y coordinates. The problem reduces exactly to the one given in section 2.2.4. The solution for the hydrodynamic pressure will be given by Eq. 2.30 for compressible water, and by Eq. 2.33 (or Eq. 2.34) for incompressible water.

2.3.6. Numerical Examples

In addition to the parameters given in page 24, Eq. 2.44 shows that the hydrodynamic pressure is further dependent on the length of the dam B. The normalized pressure will in turn be dependent on the ratio B/H.

The hydrodynamic pressure acting on the upstream dam face is calculated, using Eq. 2.44, for prescribed vibrational shapes:

$$\Psi\left(\frac{Y}{B},\frac{Z}{H}\right) = Y_i\left(\frac{Y}{B}\right) \cdot Z_j\left(\frac{Z}{H}\right) \qquad ; \quad i,j = 1,2 \tag{2.63}$$

where

1) <u>for shear deformations:</u>

$$\left.\begin{aligned} {}^{*}Y_i\left(\frac{Y}{B}\right) &= \sin\left(\beta_i \frac{Y}{B}\right) \quad ; \quad \beta_i = i\,\pi \\ {}^{*}Z_j\left(\frac{Z}{H}\right) &= \sin\left(\eta_j \frac{Z}{H}\right) \quad ; \quad \eta_j = \frac{(2j-1)\pi}{2} \end{aligned}\right\} \tag{2.64}$$

2) <u>for bending deformations:</u>

$${}^{*}Y_i\left(\frac{Y}{B}\right) = B_i\left(\frac{Y}{B}\right) / B_i(\bar{y}_i)$$

where

$$B_i\left(\frac{Y}{B}\right) = \left[\cos\left(\alpha_i \frac{Y}{B}\right) - \cosh\left(\alpha_i \frac{Y}{B}\right)\right] - c_i\left[\sin\left(\alpha_i \frac{Y}{B}\right) - \sinh\left(\alpha_i \frac{Y}{B}\right)\right]$$

in which $\alpha_i$ are roots of: $\cos(\alpha_i)\cosh(\alpha_i) = 1$

and $$c_i = \frac{\cos(\alpha_i) - \cosh(\alpha_i)}{\sin(\alpha_i) - \sinh(\alpha_i)}$$

$\bar{y}_i$ is such that $B_i(\bar{y}_i)$ is maximum.

$${}^{*}Z_j\left(\frac{Z}{H}\right) = A_j\left(\frac{Z}{H}\right) / A_j(1)$$

where $A_j\left(\frac{Z}{H}\right)$ is as given in Eqs. 2.36. (2.65)

These shapes are the first four mode shapes, two symmetric and two antisymmetric, of a shear and a bending plate, respectively.

For a full reservoir and a dam of B/H = 2, the pressure was calculated at 121 equidistant points covering the left half of the dam face, for $A\omega^2 = g$ and $\bar{\omega} = 0.7$. The vibrational shapes and the resulting pressures are shown in Figs. 2.14 and 2.15. For each case, the pressure values plotted were scaled by their maximum value (shown by a solid arrow). These maximas, and their locations $\left(\frac{Y}{B}, \frac{Z}{H}\right)$, are given in Table 2.1.

| | Prescribed Shape | 1st | 2nd | 3rd | 4th |
|---|---|---|---|---|---|
| Shear Deformations | Maximum Pressure | 0.381 | 0.259 | 0.446 | 0.280 |
| | Location | (0.5,0.6) | (0.2,0.6) | (0.5,0.3) | (0.2,0.3) |
| Bending Deformations | Maximum Pressure | 0.197 | 0.137 | 0.273 | 0.170 |
| | Location | (0.5,0.6) | (0.25,0.6) | (0.5,0.4) | (0.25,0.4) |

TABLE 2.1. Maximum Normalized Pressure and its Location

The pressure distribution was also calculated for dams of B/H ranging between 1.0 and 10.0, for the same vibrational shapes given before. The absolute maximum pressure acting on the dam as well as the maximum pressure at the left bank are given in Tables 2.2 and 2.3 for the shear and the bending vibrational shapes, respectively. It is noticed that the absolute maximum pressure increases in value as B/H

increases. Also, a comparison between the maximum value and the value at the bank shows a large variation in the pressure along any horizontal plane, as opposed to a constant value for the case of an infinitely long dam. This is also clear from Figs. 2.14 and 2.15.

| | B/H / Prescribed shape | 1.0 | 2.0 | 3.0 | 5.0 | 10.0 |
|---|---|---|---|---|---|---|
| Absolute Maximum Pressure | 1st | 0.174 | 0.197 | 0.212 | 0.229 | 0.246 |
| | 2nd | 0.093 | 0.137 | 0.165 | 0.197 | 0.231 |
| | 3rd | 0.243 | 0.273 | 0.295 | 0.327 | 0.359 |
| | 4th | 0.106 | 0.170 | 0.213 | 0.266 | 0.329 |
| Maximum Pressure at Left Bank | 1st | 0.101 | 0.088 | 0.073 | 0.048 | 0.020 |
| | 2nd | 0.052 | 0.059 | 0.067 | 0.067 | 0.040 |
| | 3rd | 0.163 | 0.137 | 0.112 | 0.073 | 0.030 |
| | 4th | 0.063 | 0.092 | 0.108 | 0.104 | 0.061 |

TABLE 2.2. Maximum Normalized Pressure (Shear Deformations)

| | B/H / Prescribed shape | 1.0 | 2.0 | 3.0 | 5.0 | 10.0 |
|---|---|---|---|---|---|---|
| Absolute Maximum Pressure | 1st | 0.174 | 0.197 | 0.212 | 0.229 | 0.246 |
| | 2nd | 0.093 | 0.137 | 0.165 | 0.197 | 0.231 |
| | 3rd | 0.243 | 0.273 | 0.295 | 0.327 | 0.359 |
| | 4th | 0.106 | 0.170 | 0.213 | 0.266 | 0.329 |
| Maximum Pressure at Left Bank | 1st | 0.101 | 0.088 | 0.073 | 0.048 | 0.020 |
| | 2nd | 0.052 | 0.059 | 0.067 | 0.067 | 0.040 |
| | 3rd | 0.163 | 0.137 | 0.112 | 0.073 | 0.030 |
| | 4th | 0.063 | 0.092 | 0.108 | 0.104 | 0.061 |

TABLE 2.3. Maximum Normalized Pressure (Bending Deformations)

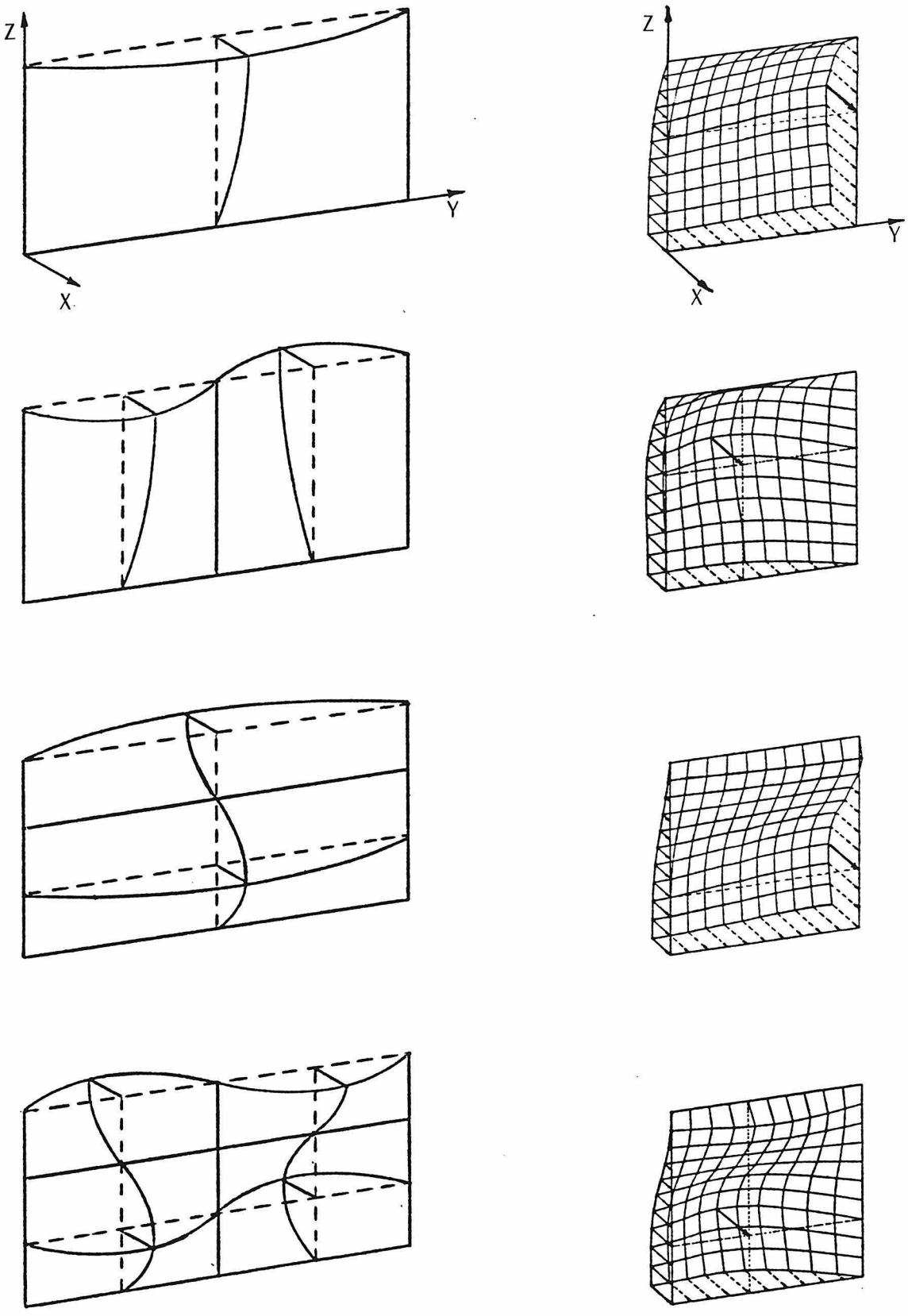


(a) Prescribed Motion (b) Hydrodynamic Pressure

Fig. 2.14 Hydrodynamic Pressure Distribution (Shear Deformation)

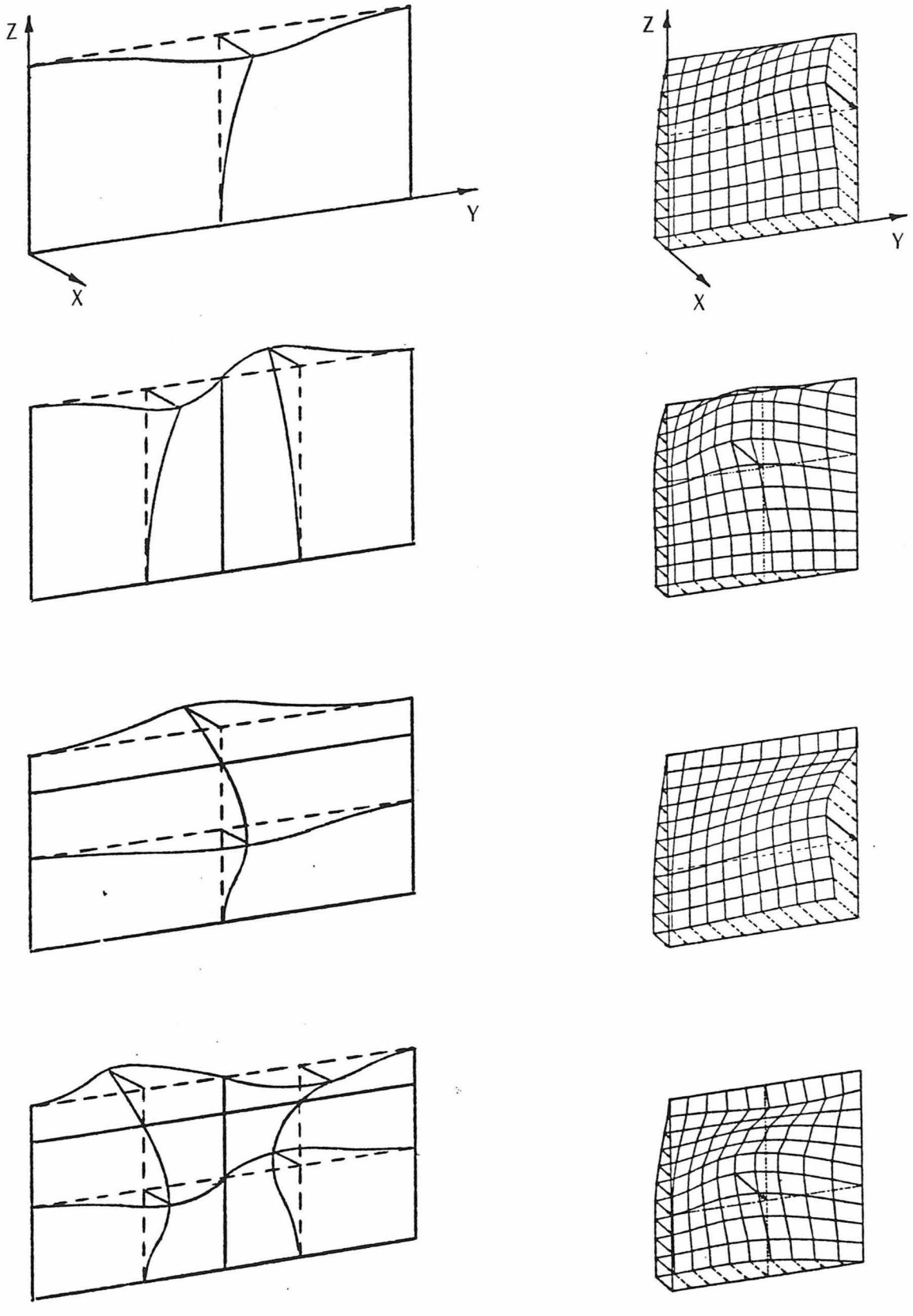


(a) Prescribed Motion (b) Hydrodynamic Pressure

Fig. 2.15 Hydrodynamic Pressure Distribution (Bending Deformation)

The effect of B/H is better illustrated in Figs. 2.16 and 2.17, in which the distribution of pressure at the mid-span of the dam, is plotted for various B/H ratios. This is done for the first and third vibrational shapes, in shear (Fig. 2.16), and in bending (Fig. 2.17).

The absolute value of the total hydrodynamic force, normalized by the hydrostatic, acting on the left half of a dam of B/H = 2.0 forced to deform according to the first and second of the prescribed shapes mentioned before, is plotted in Figs. 2.18a and 2.18b, respectively, as a function of the normalized frequency $\bar{\omega}$. The response shown is for a shear deformation. The bending case will be similar, but with smaller values.

Although the problem of a limited length gravity dam is three dimensional, the hydrodynamic pressure generated by longitudinal and by vertical ground motions turns out to be independent of the position along the dam length. For transverse ground motions, a case suppressed in infinitely long dams problem, the generated pressure is maximum at the banks and decreases to zero at the middle of the dam. Figure 2.19 shows the distribution of pressure along the vertical line y = 0, for the three components of ground motion for both incompressible and compressible water assumptions. The motion is assumed to be harmonic of frequency (normalized) $\bar{\omega} = 0.7$. In addition, the absolute total force responses are plotted in Fig. 2.20.

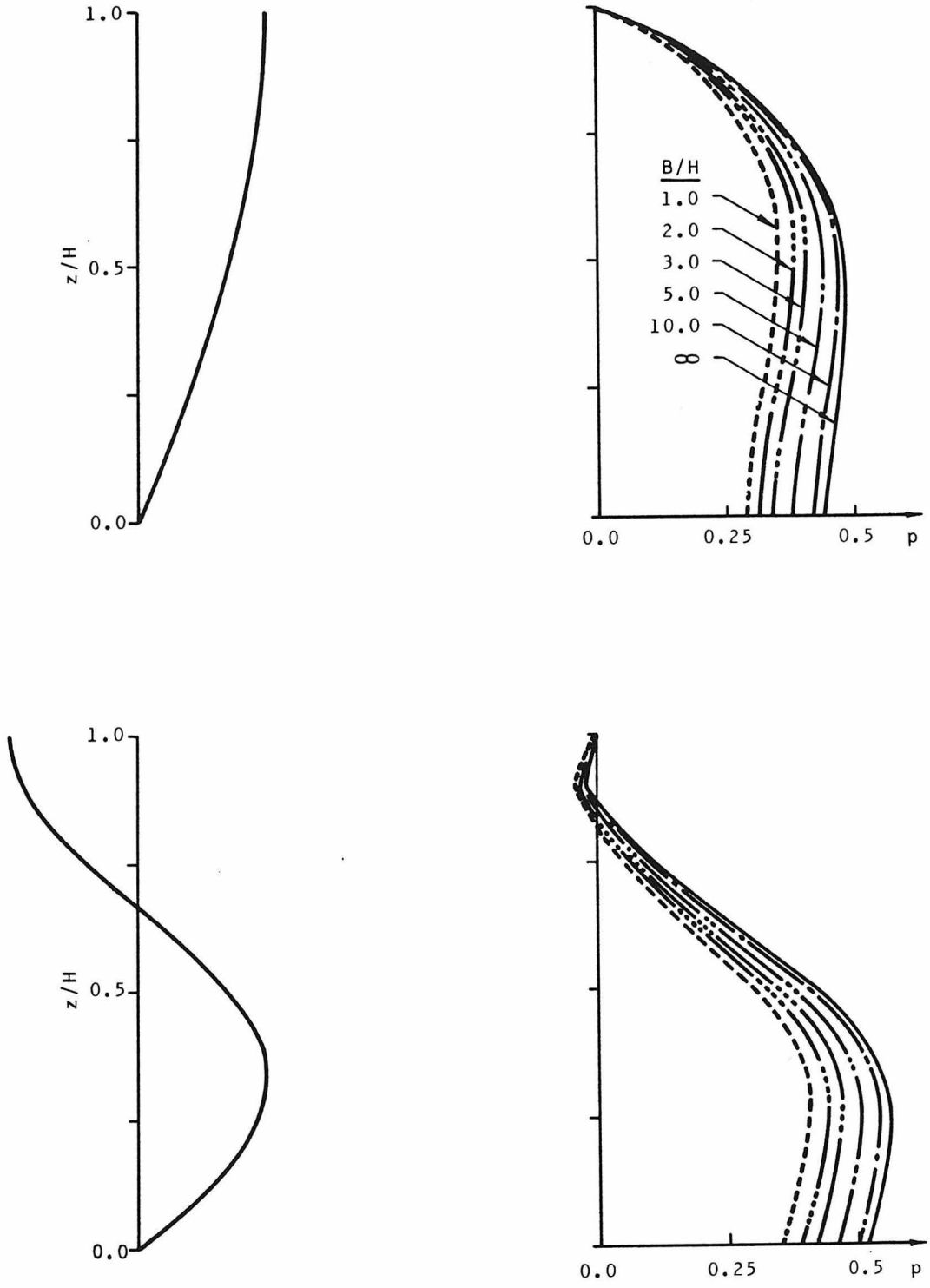


(a) Prescribed Motion (b) Normalized Pressure

Fig. 2.16 Pressure Distribution at Mid-Span (Shear Deformation)

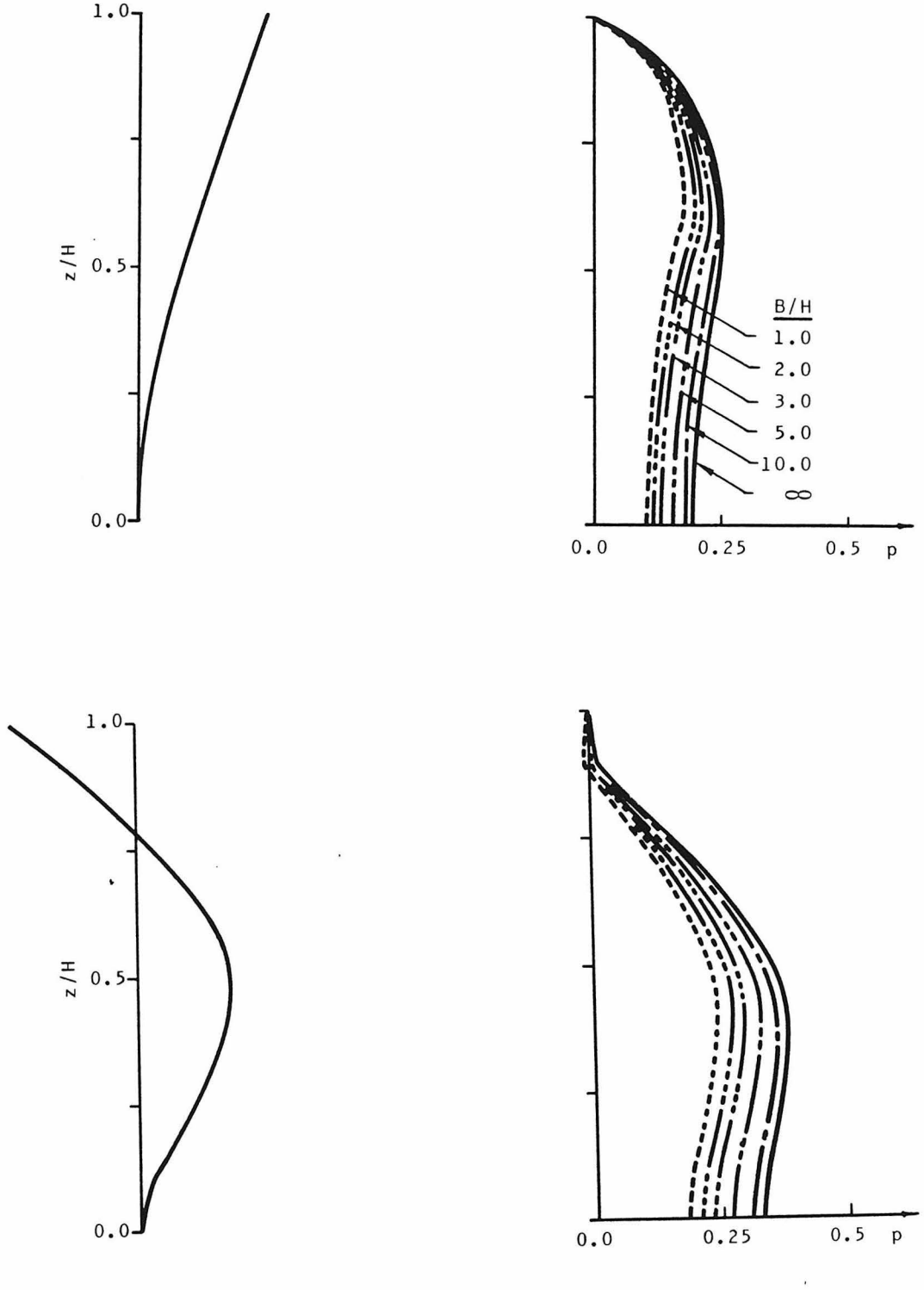


(a) Prescribed Motion (b) Normalized Pressure

Fig. 2.17 Pressure Distribution at Mid-Span (Bending Deformation)

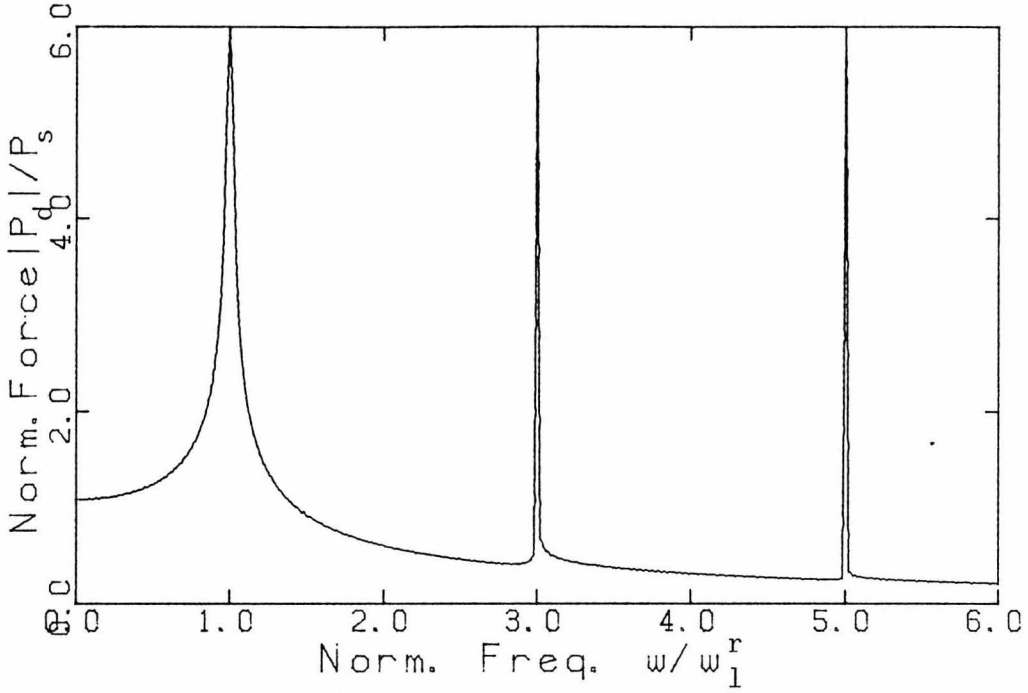


(a) 1st Mode of Vibration (Symmetric)

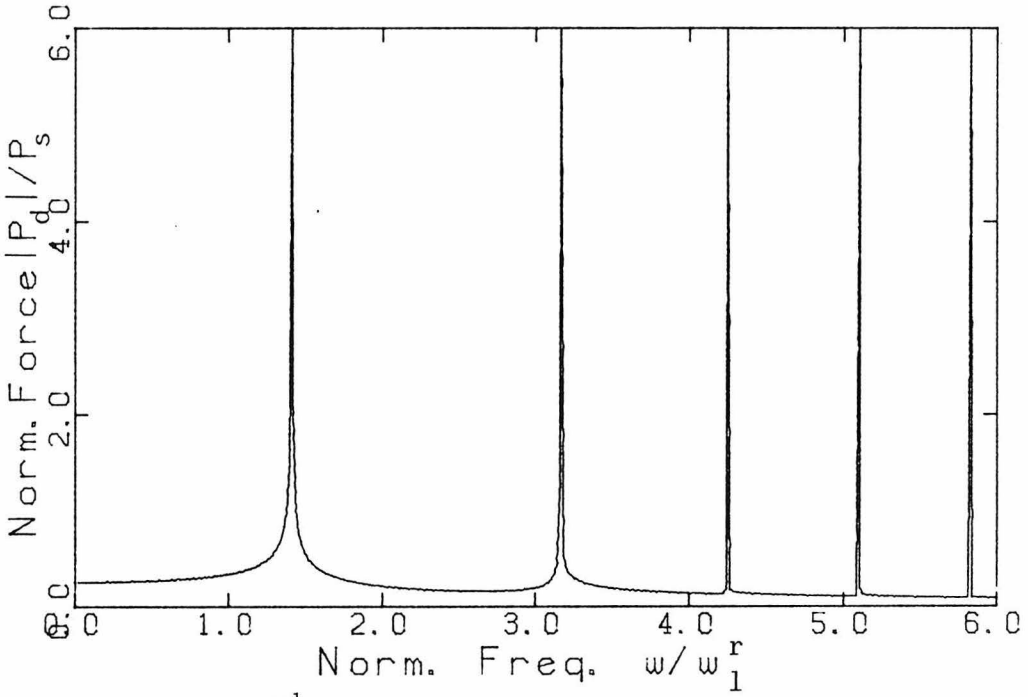


(b) 2nd Mode of Vibration (Antisymmetric)

Fig. 2.18 Hydrodynamic Force Response (Shear Deformation)

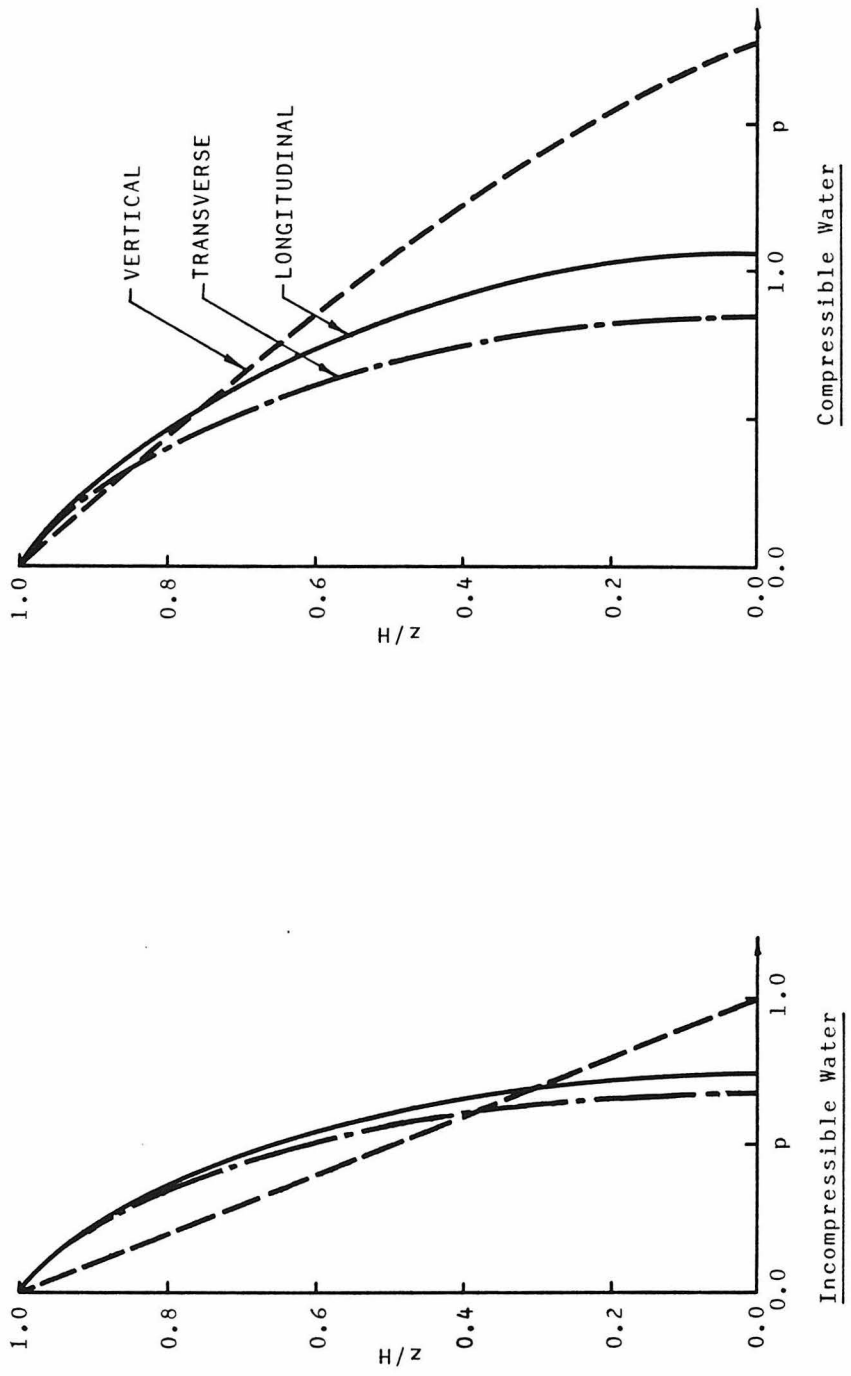


Fig. 2.19 Hydrodynamic Pressure Distribution (Rigid Dam, y/B=0.0, $\bar{\omega}$=0.7)

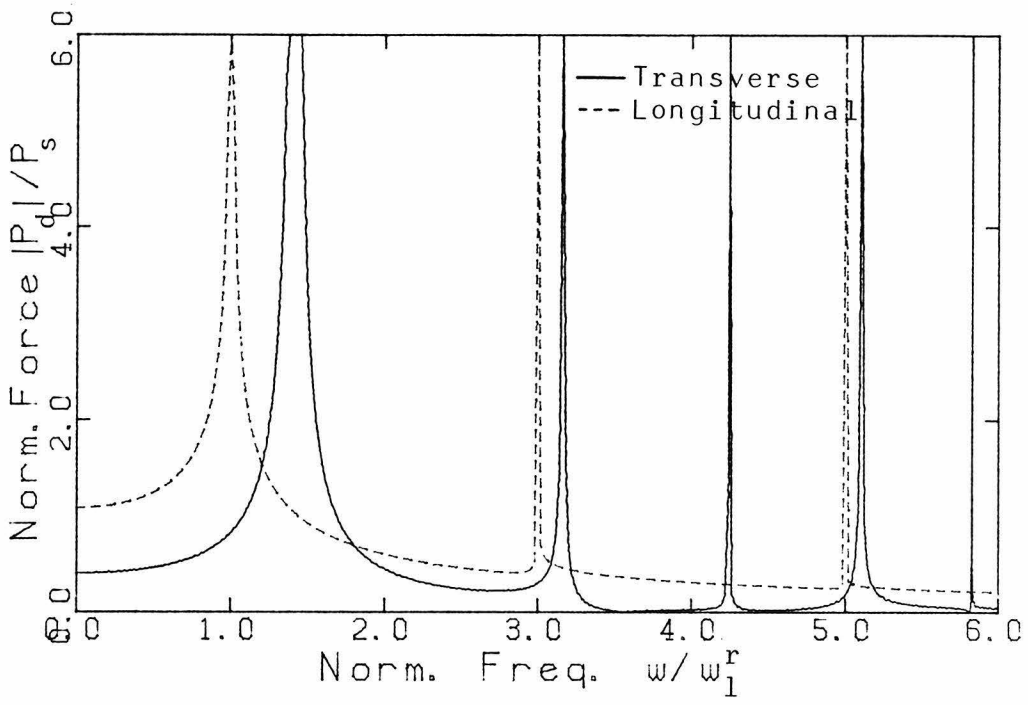


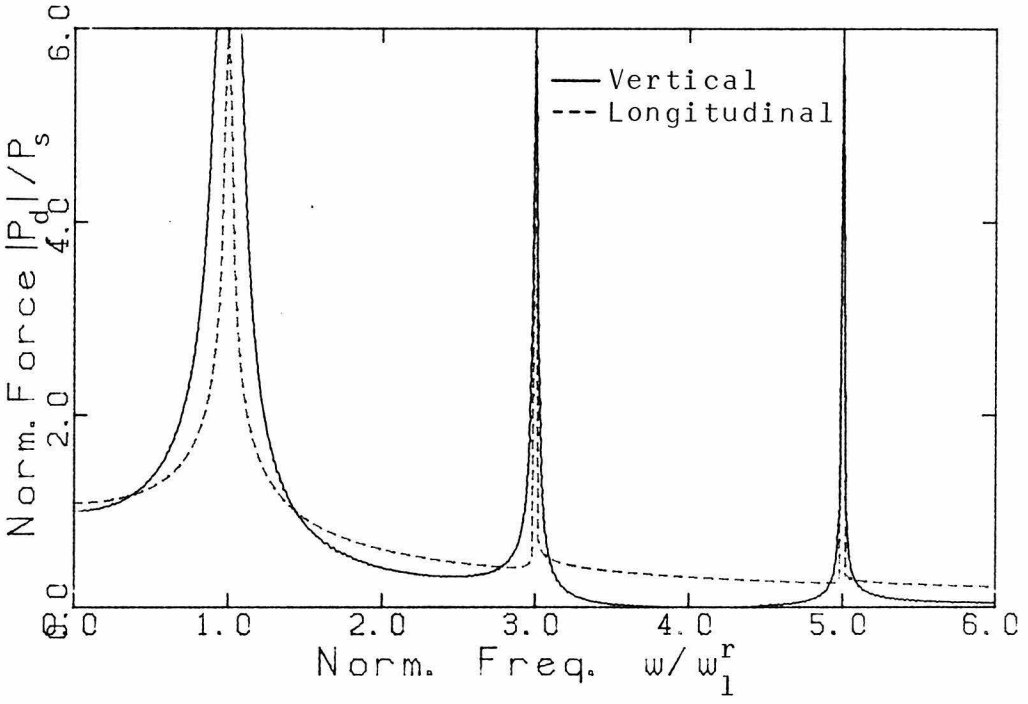


Fig. 2.20 Hydrodynamic Force Response (Rigid Dam)

## 2.4. Appendix

In this section, analytical solutions for the hydrodynamic pressures generated in some other simplified fluid domains are presented. These are:

i) Liquids stored in circular cylindrical tanks.

ii) Water around circular cylindrical intake towers or bridge piers.

iii) Reservoirs behind arch dams whose upstream faces are segments of circular cylinders.

In all cases, the assumptions made in section 2.1.1. about the fluid are also made here, so that the pressure is governed by the wave equation, Eq. 2.1. However, it is convenient to use a cylindrical coordinate frame, in which the Laplace operator is given by:

$$\nabla^2 = \frac{\partial^2}{\partial r^2} + \frac{1}{r}\frac{\partial}{\partial r} + \frac{1}{r^2}\frac{\partial^2}{\partial \theta^2} + \frac{\partial^2}{\partial z^2} \qquad (2.66)$$

Only solutions for the case of compressible fluids are presented. For incompressible fluids, the solutions can be obtained as limiting cases of the first set, by letting the sound velocity $c \rightarrow \infty$.

In cylindrical coordinates, two possible solutions for the wave equation are:

$$p(r,\theta,z,t) = \left[c_1 I_\beta(\delta r) + c_2 K_\beta(\delta r)\right] \cdot \left[c_3 \sin(\beta\theta) + c_4 \cos(\beta\theta)\right] \cdot \left[c_5 \sin(\eta z) + c_6 \cos(\eta z)\right] \cdot \left[c_7 \exp(i\tau t) + c_8 \exp(-i\tau t)\right] \quad (2.67)$$

in which $\eta^2 > (\tau/c)^2$, $\delta^2 = \eta^2 - (\tau/c)^2$, and $I_\beta$ and $K_\beta$ are the modified Bessel's functions of order $\beta$ of the first and second kinds, respectively, or

$$p(r,\theta,z,t) = \left[\bar{c}_1 J_\beta(\bar{\delta} r) + \bar{c}_2 Y_\beta(\bar{\delta} r)\right] \cdot \left[c_3 \sin(\beta\theta) + c_4 \cos(\beta\theta)\right] \cdot \left[c_5 \sin(\eta z) + c_6 \cos(\eta z)\right] \cdot \left[c_7 \exp(i\tau t) + c_8 \exp(-i\tau t)\right] \quad (2.68)$$

in which $\eta^2 < (\tau/c)^2$, $\delta^2 = (\tau/c)^2 - \eta^2$, and $J_\beta$ and $Y_\beta$ are the Bessel's functions of order $\beta$ of the first and second kinds, respectively. Equation 2.68 can be put in a second form as:

$$p(r,\theta,z,t) = \left[ \bar{c}_1 H_\beta^{(1)}(\bar{\delta}r) + \bar{c}_2 H_\beta^{(2)}(\bar{\delta}r) \right] \cdot \left[ c_3 \sin(\beta\theta) + c_4 \cos(\beta\theta) \right] \cdot \left[ c_5 \sin(\eta z) + c_6 \cos(\eta z) \right] \cdot \left[ c_7 \exp(i\tau t) + c_8 \exp(-i\tau t) \right] \quad (2.69)$$

where $H_\beta^{(1)}$ and $H_\beta^{(2)}$ are the Hankel's functions (Bessel's functions of the third kind) of order $\beta$ [13]. In the above equations, the $c_i$'s and $\bar{c}_i$'s are constant coefficients, $\delta$, $\bar{\delta}$, $\beta$, $\eta$, and $\tau$ are separation constants.

In the following subsections, these general solutions will be specialized for particular fluid domains. In all cases, the effect of surface waves are neglected.

2.4.1. Circular Cylindrical Tanks

The tank geometry and the coordinate system are illustrated in Fig. 2.21.

2.4.1.1. Vibrational Motion

Let the wall of the flexible tank vibrate according to:

$$u(\theta,z,t) = A \cos(n\theta) \cdot \varphi\left(\frac{z}{H}\right) \cdot \exp(i\omega t) \quad ; \quad n = 0,1,2,... \quad (2.70)$$

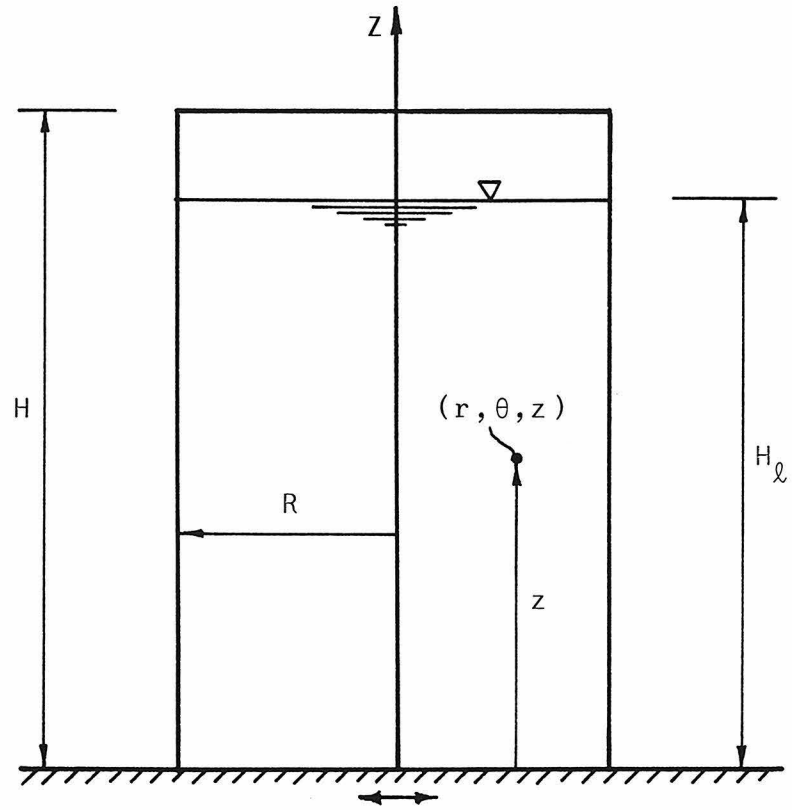


(a) Sectional Elevation

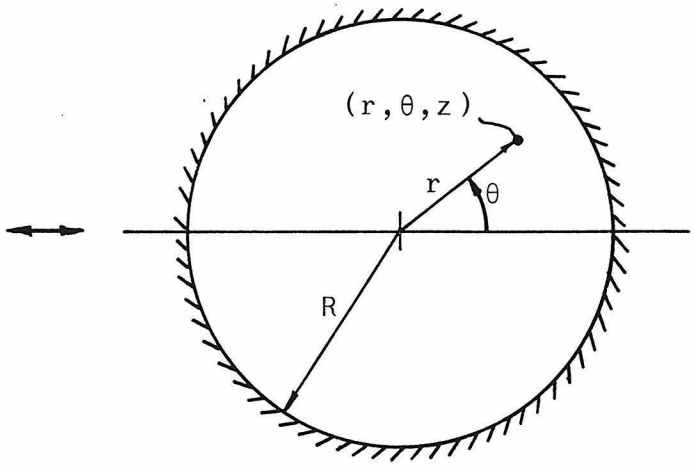


(b) Plan View

Fig. 2.21 Tank Geometry and Coordinate System

The solution is then given by:

$$p(r,\theta,z,t) = 2\,\rho_\ell H_\ell A\,\omega^2 \cos(n\theta)\cdot\exp(i\omega t)\cdot\left\{\sum_{m=1}^{m_0-1}\frac{I_{m0}}{\bar{\delta}_{m0}\,J'_n\left(\bar{\delta}_{m0}\,\frac{R}{H_\ell}\right)}J_n\left(\bar{\delta}_{m0}\,\frac{r}{H_\ell}\right)\cdot\cos\left(\eta_m\,\frac{z}{H_\ell}\right)\right.$$

$$\left.+\sum_{m=m_0}^{\infty}\frac{I_{m0}}{\delta_{m0}\,I'_n\left(\delta_{m0}\,\frac{R}{H_\ell}\right)}I_n\left(\delta_{m0}\,\frac{r}{H_\ell}\right)\cdot\cos\left(\eta_m\,\frac{z}{H_\ell}\right)\right\} \qquad (2.71)$$

where $m_0$, $\eta_m$, $\delta_{m0}$ and $I_{m0}$ are given by Eqs. 2.14 through 2.16.

2.4.1.2. Horizontal Ground Motion

Here, the wall of the rigid tank moves according to:

$$u(\theta,z,t) = u_g(t)\cos(\theta) = \bar{u}_g\cos(\theta)\exp(i\omega t) \qquad (2.72)$$

The solution is given by Eq. 2.71, with n = 1, $\varphi\left(\frac{z}{H}\right)\equiv 1$ and $A = \bar{u}_g$.

Other versions of the above solutions, as well as solutions for the case of incompressible fluid are given in [12,14-16].

2.4.2. Circular Cylindrical Intake Towers or Bridge Piers

The geometry and the coordinate system are as those illustrated in Fig. 2.21 except that the fluid is now at the outside of the cylinder.

2.4.2.1. Vibrational Motion

The deformational motion is given by Eq. 2.70, and the solution for the pressure is given by:

$$p(r,\theta,z,t) = 2\,\rho_\ell H_\ell A\,\omega^2 \cos(n\theta)\cdot \exp(i\omega t)$$

$$\cdot\left\{\sum_{m=1}^{m_0-1} \frac{I_{m0}}{\bar{\delta}_{m0}\left[H_n^{(2)}\left(\bar{\delta}_{m0}\frac{R}{H_\ell}\right)\right]'} H_n^{(2)}\left(\bar{\delta}_{m0}\frac{r}{H_\ell}\right)\cdot \cos\left(\eta_m \frac{z}{H_\ell}\right)\right.$$

$$\left. + \sum_{m=m_0}^{\infty} \frac{I_{m0}}{\delta_{m0}\left[K_n\left(\delta_{m0}\frac{R}{H_\ell}\right)\right]'} K_n\left(\delta_{m0}\frac{r}{H_\ell}\right)\cdot \cos\left(\eta_m \frac{z}{H_\ell}\right)\right\} \quad (2.73)$$

2.4.2.2. Horizontal Ground Motion

For a rigid structure, the motion is given by Eq. 2.72 and the solution is given by Eq. 2.73 with n = 1, $\varphi\left(\frac{z}{H}\right) \equiv 1$ and $A = \bar{u}_g$.

Other versions of the above solutions, as well as solutions for the cases of incompressible fluid are given in [12,15,17-19].

2.4.3. Simple Arch Dams

The geometry and the coordinate system are illustrated in Fig. 2.22.

2.4.3.1. Vibrational Motion

Let the radial motion of the upstream face of the dam be:

$$u(\theta,z,t) = A\cdot \varphi\left(\frac{\theta}{\theta_0}, \frac{z}{H}\right)\cdot \exp(i\omega t) \quad (2.74)$$

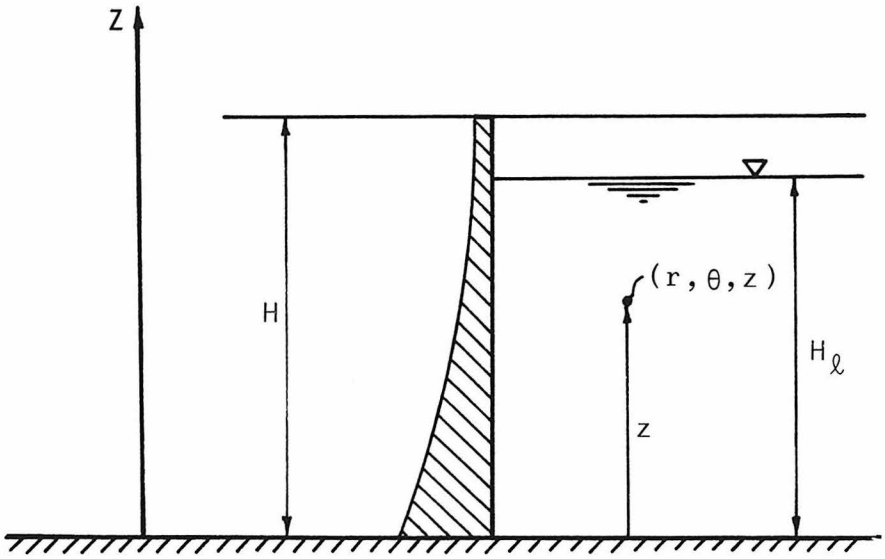


(a) Sectional Elevation

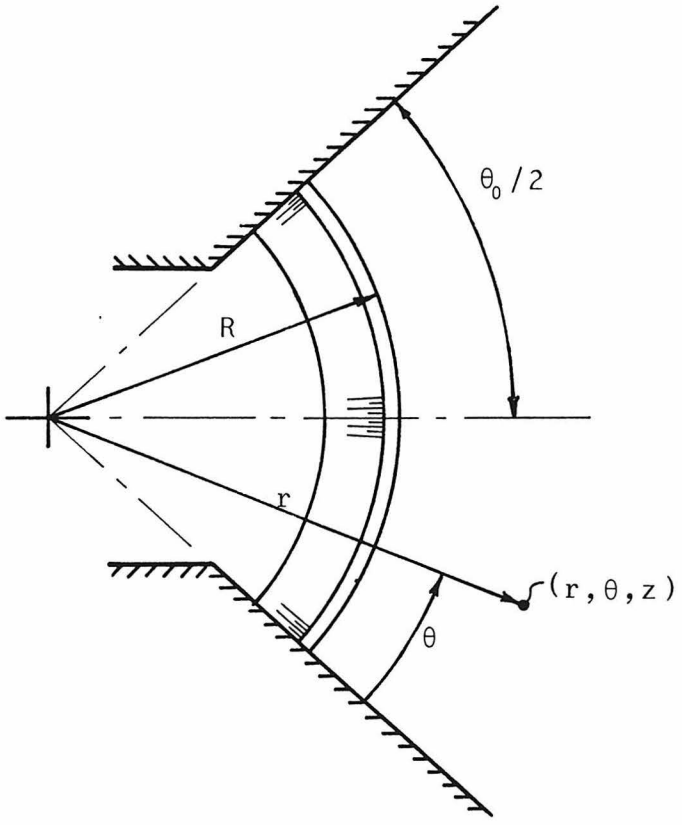


(b) Plan View

Fig. 2.22 Arch Dam Geometry and Coordinate System

The solution is obtained in the form:

$$p(r,\theta,z,t) = 4\,\rho_\ell H_\ell A\,\omega^2 \exp(i\omega t)$$

$$\cdot \left\{ \sum_{n=0}^{\infty} \sum_{m=1}^{m_n-1} \frac{I_{mn}}{\varepsilon_n \bar{\delta}_{m0}} \frac{H^{(2)}_{\beta_n}\left(\bar{\delta}_{m0}\frac{r}{H_\ell}\right)}{\left[H^{(2)}_{\beta_n}\left(\bar{\delta}_{m0}\frac{R}{H_\ell}\right)\right]'} \cos\left(\beta_n \frac{\theta}{\theta_0}\right) \cdot \cos\left(\eta_m \frac{z}{H_\ell}\right) \right.$$

$$\left. + \sum_{n=0}^{\infty} \sum_{m=m_n}^{\infty} \frac{I_{mn}}{\varepsilon_n \delta_{m0}} \frac{K_{\beta_n}\left(\delta_{m0}\frac{r}{H_\ell}\right)}{\left[K_{\beta_n}\left(\delta_{m0}\frac{R}{H_\ell}\right)\right]'} \cos\left(\beta_n \frac{\theta}{\theta_0}\right) \cos\left(\eta_m \frac{z}{H_\ell}\right) \right\} \tag{2.75}$$

where $m_n$, $\varepsilon_n$, $\beta_n$ and $\eta_m$ are as defined in Eqs. 2.45, $\bar{\delta}_{m0}$ and $\delta_{m0}$ are given by Eqs. 2.15, and $I_{mn}$ is given by Eq. 2.47 with y and B replaced by $\theta$ and $\theta_0$, respectively.

2.4.3.2. Longitudinal and Transverse Ground Motions

In these cases, exact solutions exist only when $\theta_0 = \frac{\pi}{2}$, and are given in [20,21].

Finally, for the case of vertical ground motion, the solution turns out to be the same for all three fluid domains. It is independent of the r and $\theta$ coordinates and is given by Eq. 2.30.

# CHAPTER III

# FLUID-STRUCTURE INTERACTION FOR LONG WALLS OR DAMS

## 3.1. Introduction

During an earthquake, a dam will move bodily into and away from the water in the reservoir and in addition the dam will vibrate. Both motions will generate hydrodynamic pressures in the water. Those pressures will act on the upstream face of the dam and in turn affect its deformation. Thus, an interaction between the dam and the reservoir exists. This should be included in the formulation of the problem of the dynamic response of the dam to earthquake ground motions.

In the analysis of dam-reservoir systems, investigators initially neglected the structural deformations of the dam and assumed it to be rigid [1,4-8]. This completely suppresses any interaction effects. The hydrodynamic pressure on the rigid dam was obtained and converted into an added mass of fluid which is then assumed to move with the dam [1,8]. The added mass concept was shown to be valid only when water compressibility is neglected [5,6].

The first attempt to account for the dam flexibility was made by H.A. Brahtz and C.H. Heilbron [2]. Using a linear deflected shape and an iterative procedure, they calculated the response of the coupled system. J.I. Bustamante et al. [4] prescribed a parabolic deformation shape and their solution showed clearly the effects of flexibility on the generated pressures. A.K. Chopra [9,22,23] used a parabolic shape fitted to the first mode of vibration of the dam with empty reservoir.

This approach was generalized by P. Chakrabarti and A.K. Chopra [24-26] to include additional mode shapes. W.D.L. Finn and E. Varoglu [27,28] provided an analytical solution to the problem when the dam has rectangular cross-section. For dams having general cross-sections, W.D.L. Finn and E. Varoglu [29] used a finite element formulation for the dam only and presented a solution based on their previous analytical approach.

In the analyses mentioned above [9,22-29], the water compressibility was included, leading to frequency dependent hydrodynamic pressure and dam response. The response to earthquake ground motion is obtained by using Fourier analysis techniques requiring the determination of the system transfer function. The latter is obtained by calculating the response of the dam to harmonic ground motion over a range of excitation frequencies. This requires some computational effort. Analyses [9,22-26,29] used two dimensional finite elements for the triangular cross-section dam, while [27,28] used a bending theory for the rectangular cross-section plate.

For reservoirs of relatively small depth, the water compressibility may be neglected, leading to frequency independent hydrodynamic pressure. In the following sections, the problem of long dams of walls retaining incompressible water are analysed. Two cases are considered: 1) rectangular section, and 2) triangular or trapezoidal section. The natural frequencies of vibration of the whole system, and the associated mode shapes are found by treating the dam analytically in the first case, and by finite elements in the second. In both cases, the water is

treated analytically by boundary solution techniques. The dam is modeled either by a shear or by a bending theory. When using finite element, a shear-bending theory is also used. In each of the two cases considered, a method is presented to compute the earthquake response of the dam, based on superposition of its free vibrational modes.

In all previous investigations [14-21], only the case of forced vibration was studied. Moreover, the analysis was done in the frequency domain, thus being relatively expensive with regard to computer time. The main advantage of the present method of analysis over previous approaches is that it is carried out in the time domain. This allows the study of the free vibration case, the direct outcomes of which are the natural frequencies and mode shapes. In addition, the modal analysis procedure can be used for the calculation of the structural response to earthquake ground motion. Also, for rectangular section walls, the analytical analysis is extended to the shear theory model, applicable to walls with relatively large thicknesses. The extension to a shear-bending model, although a bit complicated, is obtainable in a straightforward manner. Finally, the use of one dimensional beam elements, when the dam is modeled by finite elements, reduces considerably the number of degrees of freedom as compared to the two dimensional elements used in the previous investigations, thus resulting in substantial savings in computing effort.

## 3.2. Rectangular Cross-Section: Analytical Solution

Let the dam under consideration be assumed to have a rectangular cross-section as shown in Fig. 3.1. Since the dam is infinitely long, its deformation u(z,t) will be a function of the z-coordinate only and time. The assumptions made in Chapter II, regarding the reservoir boundaries and the water are also made here, so that the formulas obtained there for the hyrodynamic pressure will be used here directly.

### 3.2.1. Free Vibration

Consider first the case in which the dam is assumed to vibrate freely with no ground motion applied to its base, see Fig. 3.1. The analysis leads to the determination of the natural frequencies of the dam-reservoir system, as well as the corresponding mode shapes of vibration. In the following sections, the structural deformations of the dam are modeled by two different theories, namely: 1) pure shear theory, and 2) pure bending theory.

#### 3.2.1.1. Shear Theory

According to the assumptions underlying this theory, the dam deflection is purely due to shearing deformations, and any bending effects are completely neglected in the analysis.

Although vibrating freely with no ground motion applied to its base, the dam will be acted upon by the hydrodynamic pressure generated by its deflection. The equation of motion governing the dam vibration is given by:

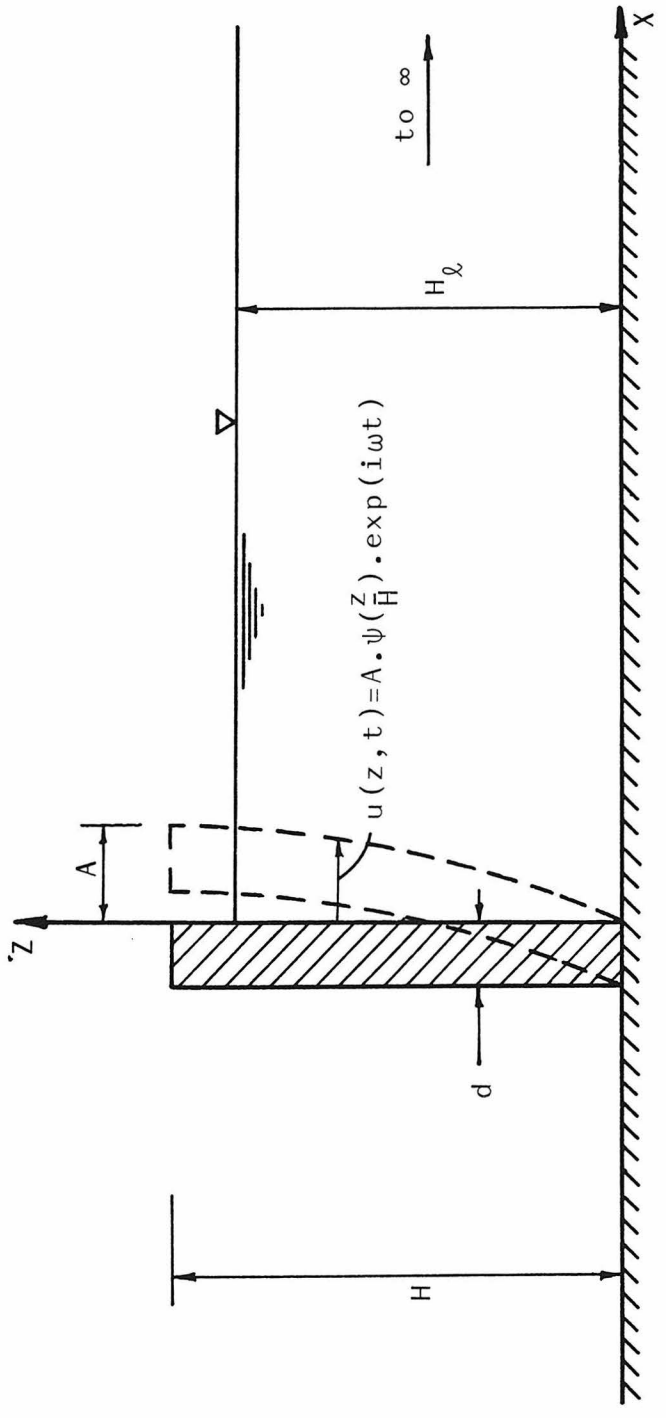


Fig. 3.1 Dam-Reservoir System , Free Vibration

$$\rho d \frac{\partial^2 u(z,t)}{\partial t^2} - G d \frac{\partial^2 u(z,t)}{\partial z^2} = -p(z,t) \quad ; \quad 0 \leq z \leq H_\ell \tag{3.1a}$$

$$= 0 \quad ; \quad H_\ell \leq z \leq H \tag{3.1b}$$

where $\rho$ is the mass density of the dam material, G its shear modulus, d is the dam constant thickness, and $p(z,t)$ is the hydrodynamic pressure acting on the upstream face of the dam. $p(z,t)$ is obtained from Eq. 2.19 by setting $x = 0$, and is given by:

$$p(z,t) = 2\rho_\ell \left\{ \sum_{m=1}^{\infty} \frac{1}{\eta_m} \cdot \left[ \int_0^{H_\ell} \ddot{u}(z,t) \cdot \cos\left(\eta_m \frac{z}{H_\ell}\right) \cdot dz \right] \cos\left(\eta_m \frac{z}{H_\ell}\right) \right\} \tag{3.2}$$

For free vibration, the dam displacement is expressed as:

$$u(z,t) = A \cdot \varphi\left(\frac{z}{H}\right) \cdot \exp(i\omega t) \tag{3.3}$$

where $\varphi\left(\frac{z}{H}\right)$ is some nondimensional function of z/H such that $\varphi(1) = 1$, A is the amplitude of motion of the dam crest, and $\omega$ is the frequency of vibration.

Substituting Eqs. 3.2 and 3.3 into Eq. 3.1 and rearranging, one obtains:

$$\varphi''(\xi) + \alpha^2\varphi(\xi) = -\frac{2\bar{H}}{\bar{\rho}\,\bar{d}} \cdot \alpha^2 \left\{ \sum_{m=1}^{\infty} \frac{\cos(\eta_m\bar{\xi})}{\eta_m} \left[ \int_0^1 \varphi(\xi) \cos(\eta_m\bar{\xi})\, d\bar{\xi} \right] \right\} \quad ; \quad 0 \le \xi \le \bar{H} \tag{3.4a}$$

$$= 0 \quad ; \quad \bar{H} \le \xi \le 1 \tag{3.4b}$$

where the (') denotes differentiation w.r.t. the argument, and

$$\xi = z/H\,, \quad \bar{\xi} = z/H_\ell\,, \quad \bar{H} = H_\ell/H\,, \quad \bar{\rho} = \rho/\rho_\ell\,, \quad \bar{d} = d/H$$

$$\alpha^2 = \left(\frac{\pi}{2}\right)^2 \cdot \frac{\bar{\rho}}{G/k} \cdot \bar{\omega}^2 \tag{3.5}$$

$$\bar{\omega} = \omega/(\omega_1^r)_f\,, \quad (\omega_1^r)_f = \frac{\pi c}{2H} \text{ and } c = \sqrt{k/\rho_\ell}$$

The solution of Eq. 3.4a is given by:

$$\varphi^I(\xi) = c_1 \cos(\alpha\xi) + c_2 \sin(\alpha\xi) + 2\sum_{m=1}^{\infty} (c_1 a_m + c_2 b_m) \frac{\lambda_m}{1-\lambda_m} \cos(\eta_m\bar{\xi}) \tag{3.6a}$$

where $c_1$ and $c_2$ are constants;

$$\left.\begin{aligned} a_m &= \int_0^1 \cos(\alpha\xi) \cos(\eta_m\bar{\xi})\, d\bar{\xi}; \\ b_m &= \int_0^1 \sin(\alpha\xi) \cos(\eta_m\bar{\xi})\, d\bar{\xi}; \end{aligned}\right\} \tag{3.7a}$$

and

$$\lambda_m = \frac{\alpha^2}{\bar{\rho}\,\bar{d}[(\eta_m/\bar{H})^2 - \alpha^2]\,(\eta_m/\bar{H})} \tag{3.7b}$$

Notice that the solution given in Eq. 3.5a is not valid when $\lambda_m = 1$ or when $(\eta_m/\bar{H}) = \alpha$. For those two limiting cases, we have the following forms:

$\underline{\lambda_i = 1}$:

$$\varphi^I(\xi) = c_1[\cos(\alpha\xi) - (a_i/b_i)\sin(\alpha\xi)] + c_2\cos(\eta_i\bar{\xi}) + 2\sum_{\substack{m=1\\ m\neq i}}^{\infty} c_1\,[a_m - (a_i/b_i)b_m]\,\frac{\lambda_m}{1-\lambda_m}\cos(\eta_m\bar{\xi}) \tag{3.6b}$$

$\underline{\eta_i/\bar{H}=\alpha}$:

$$\varphi^I(\xi) = c_1\cos(\alpha\xi) + c_2\sin(\alpha\xi) - \frac{4(c_1a_i+c_2b_i)}{1+4\bar{\rho}\,\bar{d}\,\alpha}(\alpha\xi)\sin(\alpha\xi) + 2\sum_{\substack{m=1\\ m\neq i}}^{\infty}(c_1a_m+c_2b_m)\,\frac{\lambda_m}{1-\lambda_m}\cos(\eta_m\bar{\xi}) \tag{3.6c}$$

Eq. 3.4b has solution:

$$\varphi^{II}(\xi) = \bar{c}_1\cos(\alpha\xi) + \bar{c}_2\sin(\alpha\xi) \tag{3.8}$$

Thus, for the general case of a reservoir partly filled with water to a height $H_\ell < H$, the displacement of the dam is given by:

$$\varphi(\xi) = \begin{cases} \varphi^{I}(\xi) & ; \quad 0 \leq \xi \leq \bar{H} \\ \varphi^{II}(\xi) & ; \quad \bar{H} \leq \xi \leq 1 \end{cases} \tag{3.9}$$

This solution has, in general, 4 unknown constants $c_1$, $c_2$, $\bar{c}_1$, and $\bar{c}_2$. Correspondingly, there are 4 conditions to satisfy:

i) the dam displacement vanishes at $z = 0$, i.e.,

$u(z,t)\big|_{z=0} = 0$ , $\rightarrow$

$$\varphi^{I}(0) = 0 \tag{3.10a}$$

ii) the shear force vanishes at $z = H$, i.e.,

$Gd \dfrac{\partial u(z,t)}{\partial z}\Big|_{z=H} = 0$ , $\rightarrow$

$$\left[\varphi^{II}(1)\right]' = 0 \tag{3.10b}$$

iii) the displacement at $z = H_\ell$ is the same when determined from either Eq. 3.6 or Eq. 3.8, $\rightarrow$

$$\varphi^{I}(\bar{H}) = \varphi^{II}(\bar{H}) \tag{3.10c}$$

iv) the shear force at $z = H_\ell$ is the same when calculated from both sides, $\rightarrow$

$$\left[\varphi^{I}(\bar{H})\right]' = \left[\varphi^{II}(\bar{H})\right]' \tag{3.10d}$$

Let us consider a particular case in which the reservoir is completely full of water to a height $H_\ell = H$. In this case, the vibration of the dam is governed by Eq. 3.4a whose solution is given by

Eq. 3.6. However, in these two equations $\bar{H}$ and $\bar{\xi}$ are replaced by 1 and $\xi$, respectively. Clearly, the solution given by Eq. 3.8, as well as the 3rd and 4th conditions are suppressed, and we are left with two constants $c_1$ and $c_2$ together with the 1st and 2nd boundary conditions, Eqs. 3.10a and 3.10b. By applying those two conditions, one ends up with two linear homogeneous algebraic equations for $c_1$ and $c_2$, of the form:

$$\left.\begin{aligned} A_{11}\, c_1 + A_{12}\, c_2 &= 0 \\ A_{21}\, c_1 + A_{22}\, c_2 &= 0 \end{aligned}\right\} \qquad (3.11)$$

where

$$\left.\begin{aligned} A_{11} &= 1 + 2 \sum_{m=1}^{\infty} a_m \cdot \frac{\lambda_m}{1-\lambda_m} \\ A_{12} &= 2 \sum_{m=1}^{\infty} b_m \cdot \frac{\lambda_m}{1-\lambda_m} \\ A_{21} &= -\alpha \cdot \sin(\alpha) - 2 \sum_{m=1}^{\infty} (-1)^{m+1} \cdot a_m \cdot \eta_m \cdot \frac{\lambda_m}{1-\lambda_m} \\ A_{22} &= \alpha \cdot \cos(\alpha) - 2 \sum_{m=1}^{\infty} (-1)^{m+1} \cdot b_m \cdot \eta_m \cdot \frac{\lambda_m}{1-\lambda_m} \end{aligned}\right\} \qquad (3.12)$$

The coefficients $A_{ij}$ are functions of the frequency of vibrations $\omega$. For nontrivial solution of the system of Eq. 3.11, the determinant of coefficients should vanish. This condition provides the frequency equation which is solved numerically for the natural frequencies of the

dam-reservoir. Once these are found, the associated mode shapes will be given by:

$$\varphi(\xi) = c_1 \left\{ \cos(\alpha\xi) + (c_2/c_1) \sin(\alpha\xi) + 2 \sum_{m=1}^{\infty} [a_m + (c_2/c_1) b_m] \frac{\lambda_m}{1-\lambda_m} \cos(\eta_m \xi) \right\} \tag{3.13}$$

where the ratio $(c_2/c_1)$ is determined from either of Eqs. 3.11.

Orthogonality

Consider two mode shapes $\varphi_i(\xi)$ and $\varphi_j(\xi)$, corresponding to two distinct natural frequencies $\omega_i$ and $\omega_j$, respectively. It could be shown that the following orthogonality relation holds:

$$\int_0^1 \varphi_i(\xi) \cdot \varphi_j(\xi) d\xi + \frac{2\bar{H}^2}{\bar{\rho}\,\bar{d}} \sum_{m=1}^{\infty} \frac{I_{m0}^i I_{m0}^j}{\eta_m} = 0 \quad ; i \neq j$$
$$= a_i \quad ; i = j \tag{3.14}$$

where

$$I_{m0}^i = \int_0^1 \varphi_i(\xi) \cos(\eta_m \bar{\xi}) d\bar{\xi} \tag{3.15}$$

and

$$a_i = \int_0^1 [\varphi_i(\xi)]^2 d\xi + \frac{2\bar{H}^2}{\bar{\rho}\,\bar{d}} \sum_{m=1}^{\infty} \frac{[I_{m0}^i]^2}{\eta_m} \tag{3.16}$$

3.2.1.2. Bending Theory

Here, the dam deflection is governed by the Bernoulli-Euler flexural deformations theory, in which shear distortions are neglected.

The transverse vibration of the dam is governed by the following differential equation:

$$\rho d \frac{\partial^2 u(z,t)}{\partial t^2} + \frac{Ed^3}{12(1-\nu)^2} \frac{\partial^4 u(z,t)}{\partial z^4} = -p(z,t) \quad ; \quad 0 \leq z \leq H_\ell \tag{3.17a}$$

$$= 0 \quad ; \quad H_\ell \leq z \leq H \tag{3.17b}$$

where $\rho$, d and $p(z,t)$ are as defined in the previous section, E is the Young's modulus of elasticity of the dam material and $\nu$ is its Poisson's ratio.

Using Eqs. 3.2 and 3.3 together with Eq. 3.17 and arranging:

$$\varphi''''(\xi) - \sigma^4 \varphi(\xi) = \frac{2\bar{H}}{\bar{\rho}\,\bar{d}} \sigma^4 \left\{ \sum_{m=1}^{\infty} \frac{\cos(\eta_m \bar{\xi})}{\eta_m} \left[ \int_0^1 \varphi(\xi) \cos(\eta_m \bar{\xi}) d\bar{\xi} \right] \right\} \quad ; \quad 0 \leq \xi \leq \bar{H} \tag{3.18a}$$

$$= 0 \quad ; \quad \bar{H} \leq \xi \leq 1 \tag{3.18b}$$

where $\xi$, $\bar{\xi}$, $\bar{H}$, $\bar{\rho}$ and $\bar{d}$ are as defined before and

$$\sigma^4 = 3\left(\frac{\pi}{\bar{d}}\right)^2 \cdot \frac{\bar{\rho}}{\bar{E}/k} \cdot \bar{\omega}^2 \quad ; \quad \bar{E} = \frac{E}{(1-\nu^2)}$$

Define:

$$\left.\begin{aligned} a_m &= \int_0^1 \cos(\sigma\xi) \cdot \cos(\eta_m\bar{\xi}) \cdot d\bar{\xi} \\ b_m &= \int_0^1 \sin(\sigma\xi) \cdot \cos(\eta_m\bar{\xi}) \cdot d\bar{\xi} \\ c_m &= \int_0^1 \cosh(\sigma\xi) \cdot \cos(\eta_m\bar{\xi}) \cdot d\bar{\xi} \\ d_m &= \int_0^1 \sinh(\sigma\xi) \cdot \cos(\eta_m\bar{\xi}) \cdot d\bar{\xi} \\ \lambda_m &= \frac{\sigma^4}{\bar{\rho}\,\bar{d}[(\eta_m/\bar{H})^4 - \sigma^4](\eta_m/\bar{H})} \end{aligned}\right\} \quad (3.19)$$

Now, depending on the value of $\omega$ ( and hence $\sigma$), the solution of Eq. 3.18a is given by one of the following forms:

a) $\underline{\lambda_m \neq 1 \text{ and } (\eta_m/\bar{H}) \neq \sigma \text{ for all m:}}$

$$\varphi^I(\xi) = c_1 \cos(\sigma\xi) + c_2 \sin(\sigma\xi) + c_3 \cosh(\sigma\xi) + c_4 \sinh(\sigma\xi) + 2 \sum_{m=1}^{\infty} (c_1 a_m + c_2 b_m + c_3 c_m + c_4 d_m) \cdot \frac{\lambda_m}{1-\lambda_m} \cdot \cos(\eta_m\bar{\xi}) \quad (3.20a)$$

b) $\underline{\lambda_i=1:}$

$$\varphi^I(\xi) = c_1\left[\cos(\sigma\xi) - \frac{a_i}{d_i} \cdot \sinh(\sigma\xi)\right]$$

$$+ c_2\left[\sin(\sigma\xi) - \frac{b_i}{d_i} \cdot \sinh(\sigma\xi)\right]$$

$$+ c_3\left[\cosh(\sigma\xi) - \frac{c_i}{d_i} \cdot \sinh(\sigma\xi)\right]$$

$$+ c_4 \cos(\eta_i\bar{\xi})$$

$$+ 2 \sum_{\substack{m=1 \\ m\neq i}}^{\infty} \left[c_1\left(a_m - \frac{a_i}{d_i} d_m\right) + c_2\left(b_m - \frac{b_i}{d_i} d_m\right)\right.$$

$$\left. + c_3\left(c_m - \frac{c_i}{d_i} d_m\right)\right] \cdot \frac{\lambda_m}{1-\lambda_m} \cdot \cos(\eta_m\bar{\xi})$$

(3.20b)

c) $\underline{\eta_i/\bar{H} = \sigma:}$

$$\varphi^{I}(\xi) = c_1 \cos(\sigma\xi) + c_2 \sin(\sigma\xi) + c_3 \cosh(\sigma\xi) + c_4 \sinh(\sigma\xi)$$

$$+ 2 \sum_{\substack{m=1 \\ m\neq i}}^{\infty} (c_1 a_m + c_2 b_m + c_3 c_m + c_4 d_m) \cdot \frac{\lambda_m}{1-\lambda_m} \cdot \cos(\eta_m \bar{\xi})$$

$$- 4\sigma \cdot \frac{(c_1 a_i + c_2 b_i + c_3 c_i + c_4 d_i)}{1 + 8\bar{\rho}\,\bar{d}\,\sigma} \cdot \xi \cdot \sin(\sigma\xi) \qquad (3.20c)$$

where $c_1$, $c_2$, $c_3$ and $c_4$ are constants.

Eq. 3.18b has the following solution:

$$\varphi^{II}(\xi) = \bar{c}_1 \cos(\sigma\xi) + \bar{c}_2 \sin(\sigma\xi) + \bar{c}_3 \cosh(\sigma\xi) + \bar{c}_4 \sinh(\sigma\xi) \qquad (3.21)$$

where $\bar{c}_1$, $\bar{c}_2$, $\bar{c}_3$ and $\bar{c}_4$ are also constant coefficients.

Thus, in general, the displacement of the dam will be given by Eq. 3.9 which contains, in this case, 8 unknown constants. However eight conditions must now be satisfied:

- the displacement and slope vanish at z = o.
- the bending moment and shear force vanish at z = H
- the displacement, slope, moment and shear at z = $H_\ell$ matches when either calculate from below or above the water surface.

Again, if the case of a full reservoir is considered, only the solution given by Eq. 3.20 will be present. The eight constants are reduced to only four and the boundary conditions left may be stated as follows:

$$\left.\begin{aligned} &\text{i)} \quad \varphi(0) = 0 \\ &\text{ii)} \quad \varphi'(0) = 0 \\ &\text{iii)} \quad \varphi''(1) = 0 \\ &\text{iv)} \quad \varphi'''(1) = 0 \end{aligned}\right\} \tag{3.22}$$

These conditions lead to a system of four linear homogeneous algebraic equations for $c_1$, $c_2$, $c_3$ and $c_4$, which can be put in a matrix form as shown in Fig. 3.2. For nontrivial solution, the determinant of the coefficients matrix is set equal to zero, which gives the frequency equation for the dam-reservoir system. The natural frequencies and the corresponding mode shapes are determined as outlined in the previous section. These mode shapes satisfy the general orthogonality relation given by Eq. 3.14.

3.2.1.3. Numerical Examples

In the following examples, the free lateral vibrations of dam-reservoir systems are analyzed using the method of analysis discussed earlier. The effects of the water in the reservoir on the natural frequencies and mode shapes of the dam are explored.

Example 1. Shear Theory

The method of analysis discussed in section 3.2.1.1 is applied to determine the natural frequencies of vibration and the associated mode shapes of a dam-reservoir system, for two cases: 1) empty reservoir, and 2) totally full reservoir. The dam is assumed to be made of concrete whose properties are: $E = 5 \times 10^6$ p.s.i., $\nu=0.17$, $G=\frac{E}{2(1+\nu)} = 2.14 \times 10^6$

$$\begin{bmatrix} \left(1 + 2\sum_{m=1}^{\infty} a_m \cdot \frac{\lambda_m}{1-\lambda_m}\right) & \left(2\sum_{m=1}^{\infty} b_m \cdot \frac{\lambda_m}{1-\lambda_m}\right) & \left(1 + 2\sum_{m=1}^{\infty} c_m \cdot \frac{\lambda_m}{1-\lambda_m}\right) & \left(2\sum_{m=1}^{\infty} d_m \cdot \frac{\lambda_m}{1-\lambda_m}\right) \\ 0 & 1 & 0 & 1 \\ -\cos(\sigma) & -\sin(\sigma) & \cosh(\sigma) & \sinh(\sigma) \\ \left(\sigma^3 \sin(\sigma) + 2\sum_{m=1}^{\infty} a_m\bar{\lambda}_m\right) & \left(-\sigma^3 \cos(\sigma) + 2\sum_{m=1}^{\infty} b_m\bar{\lambda}_m\right) & \left(\sigma^3 \sinh(\sigma) + 2\sum_{m=1}^{\infty} c_m\bar{\lambda}_m\right) & \left(\sigma^3 \cosh(\sigma) + 2\sum_{m=1}^{\infty} d_m\bar{\lambda}_m\right) \end{bmatrix} \cdot \begin{Bmatrix} C_1 \\ C_2 \\ C_3 \\ C_3 \end{Bmatrix} = \begin{Bmatrix} 0 \\ 0 \\ 0 \\ 0 \end{Bmatrix}$$

$$\bar{\lambda}_m = \frac{(-1)^{m+1} \cdot \lambda_m \cdot \eta_m^3}{1 - \lambda_m}$$

Fig. 3.2 Matrix Form of the System of Equations

p.s.i. and $\gamma = \rho g = 155$ p.c.f. The properties of the water are: $k = 3 \times 10^5$ p.s.i. and $\gamma_\ell = \rho_\ell g = 62.4$ p.c.f.

The dam has a rectangular section, with thickness to height ratio, $\bar{d}$, of 0.4. Since the frequencies obtained are normalized by the fundamental frequency of the full reservoir, their values are independent of the actual height of the dam.

The computed natural frequencies, for both the empty and the full reservoir cases, are presented in table 3.1. It is clear that the frequencies are reduced in value due to the presence of the water. The corresponding mode shapes, which are clearly affected by the water, are displayed in Fig. 3.3.

| Frequency | 1st | 2nd | 3rd |
|---|---|---|---|
| Empty Reservoir | 1.69 | 5.13 | 8.69 |
| Full Reservoir | 1.45 | 4.46 | 8.09 |

TABLE 3.1. Normalized Natural Frequencies

Example 2. Bending Theory

The dam considered in this example has the same proportions and properties of concrete as that of the previous example, but the analysis of section 3.2.1.2 is used instead.

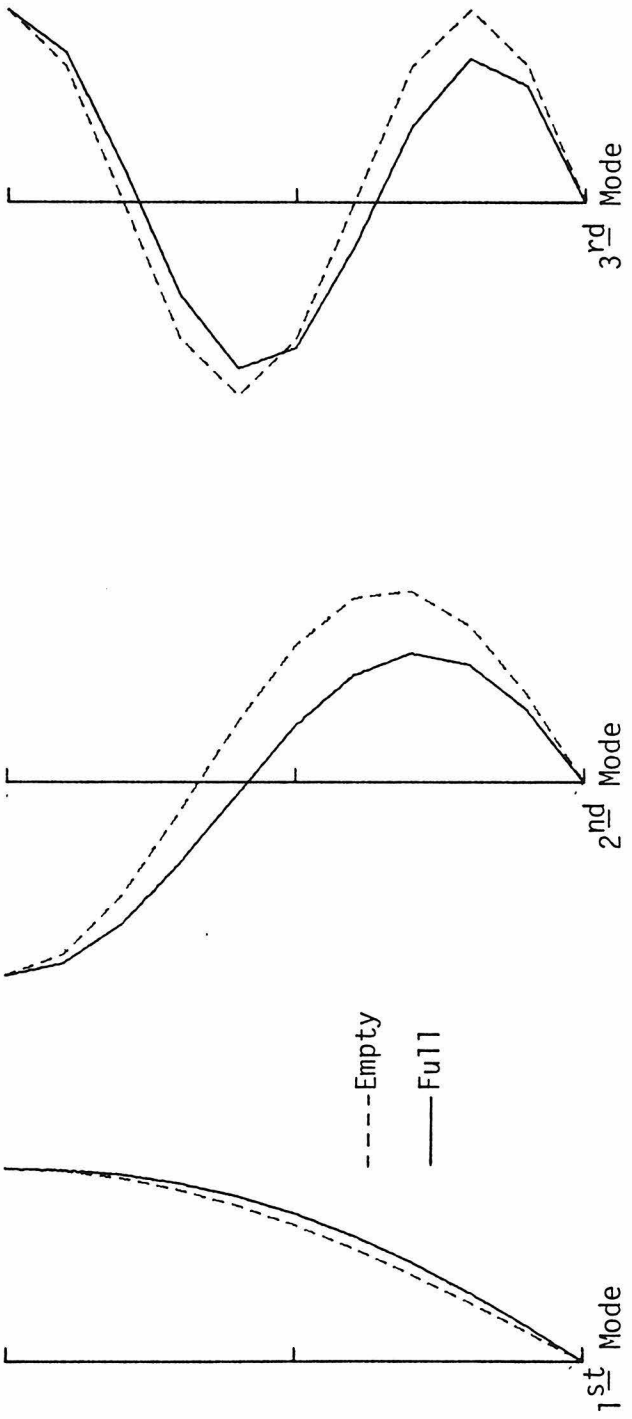


Fig. 3.3 Mode Shapes of Vibration, Shear Theory

The normalized natural frequencies of the dam, with empty or full reservoir, are presented in table 3.2, while the corresponding mode shapes are shown in Fig. 3.4.

| Frequency | 1st | 2nd | 3rd |
|---|---|---|---|
| Empty Reservoir | 0.68 | 4.26 | 11.92 |
| Full Reservoir | 0.61 | 3.73 | 11.00 |

TABLE 3.2. Normalized Natural Frequencies

3.2.2. Forced Vibration: Harmonic Ground Motion

Let us now consider the case in which the dam is forced into motion by a ground displacement applied to its base. The dam will move, as a rigid body, with the same specified ground motion, and in addition will vibrate, as shown in Fig. 3.5. For a harmonic ground motion, the analysis leads to the dam response in the frequency domain. This clearly shows the dam-reservoir interaction effects on the hydrodynamic pressures generated, and on the dam response. Again, two different theories modeling the structural deformations of the dam are considered.

3.2.2.1. Shear Theory

In addition to the inertia forces resulting from its motion, the dam will be acted upon by the hydrodynamic pressures generated by both

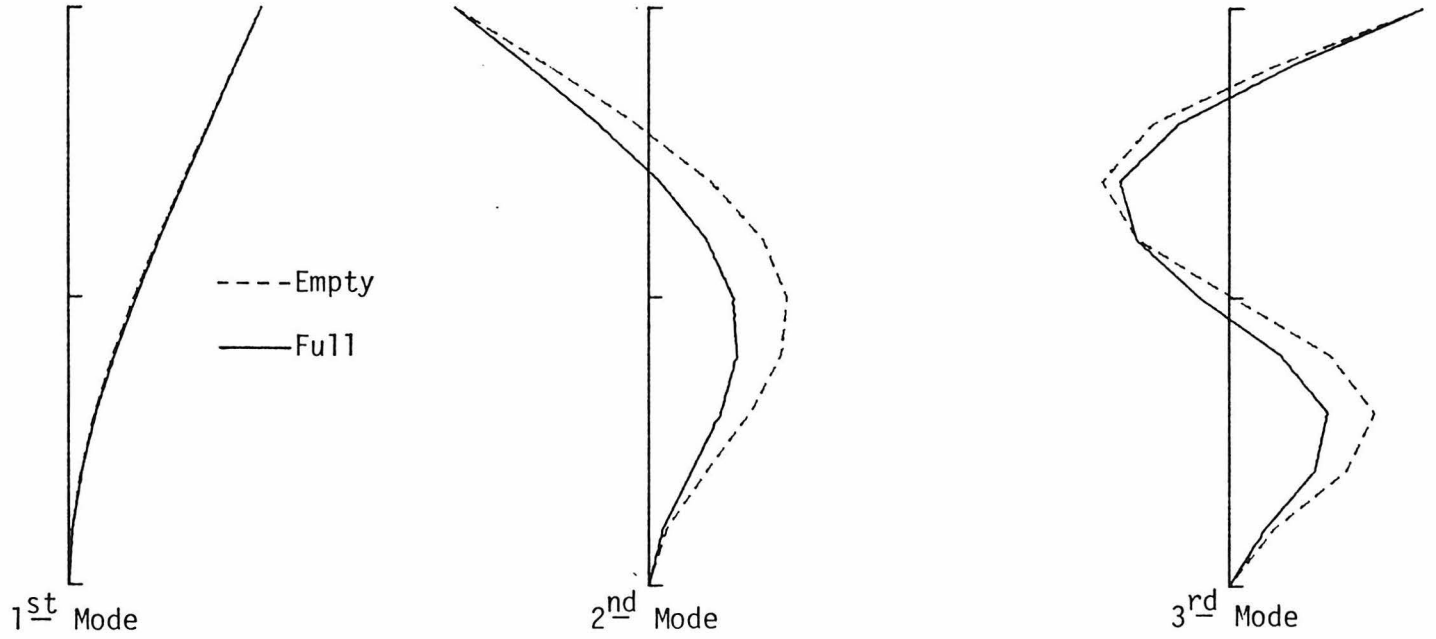


Fig. 3.4 Mode Shapes of Vibration, Bending Theory

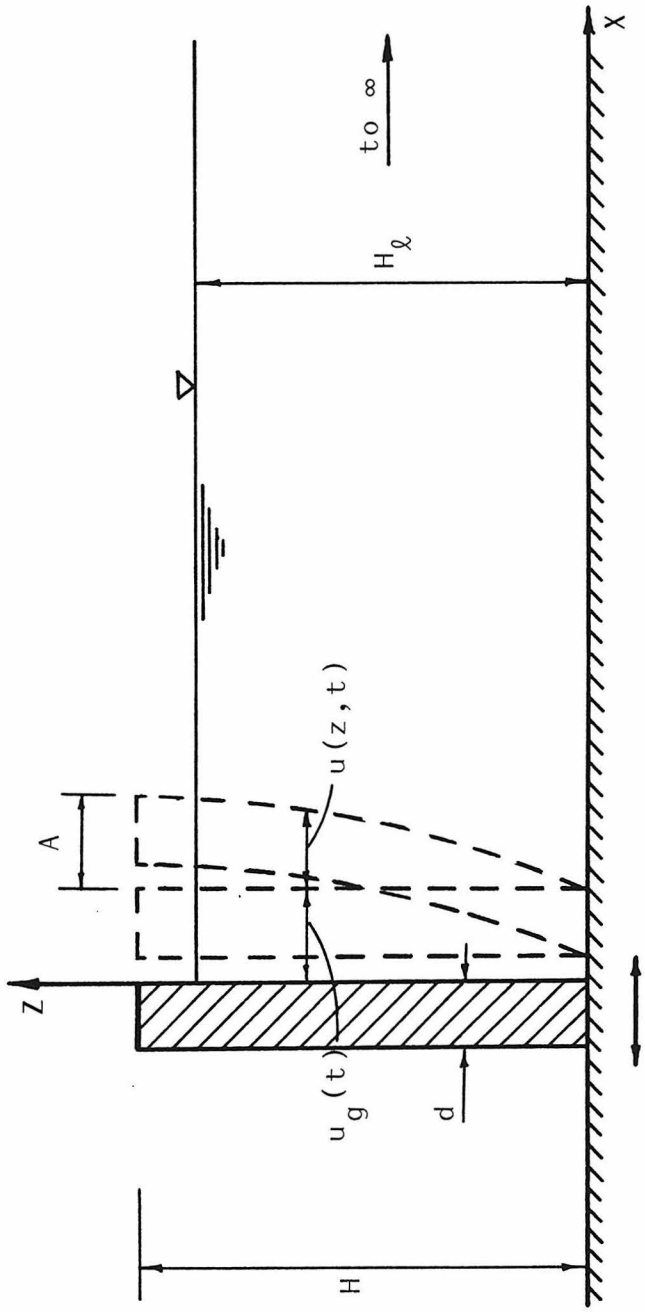


Fig. 3.5 Dam-Reservoir System , Forced Vibration

its rigid plus its deformational motions. The differential equation governing the dam vibration is written as:

$$\rho d \frac{\partial^2 u(z,t)}{\partial t^2} - Gd \frac{\partial^2 u(z,t)}{\partial z^2} = -\rho d \ddot{u}_g(t) - p_g(z,t) - p(z,t) \quad ; \quad 0 \leq z \leq H_\ell \tag{3.23a}$$

$$= -\rho d \ddot{u}_g(t) \quad ; \quad H_\ell \leq z \leq H \tag{3.23b}$$

where $\rho$, G and d are as defined before, $\ddot{u}_g(t)$ is the applied ground acceleration, and $p_g(z,t)$ is the hydrodynamic pressure acting on the upstream face of the dam, and resulting from the rigid motion. This is obtained from Eq. 2.25 by putting x = 0, and is given by:

$$p_g(z,t) = 2\rho_\ell H_\ell \ddot{u}_g(t) \left\{ \sum_{m=1}^{\infty} \frac{(-1)^{m+1}}{\eta_m^2} \cdot \cos\left(\eta_m \frac{z}{H_\ell}\right) \right\} \tag{3.24}$$

p(z,t) is the pressure resulting from the dam deflection and is given by Eq. 3.2.

Let the ground acceleration be harmonic in time, thus having the form:

$$\ddot{u}_g(t) = a_g \cdot \exp(i\omega t) \tag{3.25}$$

where $a_g$ is the amplitude of the acceleration and $\omega$ is the frequency of oscillation.

Since the system is linear and time invariant and the excitation is steady-state simple harmonic motion, the response is also steady-state simple harmonic motion of the same frequency. Thus, the dam deflection response may be expressed as:

$$u(z,t) = A \cdot U(\frac{z}{H}) \cdot \exp(i\omega t) \tag{3.26}$$

where A is the amplitude of crest motion, and $U(\frac{z}{H})$ is the nondimensional deflection shape of the dam.

Substituting from Eqs. 3.2, 3.24, 3.25 and 3.26 into eq. 3.23, and rearranging, yields:

$$U''(\xi) + \alpha^2 U(\xi) = -\frac{2\bar{H}}{\bar{\rho}\,\bar{d}}\alpha^2 \left\{ \sum_{m=1}^{\infty} \frac{\cos(\eta_m \bar{\xi})}{\eta_m} \cdot \left[ \int_0^1 U(\xi) \cdot \cos(\eta_m \bar{\xi}) \cdot d\bar{\xi} \right] \right\}$$

$$+ \frac{\alpha^2}{\bar{A}} \left[ 1 + \frac{2\bar{H}}{\bar{\rho}\,\bar{d}} \sum_{m=1}^{\infty} \frac{(-1)^{m+1}}{\eta_m^2} \cos(\eta_m \bar{\xi}) \right] \quad ; \; 0 \leq \xi \leq \bar{H} \tag{3.27a}$$

$$= \frac{\alpha^2}{\bar{A}} \quad ; \; \bar{H} \leq \xi \leq 1 \tag{3.27b}$$

where $\xi$, $\bar{\xi}$, $\bar{H}$, $\bar{\rho}$, $\bar{d}$, and $\alpha$ are as defined previously, and $\bar{A}$ is the amplitude of crest acceleration normalized by the amplitude of ground acceleration, i.e.:

$$\bar{A} = (A\,\omega^2)/a_g \tag{3.28}$$

Eq. 3.27a has one of the following solutions:

a) $\lambda_m \neq 1$ and $(\eta_m/\bar{H}) \neq \alpha$ for all m:

$$U^I(\xi) = c_1 \cos(\alpha\xi) + c_2 \sin(\alpha\xi) + 1/\bar{A} + 2 \sum_{m=1}^{\infty} (c_1 a_m + c_2 b_m) \frac{\lambda_m}{1-\lambda_m} \cos(\eta_m \bar{\xi}) \tag{3.29a}$$

b) $\lambda_i = 1$:

$$U^I(\xi) = c_1 \left[ \cos(\alpha\xi) - \frac{a_i}{b_i} \cdot \sin(\alpha\xi) \right] + c_2 \cos(\eta_i \bar{\xi}) + 1/\bar{A} + 2 \sum_{\substack{m=1 \\ m\neq i}}^{\infty} c_1 \left( a_m - \frac{a_i}{b_i} b_m \right) \cdot \frac{\lambda_m}{1-\lambda_m} \cdot \cos(\eta_m \bar{\xi}) \tag{3.29b}$$

c) $\eta_i / \bar{H} = \alpha$:

$$U^I(\xi) = c_1 \cos(\alpha\xi) + c_2 \sin(\alpha\xi) + \frac{1}{\bar{A}} - \frac{4(c_1 a_i + c_2 b_i)}{1 + 4\bar{\rho}\,\bar{d}\alpha} (\alpha\xi) \sin(\alpha\xi) + 2 \sum_{\substack{m=1 \\ m\neq i}}^{\infty} (c_1 a_m + c_2 b_m) \frac{\lambda_m}{1-\lambda_m} \cos(\eta_m \bar{\xi}) \tag{3.29c}$$

where $c_1$, $c_2$ are constants, $a_m$, $b_m$ and $\lambda_m$ are as defined by Eq. 3.7.

Eq. 3.27b has the solution:

$$U^{II}(\xi) = \bar{c}_1 \cos(\alpha\xi) + \bar{c}_2 \sin(\alpha\xi) + \frac{1}{\bar{A}} \tag{3.30}$$

Now, the deflection of the dam is given by:

$$\left.\begin{aligned} U(\xi) &= U^{I}(\xi) \qquad ; \quad 0 \leq \xi \leq \bar{H} \\ &= U^{II}(\xi) \qquad ; \quad \bar{H} \leq \xi \leq 1 \end{aligned}\right\} \tag{3.31}$$

Unlike the case of free vibration, the parameter $\alpha$ is known, since the excitation frequency $\omega$ is prescribed. Thus, the four conditions given in Eq. 3.10 will completely determine the four unknown constants $c_1$, $c_2$, $\bar{c}_1$ and $\bar{c}_2$.

For a completely full reservoir, the solution given by Eq. 3.29 will be valid over $0 \leq \xi \leq 1$, and we are left with only two constants, $c_1$ and $c_2$, to be determined by applying the two conditions, Eqs. 3.10a and 3.10b. Thus, we end up with two linear inhomogeneous algebraic equations of the form:

$$\left.\begin{aligned} A_{11}\, c_1 + A_{12}\, c_2 &= 1/\bar{A} \\ A_{21}\, c_1 + A_{22}\, c_2 &= 0 \end{aligned}\right\} \tag{3.32}$$

where $A_{11}$, $A_{12}$, $A_{21}$ and $A_{22}$ are given by Eqs. 3.12. Once $c_1$ and $c_2$ are determined, by solving the system of Eqs. 3.32, the displacement response of the dam is obtained by substituting these values in the proper equation of Eqs. 3.29.

3.2.2.2. Bending Theory

When the dam deformations are modeled by the bending theory, the differential equation for the forced vibration of the dam is written as:

$$\rho d \frac{\partial^2 u(z,t)}{\partial t^2} + \frac{\bar{E}d^3}{12} \frac{\partial^4 u(z,t)}{\partial z^4} = -\rho d \ddot{u}_g(t) - p_g(z,t) - p(z,t) \quad ; \ 0 \leq z \leq H_\ell \tag{3.33a}$$

$$= -\rho d \ddot{u}_g(t) \quad ; \ H_\ell \leq z \leq H \tag{3.33b}$$

For harmonic ground motion, the above equations become:

$$U''''(\xi) - \sigma^4 U(\xi) = \frac{2\bar{H}}{\bar{\rho}\,\bar{d}} \sigma^4 \left\{ \sum_{m=1}^{\infty} \frac{\cos(\eta_m \bar{\xi})}{\eta_m} \left[ \int_0^1 U(\xi) \cos(\eta_m \bar{\xi}) d\bar{\xi} \right] \right\}$$

$$- \frac{\sigma^4}{\bar{A}} \left[ 1 + \frac{2\bar{H}}{\bar{\rho}\,\bar{d}} \sum_{m=1}^{\infty} \frac{(-1)^{m+1}}{\eta_m^2} \cos(\eta_m \bar{\xi}) \right] \quad ; \ 0 \leq \xi \leq \bar{H} \tag{3.34a}$$

$$= - \frac{\sigma^4}{\bar{A}} \quad ; \ \bar{H} \leq \xi \leq 1 \tag{3.34b}$$

where $U(\xi)$ is as defined in Eq. 3.26.

The solutions for these equations is given by:

$$\left.\begin{aligned} U(\xi) = U^I(\xi) &= \varphi^I(\xi) + 1/\bar{A} \quad ; \ 0 \leq \xi \leq \bar{H} \\ &= U^{II}(\xi) = \varphi^{II}(\xi) + 1/\bar{A} \quad ; \bar{H} \leq \xi \leq 1 \end{aligned}\right\} \tag{3.35}$$

Where $\varphi^I(\xi)$ and $\varphi^{II}(\xi)$ are the solutions of the free vibration problem obtained previously, and are given by Eqs. 3.20 and 3.21, respectively.

Finally for the case of a full reservoir, the remaining four constants $c_1$, $c_2$, $c_3$ and $c_4$ are determined using the approach outlined in the previous section, leading to the complete solution of the dam displacement response.

3.2.2.3. Numerical Examples

In this section, the dynamic response of dam-reservoir systems to harmonic ground excitations is analysed using the approach developed in the previous two sections. The effects of the presence of water on the frequency domain response of the dam, on the hydrodynamic pressure distribution, and on the total force acting on the dam are explored.

Consider a concrete dam having dimensions and materials properties the same as those given in section 3.2.1.3. The dynamic response of the dam, to harmonic ground motion, is evaluated for two cases: 1) empty reservoir, and 2) totally full reservoir. The crest acceleration, normalized by the ground acceleration, is computed for excitation frequencies in the range 0 to 6 times the fundamental full-reservoir frequency. The amplitude of this normalized acceleration is given by:

$$\frac{|A \cdot U^I(1)| \cdot \omega^2}{a_g} = \bar{A} \cdot |U^I(1)| \qquad (3.36)$$

where $\bar{A}$ is given by Eq. 3.28, and $U^I(1)$ is found from either Eqs. 3.31 or Eqs. 3.35.

The calculated response for both the shear and bending theories is presented in Fig. 3.6. The effect of the reservoir is shown to shift the peaks of the response curve to the left as expected.

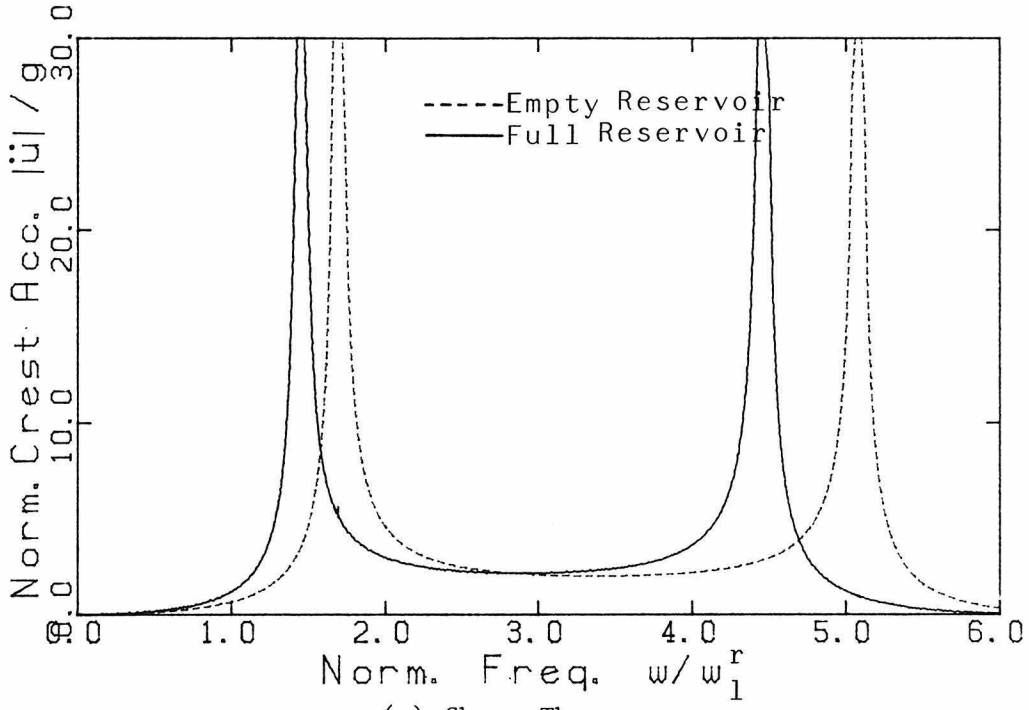


(a) Shear Theory

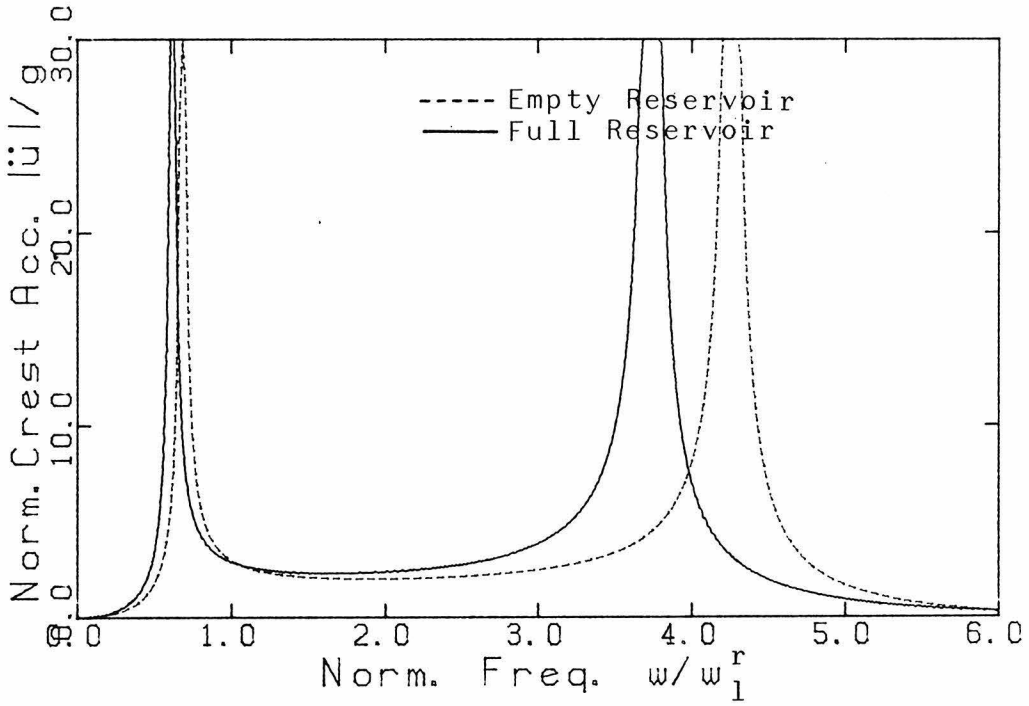


(b) Bending Theory

Fig. 3.6 Crest Acceleration Response

When normalized with the maximum hydrostatic pressure, the hydrodynamic pressure acting on the upstream face of the dam and resulting from the combined rigid and vibrational motions, will be of the form:

$$\bar{p}(z,t) = 2 \frac{a_g}{g} \left\{ \sum_{m=1}^{\infty} \left[ \frac{(-1)^{m+1}}{\eta_m^2} - \frac{\bar{A} I_m}{\eta_m} \right] \cos \left( \eta_m \frac{z}{H_\ell} \right) \right\} \exp (i\omega t) \tag{3.37}$$

where

$$I_m = \int_0^1 U^I(\xi) \cos (\eta_m \xi) d\xi \tag{3.38}$$

Eq. 3.37 is used to calculate the pressure distribution along the dam height, for ground motion of amplitude $a_g = 1g$, and normalized excitation frequencies $\bar{\omega} = 0.7$ and 1.5. The results are displayed in Fig. 3.7 for both the shear and bending theories. For comparison, the pressure due to a rigid motion alone is also presented. It is clear that the pressure distribution changes completely when the dam flexibility is included in the analysis.

Finally, by integrating the pressure over the dam height, one obtains the total hydrodynamic force which acts on a unit length of the dam. This force, when normalized by the total hydrostatic force, is given by:

$$\bar{P}(t) = 4 \frac{a_g}{g} \left\{ \sum_{m=1}^{\infty} \left[ \frac{1}{\eta_m^3} - \frac{(-1)^{m+1} \bar{A} \cdot I_m}{\eta_m^2} \right] \right\} \exp (i\omega t) \tag{3.39}$$

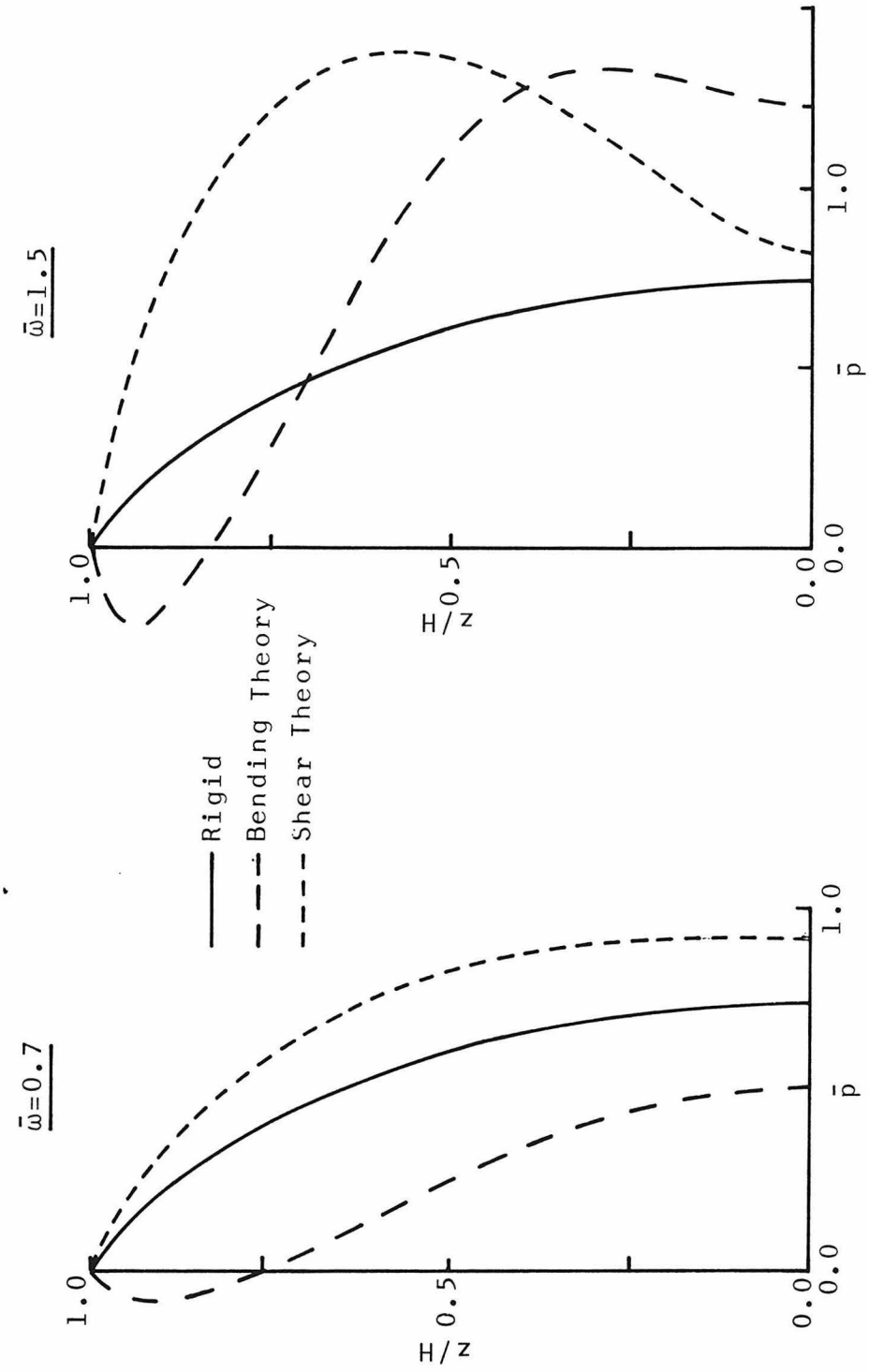


Fig. 3.7 Hydrodynamic Pressure Distribution

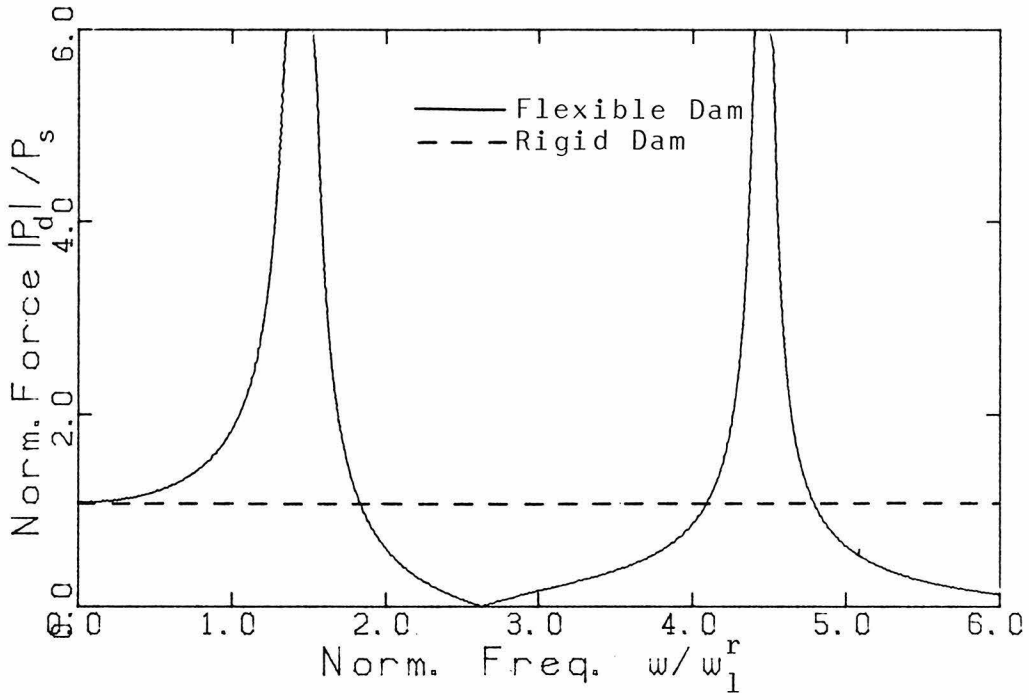


(a) Shear Theory

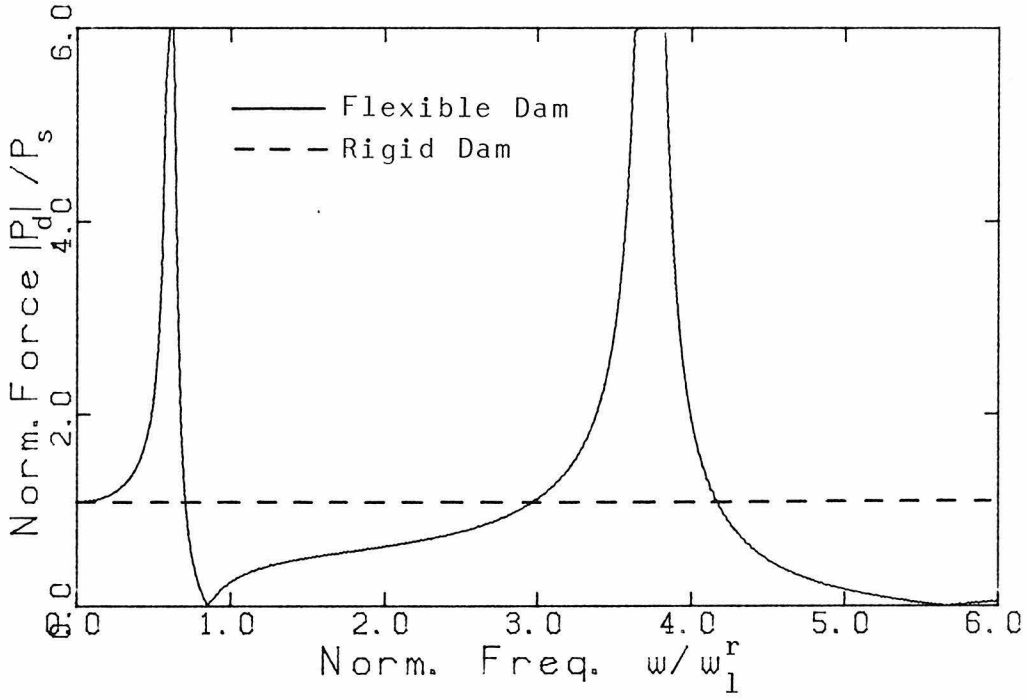


(b) Bending Theory

Fig. 3.8 Hydrodynamic Force Response

The amplitude of this normalized total force is plotted in Fig. 3.8. This can be compared with the force on a rigid dam given by the dotted line.

3.2.3. Response to Earthquake Ground Motion

The earthquake response of a dam is obtained by solving its equation of motion, Eq. 3.23 for a dam modeled by the shear theory or Eq. 3.33 when the bending theory is used. In the analysis given below, only dams modeled by the shear theory and retaining completely full reservoirs are discussed. The analysis, when the bending theory is used, is quite similar in nature. Also, the generalization for the case of partly filled reservoir is straightforward.

Two different analysis procedures are available; these are commonly known as the time domain analysis and the frequency domain analysis.

3.2.3.1. Time Domain Analysis

The mode superposition method [30,31] is used. This method, applicable only if the response is within the linear range, is generally efficient to use with earthquake type excitations because the response is essentially given by the first few modes of vibration, the contributions of the higher modes to the total response being small.

The first step in the mode superposition analysis procedure is to obtain the natural frequencies ($\omega_i$) of the dam-reservoir system and the associated mode shapes ($\varphi_i$). This is done as discussed in section 3.2.1.1.

Next, the dam deformation is expressed as a linear combination of the first N modes, as follows:

$$u(z,t) = \sum_{i=1}^{N} \varphi_i(\frac{z}{H}) \cdot u_i(t) \tag{3.40}$$

where $u_i(t)$ are the generalized modal coordinates.

Substituting into the equation of motion and using the orthogonality condition eventually yields:

$$\ddot{u}_j(t) + \omega_j^2 u_j(t) = -\frac{f_j}{a_j} \cdot \ddot{u}_g(t) \quad ; \quad j = 1,2,\ldots,N \tag{3.41}$$

where

$$f_j = \int_0^1 \varphi_j(\xi) \cdot d\xi + \frac{2}{\bar{\rho}\,\bar{d}} \sum_{m=1}^{\infty} \frac{(-1)^{m+1} I_{m0}^j}{\eta_m^2} \tag{3.42}$$

and $a_j$ is as given by Eq. 3.16.

Therefore, Eq. 3.23 reduces to N independent differential equations, Eq. 3.41. Introducing damping into these equations, they may be rewritten as:

$$\ddot{u}_j(t) + 2\zeta_j\omega_j \dot{u}_j(t) + \omega_j^2 u_j(t) = -b_j \ddot{u}_g(t) \quad ; \quad j=1,2,\ldots,N \tag{3.43}$$

where $\zeta_j$ are the modal dampings and $b_j = f_j/a_j$ are the modal participation factors.

The generalized coordinates $u_j(t)$ can be found by employing either the convolution integral or a step-by-step integration scheme. A brief description of each method is given below.

1) Convolution Integral:

In this method, one first finds the response to an impulse $\ddot{u}_g(t) = \delta(t)$, where $\delta(t)$ is the Dirac delta function. This response is readily obtained [32], Eq. 3.43 being the equation of motion of a single degree of freedom system, and has the form:

$$U_j(t) = -\frac{b_j}{\omega_j\sqrt{1-\zeta_j^2}} \cdot \exp(-\zeta_j\omega_j t) \cdot \sin\left(\omega_j\sqrt{1-\zeta_j^2}\, t\right) \tag{3.44}$$

The response to arbitrary ground motion $\ddot{u}_g(t)$ can now be obtained through the convolution integral:

$$u_j(t) = \int_0^t U_j(t-\tau) \cdot \ddot{u}_g(\tau) \cdot d\tau \tag{3.45}$$

2) Step by Step Integration:

The integration scheme used in [33] is discussed hereafter. For $\ddot{u}_g(t)$ given by a segmentally linear function, for $t^{(i)} \leq t \leq t^{(i+1)}$, Eq. 3.43 becomes:

$$\ddot{u}_j + 2\zeta_j\omega_j\dot{u}_j + \omega_j^2 u_j = -b_j\left[\ddot{u}_g^{(i)} + \frac{\Delta\ddot{u}_g}{\Delta t}(t-t^{(i)})\right] \tag{3.46}$$

where $\Delta\ddot{u}_g = \ddot{u}_g^{(i+1)} - \ddot{u}_g^{(i)}$, and $\Delta t = t^{(i+1)} - t^{(i)} =$ constant.

The solution of Eq. 3.46 at time $t = t^{(i+1)}$ can be expressed in terms of that at $t = t^{(i)}$ by:

$$\begin{Bmatrix} u_j^{(i+1)} \\ \dot{u}_j^{(i+1)} \end{Bmatrix} = [A(\zeta_j, \omega_j, \Delta t)] \begin{Bmatrix} u_j^{(i)} \\ \dot{u}_j^{(i)} \end{Bmatrix} + [B(\zeta_j, \omega_j, \Delta t, b_j)] \begin{Bmatrix} \ddot{u}_g^{(i)} \\ \ddot{u}_g^{(i+1)} \end{Bmatrix} \quad (3.47)$$

Therefore, if the generalized coordinate $u_j(t)$ and its time derivative $\dot{u}_j(t)$ are known at $t^{(i)}$, then the complete time history can be computed by a step by step application of Eq. 3.47. The advantage of this method lies in the fact that for a constant time interval $\Delta t$, the matrices [A] and [B] depend only on $\zeta_j, \omega_j$ and $b_j$, and are constant during the calculation of the response.

Using either method, the procedure of finding $u_j(t)$ is repeated for all j between 1 and N. The dam deformation u(z,t) is then calculated from Eq. 3.40. Once this is done, the stresses in the dam, the base force and moment resultants, and the hydrodynamic pressures can be evaluated.

3.2.3.2. Frequency Domain Analysis

An alternative approach to obtain the response of the dam to earthquake ground motion, is to work in the frequency domain. The response is found by superposition of the responses to individual Fourier components of the excitation, through the Fourier integral.

The first step in the analysis procedure is to obtain the dam response to steady-state simple harmonic motion of the form $\ddot{u}_g(t) = \exp(i\omega t)$. This is done as discussed in section 3.2.2.1, and the response is given by:

$$u(z,t) = A \cdot U(z,\omega) \cdot \exp(i\omega t) \tag{3.48}$$

where $U(z,\omega)$ is given by Eqs. 3.29.

Next, the Fourier transform $\ddot{U}_g(\omega)$ of the ground excitation $\ddot{u}_g(t)$ is obtained through:

$$\ddot{U}_g(\omega) = \int_{-\infty}^{\infty} \ddot{u}_g(t) \cdot \exp(-i\omega t) \cdot dt \tag{3.49}$$

The dam response $u(z,t)$, to the excitation $\ddot{u}_g(t)$, is then given by:

$$u(z,t) = \frac{1}{2\pi} \int_{-\infty}^{\infty} U(z,\omega) \cdot \ddot{U}_g(\omega) \cdot \exp(i\omega t) \cdot d\omega \tag{3.50}$$

## 3.3. Triangular Cross-Section: Finite Element Solution

In this case, the dam under consideration is assumed to have a triangular cross-section, as shown in Fig. 3.9. However, the analysis can be applied to dams of arbitrary cross-sectional shape provided the upstream face is vertical.

The finite element method is now recognized as an effective discretization procedure which is applicable to a variety of engineering problems. It provides a convenient and reliable idealization of the system and is particularly effective in digital-computer analyses. In

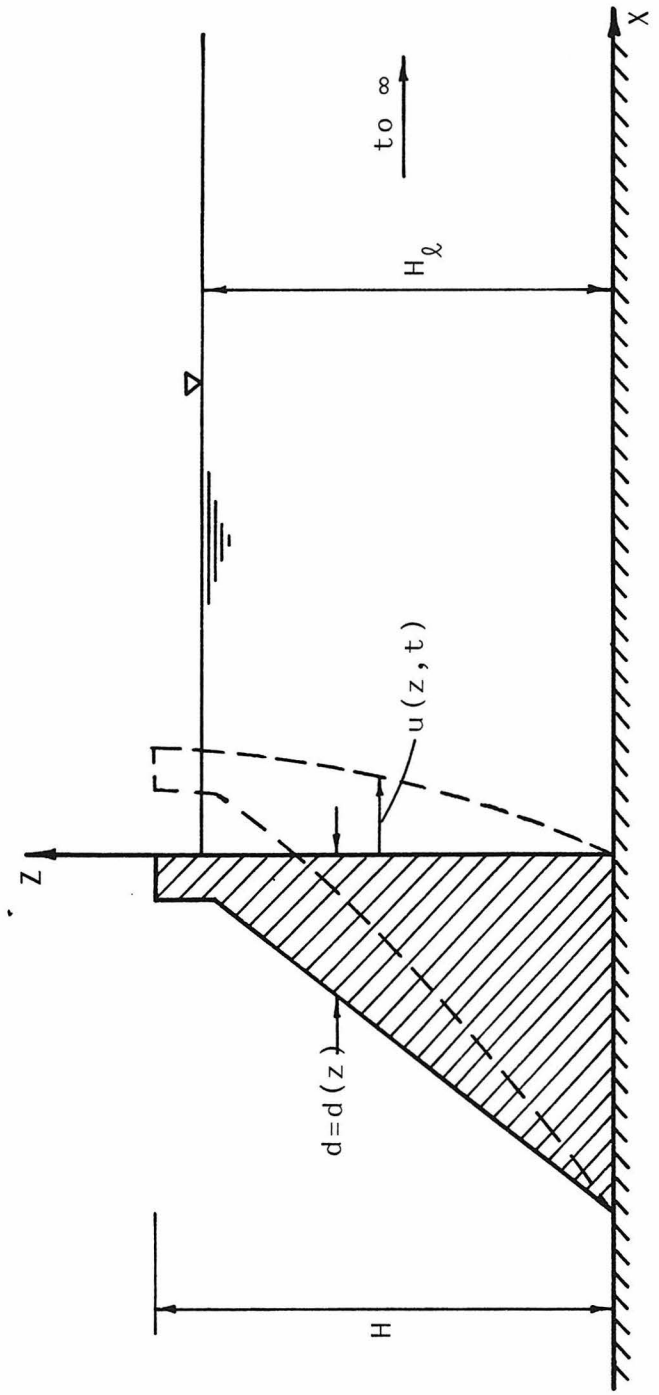


Fig. 3.9 Dam-Reservoir System , Free Vibration

the following analysis, the dam is modeled by finite elements, while the reservoir is still treated as a continuum, since the dam has a vertical upstream face. Thus, the analytical solution for the hydrodynamic pressure, given in Chapter II, are also used here.

3.3.1. Free Vibration

In this section, the partial differential equation governing the free vibration of a dam, retaining a partly filled reservoir, is discretized and converted into a matrix equation of motion. This leads to a generalized matrix eigenvalue problem, which is solved for the natural frequencies of vibration and the associated mode shapes. In addition to considering the dam behaving according to both the pure shear and the pure bending theories, a combined shear-bending theory is also presented.

3.3.1.1. Shear Theory

When the pure shear theory described previously is used, the vibration of a dam, whose thickness varies along its height, is governed by the following differential equation:

$$\rho\, d(z)\, \frac{\partial^2 u(z,t)}{\partial t^2} - \frac{\partial}{\partial z}\left[\, G\, d(z)\, \frac{\partial u(z,t)}{dz}\,\right] = -p(z,t) \tag{3.51}$$

where

$$p(z,t) = 2\,\rho_\ell \left\{ \sum_{m=1}^{\infty} \frac{\cos\left(\eta_m \frac{z}{H_\ell}\right)}{\eta_m} \left[ \int_0^{H_\ell} \ddot{u}\,(z,t)\, \cos\left(\eta_m \frac{z}{H_\ell}\right) dz \right] \right\}; \quad 0 \le z \le H_\ell \tag{3.52}$$

$$= 0 \qquad ; \quad H_\ell \le z \le H$$

The associated boundary conditions have been discussed previously, and are stated as:

$$[u(z,t)]_{z=0} = 0 \tag{3.53a}$$

$$\left[ G\, d(z) \frac{\partial u(z,t)}{\partial z} \right]_{z=H} = 0 \tag{3.53b}$$

Equations 3.51 and 3.53 constitute the "Strong" formulation of the problem under consideration.

Define $H_0^1(0,H)$ as the space of piecewise continuous functions, which are defined over the domain $0 \leq z \leq H$, are square integrable over the same domain, have square integrable first derivatives, and vanish at $z = 0$. Thus a function $v(z)$ belonging to $H_0^1(0,H)$ satisfies:

$$\int_0^H [v(z)]^2\, dz < \infty \quad ; \quad \int_0^H [v_z(z)]^2\, dz < \infty \quad ; \quad v(0) = 0 \tag{3.54}$$

Now, the "Weak-Galerkin" formulation is obtained from the "Strong" formulation by multiplying Eq. 3.51 by $v(z) \in H_0^1$, integrating over the dam height, performing an integration by parts on the second term and using the second boundary condition and the properties of $v(z)$. The "Weak" formulation may be stated as:

$$\int_0^H \rho\, d(z)\, v(z)\, \ddot{u}(z,t)\, dz + \int_0^H G\, d(z)\, v_z(z)\, u_z(z,t) dz$$

$$= -2\, \rho_\ell \sum_{m=1}^{\infty} \frac{1}{\eta_m} \left( \int_0^{H_\ell} v(z) \cos\left(\eta_m \frac{z}{H_\ell}\right) dz \right) \left( \int_0^{H_\ell} \ddot{u}(z,t) \cos\left(\eta_m \frac{z}{H_\ell}\right) dz \right) \tag{3.55}$$

Discretizing the dam into an appropriate number of finite elements, interconnected only at their ends (nodes) as shown in Fig. 3.10a, Eq. 3.55 is written as:

$$\sum_{e=1}^{NH} \int_0^{h_e} \rho\, d(\bar{z})\, v^e(\bar{z})\, \ddot{u}^e(\bar{z},t)\, d\bar{z} + \sum_{e=1}^{NH} \int_0^{h_e} G\, d(\bar{z})\, v_z^e(\bar{z})\, u_z^e(\bar{z},t)\, d\bar{z}$$

$$+ 2\, \rho_\ell \sum_{m=1}^{\infty} \frac{1}{\eta_m} \left( \sum_{e=1}^{NW} \int_0^{h_e} v^e(\bar{z}) \cos\left(\eta_m \frac{z}{H_\ell}\right) d\bar{z} \right) .$$

$$\left( \sum_{e=1}^{NW} \int_0^{h_e} \ddot{u}^e(\bar{z},t) \cos\left(\eta_m \frac{z}{H_\ell}\right) d\bar{z} \right) = 0 \qquad (3.56)$$

where e is the element number, NH is the total number of elements of which NW elements are below the water surface, $h_e$ is the element length, and $\bar{z}$ is the local z-coordinate, as shown in Fig. 3.10b.

$v^e(\bar{z})$ and $u^e(\bar{z},t)$ are v(z) and u(z,t) expressed in the local z-coordinate.

Define the vector of nodal displacements $\{r(t)\}_e$, and a constant vector $\{q\}_e$ as:

$$\{r(t)\}_e = \begin{Bmatrix} u_1^e(t) \\ u_2^e(t) \end{Bmatrix} \quad ; \quad \{q\}_e = \begin{Bmatrix} v_1^e \\ v_2^e \end{Bmatrix} \qquad (3.57)$$

then $u^e(\bar{z},t)$ and $v^e(\bar{z})$ can be expressed as:

$$u^e(\bar{z},t) = \{N(\bar{z})\}^T \{r(t)\}_e \quad ; \quad v^e(\bar{z}) = \{q\}_e^T \{N(\bar{z})\} \qquad (3.58)$$

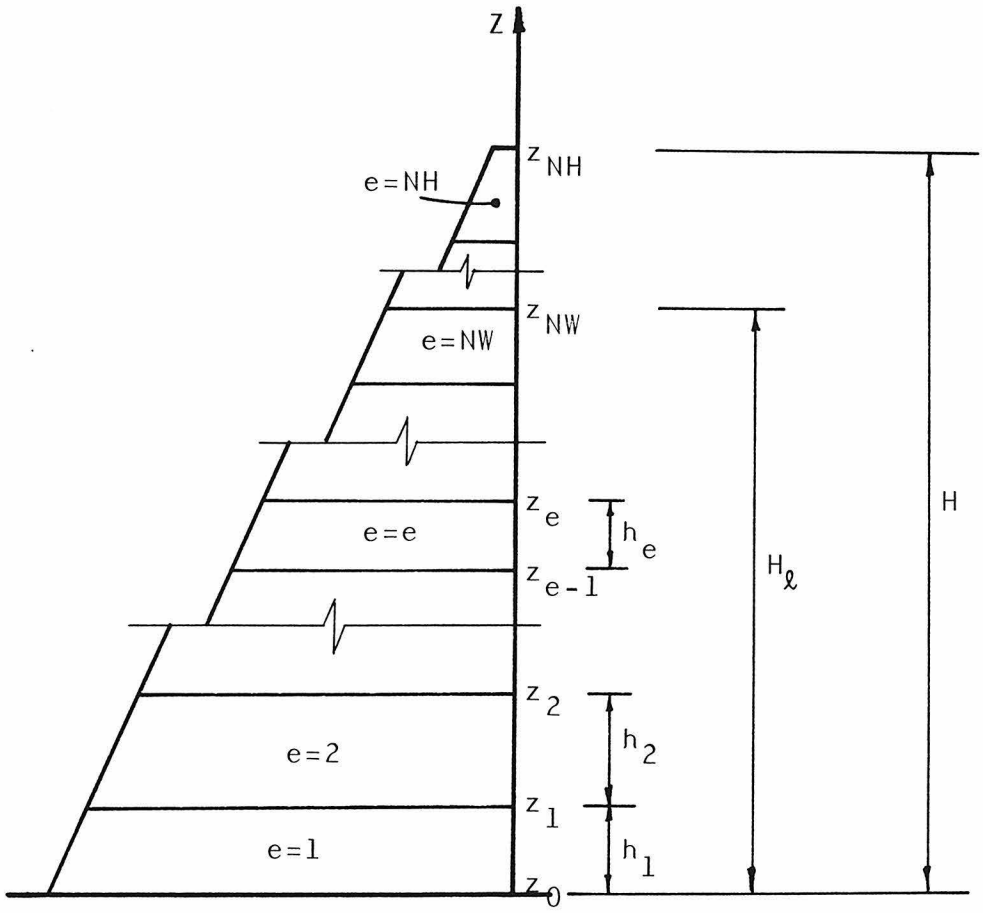


(a) Finite Element Idealization of the Dam

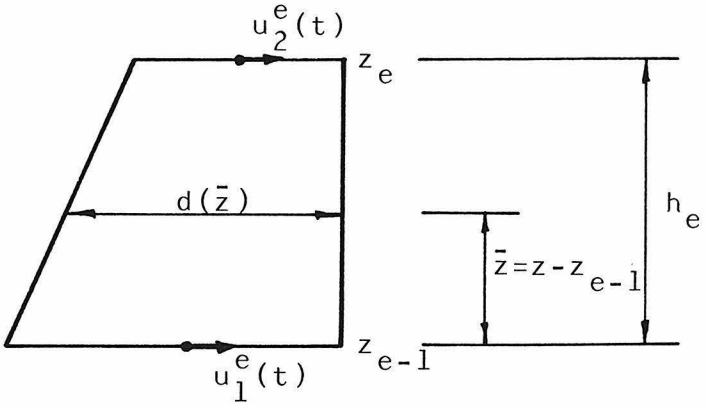


(b) Dam Element

Fig. 3.10 Finite Element Definition Diagram

where $\{N(\bar{z})\}$ is the vector of shape or interpolation functions, the elements of which are given by:

$$N_1(\bar{z}) = 1-\bar{z}/h_e \quad ; \quad N_2(\bar{z}) = \bar{z}/h_e \tag{3.59}$$

Substituting from Eqs. 3.58 into Eq. 3.56, the matrix equations of motion are eventually obtained. However, for simplicity, each term is considered separately.

The Dam Mass Matrix

Considering the first term in Eq. 3.56, substituting from Eqs. 3.58 and rearranging, one obtains:

$$\sum_{e=1}^{NH} \int_0^{h_e} \rho\, d(\bar{z})\, v^e(\bar{z})\, \ddot{u}^e(\bar{z},t)d\bar{z} = \sum_{e=1}^{NH} \{q\}_e^T\, [M_d]_e\, \{\ddot{r}(t)\}_e \tag{3.60}$$

where $[M_d]_e$ is the element mass matrix defined as:

$$[M_d]_e = \int_0^{h_e} \rho\, d(\bar{z})\{N(\bar{z})\}\{N(\bar{z})\}^T d\bar{z} \tag{3.61}$$

which after performing the necessary integrations yields:

$$[M_d]_e = \rho\, d_e\, h_e \begin{bmatrix} 1/3 & 1/6 \\ 1/6 & 1/3 \end{bmatrix} \tag{3.62}$$

where $d_e$ is the average thickness of element e.

The R.H.S. of Eq. 3.60 is assembled by a process based on the nodal compatibility. By matching the displacements at the nodes, the masses are added at these locations. Thus, the overall mass matrix of the dam will be:

$$[M_d] = \sum_{e=1}^{NH} [M_d]_e \tag{3.63}$$

By defining overall nodal displacement and constant vectors as:

$$\{R(t)\} = \sum_{e=1}^{NH} \{r(t)\}_e \quad \text{and} \quad \{Q\} = \sum_{e=1}^{NH} \{q\}_e \tag{3.64}$$

Equation 3.60 is expressed as:

$$\sum_{e=1}^{NH} \int_0^{h_e} \rho\, d(\bar{z})\, v^e(\bar{z})\, \ddot{u}^e(\bar{z},t)\, d\bar{z} = \{Q\}^T [M_d] \{\ddot{R}(t)\} \tag{3.65}$$

The Dam Stiffness Matrix

Going through the same steps, the second term in Eq. 3.56 eventually yields:

$$\sum_{e=1}^{NH} \int_0^{h_e} G\, d(\bar{z})\, v_z^e(\bar{z})\, u_z^e(\bar{z},t)\, d\bar{z} = \{Q\}^T [K_d] \{R(t)\} \tag{3.66}$$

where $[K_d]$ is the overall stiffness matrix, obtained by superposing the element stiffness matrices $[K_d]_e$ defined as:

$$[K_d]_e = \int_0^{h_e} G\, d(\bar{z}) \{N_z(\bar{z})\} \{N_z(\bar{z})\}^T d\bar{z} \tag{3.67}$$

Equation 3.67 yields:

$$[K_d]_e = \frac{G\, d_e}{h_e} \begin{bmatrix} 1 & -1 \\ -1 & 1 \end{bmatrix} \tag{3.68}$$

The Added Mass Matrix

Substituting from Eqs. 3.58 into the third term of Eq. 3.56, yields:

$$AM = 2\,\rho_\ell \sum_{m=1}^{\infty} \frac{1}{\eta_m} \left( \sum_{e=1}^{NW} \int_0^{h_e} v^e(\bar{z}) \cos\left(\eta_m \frac{z}{H_\ell}\right) d\bar{z} \right) \left( \sum_{e=1}^{NW} \int_0^{h_e} \ddot{u}^e(\bar{z},t) \cos\left(\eta_m \frac{z}{H_\ell}\right) d\bar{z} \right)$$

$$= 2\,\rho_\ell \sum_{m=1}^{\infty} \frac{1}{\eta_m} \left( \sum_{e=1}^{NW} \{q\}_e^T \{f^{(m)}\}_e \right) \left( \sum_{e=1}^{NW} \{f^{(m)}\}_e^T \{\ddot{r}(t)\}_e \right) \tag{3.69}$$

$$\{f^{(m)}\}_e = \int_0^{h_e} \{N(\bar{z})\} \cos\left(\eta_m \frac{z}{H_\ell}\right) d\bar{z} \tag{3.70}$$

Defining the vector $F^{(m)}$ as:

$$\{F^{(m)}\} = \sum_{e=1}^{NW} \{f^{(m)}\}_e \tag{3.71}$$

Equation 3.69 can be written as:

$$AM = \{Q\}^T [M_\ell] \{\ddot{R}\} \tag{3.72}$$

where $[M_\ell]$ is the overall added mass matrix, defined as:

$$[M_\ell] = 2\,\rho_\ell \sum_{m=1}^{\infty} \frac{1}{\eta_m} \{F^{(m)}\} \{F^{(m)}\}^T \tag{3.73}$$

Substituting from Eqs. 3.59 into Eq. 3.70, the elements of the vector $\{f^{(m)}\}_e$ are obtained as:

$$f_1^{(m)} = h_e \left[ -\frac{1}{\gamma_m} \sin\left(\gamma_m \frac{z_{e-1}}{h_e}\right) + \frac{1}{\gamma_m^2} \cos\left(\gamma_m \frac{z_{e-1}}{h_e}\right) - \frac{1}{\gamma_m^2} \cos\left(\gamma_m \frac{z_e}{h_e}\right) \right] \tag{3.74a}$$

$$f_2^{(m)} = h_e \left[ -\frac{1}{\gamma_m^2} \cos\left(\gamma_m \frac{z_{e-1}}{h_e}\right) + \frac{1}{\gamma_m} \sin\left(\gamma_m \frac{z_e}{h_e}\right) + \frac{1}{\gamma_m^2} \cos\left(\gamma_m \frac{z_e}{h_e}\right) \right] \tag{3.74b}$$

where $\gamma_m = \eta_m\, h_e / H_\ell$.

The Matrix Equations of Motion

Substituting from Eqs. 3.65, 3.66 and 3.72 into Eq. 3.56, leads to:

$$[[M_d] + [M_\ell]] \{\ddot{R}(t)\} + [K_d] \{R(t)\} = \{0\} \tag{3.75}$$

which is the matrix equation governing the free vibration of the dam-reservoir system.

The dam mass and stiffness matrices are symmetric, banded and positive definite matrices, while the added mass matrix is symmetric, not banded and has zero elements corresponding to the nodes located above the water surface. After deleting the column and row corresponding to the fixed node at the dam base, the general forms of these matrices are shown schematically in Fig. 3.11; only the hatched blocks are non-zero elements.

The Eigenvalue Problem

The matrix equation for the free lateral undamped vibration of the dam is given by:

$$[M] \{\ddot{R}\} + [K] \{R\} = \{0\} \tag{3.76}$$

where

$$[M] = [M_d] + [M_\ell] \; ; \quad \text{and} \quad [K] = [K_d]$$

By writing the solution of Eq. 3.76 in the familiar form:

$$\{R(t)\} = \{\phi\} \exp(i\omega t) \qquad ; \quad i = \sqrt{-1} \tag{3.77}$$

and substituting Eq. 3.77 into Eq. 3.76 [leaving out the common factor $\exp(i\omega t)$], the following equation is obtained:

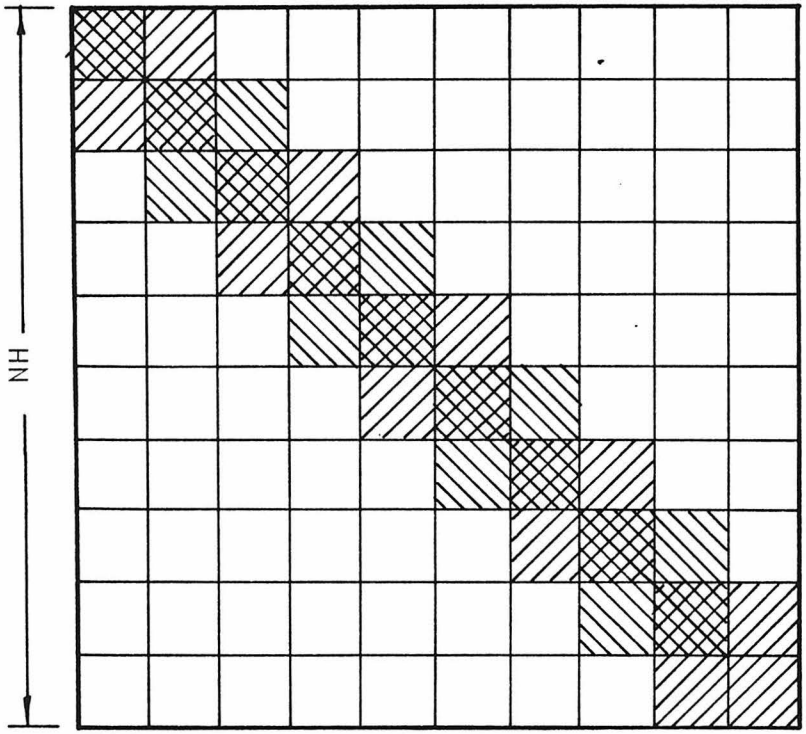


General Form of the "Banded" Mass
or Stiffness Matrix

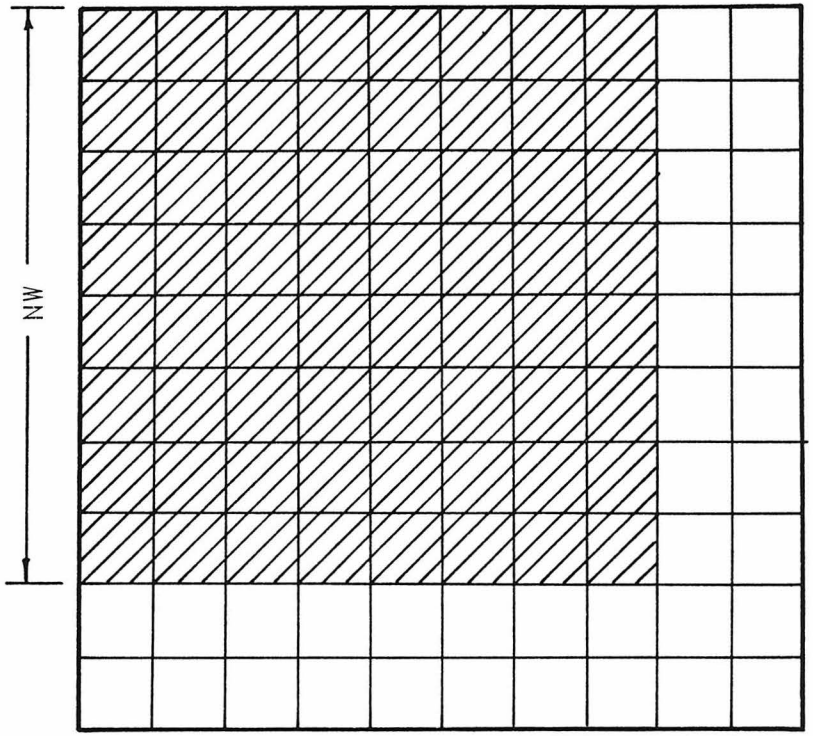


General Form of the "Full" Added
Mass Matrix

Fig. 3.11 Schematics of the Form of the Mass, Stiffness and Added Mass Matrix

$$\left[ -\omega^2 \, [M] + [K] \right] \{\phi\} = \{0\} \tag{3.78}$$

where $\{\phi\}$ is the vector of the displacement amplitudes of vibration (which does not change with time), and $\omega$ is the natural circular frequency.

A non-trivial solution of Eq. 3.78 is possible only if the determinant of the coefficients vanishes, i.e.,

$$|| \, [K] - \omega^2 \, [M] \, || = 0 \tag{3.79}$$

Expanding the determinant will give an algebraic equation of $NH^{th}$ degree in the frequency parameter $\omega^2$ for a system having NH elements.

Because of the positive definitiveness of [M] and [K], the eigenvalues $\omega_1^2, \omega_2^2, \ldots, \omega_{NH}^2$ are real and positive quantities; Eq. 3.78 provides nonzero solution vectors $\{\phi\}_i$ (eigenvectors) for each eigenvalue $\omega_i^2$.

3.3.1.2. Bending Theory

The differential equation governing the free vibration of a variable thickness dam, modeled by the pure bending theory, is as follows:

$$\rho \, d(z) \, \frac{\partial^2 u(z,t)}{\partial t^2} + \frac{\partial^2}{\partial z^2} \left[ \frac{\bar{E}}{12} \, d^3(z) \, \frac{\partial^2 u(z,t)}{\partial z^2} \right] = -p(z,t) \tag{3.80}$$

where $p(z,t)$ is given by Eq. 3.52.

The boundary conditions, associated with this equation, have been discussed before, and may be stated as follows:

$$[u(z,t)]_{z=0} = 0 \tag{3.81a}$$

$$[u_z(z,t)]_{z=0} = 0 \tag{3.81b}$$

$$\left[ \bar{E} \frac{d^3(z)}{12} u_{zz}(z,t) \right]_{z=H} = 0 \tag{3.81c}$$

$$\left[ \frac{\partial}{\partial z} \left( \bar{E} \frac{d^3(z)}{12} u_{zz}(z,t) \right) \right]_{z=H} = 0 \tag{3.81d}$$

Define $H^2_{00}(0,H)$ as the space of continuous functions defined over the domain $0 \leq z \leq H$ and having piecewise continuous first derivatives. Each function in $H^2_{00}$, as well as its first and second derivatives, are square integrable over the domain. In addition, each function and its first derivative vanish at $z = 0$. Thus, a function $v(z)$ belonging to $H^2_{00}$ satisfies:

$$\int_0^H [v(z)]^2 \, dz < \infty \; ; \; \int_0^H [v_z(z)]^2 \, dz < \infty \; ; \; \int_0^H [v_{zz}(z)]^2 \, dz < 0$$

$$v(0) = 0 \; ; \; v_z(0) = 0 \tag{3.82}$$

Multiplying Eq. 3.80 by $v(z) \in H^2_{00}(0,H)$, integrating over the domain, performing an integration by parts twice on the second term, and using the boundary conditions Eqs. 3.81c and 3.81d as well as the properties of $v(z)$, one obtains the "Weak" form:

$$\int_0^H \rho\, d(z)\, v(z)\, \ddot{u}(z,t)\, dz + \int_0^H \bar{E}\, \frac{d^3(z)}{12}\, v_{zz}(z)\, u_{zz}(z,t)\, dz$$

$$= -2\, \rho_\ell \sum_{m=1}^{\infty} \frac{1}{\eta_m} \left( \int_0^{H_\ell} v(z)\, \cos\left(\eta_m \frac{z}{H_\ell}\right) dz \right) \left( \int_0^{H_\ell} \ddot{u}(z,t)\, \cos\left(\eta_m \frac{z}{H_\ell}\right) dz \right) \qquad (3.83)$$

When the dam is discretized into NH finite elements, NW of which are below the water surface, Eq. 3.83 can be written as:

$$\sum_{e=1}^{NH} \int_0^{h_e} \rho\, d(\bar{z})\, v^e(\bar{z})\, \ddot{u}^e(\bar{z},t) d\bar{z} + \sum_{e=1}^{NH} \int_0^{h_e} \bar{E}\, \frac{d^3(\bar{z})}{12}\, v^e_{zz}(\bar{z})\, u^e_{zz}(\bar{z}) d\bar{z}$$

$$+ 2\, \rho_\ell \sum_{m=1}^{\infty} \frac{1}{\eta_m} \left( \sum_{e=1}^{NW} \int_0^{h_e} v^e(\bar{z})\, \cos\left(\eta_m \frac{z}{H_\ell}\right) d\bar{z} \right) \cdot$$

$$\left( \sum_{e=1}^{NW} \int_0^{h_e} \ddot{u}^e(\bar{z},t)\, \cos\left(\eta_m \frac{z}{H_\ell}\right) d\bar{z} \right) = 0 \qquad (3.84)$$

where $\bar{z}$, $h_e$, $v^e(\bar{z})$ and $u^e(\bar{z},t)$ are as defined previously. The displacement $u^e(\bar{z},t)$ and the variational function $v^e(\bar{z})$ can be expressed as:

$$\left.\begin{aligned} u^e(\bar{z},t) &= \sum_{i=1}^{2} \left( N_i(\bar{z})\, u^e_i(t) + \hat{N}_i(\bar{z})\, u^e_{zi}(t) \right) \\ v^e(\bar{z}) &= \sum_{j=1}^{2} \left( N_j(\bar{z})\, v^e_j + \hat{N}_j(\bar{z})\, v^e_{zj} \right) \end{aligned}\right\} \qquad (3.85)$$

where $u_i^e(t)$ are the nodal displacements, $u_{zi}^e(t)$ are the slopes at the nodes, $v_j^e$ and $v_{zj}^e$ are constants. $N_i(\bar{z})$ and $\hat{N}_i(\bar{z})$ are the shape functions, chosen cubic Hermitian polynomials to assure slope continuity at the nodes.

Define the vector of generalized nodal displacement as:

$$\{r(t)\}_e = \{u_1^e(t) \quad h_e\, u_{z1}^e(t) \quad u_2^e(t) \quad h_e\, u_{z2}^e(t)\}^T \tag{3.86a}$$

and a constant vector as:

$$\{q\}_e = \{v_1^e \quad h_e\, v_{z1}^e \quad v_2^e \quad h_e\, v_{z2}^e\}^T \tag{3.86b}$$

and the vector of shape functions as:

$$\{N(\bar{z})\} = \begin{Bmatrix} N_1(\bar{z}) \\ \hat{N}_1(\bar{z}) \\ N_2(\bar{z}) \\ \hat{N}_2(\bar{z}) \end{Bmatrix} = \begin{Bmatrix} \left(1 - 3\,\dfrac{\bar{z}^2}{h_e^2} + 2\,\dfrac{\bar{z}^3}{h_e^3}\right) \\ \left(\dfrac{\bar{z}}{h_e} - 2\,\dfrac{\bar{z}^2}{h_e^2} + \dfrac{\bar{z}^3}{h_e^3}\right) \\ \left(3\,\dfrac{\bar{z}^2}{h_e^2} - 2\,\dfrac{\bar{z}^3}{h_e^3}\right) \\ \left(-\dfrac{\bar{z}^2}{h_e^2} + \dfrac{\bar{z}^3}{h_e^3}\right) \end{Bmatrix} \tag{3.86c}$$

Thus, Eqs. 3.85 can be now expressed by the same form given in Eqs. 3.58.

The overall mass and stiffness matrices of the dam are obtained by substituting from Eq. 3.58 into the first and second terms of Eq. 3.84, respectively. They are expressed as the assemblage of the individual element mass and stiffness matrices, which are given by:

$$[M_d]_e = \int_0^{h_e} \rho\, d(z)\, \{N(\bar{z})\}\, \{N(\bar{z})\}^T\, d\bar{z} = \rho\, d_e h_e \begin{bmatrix} \frac{13}{35} & \frac{11}{210} & \frac{9}{70} & \frac{-13}{420} \\ \frac{11}{210} & \frac{1}{105} & \frac{13}{420} & \frac{-1}{140} \\ \frac{9}{70} & \frac{13}{420} & \frac{13}{35} & \frac{-11}{210} \\ \frac{-13}{420} & \frac{-1}{140} & \frac{-11}{210} & \frac{1}{105} \end{bmatrix} \quad (3.87)$$

and

$$[K_d]_e = \int_0^{h_e} \bar{E}\, \frac{d^3(\bar{z})}{12}\, \{N_{zz}(\bar{z})\}\{N_{zz}(\bar{z})\}^T d\bar{z} = \frac{\bar{E}\, d_e^3}{12\, h_e^3} \begin{bmatrix} 12 & 6 & -12 & 6 \\ 6 & 4 & -6 & 2 \\ -12 & -6 & 12 & -6 \\ 6 & 2 & -6 & 4 \end{bmatrix} \quad (3.88)$$

The overall added mass matrix is as defined in Eq. 3.73 in which the vector $\{f^{(m)}\}_e$, defined by Eq. 3.70, has elements:

$$f_1^{(m)} = \int_0^{h_e} N_1(\bar{z}) \cos\left(\eta_m \frac{z}{H_\ell}\right) d\bar{z}$$

$$= h_e \left[ -\left(\frac{1}{\gamma_m} + \frac{6}{\gamma_m^3}\right) \sin\left(\gamma_m \frac{z_{e-1}}{h_e}\right) + \frac{12}{\gamma_m^4} \cos\left(\gamma_m \frac{z_{e-1}}{h_e}\right) \right.$$

$$\left. - \frac{6}{\gamma_m^3} \sin\left(\gamma_m \frac{z_e}{h_e}\right) - \frac{12}{\gamma_m^4} \cos\left(\gamma_m \frac{z_e}{h_e}\right) \right] \qquad (3.89a)$$

$$f_2^{(m)} = \int_0^{h_e} \hat{N}_1(\bar{z}) \cos\left(\eta_m \frac{z}{H_\ell}\right) d\bar{z}$$

$$= h_e \left[ -\frac{4}{\gamma_m^3} \sin\left(\gamma_m \frac{z_{e-1}}{h_e}\right) - \left(\frac{1}{\gamma_m^2} - \frac{6}{\gamma_m^4}\right) \cos\left(\gamma_m \frac{z_{e-1}}{h_e}\right) \right.$$

$$\left. - \frac{2}{\gamma_m^3} \sin\left(\gamma_m \frac{z_e}{h_e}\right) - \frac{6}{\gamma_m^4} \cos\left(\gamma_m \frac{z_e}{h_e}\right) \right] \qquad (3.89b)$$

$$f_3^{(m)} = \int_0^{h_e} N_2(\bar{z}) \cos\left(\eta_m \frac{z}{H_\ell}\right) d\bar{z}$$

$$= h_e \left[ \frac{6}{\gamma_m^3} \sin\left(\gamma_m \frac{z_{e-1}}{h_e}\right) - \frac{12}{\gamma_m^4} \cos\left(\gamma_m \frac{z_{e-1}}{h_e}\right) \right.$$

$$\left. + \left(\frac{1}{\gamma_m} + \frac{6}{\gamma_m^3}\right) \sin\left(\gamma_m \frac{z_e}{h_e}\right) + \frac{12}{\gamma_m^4} \cos\left(\gamma_m \frac{z_e}{h_e}\right) \right] \qquad (3.89c)$$

$$f_4^{(m)} = \int_0^{h_e} \hat{N}_2(\bar{z}) \cos\left(\eta_m \frac{z}{H_\ell}\right) d\bar{z}$$

$$= h_e \left[ -\frac{2}{\gamma_m^3} \sin\left(\gamma_m \frac{z_{e-1}}{h_e}\right) + \frac{6}{\gamma_m^4} \cos\left(\gamma_m \frac{z_{e-1}}{h_e}\right) \right.$$

$$\left. - \frac{4}{\gamma_m^3} \sin\left(\gamma_m \frac{z_e}{h_e}\right) + \left(\frac{1}{\gamma_m^2} - \frac{6}{\gamma_m^4}\right) \cos\left(\gamma_m \frac{z_e}{h_e}\right) \right] \qquad (3.89d)$$

where $\gamma_m = \eta_m / H_\ell$.

Having obtained the overall mass, stiffness and added mass matrices, Eq. 3.83 is reduced to a matrix equation of motion of the form given by Eq. 3.75. The matrices involved have the same properties as discussed in the previous section; however, their size is 2 NH rather than NH, since we have two generalized nodal displacements associated with each node. The generalized eigenvalue problem, as given by Eq. 3.78, is obtained and solved for the natural frequencies and mode shapes.

3.3.1.3. Shear-Bending Theory

In this section, an analysis, more accurate than those described in the previous two sections, is discussed. In addition to the pure bending deformations, the deflection due to shear as well as the effect of rotary inertia are taken into account. This problem was first investigated by S. Timoshenko [34] who obtained a single differential equation for the vibration of beams, involving only the total (bending + shear) deflection. However, the boundary conditions associated with

this equation were not easy to define. Later, R. A. Anderson [35] and J. Miklowitz [36] used another formulation of the Timoshenko theory, in which they dealt with two coupled differential equations in the two separate bending and shear deflections. The studies mentioned involve only prismatic beams of uniform cross-section. In the following, "Strong" formulation of the transverse free vibration problem of a variable section plate (dam) is presented and the finite element matrix equation of motion developed in a manner analogous to the one used in the previous two sections.

According to the Timoshenko theory, the slope of the deflection curves depends not only on the rotation of cross-sections, but also on the shearing deformations. If $\phi$ denotes the slope of the deflection curve when shear is neglected, and $\beta$ denotes the angle of shear at the neutral axis in the same cross-section, then the total slope is:

$$\frac{\partial u}{\partial z} = \phi + \beta \tag{3.90}$$

Thus, of the three variables, u, $\phi$ and $\beta$, only two can vary independently, while the third is determined from Eq. 3.90. Choosing u, the total deflection, and $\phi$, the slope due to bending only, as our two variables, the two coupled differential equations governing the transverse vibration of a variable thickness dam can be written in the following form:

$$\rho\, d(z)\, \frac{\partial^2 u(z,t)}{\partial t^2} - \frac{\partial}{\partial z}\left[G\, d(z)\left(\frac{\partial u(z,t)}{\partial z} - \phi(z,t)\right)\right] = -\, p(z,t) \tag{3.91}$$

$$\rho\, \frac{d^3(z)}{12}\, \frac{\partial^2 \phi(z,t)}{\partial t^2} - \frac{\partial}{\partial z}\left[\, \frac{\bar{}}{E}\, \frac{d^3(z)}{12}\, \frac{\partial \phi(z,t)}{\partial z}\,\right]$$

$$- G\, d(z)\left[\, \frac{\partial u(z,t)}{\partial z} - \phi(z,t)\,\right] = 0 \tag{3.92}$$

where $p(z,t)$ is given by Eq. 3.52.

Now, the boundary conditions associated with Eqs. 3.91 and 3.92 can be expressed in terms of the variables $u(z,t)$ and $\phi(z,t)$ as follows:

i) the total deflection at the dam base vanishes, i.e.,

$$[u(z,t)]_{z=0} = 0 \tag{3.93a}$$

ii) the slope, due to bending only, vanishes at the dam base, i.e.,

$$[\phi(z,t)]_{z=0} = 0 \tag{3.93b}$$

iii) the bending moment at the dam crest vanishes, i.e.,

$$\left[\, \frac{\bar{}}{E}\, \frac{d^3(z)}{12}\, \frac{\partial \phi(z,t)}{\partial z}\,\right]_{z=H} = 0 \tag{3.93c}$$

iv) the shear force at the dam crest vanishes, i.e.,

$$\left[\, G\, d(z)\left(\frac{\partial\, u(z,t)}{\partial z} - \phi(z,t)\right)\right]_{z=H} = 0 \tag{3.93d}$$

Equations 3.91, 3.92 and 3.93 constitute the "Strong" formulation. The "Weak" formulation is obtained by multiplying Eqs. 91 and 92 by variation functions $v(z)$ and $\Omega(z) \in H_0^1(0,H)$, respectively, adding, integrating over the dam height and performing the necessary

integrations by parts. The final form will be:

$$\int_0^H \rho\, d(z)\, v(z)\, \ddot{u}(z,t)dz + \int_0^H G\, d(z)\, v_z(z)\, u_z(z,t)dz$$

$$- \int_0^H G\, d(z)\, v_z(z)\, \phi(z,t)dz$$

$$+ 2\, \rho_\ell \sum_{m=1}^{\infty} \frac{1}{\eta_m} \left( \int_0^{H_\ell} v(z) \cos\left(\eta_m \frac{z}{H_\ell}\right) dz \right) \left( \int_0^{H_\ell} \ddot{u}(z,t) \cos\left(\eta_m \frac{z}{H_\ell}\right) dz \right)$$

$$+ \int_0^H \rho \frac{d^3(z)}{12} \Omega(z)\, \ddot{\phi}(z,t)dz$$

$$+ \int_0^H \bar{E} \frac{d^3(z)}{12} \Omega_z(z)\, \phi_z(z,t)dz$$

$$- \int_0^H G\, d(z)\, \Omega(z)\, u_z(z,t)dz$$

$$+ \int_0^H G\, d(z)\, \Omega(z)\, \phi(z,t)dz = 0 \qquad (3.94)$$

By discretizing the dam, Eq. 3.94 takes the form:

$$\sum_{e=1}^{NH} \int_0^{h_e} \rho\, d(\bar{z})\, v^e(\bar{z})\, \ddot{u}^e(\bar{z},t)d\bar{z} + \sum_{e=1}^{NH} \int_0^{h_e} G\, d(\bar{z})\, v_z^e(\bar{z})\, u_z^e(\bar{z},t)d\bar{z}$$

$$- \sum_{e=1}^{NH} \int_0^{h_e} G\, d(\bar{z})\, v_z^e(\bar{z})\, \phi^e(\bar{z},t)d\bar{z}$$

$$+ 2\,\rho_\ell \sum_{m=1}^{\infty} \frac{1}{\eta_m} \left( \sum_{e=1}^{NW} \int_0^{h_e} v^e(\bar{z}) \cos\left(\eta_m \frac{z}{H_\ell}\right) d\bar{z} \right)$$

$$\cdot \left( \sum_{e=1}^{NW} \int_0^{h_e} \ddot{u}^e(\bar{z},t) \cos\left(\eta_m \frac{z}{H_\ell}\right) d\bar{z} \right)$$

$$+ \sum_{e=1}^{NH} \int_0^{h_e} \rho \frac{d^3(\bar{z})}{12}\, \Omega^e(\bar{z})\, \ddot{\phi}^e(\bar{z},t)d\bar{z}$$

$$+ \sum_{e=1}^{NH} \int_0^{h_e} \bar{E} \frac{d^3(\bar{z})}{12}\, \Omega_z^e(\bar{z})\, \phi_z^e(\bar{z},t)dz$$

$$- \sum_{e-1}^{NH} \int_0^{h_e} G\, d(\bar{z})\, \Omega^e(\bar{z})\, u_z^e(\bar{z},t)d\bar{z}$$

$$+ \sum_{e=1}^{NH} \int_0^{h_e} G\, d(\bar{z})\, \Omega^e(\bar{z})\, \phi^e(\bar{z},t)d\bar{z} = 0 \qquad (3.95)$$

Now, define $u^e(\bar{z},t)$ , $v^e(\bar{z})$ , $\phi^e(\bar{z},t)$ and $\Omega^e(\bar{z})$ as follows:

$$\left.\begin{aligned} u^e(\bar{z},t) &= \{N(\bar{z})\}^T \{r(t)\}_e \quad ; \quad v^e(\bar{z}) = \{q\}_e^T \{N(\bar{z})\} \\ \phi^e(\bar{z},t) &= \{S(\bar{z})\}^T \{r(t)\}_e \quad ; \quad \Omega^e(\bar{z}) = \{q\}_e^T \{S(\bar{z})\} \end{aligned}\right\} \qquad (3.96)$$

where

$$\left.\begin{aligned} \{r(t)\}_e &= \begin{Bmatrix} u_1^e(t) \\ h_e \phi_1^e(t) \\ u_2^e(t) \\ h_e \phi_2^e(t) \end{Bmatrix} \quad ; \quad \{q\}_e = \begin{Bmatrix} v_1^e \\ h_e \Omega_1^e \\ v_2^e \\ h_e \Omega_2^e \end{Bmatrix} \\ \{N(\bar{z})\} &= \begin{Bmatrix} N_1(\bar{z}) \\ 0 \\ N_2(\bar{z}) \\ 0 \end{Bmatrix} \quad ; \quad \{S(\bar{z})\} = \begin{Bmatrix} 0 \\ \frac{1}{h_e} N_1(\bar{z}) \\ 0 \\ \frac{1}{h_e} N_2(\bar{z}) \end{Bmatrix} \end{aligned}\right\} \tag{3.97}$$

where $u_i^e(t)$ and $\phi_i^e(t)$ are the nodal displacements and slopes, respectively, $v_i^e$ and $\Omega_i^e$ are constants, and $N_i(\bar{z})$ are the same shape functions given by Eq. 3.59.

The matrix equations of motion can be obtained by substituting from Eqs. 3.96 into Eq. 3.95. However, for the sake of clarity, the mass, stiffness and added mass matrices will be developed separately.

The Dam Mass Matrix

The overall mass matrix of the dam is obtained, from the sum of the first and fifth terms of Eq. 3.95, as the assemblage of the element mass matrices, which are given by:

$$[M_d]_e = \int_0^{h_e} \left[ \rho\, d(\bar{z})\ \{N(\bar{z})\}\ \{N(\bar{z})\}^T + \rho\, \frac{d^3(\bar{z})}{12}\ \{S(\bar{z})\}\ \{S(\bar{z})\}^T \right] d\bar{z} \tag{3.98}$$

which yields:

$$[M_d]_e = \rho\, d_e\, h_e \begin{bmatrix} \frac{1}{3} & 0 & \frac{1}{6} & 0 \\ 0 & \frac{1}{36}\left(\frac{d_e}{h_e}\right)^2 & 0 & \frac{1}{72}\left(\frac{d_e}{h_e}\right)^2 \\ \frac{1}{6} & 0 & \frac{1}{3} & 0 \\ 0 & \frac{1}{72}\left(\frac{d_e}{h_e}\right)^2 & 0 & \frac{1}{36}\left(\frac{d_e}{h_e}\right)^2 \end{bmatrix} \tag{3.99}$$

The Dam Stiffness Matrix

The element stiffness matrices, which upon assemblage produce the overall stiffness matrix, are generated from the remaining terms of Eq. 3.95, excluding the fourth term. It is given by:

$$[K_d]_e = \int_0^{h_e} \Big[ G\, d(\bar{z}) \Big( \{N_z(\bar{z})\}\{N_z(\bar{z})\}^T - \{N_z(\bar{z})\}\ \{S(\bar{z})\}^T - \{S(\bar{z})\}\ \{N_z(\bar{z})\}^T + \{S(\bar{z})\}\ \{S(\bar{z})\}^T \Big) + \bar{E}\, \frac{d^3(\bar{z})}{12} \Big( \{S_z(\bar{z})\}\ \{S_z(\bar{z})\}^T \Big) \Big] d\bar{z} \tag{3.100}$$

A term by term integration of the above equation yields:

$$[K_d]_e = \frac{G\, d_e}{h_e} \begin{bmatrix} 1 & \frac{1}{2} & -1 & \frac{1}{2} \\ \frac{1}{2} & \left(\frac{1}{3} + K\right) & -\frac{1}{2} & \left(\frac{1}{6} - K\right) \\ -1 & -\frac{1}{2} & 1 & -\frac{1}{2} \\ \frac{1}{2} & \left(\frac{1}{6} - K\right) & -\frac{1}{2} & \left(\frac{1}{3} + K\right) \end{bmatrix} \tag{3.101}$$

where

$$K = \frac{1}{12} \frac{\bar{E}}{G} \left(\frac{d_e}{h_e}\right)^2 \tag{3.102}$$

The Added Mass Matrix

The fourth term of Eq. 3.95 will furnish the overall added mass matrix in the same form given by Eq. 3.73, in which the first and third elements of $\{f^{(m)}\}_e$ are given by Eqs. 3.74a and 3.74b, respectively, while the second and fourth terms are zero.

The matrix equation of motion can now be written and solved exactly as discussed in the preceding two sections.

3.3.1.4: Numerical Examples

The method developed in the previous three sections is used to compute the natural frequencies of vibration and the corresponding mode shapes of a concrete dam having a triangular cross-section. Three different computer programs, one for each of the three theories used to model the dam, have been written in accordance with the method mentioned above. Each program develops the appropriate element mass and stiffness matrices, constructs the added mass matrix, and extracts the eigenvalues (natural frequencies) and the eigenvectors (mode shapes), for two

different cases: (1) dam with empty reservoir, and (2) dam with a completely full reservoir.

The dam examined has a vertical upstream face, and a 0.8:1 sloping downstream face. The properties of concrete and water are as given in section 3.2.1.3. The first three frequencies, normalized w.r.t. the fundamental frequency of the reservoir, are listed in Table 3.3, for empty and for full reservoir, for the three different theories considered. The corresponding mode shapes are displayed in Figs. 3.12-3.14.

| Freq. | Shear Theory | | Bending Theory | | Shear-Bending | |
|---|---|---|---|---|---|---|
| | Empty | Full | Empty | Full | Empty | Full |
| 1st | 2.59 | 2.04 | 1.99 | 1.57 | 1.60 | 1.26 |
| 2nd | 5.95 | 5.18 | 4.86 | 4.23 | 3.72 | 3.21 |
| 3rd | 9.41 | 8.56 | 8.23 | 7.45 | 6.28 | 5.73 |

TABLE 3.3. Normalized Natural Frequencies

### 3.3.2. Response to Earthquake Ground Motion

In this section, a method for analyzing the earthquake response of dams of arbitrary cross-sections is presented. The method is based on superposition of the free lateral vibrational modes obtained by a finite element approach. A procedure for computing the natural modes of vibration was given in preceding sections.

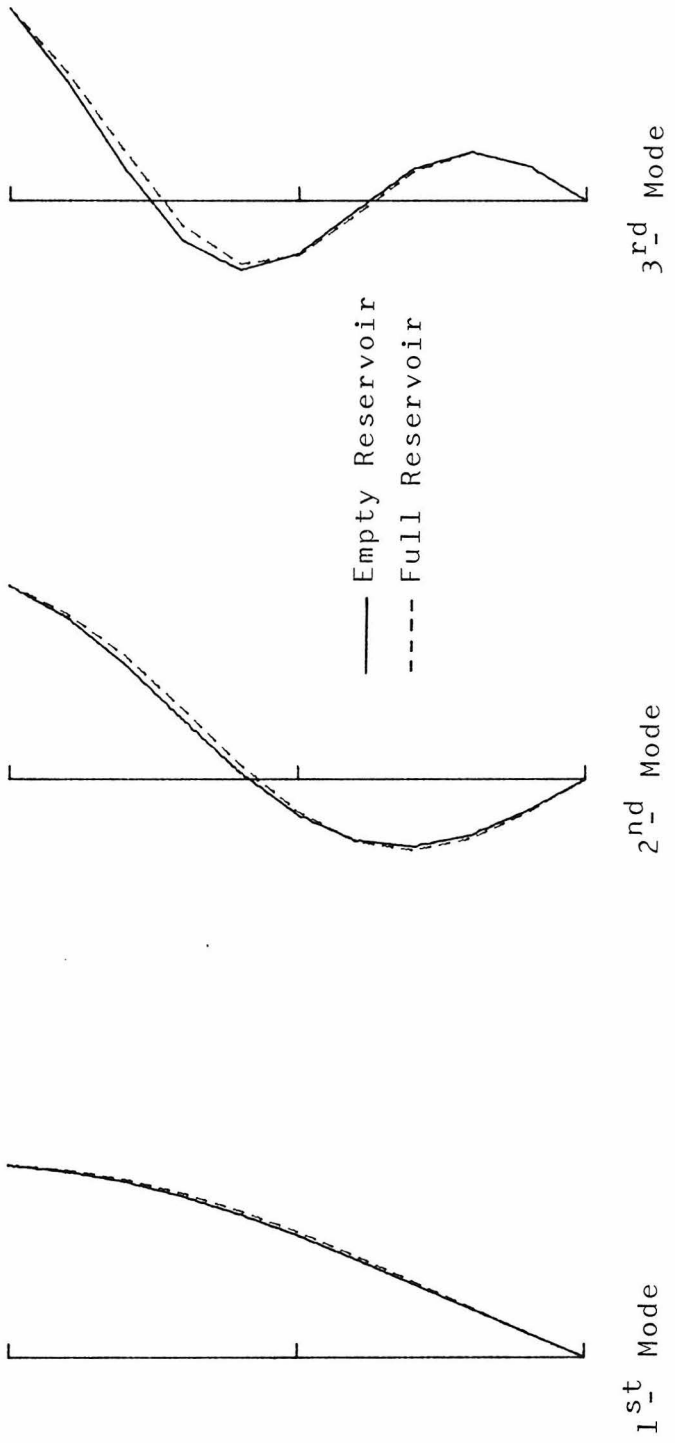


Fig. 3.12 Mode Shapes of Vibration, Shear Theory

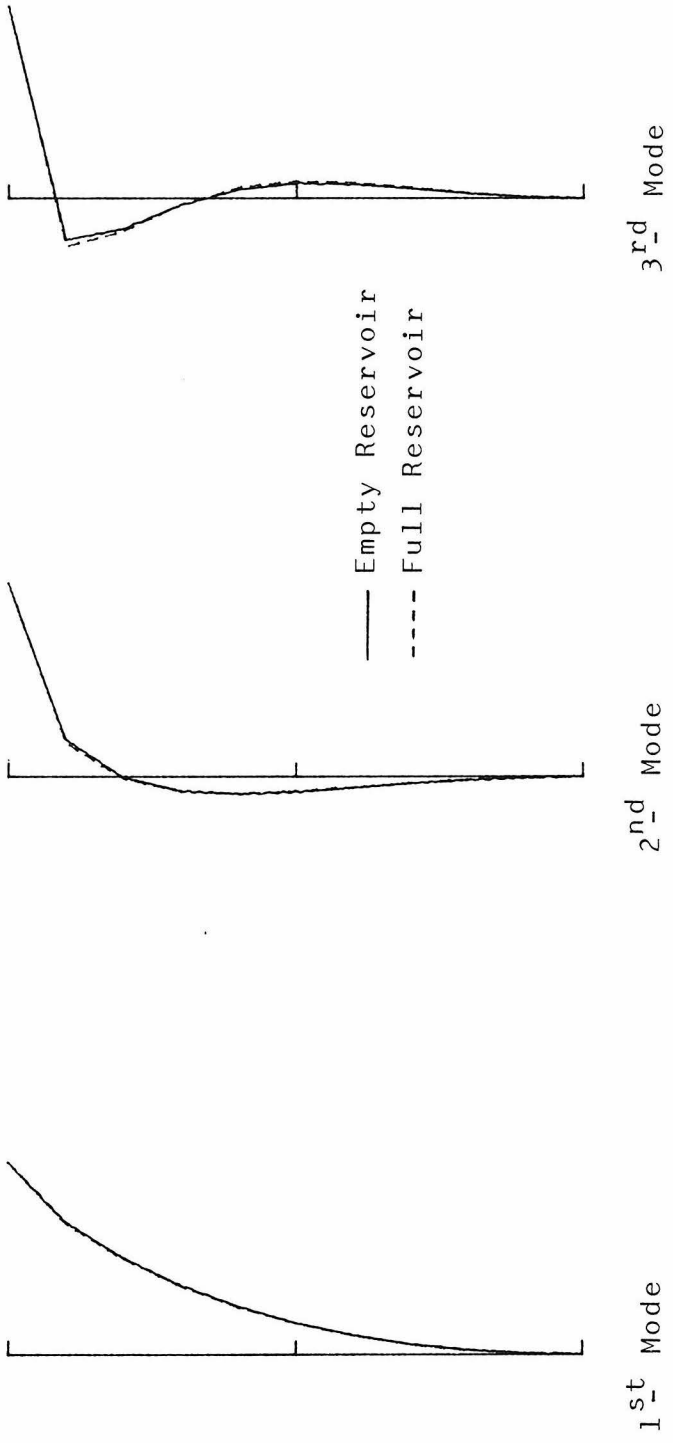


Fig. 3.13 Mode Shapes of Vibration, Bending Theory

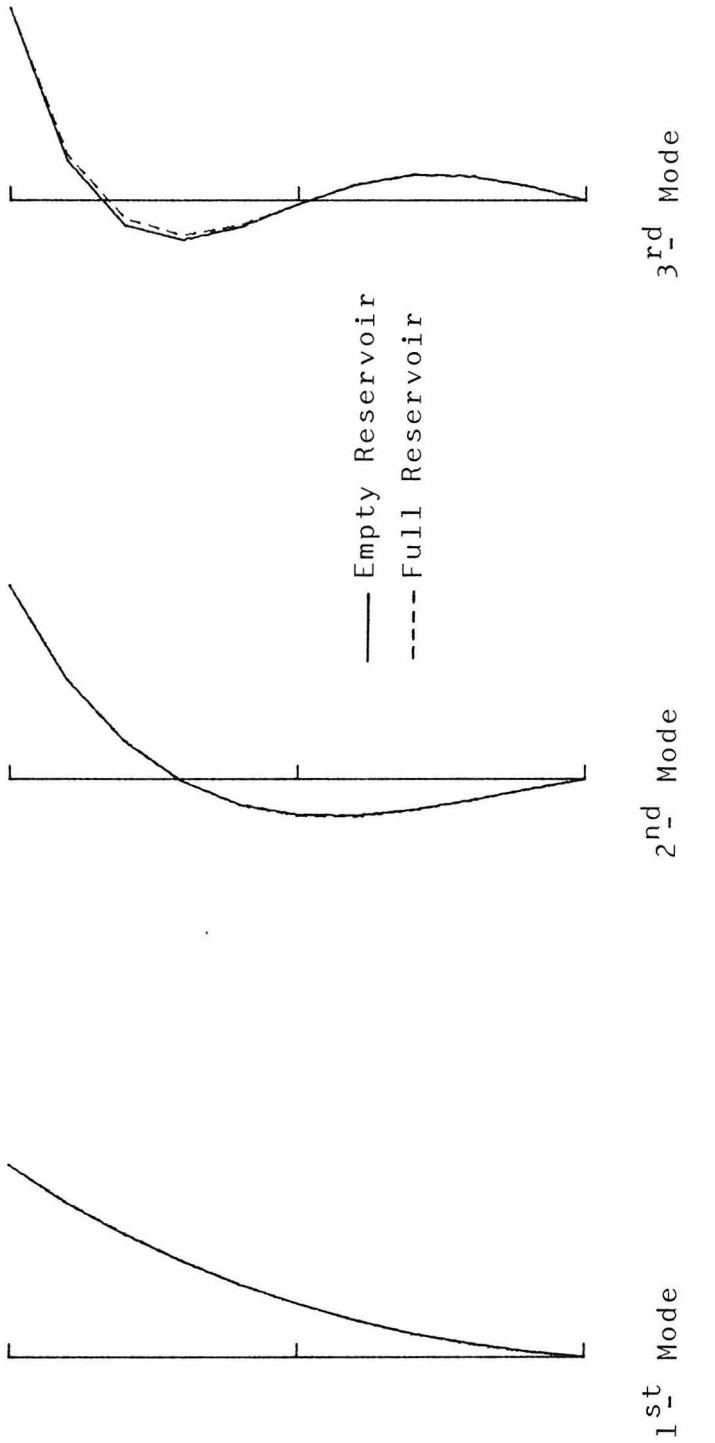


Fig. 3.14 Mode Shapes of Vibration, Shear-Bending Theory

The analysis is done in two steps: 1) the effective load resulting from the prescribed ground motion is evaluated and entered, as a force vector, in the R.H.S. of the matrix equation of motion, and 2) a modal analysis is used to reduce this matrix equation into a set of equations, each of which can be independently solved.

3.3.2.1. The Effective Force Vector

When a ground acceleration $\ddot{u}_g(t)$, in the direction normal to the dam axis, is applied to the base of the dam, its resulting total displacement will be the sum of two components: (1) the relative (or deformational) displacement u(z,t), and (2) the rigid body displacement which equals the ground displacement $u_g(t)$.

The external forces acting on the dam due to ground motion $u_g(t)$ include:

i) the distributed inertia force of the dam, which is given by

$$\rho\, d(z)\, \ddot{u}_g(t) \tag{3.103}$$

ii) the hydrodynamic pressure on the upstream face of the dam, due to its rigid motion. This is denoted by $p_g(z,t)$ and given by Eq. 3.24.

iii) the hydrodynamic pressure on the upstream face of the dam, due to its relative displacement. This is denoted by p(z,t) and given by Eq. 3.2.

Now, the differential equation governing the dam motion in the case under consideration can be obtained by inserting the first and second components of the external force, with minus sign, into the R.H.S. of the equation governing the free vibration of the dam, namely Eqs. 3.51, 3.80 and 3.91 for the cases of shear, bending and shear-bending theories, respectively. It is noted that the third component is readily incorporated in the free vibration equation.

The effective force vector to be entered in the R.H.S. of the matrix equation of motion, Eq. 3.76, is obtained from the first and second force components as follows:

a) Inertia Force

Multiplying the term in Eq. 3.103 by the variational function v(z) and integrating between 0 and H, one obtains:

$$\int_0^H v(z)\ \rho d(z)\ \ddot{u}_g(t)\ dz$$

Discretizing and carrying on the process, the above equation yields:

$$\left(\{Q\}^T\ \{L^{(1)}\}\right)\ddot{u}_g(t) \tag{3.104}$$

where {Q} is given by Eq. 3.64, and

$$\{L^{(1)}\} = \sum_{e=1}^{NH} \{\ell^{(1)}\}_e \tag{3.105}$$

in which

$$\{\ell^{(1)}\}_e = \int_0^{h_e} \rho d(\bar{z}) \{N(\bar{z})\} d\bar{z} \tag{3.106}$$

b) Hydrodynamic Force

Multiplying Eq. 3.24 by v(z) and integrating, one gets:

$$\int_0^{H_\ell} 2\rho_\ell H_\ell \ddot{u}_g(t) \left[ \sum_{m=1}^{\infty} \frac{(-1)^{m+1}}{\eta_m^2} v(z) \cos\left(\eta_m \frac{z}{H_\ell}\right) \right] dz$$

which, upon discretization and carrying on the process, eventually leads to:

$$\left(\{Q\}^T \{L^{(2)}\}\right) \ddot{u}_g(t) \tag{3.107}$$

where

$$\{L^{(2)}\} = 2\rho_\ell H_\ell \sum_{m=1}^{\infty} \frac{(-1)^{m+1}}{\eta_m^2} \{F^{(m)}\}$$

with $\{F^{(m)}\}$ as defined in Eq. 3.71.

Now, the effective force vector can be defined as:

$$\{P_{eff}\} = - \{L\} \ddot{u}_g(t) \tag{3.108}$$

where $\{L\} = \{L^{(1)}\} + \{L^{(2)}\}$.

Finally, the matrix equation which governs the earthquake response of the undamped dam-reservoir system is obtained by inserting the effective force vector, Eq. 3.108, into the R.H.S. of Eq. 3.76, resulting in:

$$[M]\{\ddot{R}\} + [K]\{R\} = - \{L\} \ddot{u}_g(t) \tag{3.109}$$

3.3.2.2. Modal Analysis

Eq. 3.109 can be solved directly by the step-by-step numerical integration method [37]. However, as discussed previously, it is more efficient to use modal superposition to evaluate the earthquake response of linear structures. Let

$$\{R(t)\} = [\Phi]\ \{Y(t)\} \tag{3.110}$$

where $[\Phi]$ is a rectangular matrix of order NXJ which contains the modal displacement vectors associated with the lowest J natural frequencies, N is the number of degrees of freedom, and $\{Y(t)\}$ is the modal amplitude vector.

Substituting from Eq. 3.110 into Eq. 3.109 and premultiplying by $[\Phi]^T$, one obtains:

$$[M^*]\ \{\ddot{Y}\} + [K^*]\ \{Y\} = -\ \{L^*\}\ \ddot{u}_g(t) \tag{3.111}$$

where $[M^*]$ and $[K^*]$ are the generalized mass and stiffness matrices, respectively, of order $J \times J$; and $\{L^*\}\ \ddot{u}_g(t)$ is the generalized force vector of order $J \times 1$.

Because of the orthogonality conditions of the natural modes, namely,

$$\{\phi\}_i^T\ [M]\ \{\phi\}_j = \{\phi\}_i^T\ [K]\ \{\phi\}_j = 0 \qquad (i \neq j) \tag{3.112}$$

the generalized mass and stiffness matrices are diagonal. Furthermore, the diagonal terms of the generalized stiffness matrix can be written as:

$$K^*_{jj} = \omega_j^2 M^*_{jj} = \omega_j^2 \{\phi\}_j^T [M] \{\phi\}_j \qquad ; j = 1,2,\ldots,J \tag{3.113}$$

Therefore, Eq. 3.111 reduces to J independent differential equations for the unknowns $Y_j(t)$

$$\ddot{Y}_j + \omega_j^2 Y_j = -\frac{L^*_j}{M^*_{jj}} \ddot{u}_g(t) \qquad ; j = 1,2,\ldots,J \tag{3.114}$$

Introducing damping into Eq. 3.114, one can rewrite such equation as follows:

$$\ddot{Y}_j + 2\zeta_j\omega_j\dot{Y}_j + \omega_j^2 Y_j = -b_j \ddot{u}_g(t) \qquad ; j = 1,2,\ldots,J \tag{3.115}$$

where $b_j = L^*_j/M^*_{jj}$ are the modal participation factors. Eq. 3.115 is identical to Eq. 3.43, and its solution can be found by using either the convolution integral or the step-by-step integration, both discussed in section 3.2.3.1.

# CHAPTER IV

# FLUID-STRUCTURE INTERACTION FOR SHORT DAMS OR WALLS

## 4.1. Introduction

In analytically analyzing the dynamic response of concrete gravity dams, most work to date has considered the dam to be infinitely long, an assumption which simplifies the problem to one in two dimensions. This would be expected to be satisfactory for dams of length B, relatively large as compared to their height H. Judgment and intuition would indicate that a two dimensional solution would err considerably for a system with relatively small B/H. This conclusion is supported by the results of a vibration experiment done by A. Selby and R.T. Severn [10] on a wall of B/H = 2.0, storing a body of water. A quick review of the gravity dams existing in the United States, as given by T.W. Mermel [11], reveals that a considerable number have small B/H ratios. Thus, it is important to develop a procedure for the dynamic analysis of short length dams or walls so that the significance of the B/H ratio can be evaluated.

A free vibration analysis of the dam-reservoir system is carried out neglecting water compressibility, with the dam modeled by both the shear theory and the bending theory. The natural frequencies and the associated mode shapes are found using the Rayleigh-Ritz method. The effects of the presence of the water and of the B/H ratio, on these dynamic properties are studied.

A forced vibration analysis is carried out, in which the Assumed-Modes method is used to obtain the dam response to all three components of the ground motion. Taking water compressibility into consideration, and assuming harmonic ground motions, frequency domain responses of the dam are obtained. The effects of the reservoir presence, the water compressibility, the dam-reservoir interaction, and the B/H ratio on these responses are illustrated.

## 4.2. Free Vibration

Consider a dam of rectangular cross-section and of finite length, as shown in Fig. 4.1. In this case, the dam deformation u(y,z,t) will be a function of the y and z coordinates, and time. With assumptions about the water and the reservoir boundaries made as in Chapter II, one may use here the formulas derived previously for the hydrodynamic pressure.

Assuming the dam to vibrate freely with no ground motion applied to its base, its natural frequencies and mode shapes are determined under an incompressible water assumption. The structural deformations of the dam are modeled by two different theories: 1) a pure shear theory, and 2) a pure bending theory.

### 4.2.1. Shear Theory

Neglecting any bending effects and considering only shear deformations, the differential equation governing the lateral (out-of-plane) vibration of the dam is written as follows:

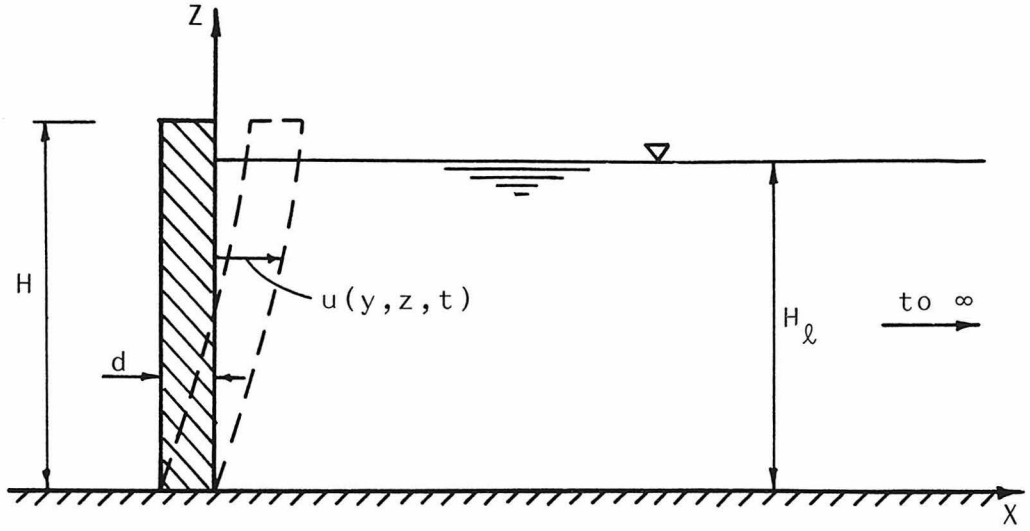


(a) Sectional Elevation

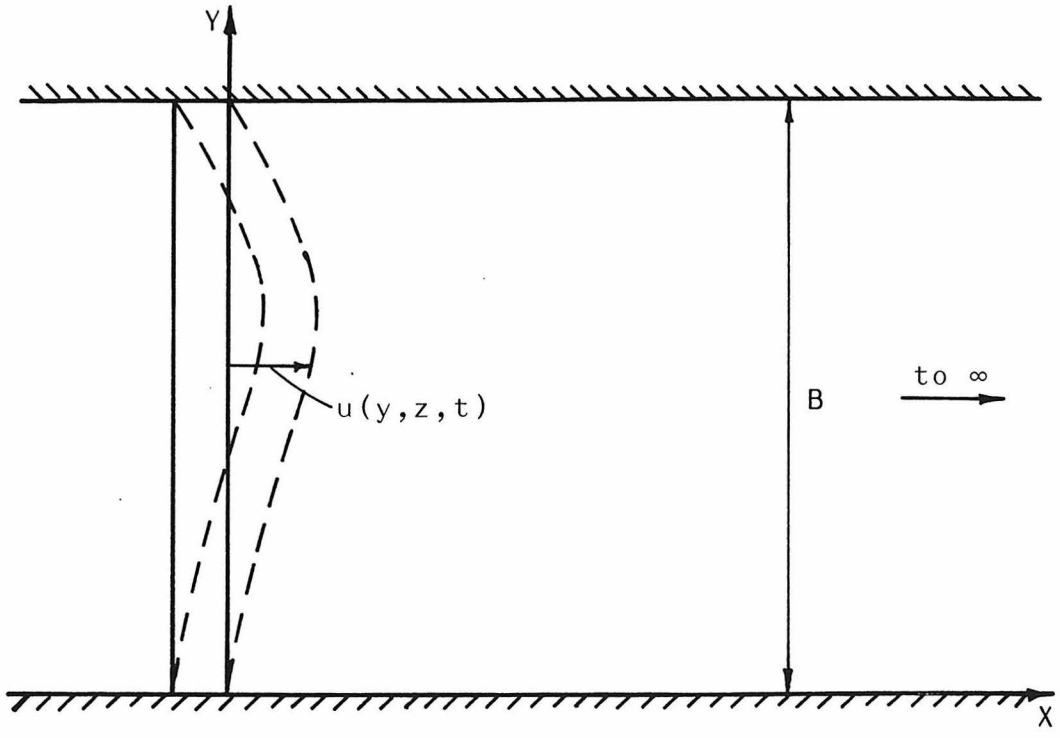


(b) Plan View

Fig. 4.1 Dam-Reservoir and Coordinate System

$$\left.\begin{aligned} \rho d \frac{\partial^2 u(y,z,t)}{\partial t^2} - Gd \nabla^2 u(y,z,t) &= -p(y,z,t) \quad ; \quad 0 \leq z \leq H_\ell \\ &= 0 \quad ; \quad H_\ell \leq z \leq H \end{aligned}\right\} \tag{4.1}$$

where $\rho$, G and d are as defined previously, u(y,z,t,) is the horizontal out-of-plane displacement of the dam, and $\nabla^2$ is the Laplace operator in two dimensions, defined as:

$$\nabla^2 = \frac{\partial^2}{\partial y^2} + \frac{\partial^2}{\partial z^2} \tag{4.2}$$

p(y,z,t) is obtained from Eq. 2.49 by setting x = 0, and is given by:

$$p(y,z,t) = \frac{4\rho_\ell}{B} \left\{ \sum_{n=0}^{\infty} \sum_{m=1}^{\infty} \frac{J_{mn}}{\varepsilon_n \mu_{mn}} \cos\left(\beta_n \frac{y}{B}\right) \cos\left(\eta_m \frac{z}{H_\ell}\right) \right\} \tag{4.3}$$

Equation 4.1 is solved approximately by using the Rayleigh-Ritz method [38] in which the dam deformation is expressed as a linear combination of N admissible functions, as follows:

$$u(y,z,t) = \left[ \sum_{j=1}^{N} e_j \Psi_j \left( \frac{y}{B}, \frac{z}{H} \right) \right] \exp(i\omega t) \tag{4.4}$$

where the $\Psi_j$ are known functions of the spatial coordinates satisfying only the geometric boundary conditions, and $e_j$ are unknown coefficients to be determined.

Substituting Eqs. 4.3 and 4.4 into Eq. 4.1, constructing and minimizing the Rayleigh's quotient, one eventually obtains an eigenvalue problem of the form:

$$\left[ -\omega^2 \left[ [M_d] + [M_\ell] \right] + [K] \right] \{E\} = 0 \tag{4.5}$$

where $\omega$ is the frequency of vibration, $\{E\}$ is the vector of unknown coefficients $e_j$, and $[K]$, $[M_d]$ and $[M_\ell]$ are the stiffness, mass and added mass matrices, the elements of which are given by:

$$k_{ij} = -G\, d \int_0^H \int_0^B \Psi_i \nabla^2 \Psi_j \, dydz \tag{4.6}$$

$$(m_d)_{ij} = \rho\, d \int_0^H \int_0^B \Psi_i \Psi_j \, dydz \tag{4.7}$$

$$(m_\ell)_{ij} = 4 \frac{\rho_\ell}{B} \sum_{n=0}^{\infty} \sum_{m=1}^{\infty} \frac{I^i_{mn} I^j_{mn}}{\varepsilon_n \mu_{mn}} \tag{4.8}$$

where

$$I^i_{mn} = \int_0^{H_\ell} \int_0^B \Psi_i \cos\left(\beta_n \frac{y}{B}\right) \cos\left(\eta_m \frac{z}{H_\ell}\right) dydz \tag{4.9}$$

Solution of Eq. 4.5 yields the natural frequencies $\omega_i$ and the eigenvectors $\{E^{(i)}\}$. The associated mode shapes are given by:

$$\Phi_i\left(\frac{y}{B}, \frac{z}{H}\right) = \sum_{j=1}^{N} e_j^{(i)} \Psi_j\left(\frac{y}{B}, \frac{z}{H}\right) \tag{4.10}$$

4.2.2. Bending Theory

In this case, the governing equation is stated as:

$$\left.\begin{aligned} \rho d \frac{\partial^2 u(y,z,t)}{\partial t^2} + \frac{Ed^3}{12(1-\nu^2)} \nabla^4 u(y,z,t) &= -p(y,z,t) \quad ; 0 \le z \le H_\ell \\ &= 0 \quad ; H_\ell \le z \le H \end{aligned}\right\} \tag{4.11}$$

where $\rho, E, \nu$ and $d$ are as defined previously, and

$$\nabla^4 = \frac{\partial^4}{\partial y^4} + 2\,\frac{\partial^4}{\partial y^2 \partial z^2} + \frac{\partial^4}{\partial z^4} \tag{4.12}$$

and $p(y,z,t)$ as given by Eq. 4.3.

Using the Rayleigh-Ritz method, an eigenvalue problem similar to the one given in Eq. 4.5 is obtained. The elements of the mass and added mass matrices are defined as in Eqs. 4.7 and 4.8, while the elements of the stiffness matrix are given by:

$$k_{ij} = \frac{Ed^3}{12(1-\nu^2)} \int_0^H \int_0^B \Psi_i \, \nabla^4 \, \Psi_j \; dydz \tag{4.13}$$

4.2.3. Numerical Examples

The method of analysis described in the previous two sections is applied to a dam whose thickness to height ratio and material properties are as given in section 3.2.1.3. The four prescribed shapes given by Eq. 2.63, and illustrated in Figs. 2.14 and 2.15 for the shear and bending deformations, respectively, are used as admissible functions.

The natural frequencies of a dam having a B/H ratio of 2.0 are calculated for both an empty and a full reservoir. The results, normalized by the fundamental frequency of the full reservoir, are presented in Tables 4.1 and 4.2, for the shear and bending theories, respectively.

| Frequency | 1st | 2nd | 3rd | 4th |
|---|---|---|---|---|
| Empty Reservoir | 2.39 | 3.79 | 5.35 | 6.11 |
| Full Reservoir | 2.07 | 3.39 | 4.75 | 5.56 |

TABLE 4.1. Normalized Natural Frequencies (Shear)

| Frequency | 1st | 2nd | 3rd | 4th |
|---|---|---|---|---|
| Empty Reservoir | 1.22 | 3.03 | 4.72 | 6.15 |
| Full Reservoir | 1.11 | 2.83 | 4.18 | 5.58 |

TABLE 4.2. Normalized Natural Frequencies (Bending)

The effect of the length to height ratio is studied by computing the normalized natural frequencies of dams having a B/H ratio ranging between 1.0 and 10.0. For an empty reservoir, these values are given in Table 4.3. It is observed that the frequencies increase as B/H decreases. This is better illustrated in Fig. 4.2, where the 1st and 2nd dam frequencies are plotted versus B/H, for both the shear and bending theories. For a shear model, the fundamental frequency of a dam having a B/H of 2.0 is 41% larger than that of an infinitely long dam. When B/H = 5.0, the increase is only 7.7%. For a bending model, a B/H = 2.0 dam has a fundamental frequency which is 82% larger than that of an infinitely long dam. The increase is 1.5% when B/H = 5.0.

| | B/H | 1.0 | 2.0 | 3.0 | 5.0 | 10.0 | ∞ |
|---|---|---|---|---|---|---|---|
| Shear | 1st | 3.79 | 2.39 | 2.04 | 1.82 | 1.73 | 1.69 |
| Theory | 2nd | 6.11 | 3.79 | 2.82 | 2.17 | 1.82 | - |
| Bending | 1st | 4.36 | 1.22 | 0.79 | 0.68 | 0.67 | 0.67 |
| Theory | 2nd | 6.96 | 3.03 | 1.42 | 0.77 | 0.68 | - |

TABLE 4.3. Normalized Natural Frequencies (Empty Reservoir)

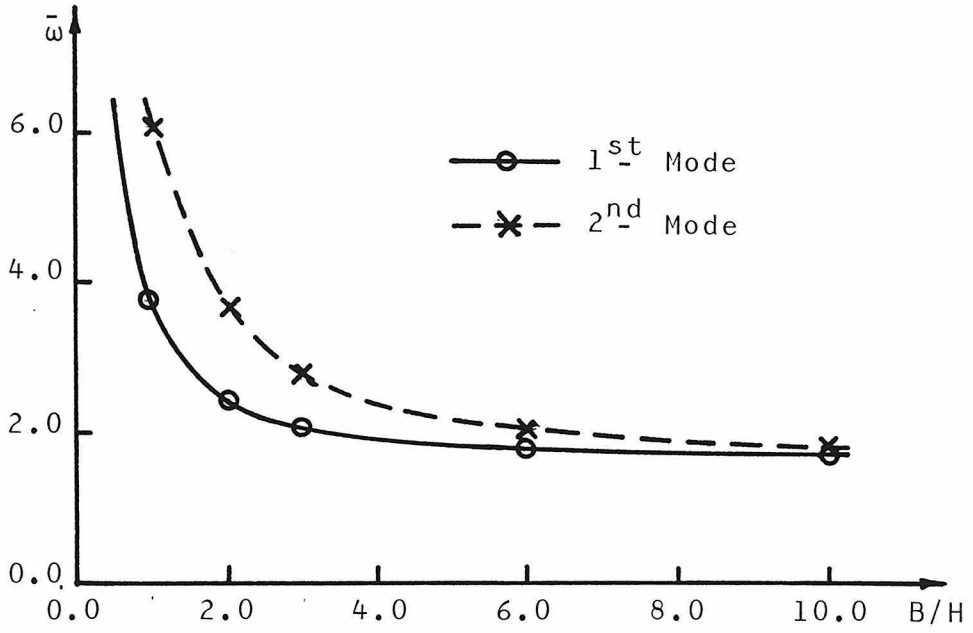


(a) Shear Theory

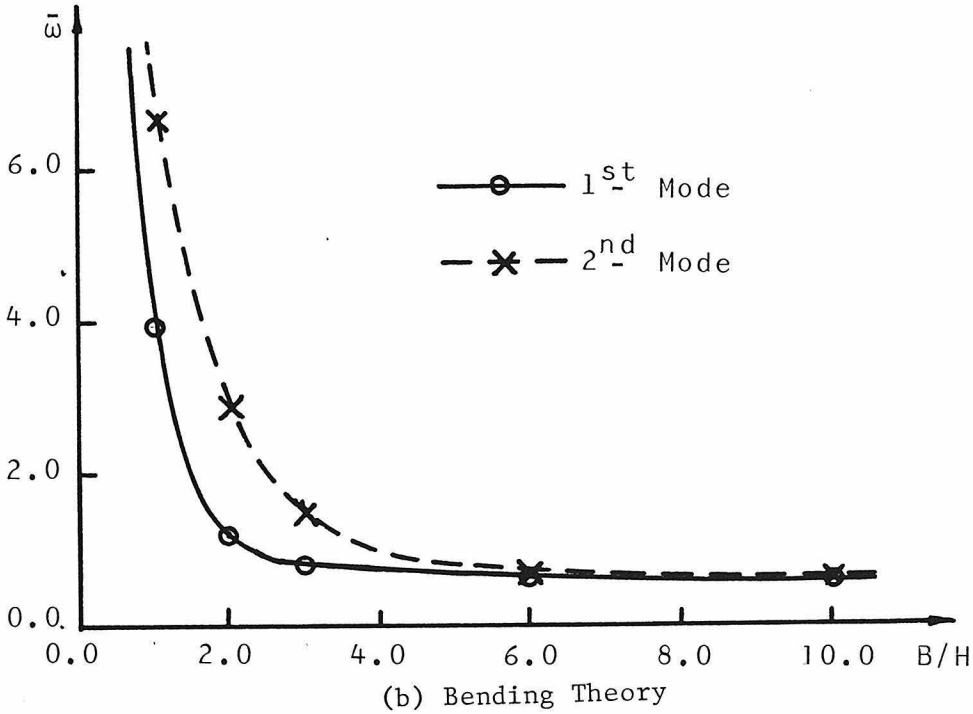


(b) Bending Theory

Fig. 4.2 Effect of B/H on Natural Frequencies

## 4.3. Forced Vibration: Harmonic Ground Motion

In this section, the problem of a dam forced into motion by a ground displacement applied to its base, is studied. All three components of ground motion are considered. These are: 1) longitudinal component (in the upstream-downstream direction), 2) transverse component (in the cross-stream direction), and 3) vertical component. Only the case of dams modeled by the shear theory is presented. The analysis, for the case of bending theory, is exactly the same except that the stiffness term of the equation of motion should be changed as discussed in the free vibration problem. This leads to a different definition of the elements of the stiffness matrix arising in the resulting matrix equation of motion. The water compressibility is taken into consideration. The applied ground motion is assumed to be harmonic, thus the analysis leads to the dam response in the frequency domain.

Approximate solutions to the governing differential equations are obtained through the use of the Assumed-Modes method [39]. This method is the extension, to the forced vibration case, of the Rayleigh-Ritz method discussed in conjunction with the free vibration problem.

### 4.3.1. Longitudinal Ground Motion

Let the dam be subjected to a ground acceleration $\ddot{u}_g(t)$ in the upstream-downstream direction. The differential equation governing its

deformation is given by:

$$\rho d \frac{\partial^2 u(y,z,t)}{\partial t^2} - Gd\nabla^2 u(y,z,t) =$$

$$\left.\begin{aligned} &= -\rho d\, \ddot{u}_g(t) - p_{gx}(z,t) - p(y,z,t) && ;\ 0 \leq z \leq H_\ell \\ &= -\rho d\, \ddot{u}_g(t) && ;\ H_\ell \leq z \leq H \end{aligned}\right\} \quad (4.14)$$

where $p(y,z,t)$ and $p_{gx}(z,t)$ are the hydrodynamic pressures resulting from the vibrational and rigid motions of the dam, respectively. For harmonic excitation as given by Eq. 3.25, these are frequency dependent and are obtained from Eqs. 2.44 and 2.24 by setting $x = 0$.

Expressing the dam deformation in the form given by Eq. 4.4, substituting into Eq. 4.14, multiplying by $\Psi_j$ ($j = 1,2,\ldots N$), and integrating over the dam face, one ends up with the following matrix equation of motion:

$$\left[\omega^2 \left[ [M_d] + [M_\ell] \right] + [K]\right]\{E\} = -\{F^I\} - \{F^x\} \quad (4.15)$$

where the elements of the mass and stiffness matrices, $[M_d]$ and $[K]$, are as defined in the previous section, and $\{E\}$ is the vector of the generalized coordinate displacements $e_j$. $[M_\ell]$ is the frequency dependent added mass matrix, whose elements are given by:

$$(m_\ell)_{ij} = \frac{4\rho_\ell}{B}\left\{-i\sum_{n=0}^{\infty}\sum_{m=1}^{m_n-1} \frac{I^i_{mn}\, I^j_{mn}}{\varepsilon_n \bar{\delta}_{mn}} + \sum_{n=0}^{\infty}\sum_{m=m_n}^{\infty} \frac{I^i_{mn}\, I^j_{mn}}{\varepsilon_n \delta_{mn}}\right\} \quad (4.16)$$

in which $I^i_{mn}$ is as given by Eq. 4.9. $\{F^I\}$ is the inertia load vector,

whose elements are given by:

$$f_j^I = \rho d\, a_g \int_0^H \int_0^B \Psi_j \, dydz \tag{4.17}$$

$\{F^x\}$ is the frequency dependent added load vector, the elements of which are defined as:

$$f_j^x = 2\rho_\ell H_\ell \, a_g \left\{ -i \sum_{m=1}^{m_0-1} \frac{(-1)^{m+1} I_{m0}^j}{\eta_m \bar{\delta}_{m0}} + \sum_{m=m_0}^{\infty} \frac{(-1)^{m+1} I_{m0}^j}{\eta_m \delta_{m0}} \right\} \tag{4.18}$$

in which

$$I_{m0}^j = \int_0^{H_\ell} \int_0^B \Psi_j \cos\left(\eta_m \frac{z}{H_\ell}\right) dydz \tag{4.19}$$

4.3.2. Transverse Ground Motion

Consider the case in which the dam-reservoir system is subjected to a cross-stream ground acceleration $\ddot{v}_g(t)$. For harmonic motion, this is expressed as:

$$\ddot{v}_g(t) = a_g \cdot \exp(i\omega t) \tag{4.20}$$

The dam motion will be governed by Eq. 4.14, with the inertia term on the R.H.S. dropped, and $p_{gx}(z,t)$ replaced by $p_{gy}(y,z,t)$, which is the hydrodynamic pressures acting on the dam, assumed as rigid, due to the motion of the reservoir banks. This is obtained from Eq. 2.59, by replacing $(-\bar{v}_g\omega^2)$ by $a_g$.

When applied to the governing differential equation, the Assumed-Modes method will yield the following matrix equation:

$$\left[-\omega^2 \left[[M_d] + [M_\ell]\right] + [K]\right]\{E\} = -\{F^y\} \tag{4.21}$$

The L.H.S. is exactly the same as in Eq. 4.15, while $\{F^y\}$ is the added load vector, whose elements are:

$$f_j^y = 2\rho_\ell H_\ell a_g \left\{ \sum_{m=1}^{m_0-1} \frac{(-1)^{m+1} \bar{J}_{m0}^j}{\eta_m \bar{\delta}_{m0}} + \sum_{m=m_0}^{\infty} \frac{(-1)^{m+1} J_{m0}^j}{\eta_m \delta_{m0}} \right\} \tag{4.22}$$

$$\left.\begin{aligned} \bar{J}_{m0}^j &= \frac{1}{\cos(B\bar{\delta}_{m0}/2H_\ell)} \int_0^{H_\ell} \int_0^B \Psi_j \cdot \sin\left[\bar{\delta}_{m0}(\tfrac{B}{2} - y)/H_\ell\right] \cdot \cos\left(\eta_m \tfrac{z}{H_\ell}\right) dydz \\ J_{m0}^j &= \frac{1}{\cosh(B\delta_{m0}/2H_\ell)} \int_0^{H_\ell} \int_0^B \Psi_j \cdot \sinh\left[\delta_{m0}(\tfrac{B}{2} - y)/H_\ell\right] \cdot \cos\left(\eta_m \tfrac{z}{H_\ell}\right) dydz \end{aligned}\right\} \tag{4.23}$$

4.3.3. Vertical Ground Motion

Let a harmonic vertical ground acceleration of the form:

$$\ddot{w}_g(t) = a_g \cdot \exp(i\omega t) \tag{4.24}$$

be applied to the dam-reservoir system. The equation of motion is obtained from Eq. 4.4 by dropping the inertia term, and replacing $p_{gx}(z,t)$ by $p_{gz}(z,t)$. The latter is given by Eq. 2.30, with $(-\bar{w}_g\omega^2)$ replaced by $a_g$. The resulting matrix equation is then:

$$\left[-\omega^2 \left[[M_d] + [M_\ell]\right] + [K]\right]\{E\} = -\{F^z\} \tag{4.25}$$

in which the added force vector $\{F^z\}$ has elements:

$$f_j^z = \frac{\rho_\ell H_\ell a_g}{\frac{\omega}{c}H_\ell \cdot \cos(\frac{\omega}{c}H_\ell)} \int_0^{H_\ell} \int_0^B \Psi_j \cdot \sin\left[\tfrac{\omega}{c} H_\ell (1 - \tfrac{z}{H_\ell})\right] dydz \tag{4.26}$$

A solution of Eq. 4.15 (or 4.21 or 4.25) for all values of excitation frequency $\omega$ would give the frequency domain response for the $e_j$'s which, upon substitution into Eq. 4.4, would yield the dam displacement response. 4.3.4. Numerical Examples

The method of analysis developed above is applied to a limited length dam modeled by the shear theory. The dam has a thickness to height ration of 0.4, and its material properties are as chosen in section 3.2.1.3. The four admissible functions used in the free vibration analysis, section 4.2.3., are also used here.

To study the effects of presence of the water, water compressibility, and dam-reservoir interaction on the response of the dam, five different cases are considered:

Case (1): empty reservoir.

Case (2): full reservoir, compressibility neglected, interaction neglected.

Case (3): full reservoir, compressibility neglected, interaction included.

Case (4): full reservoir, compressibility included, interaction neglected.

Case (5): full reservoir, compressibility included, interaction included.

For longitudinal ground motion, the dam response in each case is obtained by solving Eq. 4.15, after a proper specialization: In case (1), the added mass matrix $[M_\ell]$ and the added load vector $\{F^x\}$ are dropped; In cases (2) and (3), the water compressibility is neglected in calculating the elements of $[M_\ell]$ and $\{F^x\}$, with $[M_\ell]$ dropped in case (2) and kept in case (3); Cases (4) and (5) are analogous to cases (2) and (3), but with compressibility considered. Clearly, case (1) does

not exist for both the transverse and vertical motion cases in which the hydrodynamic pressure is the only loading on the dam.

A structural damping has been incorporated into the problem by adding the term ($i\omega[C]$) to the L.H.S. of the matrix equations of motion. The damping matrix [C] is chosen as:

$$[C] = \alpha[M_d] + \beta[K] \tag{4.26}$$

where $\alpha$ and $\beta$ are determined such that the fraction of critical damping $\zeta$ in the first two symmetric or antisymmetric modes be the same. A value of $\zeta = 3\%$ is taken, based on the results of the vibration test performed by D. Rea, C.Y. Liaw and A.K. Chopra [40].

For a dam of B/H = 2.0, the frequency domain responses of the generalized coordinate $e_j$'s are obtained for all five cases. The crest acceleration, at mid-span for longitudinal and vertical excitations and at quarter-span for transverse excitation, is then computed and plotted in Figs. 4.3, 4.4 and 4.5 for the x,y and z components of ground motion, respectively. Part (a) of each figure is for incompressible water, while part (b) is for compressible water. The ordinate of each plot is for the absolute value of the crest acceleration, normalized by the amplitude of ground acceleration, while the abcissa is for the excitation frequency, normalized by the fundamental frequency of the reservoir.

By examining Fig. 4.3, it is concluded that:

i) When the water compressibility is neglected, the effect of water is, with interaction neglected, to increase the response

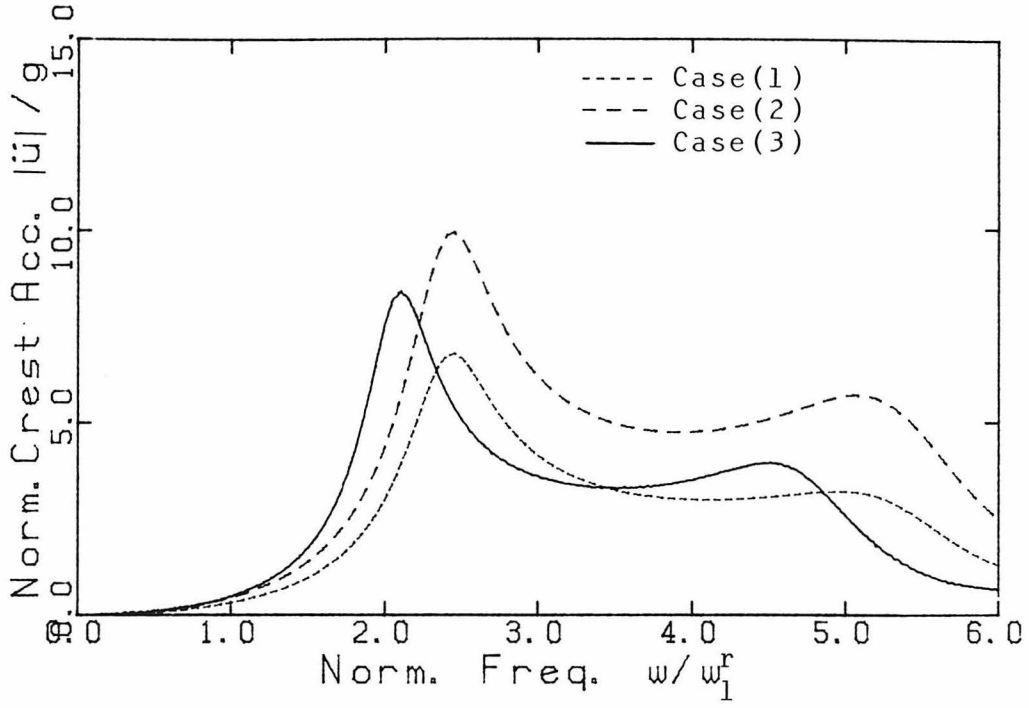


(a) Incompressible Water

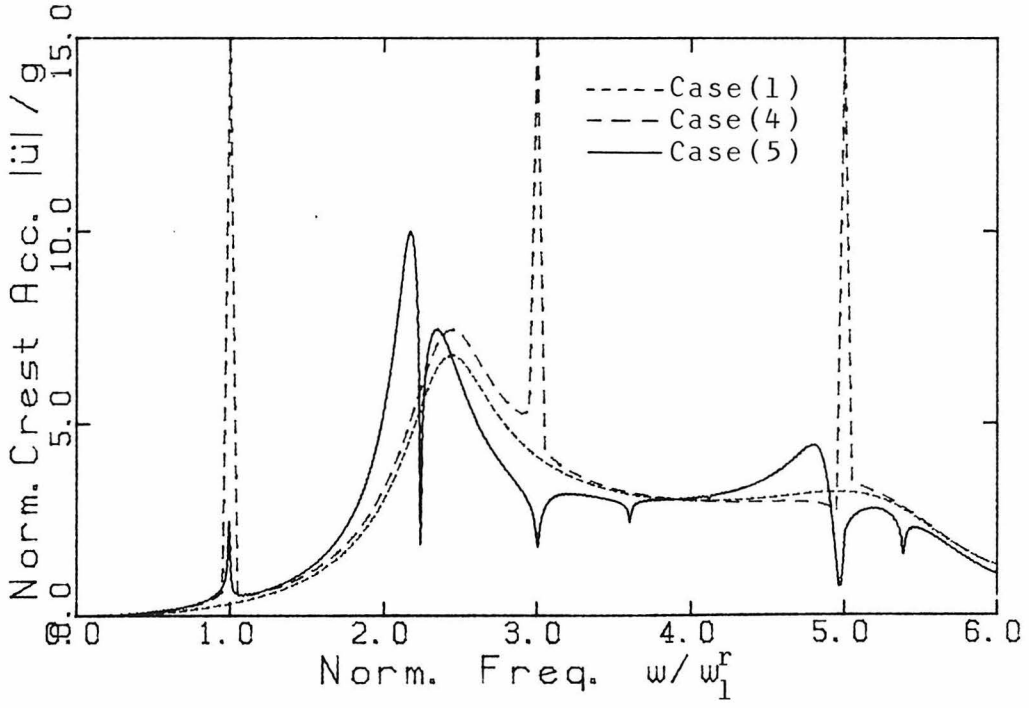


(b) Compressible Water

Fig. 4.3 Crest Acceleration Response (Longitudinal Ground Motion)

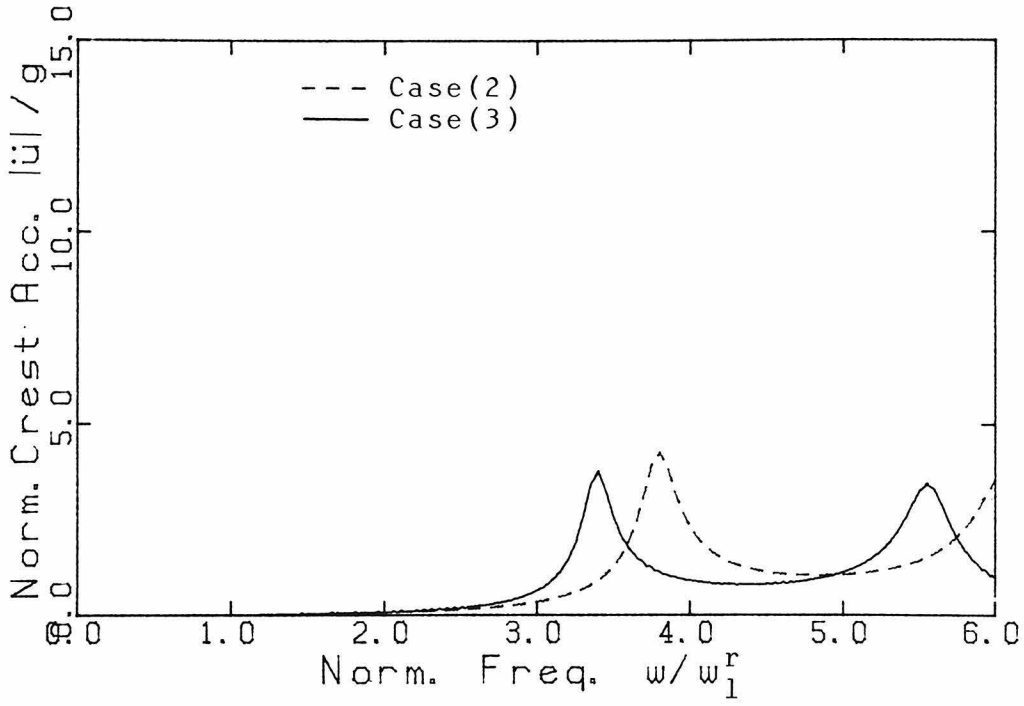


(a) Incompressible Water

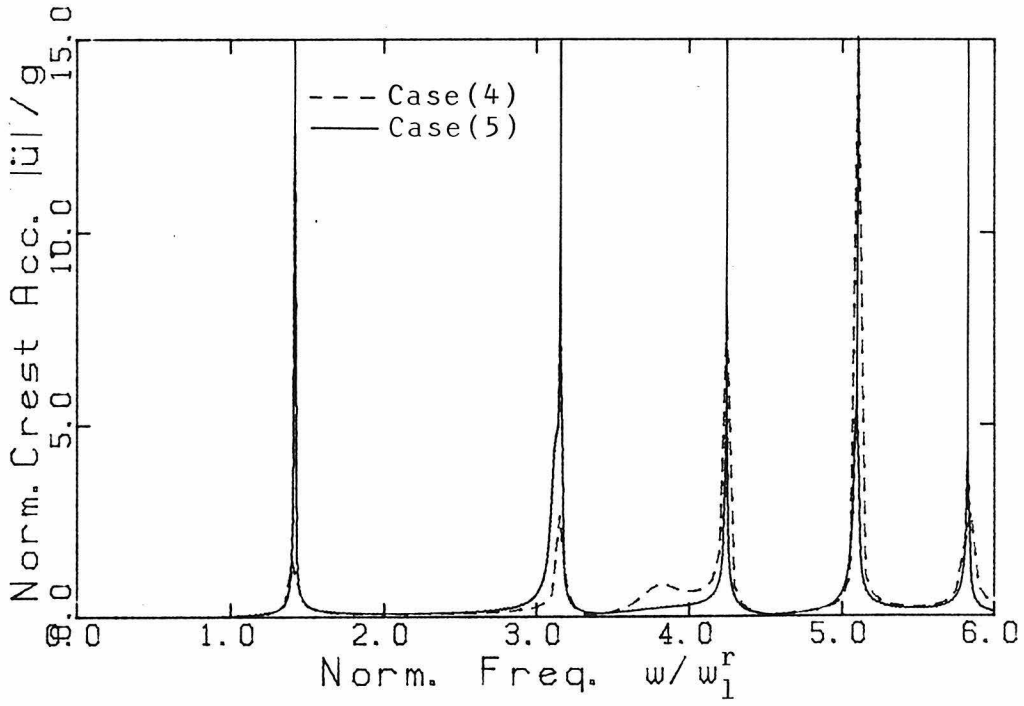


(b) Compressible Water

Fig. 4.4 Crest Acceleration Response (Transverse Ground Motion)

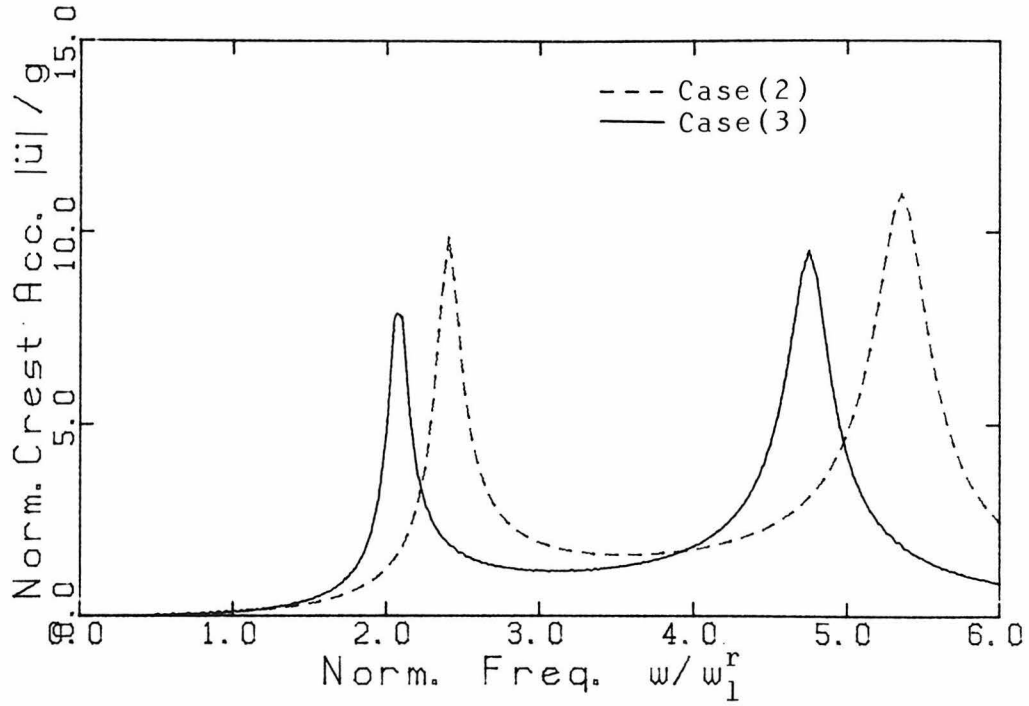


(a) Incompressible Water

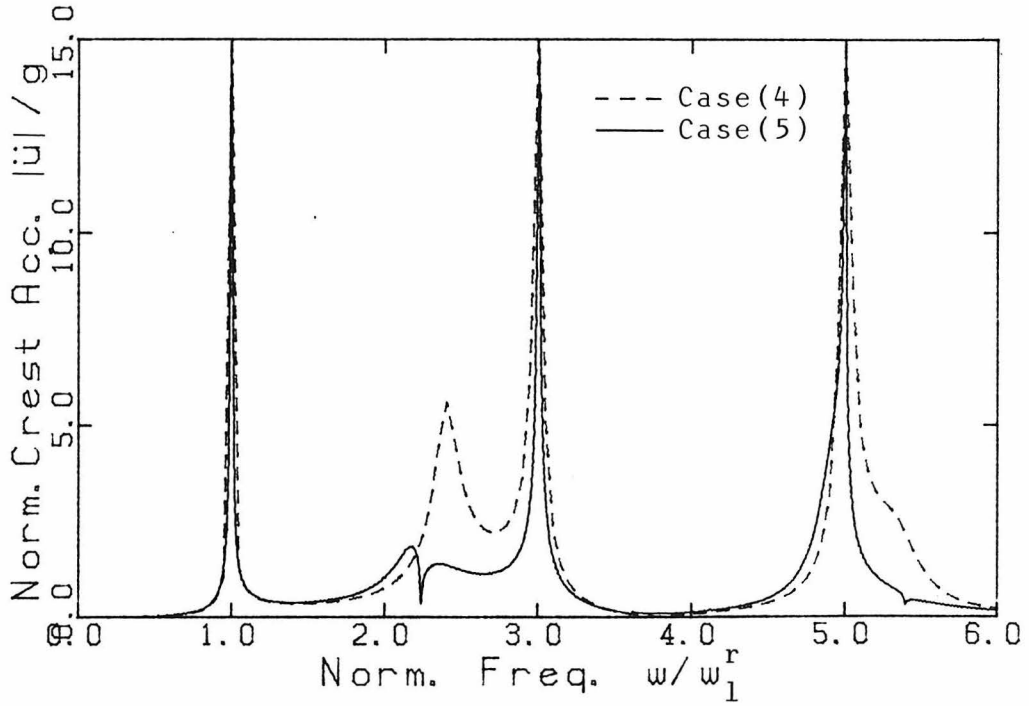


(b) Compressible Water

Fig. 4.5 Crest Acceleration Response (Vertical Ground Motion)

without any shift in the resonant frequencies. With interaction included, the resonant frequencies are reduced, with smaller increase in the response.

ii) When water compressibility is included, and interaction neglected, the response is affected locally at excitation frequencies close to the natural frequencies of the reservoir, becoming unbounded at exactly these frequencies. When interaction is included, the response changes completely, the effect of radiation damping being incorporated.

The level of contribution to the response, of each component of ground motion, is best illustrated by plotting the crest acceleration response, to all three components, on the same plot as shown in Fig. 4.6. It is concluded that the vertical component contribution is about 18% of the longitudinal component contribution. The transverse component produces, at the quarter-span, an acceleration which is roughly 1% of what the longitudinal component produces at mid-span (response values at $\bar{\omega} = 2.2$).

The effect of B/H is studied by computing the crest acceleration responses of dams having different B/H ratios. The responses to longitudinal ground motion, of dams with B/H = 1.0, 2.0, 3.0 and 5.0, are plotted in Fig. 4.7. For B/H = 2.0 and 5.0, response to transverse and vertical excitation are given in Figs. 4.8 and 4.9, respectively. It is clear how the change in B/H affects the frequency domain response, both in value and shape, which in turn

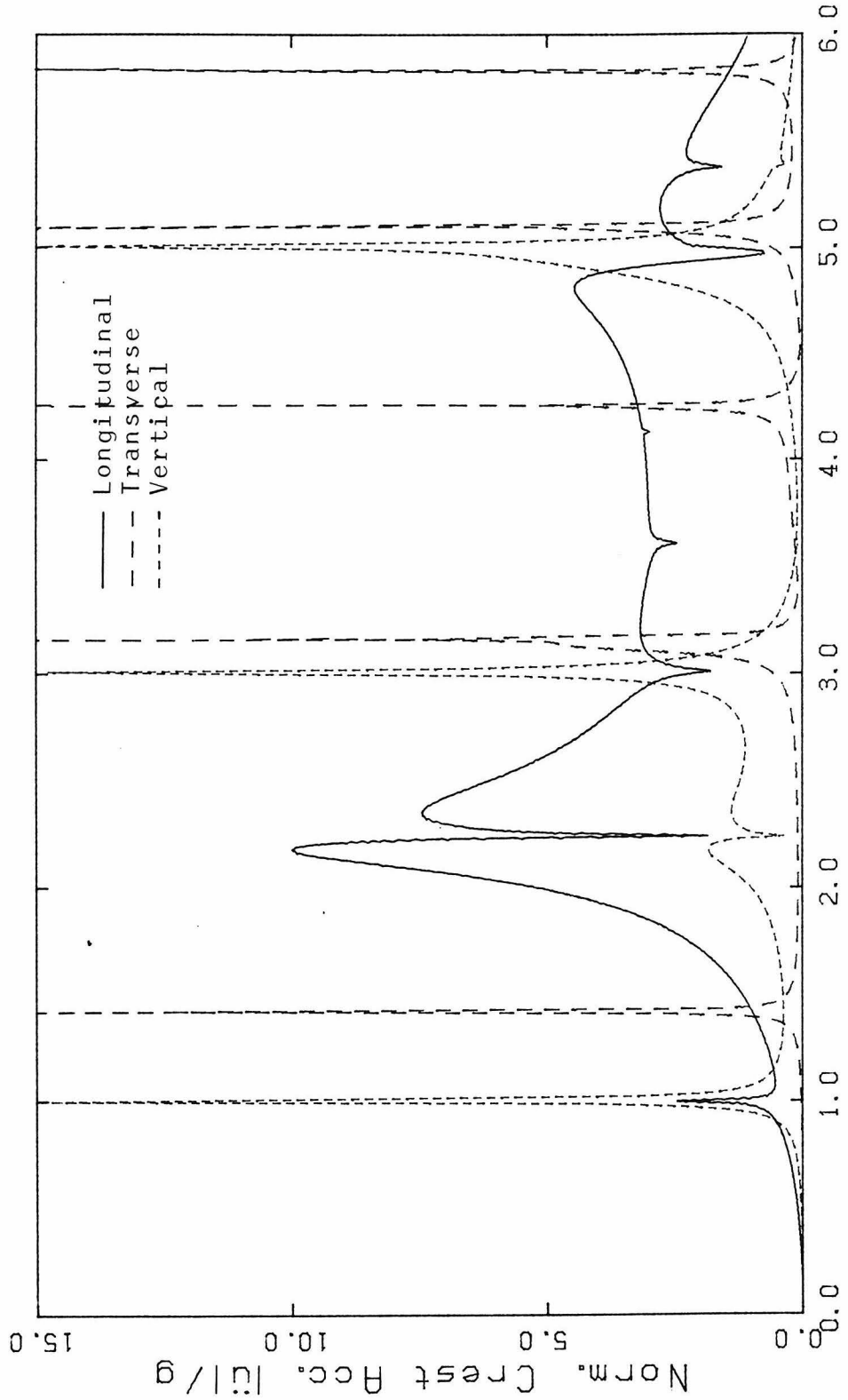


Fig. 4.6 Crest Acceleration Response (All Three Components of Ground Motion)

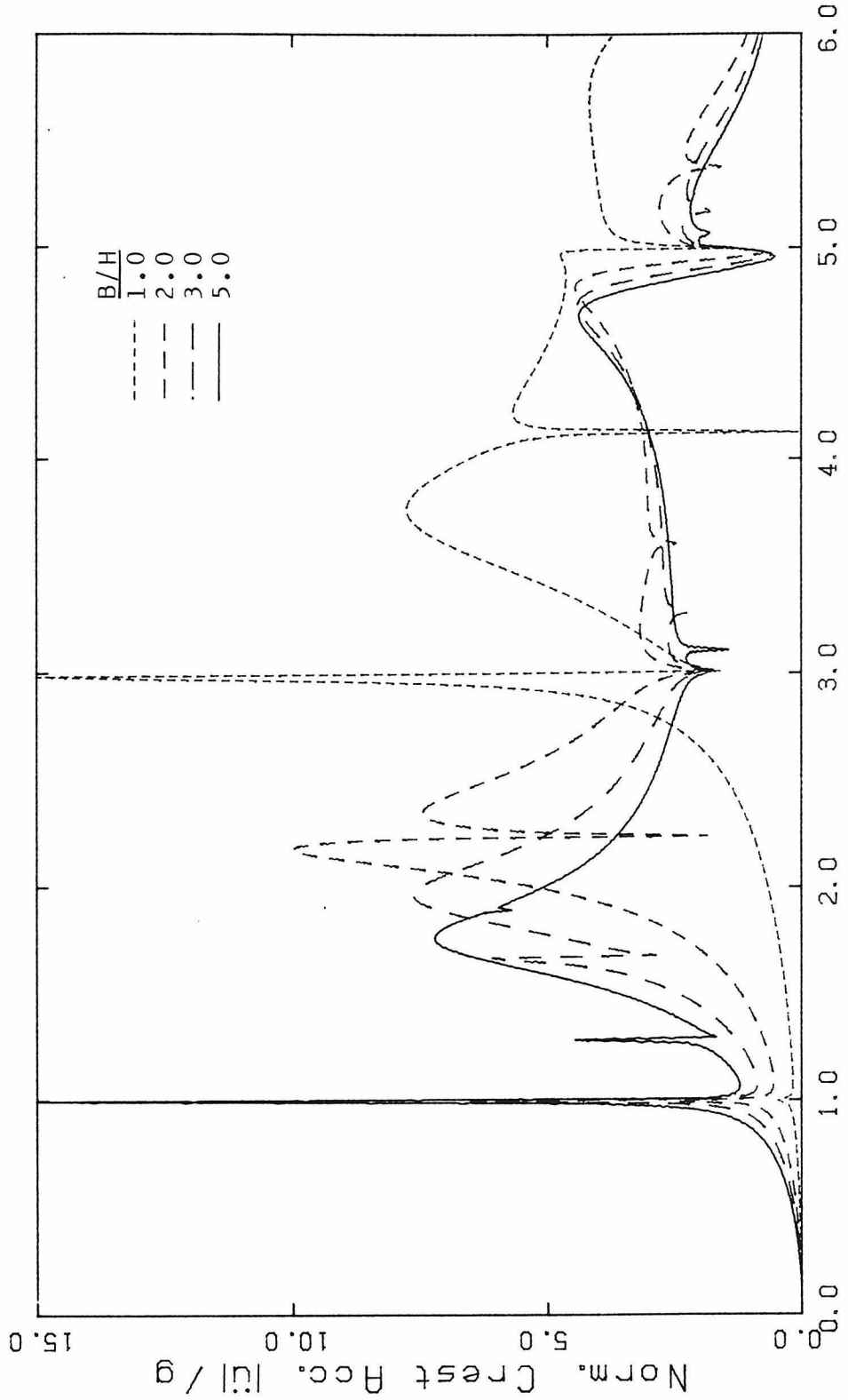


Fig. 4.7 Crest Acceleration Response (Longitudinal Ground Motion)

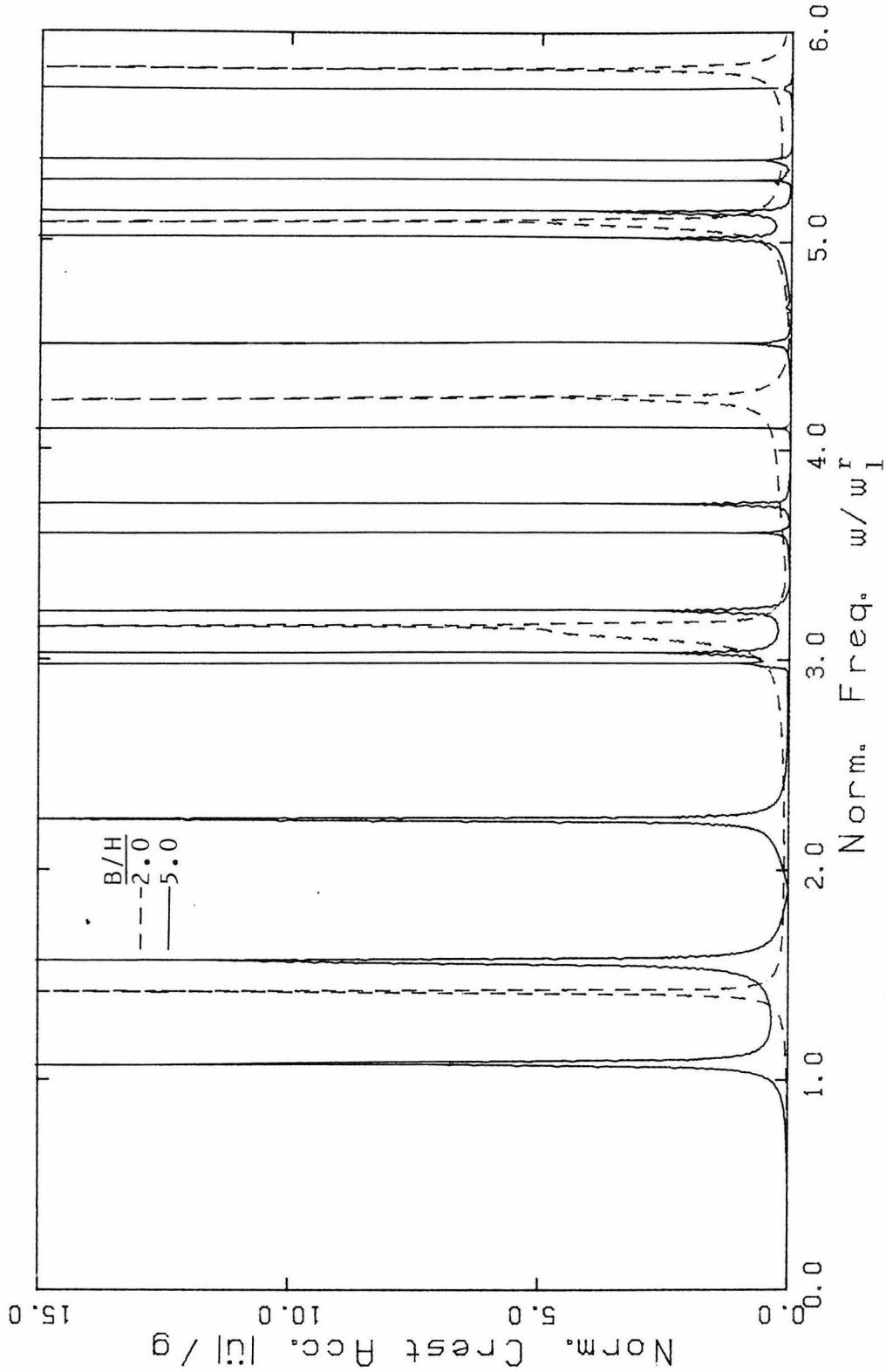


Fig. 4.8 Crest Acceleration Response (Transverse Ground Motion)

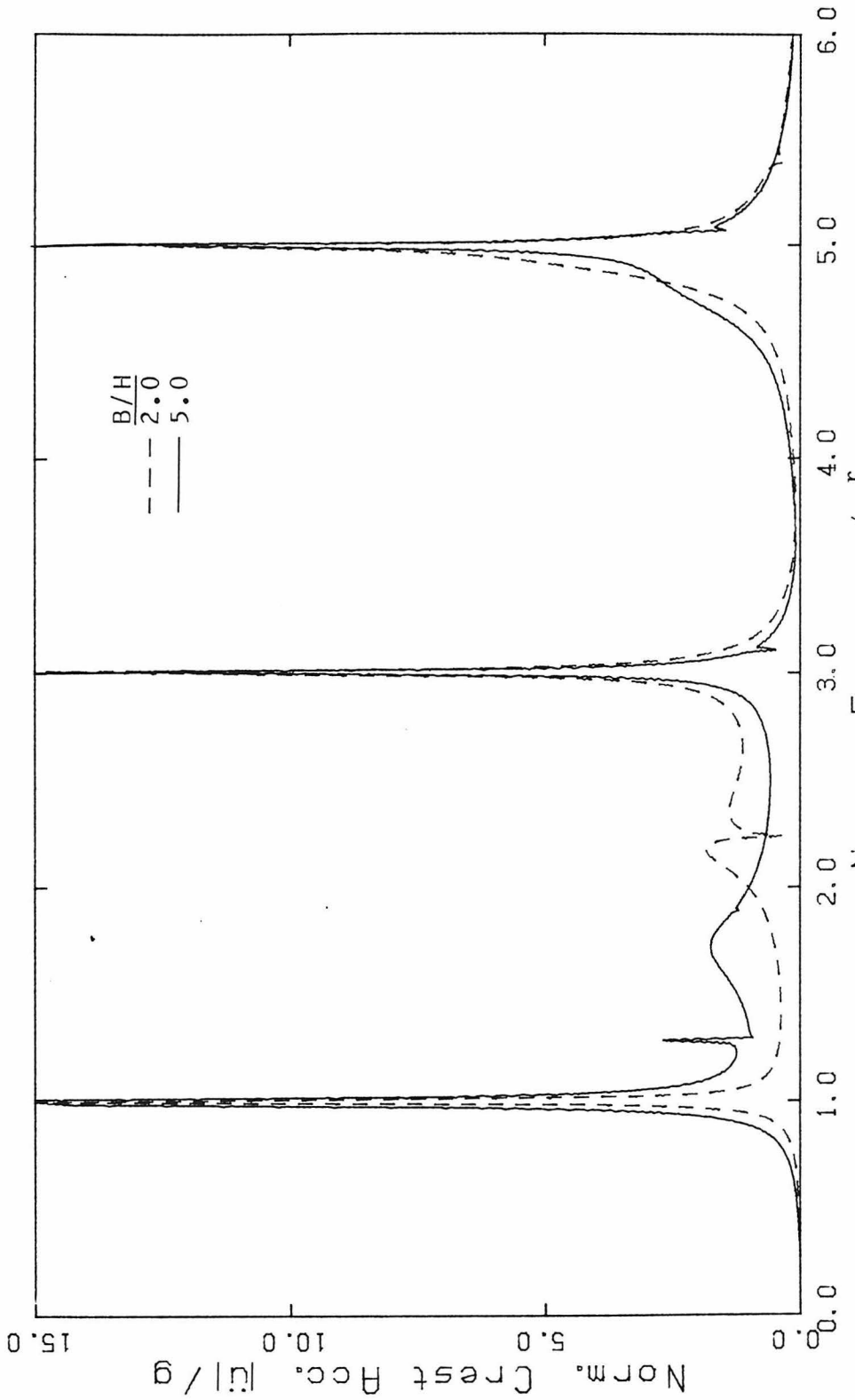


Fig. 4.9 Crest Acceleration Response (Vertical Ground Motion)

would result in a change in the response to earthquake ground motion. This will be discussed in the next chapter.

# CHAPTER V

# EARTHQUAKE RESPONSE OF SHORT DAMS OR WALLS

## 5.1 Introduction

In the previous chapter, the effects of the length to height ratio (B/H) on the dynamic properties, and on the frequency domain response of short dams or walls, have been studied. It has been shown that a change in B/H results in a change in the values of the resonant frequencies of the dam-reservoir system, which in turn results in changes in the transfer functions of the system response to all three components of ground motion. In addition, the response to the transverse component, a feature pertinent only to dams of finite length, has been established.

In this chapter, the previously obtained transfer functions are used to compute time domain responses to arbitrary ground motions. The structural response is obtained using the frequency domain analysis outlined in section 3.2.3.2. The efficiency of computation is increased by using a Fast Fourier Transform algorithm [41], especially suited for structural dynamics, for both the forward transform of the ground excitation and the inverse transform of the Fourier Integral.

Using all three components of the ground motion recorded at the abutment of Pacoima Dam during the San Fernando earthquake of February 9, 1971, crest acceleration and displacement responses of dams with different B/H ratios are evaluated in order to: 1) establish the effect of B/H on the earthquake response of short dams, and 2) to

investigate the significance of the transverse and vertical components, as compared to the longitudinal, on the dam response.

In addition, the time histories of the hydrodynamic pressure at points lying on the upstream face of the dam, along the vertical line at mid-span, are evaluated and the possibility of cavitation is investigated.

## 5.2. Inclusion of Flexibility of Reservoir Boundaries

In the response analysis of short dams, carried out in Chater IV, the problem was reduced to solving the three matrix equations given by Eqs. 4.15, 4.21, and 4.24 for ground excitation in the longitudinal, transverse and vertical directions, respectively. In those equations, the frequency dependent added mass matrix $[M_\ell]$ arises from the hydrodynamic pressure generated by the vibrational motion of the dam, while the frequency dependent added load vectors $\{F^x\}$, $\{F^y\}$ and $\{F^z\}$ result from the pressures caused by the x, y and z components of the ground motion. Those pressures, and consequently the elements of $[M_\ell]$, $\{F^x\}$, $\{F^y\}$ and $\{F^z\}$, were shown to be unbounded at excitation frequencies equal to the resonant frequencies of the reservoir, $\omega_n^r$. In the neighborhood of $\omega_n^r$, $[M_\ell]$ and $\{F^x\}$ are controlled by the term $1/\sqrt{\omega^2 - (\omega_n^r)^2}$, while $\{F^y\}$ and $\{F^z\}$ by $1/[\omega^2 - (\omega_n^r)^2]$. Thus, the dam response to longitudinal ground motion is bounded at excitation frequencies equal to $\omega_n^r$ because the ratios of the terms of $\{F^x\}$ to the

terms of $[M_\ell]$ approach finite values. On the contrary, dam responses to transverse and vertical ground motions are unbounded at those frequencies. However, the Fourier Analysis procedure for computing responses to arbitrary ground motions is, in principle, applicable because the transfer function approaches infinity, as $\omega \rightarrow \omega_n^r$, at a slow enough rate so that the areas under the undounded peaks are finite. This requires a special technique of numerical integration having a variable frequency step, thus eliminating the use of the efficient Fast Fourier Transform algorithm.

Unbounded responses are due to unbounded hydrodynamic pressures resulting from the unrealistic assumption of rigid reservoir boundaries. In actuality, these boundaries are flexible, thus allowing some energy loss by radiation through the boundaries, which results in bounded responses at the reservoir frequencies.

In this section, the formulas derived in Chapter II for the hydrodynamic pressures, under the assumption of rigid reservoir boundaries, are modified according to a flexible boundary model similar to the one used by J.F. Hall and A.K. Chopra [42]. This model provides some fluid-boundary interaction, which allows the absorption of a part of the incident energy associated with a pressure wave striking the reservoir boundary. At the fluid-boundary interface, the boundary condition stating proportionality between the pressure normal to the boundary and the normal component of acceleration is still valid. However, these accelerations cannot be specified as in the rigid boundaries case

because they depend on the fluid-boundary interaction. The actual acceleration is then composed of a free-field part and a part caused by interaction.

5.2.1. Vibrational Motion

Let the geometry of the dam-reservoir system be as described in section 3.2.1. Using the flexible boundaries model mentioned above, the boundary conditions given by Eqs. 2.40, 2.41 and 2.42 are replaced respectively by:

$$\rho_\ell \ddot{w}_\ell(x,y,0,t) = -i\omega q\, p(x,y,0,t) \tag{5.1}$$

$$\rho_\ell \ddot{v}_\ell(x,0,z,t) = -i\omega q\, p(x,0,z,t) \tag{5.2}$$

$$v_\ell(x,B/2,z,t) = 0 \qquad \text{(symmetric dam motion)} \tag{5.3a}$$

$$p(x,B/2,z,t) = 0 \qquad \text{(antisymmetric dam motion)} \tag{5.3b}$$

where q is a damping coefficient defined as:

$$q = \frac{1}{c}\frac{1-\alpha_r}{1+\alpha_r} \tag{5.4}$$

in which $\alpha_r$ is the reflection coefficient of the hydrodynamic pressure wave at the fluid-boundary interface, and c in the sound velocity in the fluid. The conditions given by Eqs. 2.38, 2.39 and 2.43 remain unchanged.

With the new set of boundary conditions, Eq. 2.44 changes to:

$$p(x,y,z,t) = -4\rho_\ell H_\ell A\omega^2 \exp(i\omega t) \left\{ \sum_{n=1}^{\infty} \sum_{m=1}^{\infty} \frac{I_{mn}}{\delta_{mn} A_n B_m} \cdot \exp\left(-\delta_{mn} \frac{x}{H_\ell}\right) \cdot Y_n\left(\frac{y}{B}\right) \cdot Z_m\left(\frac{z}{H_\ell}\right) \right\} \tag{5.5}$$

where

$$Y_n\left(\frac{y}{B}\right) = \cos\left(\beta_n \frac{y}{B}\right) + \frac{iV}{\beta_n} \sin\left(\beta_n \frac{y}{B}\right) \quad ; \quad n = 1,2,\ldots \tag{5.6}$$

$\beta_n$ are the complex valued roots of:

$$\exp(i\beta_n) = (\beta_n - V) / (\beta_n + V) \qquad \text{(symmetric)} \tag{5.7a}$$

$$\exp(i\beta_n) = (V - \beta_n) / (V + \beta_n) \quad \text{(antisymmetric)} \tag{5.7b}$$

$$V = \omega q B \tag{5.8}$$

and

$$Z_m\left(\frac{z}{H_\ell}\right) = \cos\left(\eta_m \frac{z}{H_\ell}\right) + \frac{iW}{\eta_m} \sin\left(\eta_m \frac{z}{H_\ell}\right) \quad ; m = 1,2,\ldots \tag{5.9}$$

$\eta_m$ are the complex roots of:

$$\exp(2i\eta_m) = (W - \eta_m) / (W + \eta_m) \tag{5.10}$$

$$W = \omega q H_\ell \tag{5.11}$$

The coefficients $\delta_{mn}$, $I_{mn}$, $A_n$ and $B_m$ are defined as:

$$\delta_{mn} = H_\ell \sqrt{(\beta_n/B)^2 + (\eta_m/H_\ell)^2 - (\omega/c)^2} \tag{5.12}$$

$$I_{mn} = \frac{1}{B H_\ell} \int_0^{H_\ell} \int_0^{B} \varphi\left(\frac{y}{B}, \frac{z}{H}\right) \cdot Y_n\left(\frac{y}{B}\right) \cdot Z_m\left(\frac{z}{H_\ell}\right) dy\, dz \tag{5.13}$$

$$A_n = \frac{2}{B}\int_0^B \left[ Y_n\left(\frac{y}{B}\right)\right]^2 dy \tag{5.14}$$

$$B_m = \frac{2}{H_\ell}\int_0^{H_\ell} \left[ Z_m\left(\frac{z}{H_\ell}\right)\right]^2 dz \tag{5.15}$$

5.2.2. Longitudinal Ground Motion

In this case, the dam is assumed to be rigid, and the prescribed motion is given by Eq. 2.22. The solution is a special case of Eq. 5.5 in which A is replaced by $\bar{u}_g$ and $\varphi\left(\frac{y}{B},\frac{z}{H}\right) \equiv 1$. Unlike the case of rigid reservoir boundaries, the pressure is now dependent on the y-coordinate as well.

5.2.3. Transverse Ground Motion

Under the flexible boundaries assumption, the boundary condition given by Eq. 2.55 remains unchanged, while those given by Eqs. 2.56, 2.57 and 2.58 are replaced by:

$$\rho_\ell \ddot{w}_\ell(y,0,t) = -i\omega q\, p(y,0,t) \tag{5.16}$$

$$\rho_\ell \ddot{v}_\ell(0,z,t) = \rho_\ell \ddot{v}_g(t) - i\omega q\, p(0,z,t) \tag{5.17}$$

$$p(B/2,z,t) = 0 \tag{5.18}$$

where $v_g(t)$ is now a free-field ground motion acting on the left bank of the reservoir, and assumed of the form given by Eq. 2.54.

The hydrodynamic pressure generated in this case is given by the expression:

$$p_{gy}(y,z,t) = -2\ \rho_\ell H_\ell \bar{v}_g\ \omega^2\ \exp(i\omega t)$$

$$\left\{ \sum_{m=1}^{\infty} \frac{I_m \cdot \sinh\left[\delta_{m0}\left(\frac{\beta}{2}-y\right)/H_\ell\right] \cdot Z_m\left(\frac{z}{H_\ell}\right)}{B_m\left[\cosh(B\delta_{m0}/2H_\ell) + iW \sinh(B\delta_{m0}/2H_\ell)\right]} \right\} \tag{5.19}$$

where

$$I_m = \frac{1}{H_\ell} \int_0^{H_\ell} Z_m\left(\frac{z}{H_\ell}\right) dz \tag{5.20}$$

$$\delta_{m0} = H_\ell \sqrt{(\eta_m/H_\ell)^2 - (\omega/c)^2} \tag{5.21}$$

and $Z_m\left(\frac{z}{H_\ell}\right)$, $\eta_m$, W and $B_m$ are as defined by Eqs. 5.9, 5.10, 5.11 and 5.15, respectively.

5.2.4. Vertical Ground Motion

When the flexibility of the reservoir boundaries is included in the analysis, the pressure becomes dependent on the y-coordinate. The boundary conditions are now stated as:

$$p(y,H_\ell,t) = 0 \tag{5.22}$$

$$\rho_\ell \ddot{w}_\ell(y,0,t) = \rho_\ell \ddot{w}_g(t) - i\omega q\ p(y,0,t) \tag{5.23}$$

$$\rho_\ell \ddot{v}_\ell(0,z,t) = -i\omega q\ p(0,z,t) \tag{5.24}$$

$$v_\ell(B/2,z,t) = 0 \tag{5.25}$$

where $w_g(t)$ is a free-field vertical ground motion at the reservoir bottom, given by Eq. 2.27.

Application of these conditions to the general solution for the pressure yields:

$$p_{gz}(y,z,t) = -\rho_\ell H_\ell \bar{w}_g \omega^2 \exp(i\omega t)$$

$$\left\{ \sum_{n=1}^{\infty} \frac{2 \cdot I_n \cdot Y_n\left(\frac{Y}{B}\right) \cdot \sin\left[\eta_m\left(1 - \frac{z}{H_\ell}\right)\right]}{A_n\left[\eta_n \cos(\eta_n) + iW \sin(\eta_n)\right]} \right\} \tag{5.26}$$

where

$$I_n = \frac{1}{B} \int_0^B Y_n\left(\frac{Y}{B}\right) dz \tag{5.27}$$

$$\eta_n = H_\ell \sqrt{(\omega/c)^2 - (\beta_n/B)^2} \tag{5.28}$$

and $Y_n\left(\frac{Y}{B}\right)$, $\beta_n$, W and $A_n$ are as defined by Eqs. 5.6, 5.7a, 5.11 and 5.14, respectively.

5.2.5. Numerical Examples

The expressions derived above for the hydrodynamic pressure are used to compute the elements of the added mass matrix and added load vectors arising in the matrix equations of motion governing the forced vibrations of a finite length dam. The dam has a B/H ratio of 2.0, and a thickness and material properties as chosen before. Frequency domain responses to all three components of ground motion are evaluated and plotted (dashed line) in Fig. 5.1. On the same plots, the responses obtained previously under a rigid boundaries assumption are displayed by solid lines.

For longitudinal ground motion (Fig. 5.1a), it is observed that the radiation damping associated with the fluid-boundary interaction reduces the response amplitudes, the reductions being primarily in the

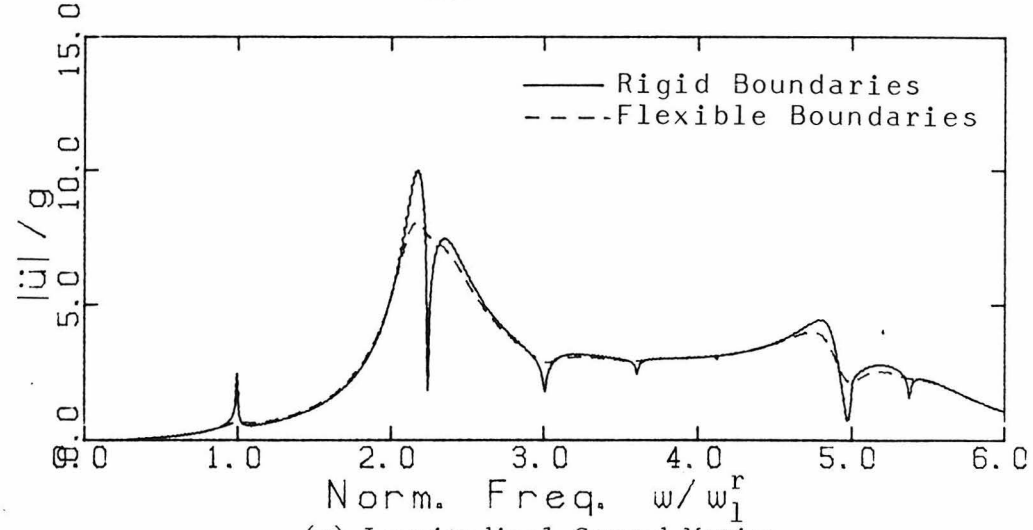


(a) Longitudinal Ground Motion

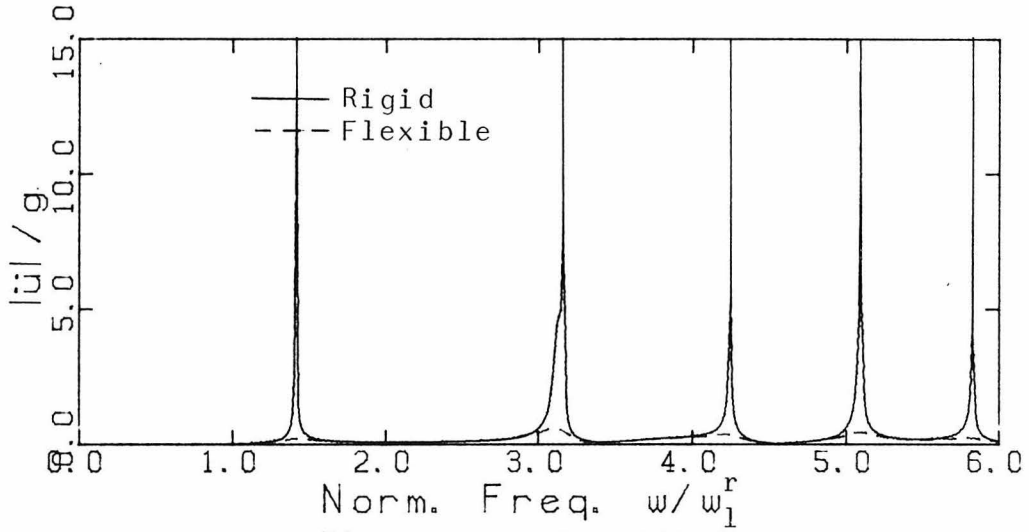


(b) Transverse Ground Motion

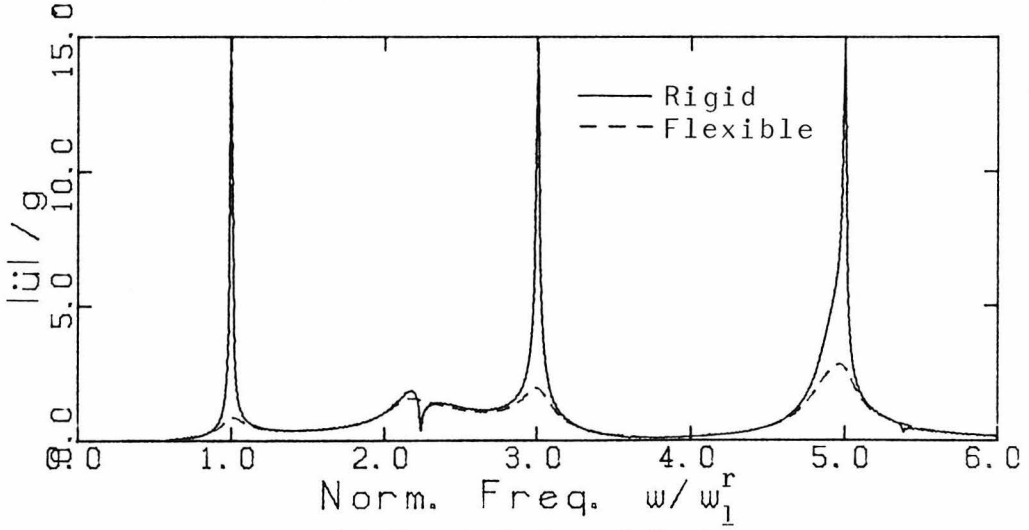


(c) Vertical Ground Motion

Fig. 5.1 Crest Acceleration Response (Harmonic Ground Motion)

vicinities of the resonant frequencies of the reservoir. For transverse and vertical ground motions (Fig. 5.1, b and c), the dam responses at excitation frequencies equal to $\omega_n^r$, which are unbounded when the boundaries are assumed rigid, are reduced to bounded values. This is a consequence of the pressures being bounded functions of excitation frequency when fluid-boundary interaction is included.

## 5.3. Earthquake Responses of Dams

In this section, the crest acceleration and displacement responses of dams to existing earthquake ground motions are evaluated. All dams considered thereafter have rectangular cross-sections, are 300 ft high and 120 ft thick. They are all made of concrete whose properties are as given previously in section 3.2.1.3. The only variable is the B/H ratio.

The ground accelerations applied to the dam-reservoir system in the longitudinal, transverse and vertical directions are the N-S, E-W and vertical components of the motion recorded at the abutment of Pacoima Dam, during the San Fernando earthquake of February 9, 1971. Only the first 12 seconds of the record are used. These are plotted in Fig. 5.2, while their Fourier transforms, obtained through the use of a Fast Fourier Transform algorithm [41], are plotted in Fig. 5.3.

Transfer functions of relative crest acceleration, for dams of varying B/H, are plotted in Fig. 5.4. These are computed at mid-span for the x and z components of ground motion, and at quarter-span for the y-component. Earthquake responses of absolute crest acceleration are

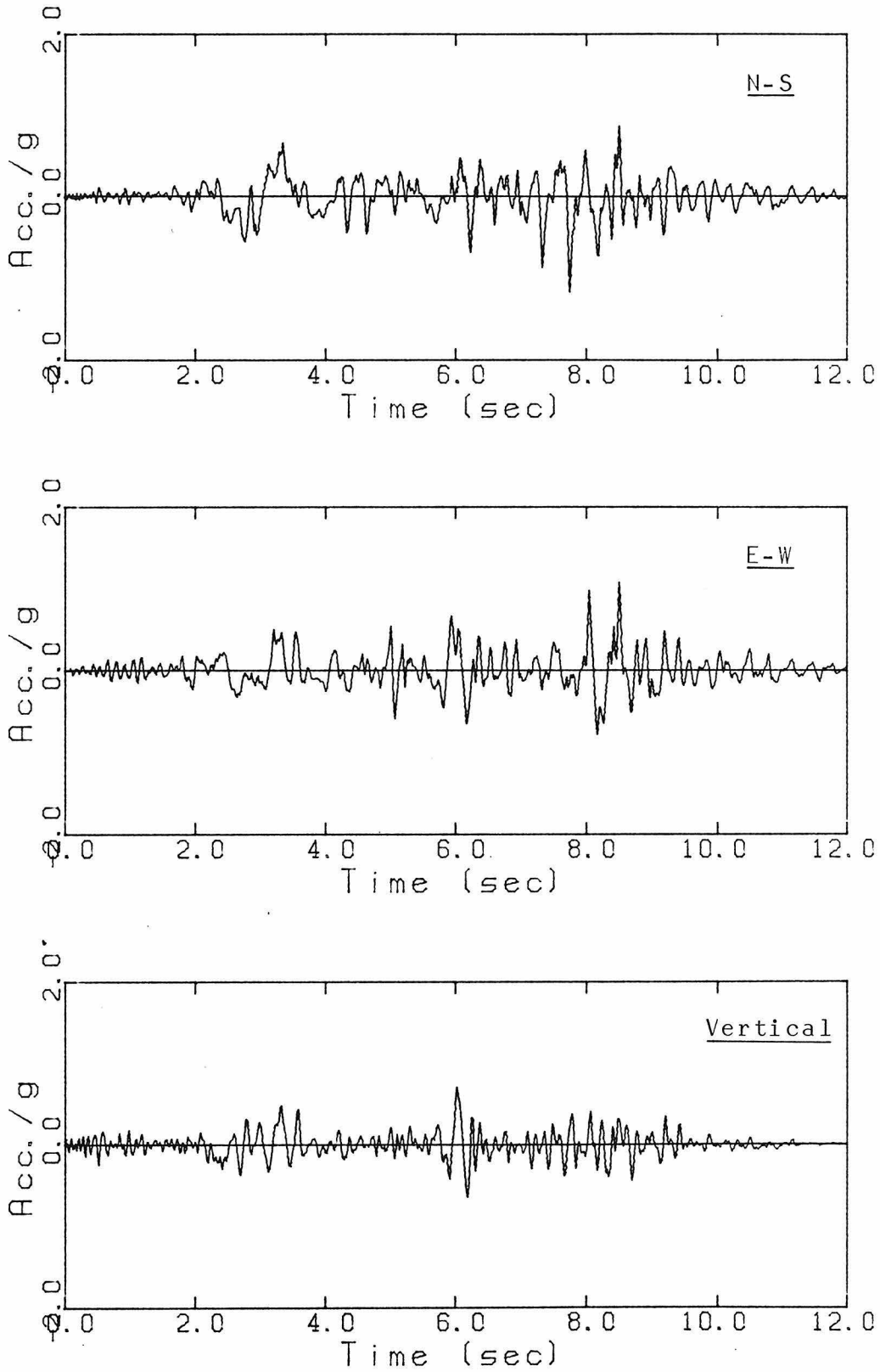


Fig. 5.2 Pacoima Dam Record of the San Fernando Earthquake

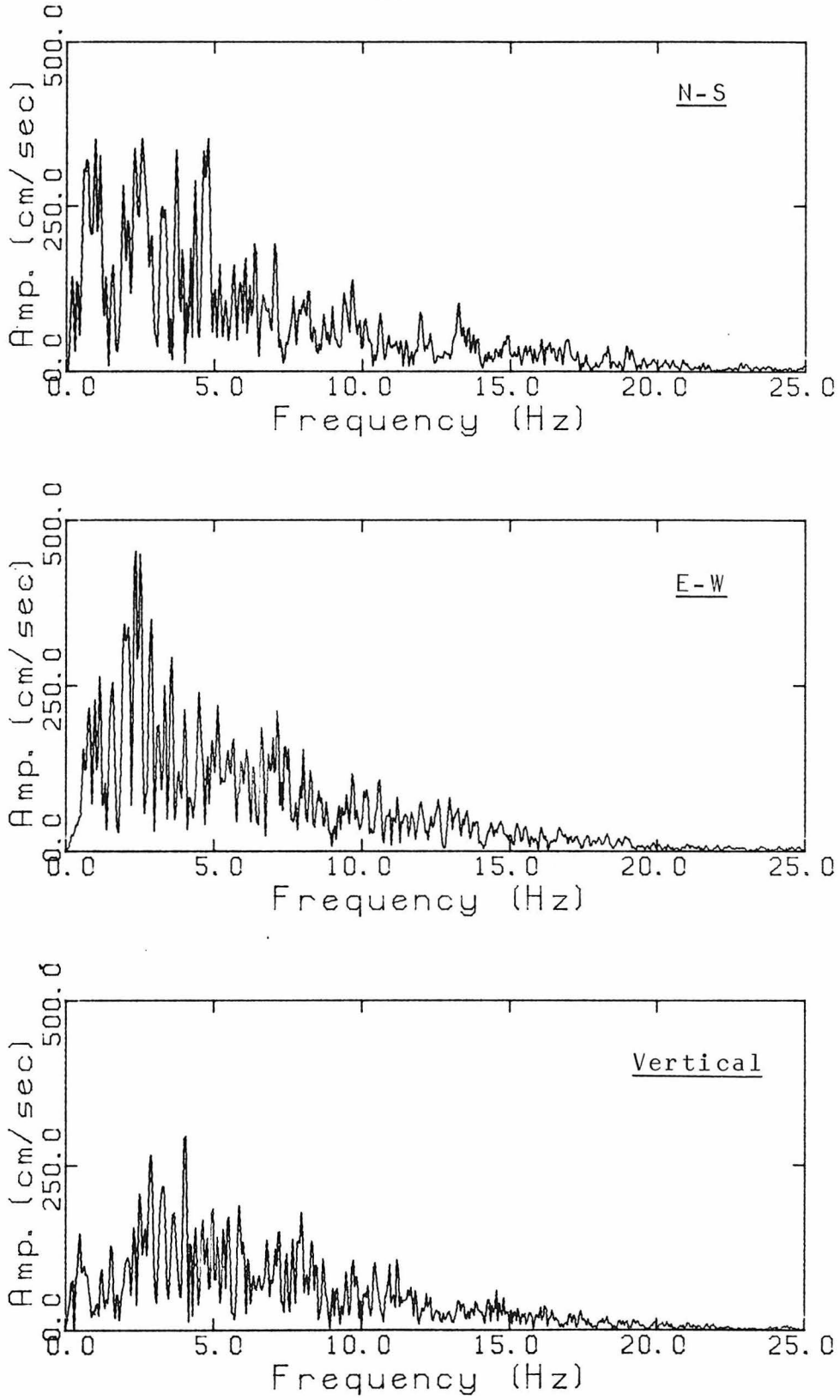


Fig. 5.3 Fourier Amplitude Spectra (Pacoima Dam Record)

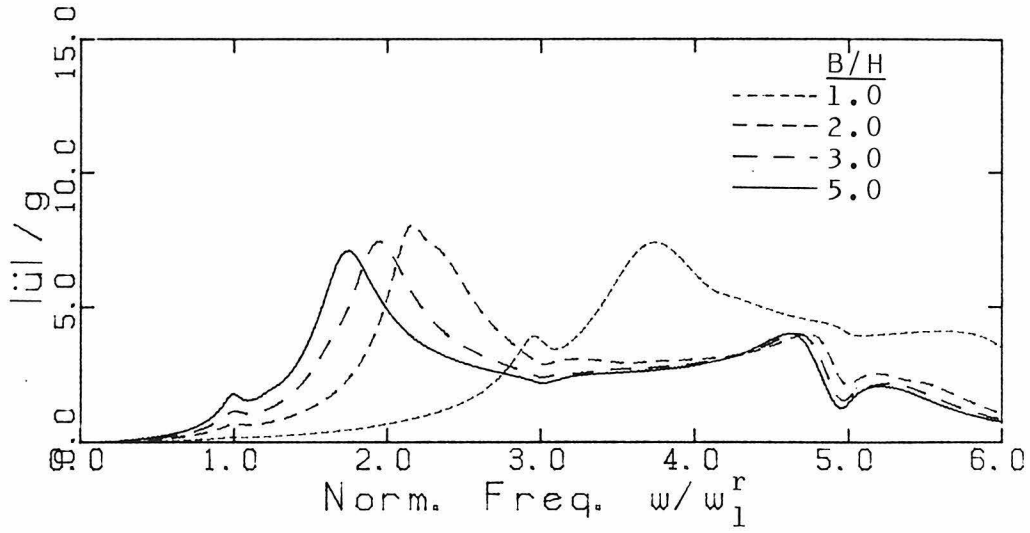


(a) Longitudinal Ground Motion

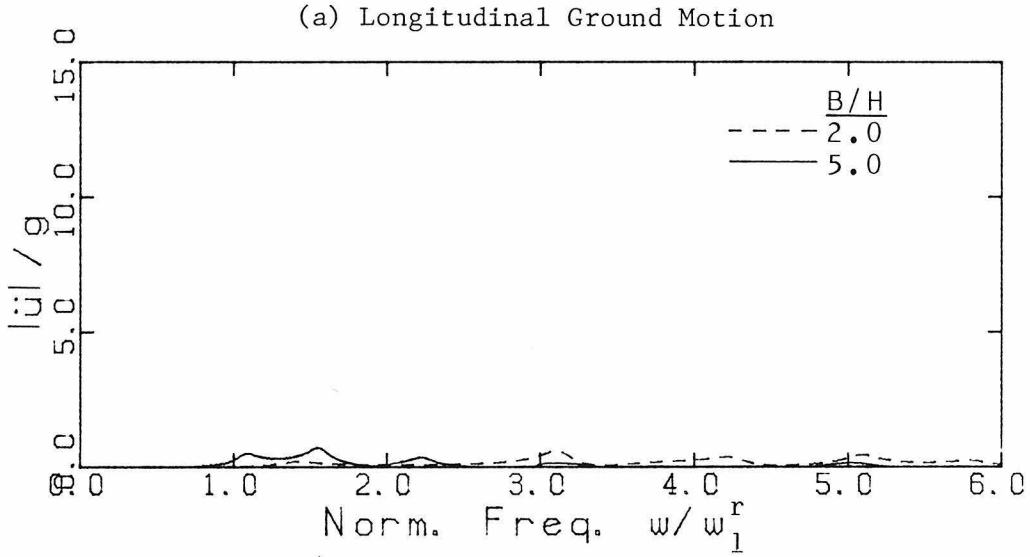


(b) Transverse Ground Motion

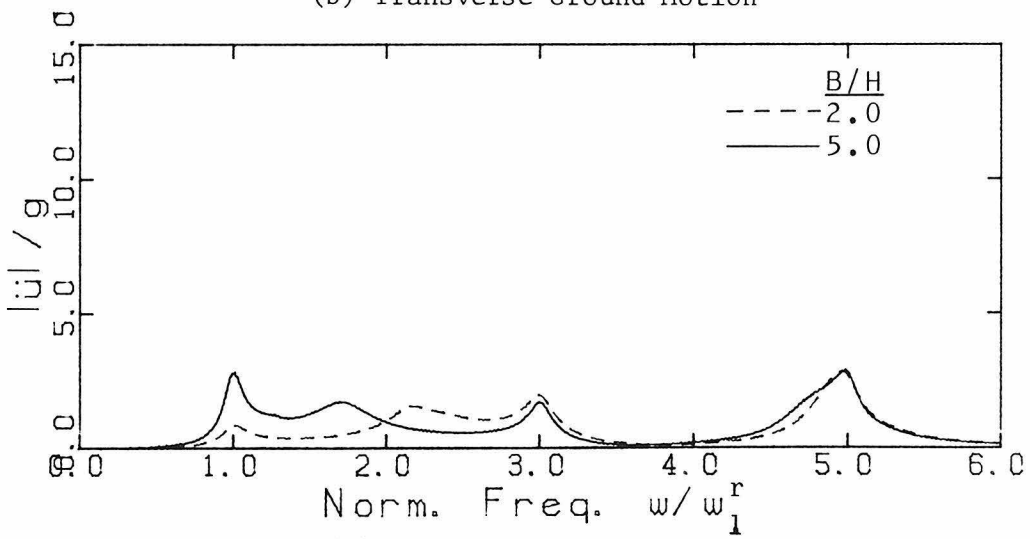


(c) Vertical Ground Motion

Fig. 5.4 Transfer Functions of Relative Crest Acceleration

obtained by evaluating the Fourier Integrals using the FFT algorithm mentioned above. These are plotted in Figs. 5.5, 5.6 and 5.7. It is observed that:

1) While the change in B/H affects the transfer functions in the sense of shifting the resonant frequencies, with small variations in the maximum values (less than 10%), it affects the peak absolute acceleration response to longitudinal motion by as much as 20% for B/H = 2.0, and 42% for B/H = 1.0 as compared to B/H = 5.0. For transverse and vertical motions, the peak response decreases respectively by 51% and 43%, when B/H changes from 5.0 to 2.0.
2) For B/H = 2.0, the transverse component produces, a quarter-span peak acceleration which is 3.6% of what the longitudinal component produces at mid-span. The vertical component contribution is 23% of the longitudinal. For B/H = 5.0, the values are 6% and 32%, respectively.

Transfer functions and earthquake responses of relative crest displacement are given in Figs. 5.8 through 5.11. The effect of B/H on the peak displacement response is displayed in Table 5.1, which contains the peak values for all B/H ratios considered and all three components of ground motion. The difference (in percentage) from the peak response when B/H = 5.0 is given in parentheses. The effect of B/H on displacement response is shown to be greater than on acceleration.

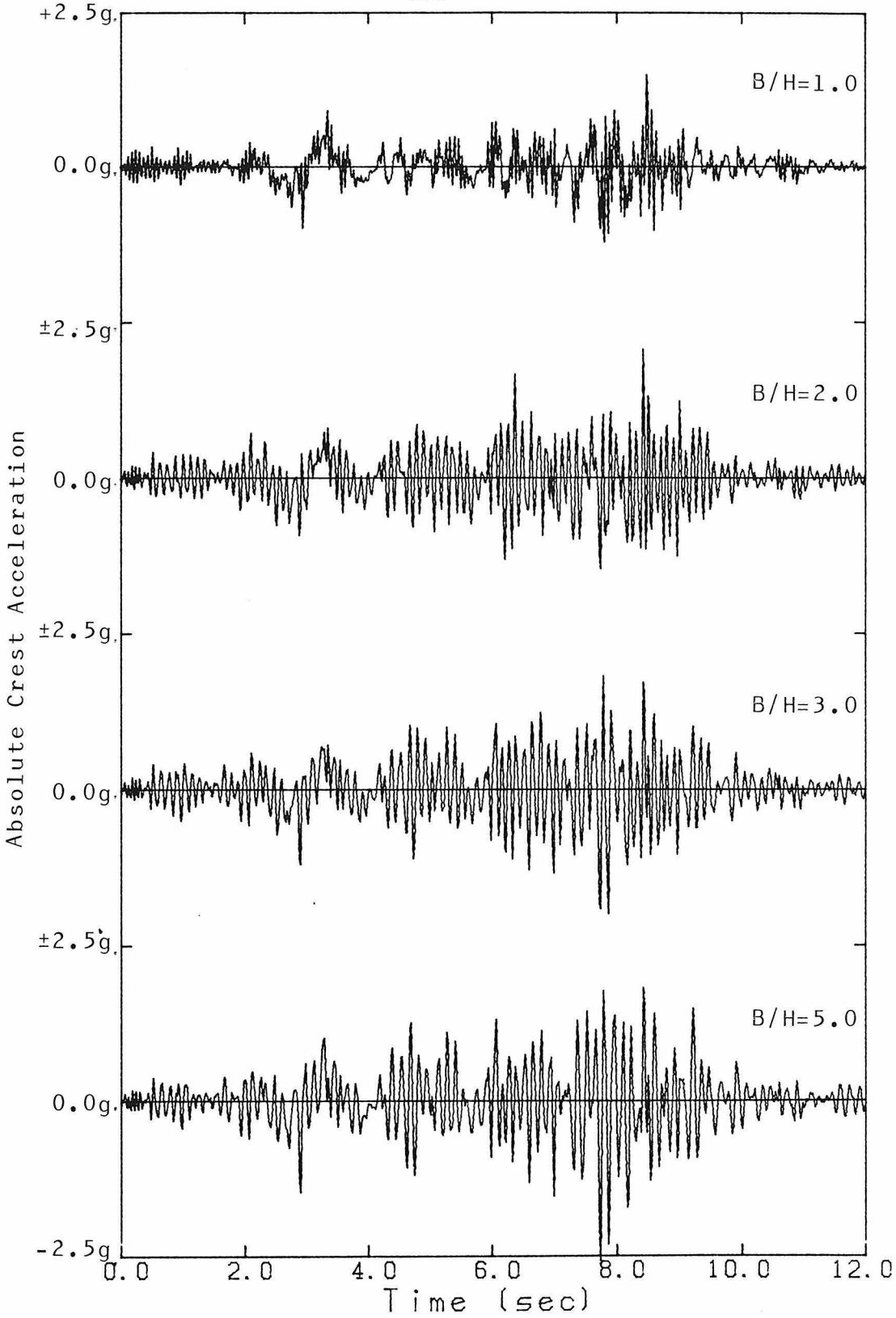


Fig. 5.5 Time Histories of Absolute Crest Acceleration
(Longitudinal Ground Motion)

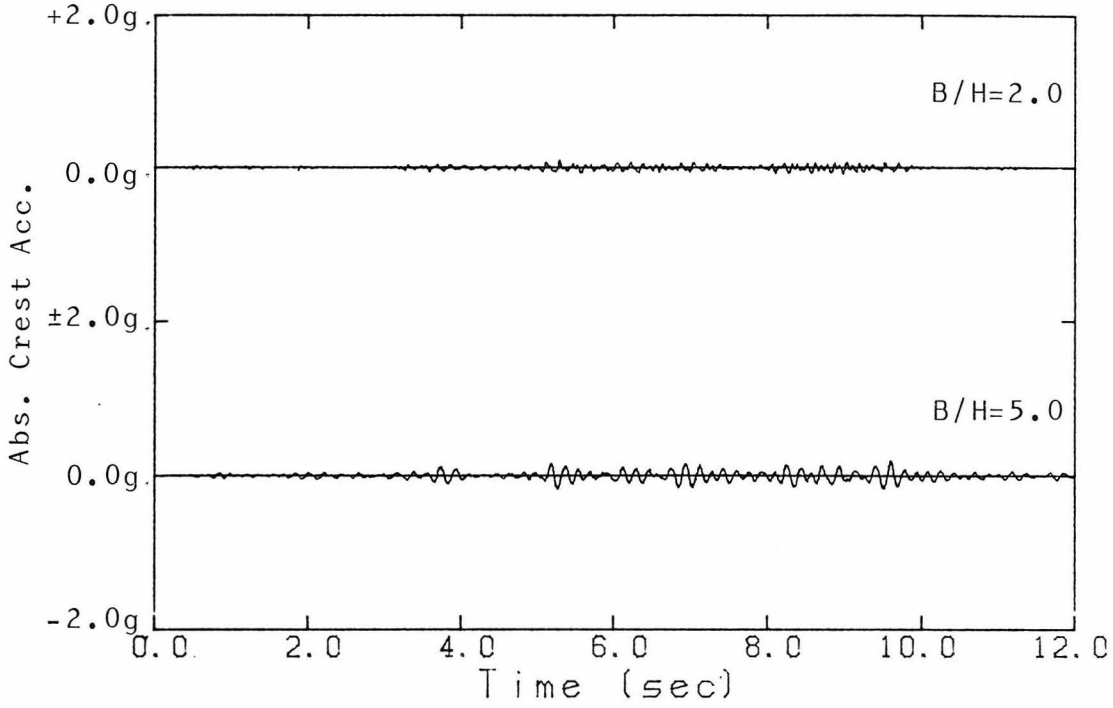


Fig. 5.6 Time Histories of Absolute Crest Acceleration
(Transverse Ground Motion)

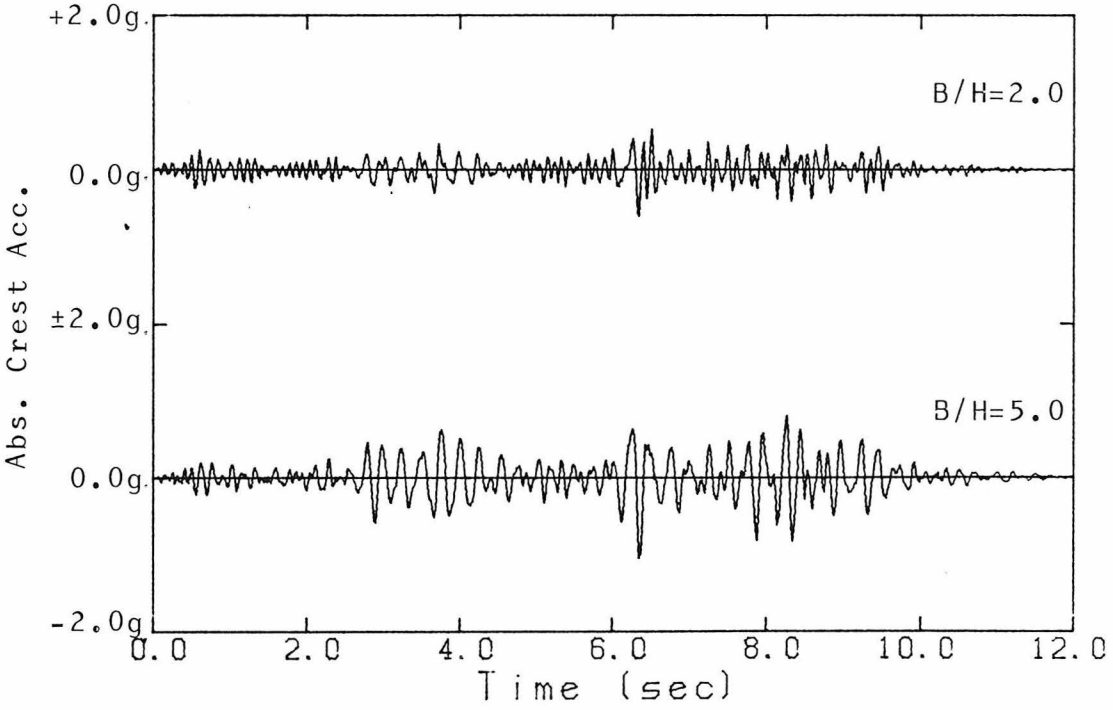


Fig. 5.7 Time Histories of Absolute Crest Acceleration
(Vertical Ground Motion)

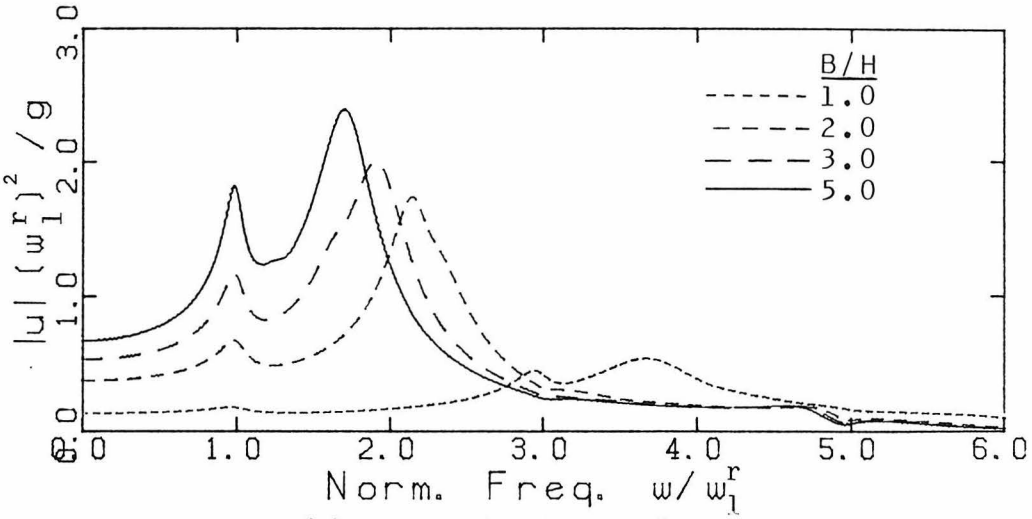


(a) Longitudinal Ground Motion

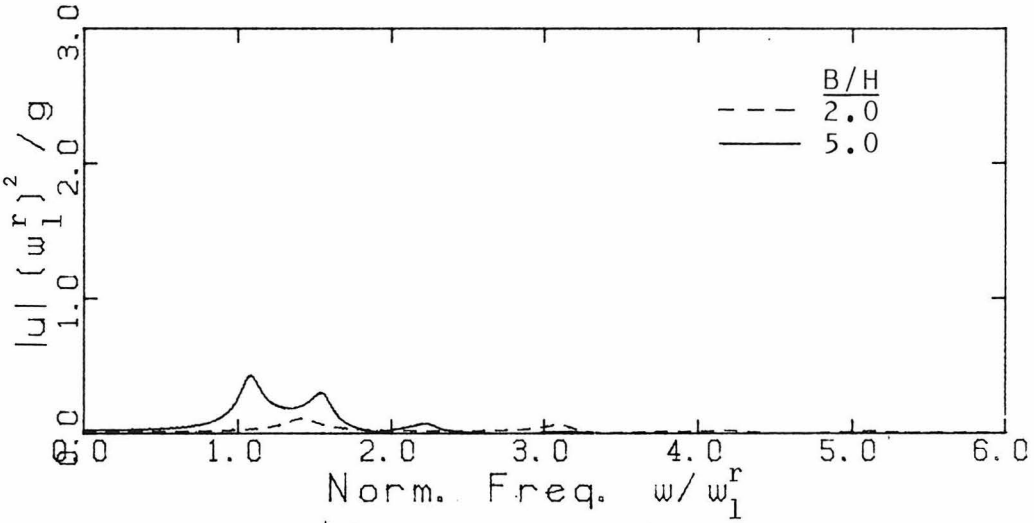


(b) Transverse Ground Motion

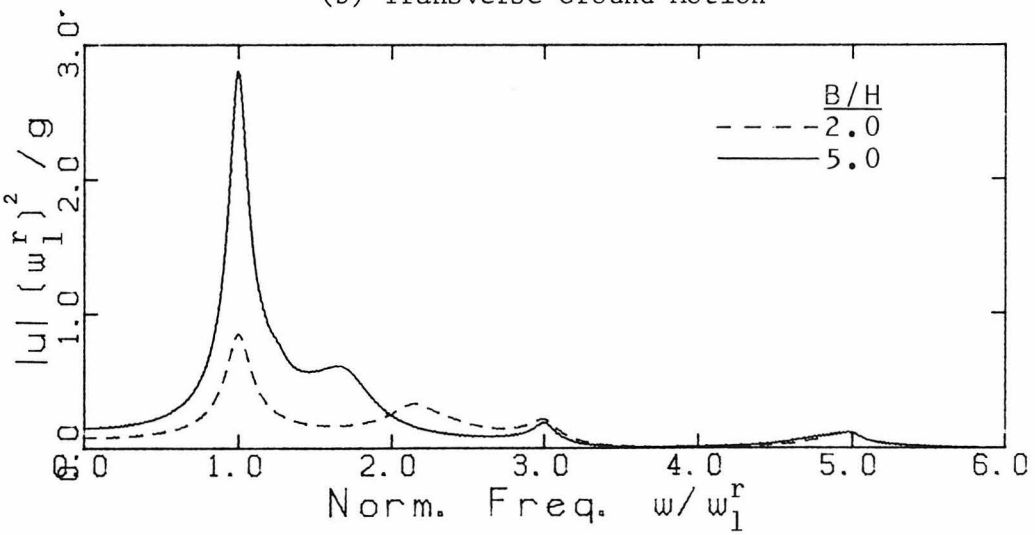


(c) Vertical Ground Motion

Fig. 5.8 Transfer Functions of Relative Crest Displacement

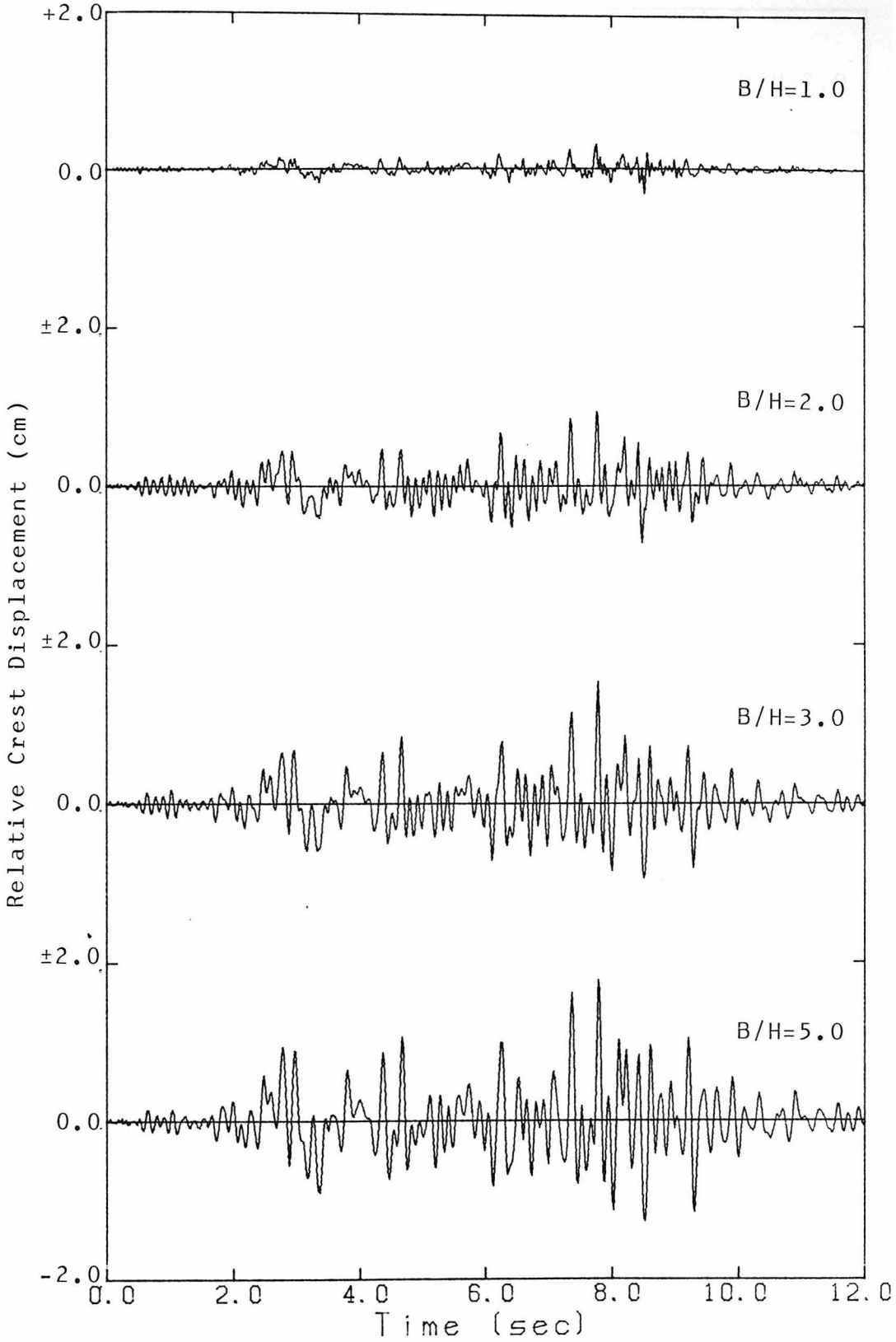


Fig. 5.9 Time Histories of Relative Crest Displacement
(Longitudinal Ground Motion)

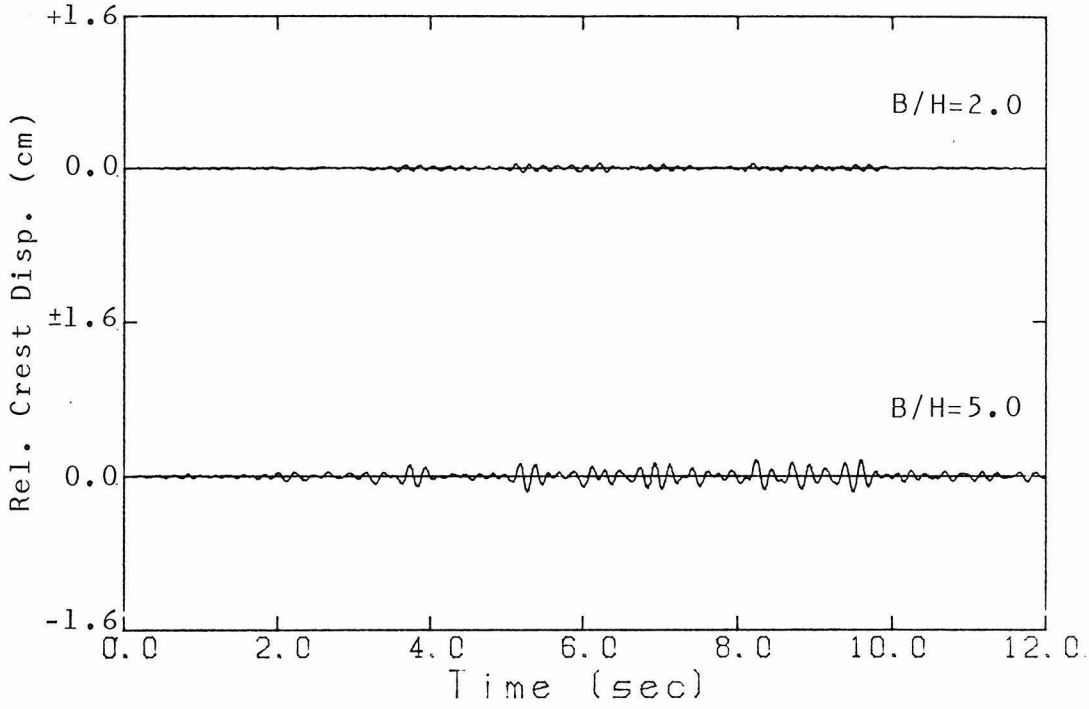


Fig. 5.10 Time Histories of Relative Crest Displacement
(Transverse Ground Motion)

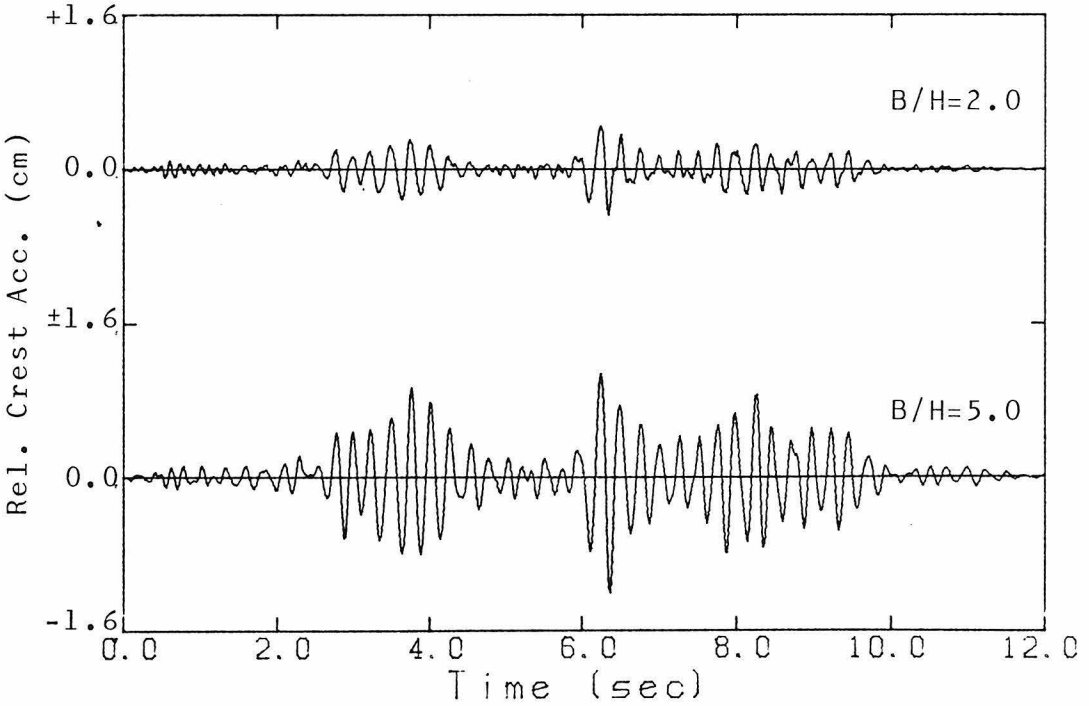


Fig. 5.11 Time Histories of Relative Crest Displacement
(Vertical Ground Motion)

| B/H | Longitudinal Ground Motion | Transverse Ground Motion | Vertical Ground Motion |
|---|---|---|---|
| 1.0 | 0.32(82) | - | - |
| 2.0 | 0.94(47) | 0.04(71) | 0.38(61) |
| 3.0 | 1.53(14) | - | - |
| 5.0 | 1.78(0) | 0.14(0) | 0.97(0) |

TABLE 5.1. Peak Crest Displacement (cm)

As mentioned at the beginning of section 2.2, the validity of neglecting the effect of gravity waves at the reservoir surface has been examined and established by J.I. Bustamante et al. [4], in case of longitudinal ground motion, and by A.K. Chopra [6], in case of vertical ground motion.

When an infinitely long reservoir of finite width is acted upon by a transverse ground motion, the water behaves exactly as in the case of a fluid contained in a rigid rectangular tank. Thus, gravity sloshing modes at the free surface are excited and additional hydrodynamic pressure generated. The effect of these gravity waves has been neglected in obtaining the expression for the pressure generated by transverse ground motion (see section 2.3.4), and this is validated hereafter.

The problem of sloshing of liquids contained in rectangular tanks has been investigated by M.A. Haroun [43]. The natural frequencies of sloshing are given by:

$$\omega_n^2 = \frac{(2n-1)\pi g}{B} \tanh\left[\frac{(2n-1)\pi H_\ell}{B}\right] = (2\pi f_n)^2 \qquad (5.29)$$

where $H_\ell$ is the height of liquid and B is the tank length in the direction of motion. For $H_\ell$ = 300 ft and B = 600 ft, the above equation yields $f_1$ = 0.063 Hz and $f_{10}$ = 0.285 Hz, which are well below the

fundamental frequency of the 300 ft high, 120 ft thick and 600 ft long dam. The higher sloshing modes, which correspond to frequencies lying within the range of the dam frequencies, will have very small participation factors and hence are of negligible effect.

The maximum height of sloshing can be obtained from [43] as:

$$|\eta_{max}| = \frac{4B}{\pi^2 g} \sum_{n=1}^{\infty} \frac{S_{an}}{(2n-1)^2} \qquad (5.30)$$

where $S_{an}$ is the spectral acceleration corresponding to $\omega_n$.

Considering only the first ten sloshing modes, with $S_{an}$ as obtained from the response spectrum of the E-W component of Pacoima Dam record [44], Eq. 5.30 yields: $|\eta_{max}| = 1.69$ ft, which is about 0.55% of the reservoir depth. Thus, the sloshing effects are shown to be negligible without introducing considerable errors in the analysis of dam responses, to transverse ground motion.

## 5.4. Hydrodynamic Pressure Response

When the total absolute pressure (hydrodynamic plus hydrostatic and atmospheric) at any point in the reservoir becomes negative, cavitation takes place because water cannot sustain tension. To examine this possibility, the hydrodynamic pressure response to the longitudinal component of ground motion, applied to a dam of B/H = 5.0, is evaluated. The pressure is calculated at ten equidistant points lying on the upstream dam face, along the vertical line at mid-span. At any of these points, the time history of the hydrodynamic pressure is computed and normalized

by the sum of the atmospheric and hydrodynamic pressure at that point. The results are shown in Fig. 5.12.

Clearly, for the example under consideration, cavitation occurs at all the points except at the one just below the water surface. This is because the absolute value of the normalized pressure exceeds 1.0 at those points.

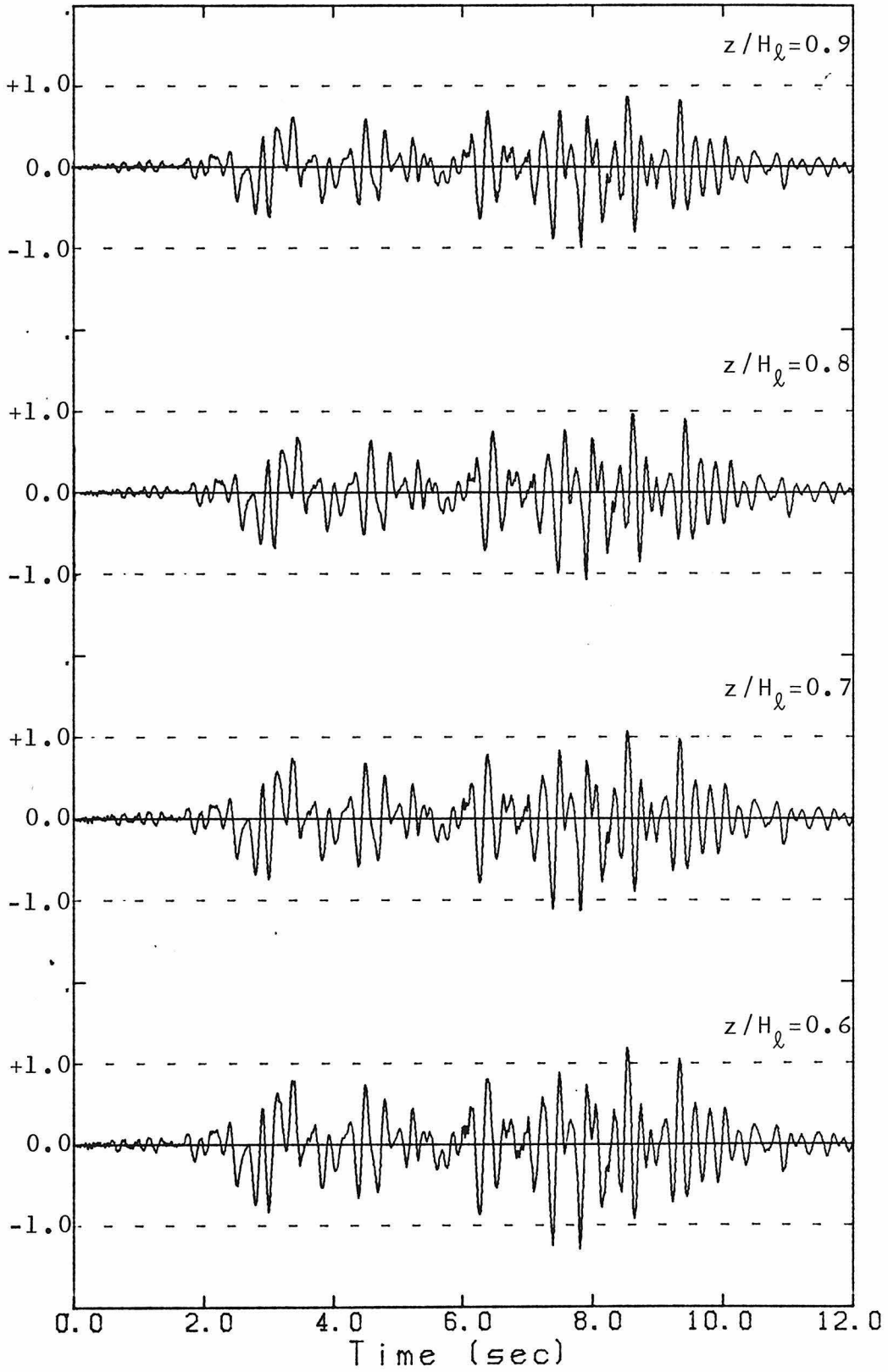


Fig. 5.12 Time Histories of Normalized Hydrodynamic Pressure

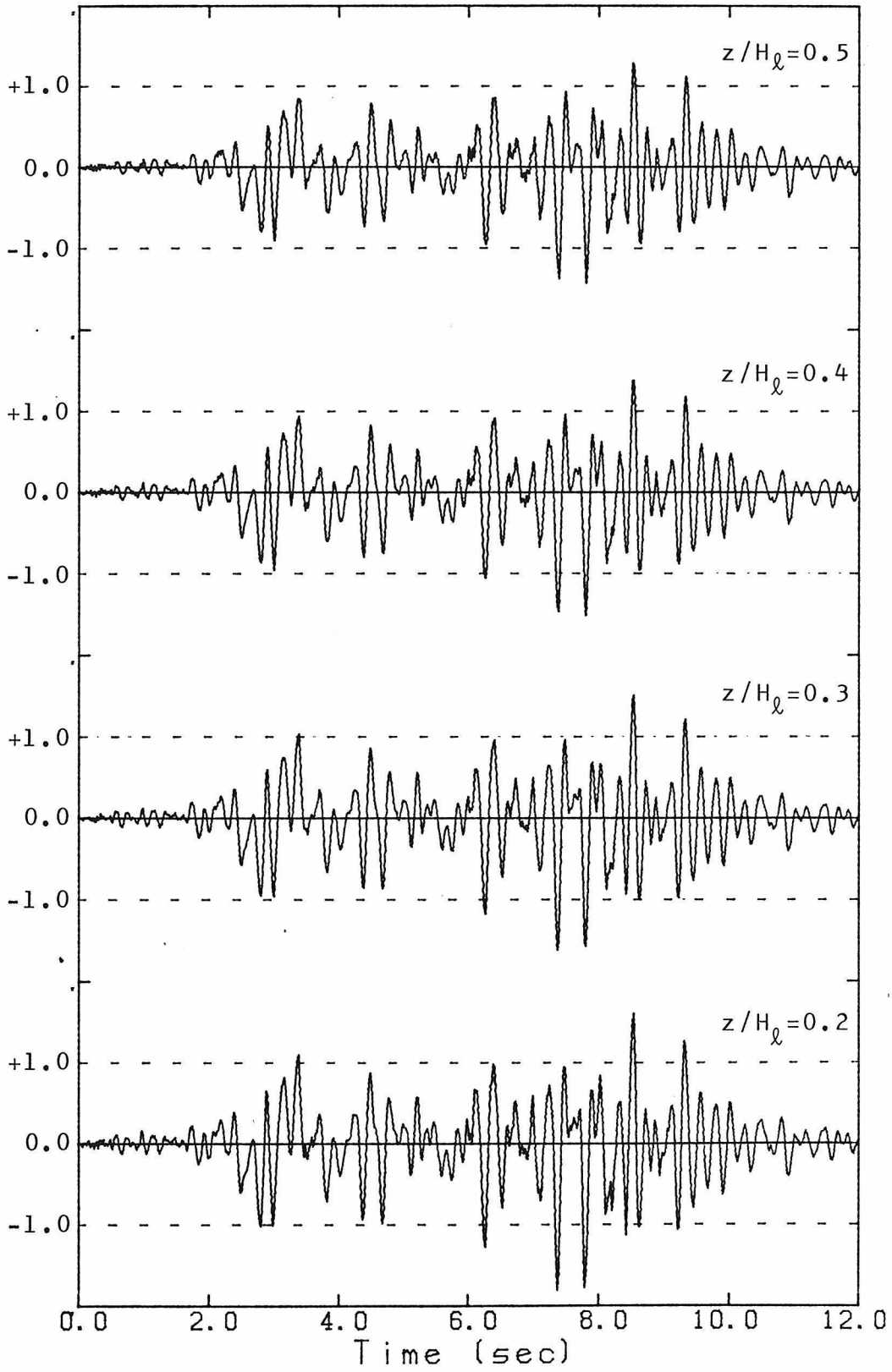


Fig. 5.12 Time Histories of Normalized Hydrodynamic Pressure (continued)

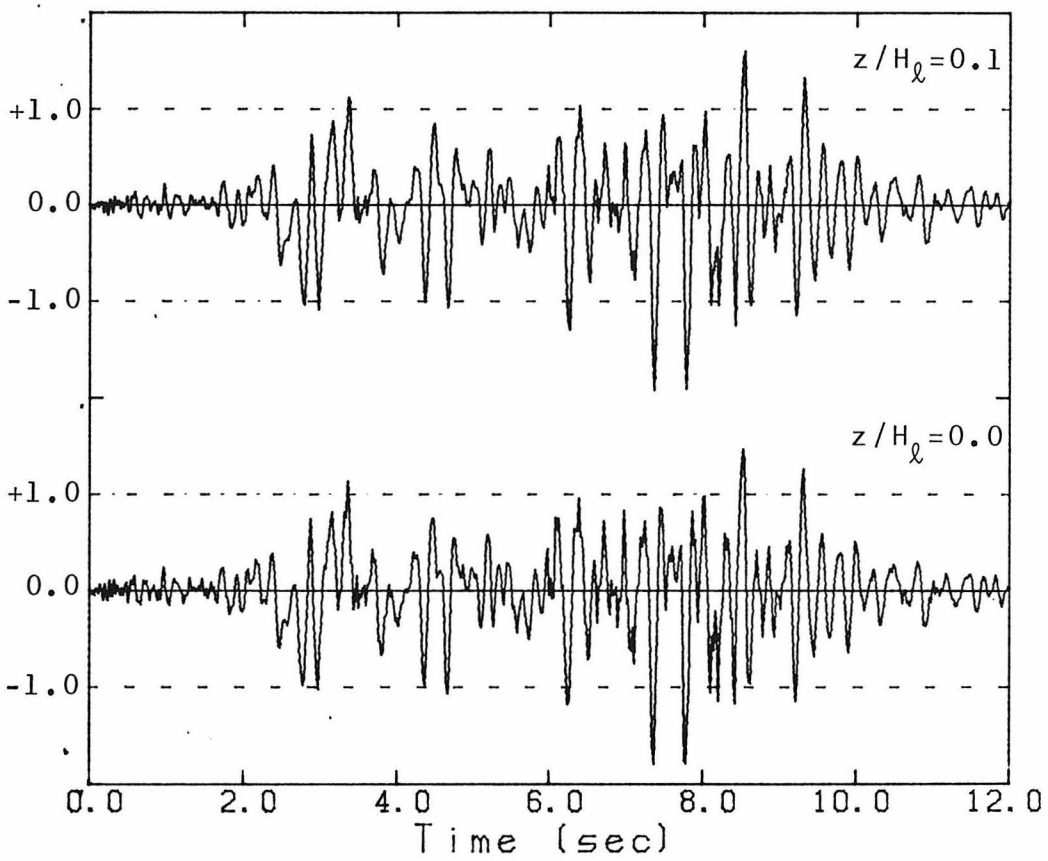


Fig. 5.12 Time Histories of Normalized Hydrodynamic Pressure (continued)

# CHAPTER VI

## SUMMARY AND CONCLUSIONS

Analytical expressions are developed for the hydrodynamic pressures generated, in reservoirs behind short dams or walls, by the vibrational motion of the structure and by all three components of ground motion. The water compressibility is taken into consideration and solutions of the three dimensional wave equation are obtained under both rigid and flexible boundaries assumptions.

Inclusion of water compressibility leads to a frequency dependent pressure. In the rigid case, the pressure becomes unbounded at excitation frequency equal to the natural frequencies of the reservoir. In the flexible case, some fluid-boundary interaction takes place leading to a damping boundary condition at the reservoir floor and sides. This allows some energy dissipation, making the pressure finite at all frequencies. It is observed that the reduction in the pressure response due to radiation damping is primarily in the vicinities of the resonant frequencies of the reservoir.

Contrary to the two-dimensional case of infinitely long dams, the pressure is found to vary along the dam length, and to depend on the length to height ratio of the dam, with values at mid-span approaching those of the 2-D case, as B/H becomes large. In addition, pressures are also generated by the transverse component of ground motion, a feature pertinent to the 3-D case only. When the reservoir boundaries are assumed rigid, the pressure arising from longitudinal and vertical

motions is independent of the y-coordinate, and identical to those obtained under the 2-D assumption.

Dynamic analyses of long dams retaining incompressible water are carried out in the time domain. Dams with rectangular cross-sections are treated analytically, while dams with variable thicknesses are discretized into finite elements. In both cases, the water is treated as a continuum by boundary solution techniques. The dam is modeled either by a shear or a bending theory. The natural frequencies of the system, and the associated mode shapes are determined from a free vibration analysis. The effect of the presence of water is equivalent to an added mass, thus reducing the resonant frequencies. The mode shapes are also altered, especially the higher ones. A method is also presented to compute the earthquake response of the dam, based on superposition of its free vibrational modes.

An analysis procedure, based on the Rayleigh-Ritz method, is developed for the dynamic response of short dam-reservoir systems. The dam is modeled by both shear and bending theories. The water is treated as a continuum, and the model can account for water compressibility and can approximately account for fluid-boundary interaction. The dam foundation is assumed rigid.

Neglecting water compressibility, the natural frequencies and mode shapes are obtained through a free vibration analysis. The effects of the dam being of finite length are as follows:

1) Antisymmetric modes of vibration are developed, in addition to the symmetric pattern.
2) Compared to the case of infinitely long dams, the natural frequencies of the structure increase as its length to height ratio decreases. For the shear model, the increase in the fundamental frequency is less than 8% for $B/H > 5.0$. The increase is as high as 42% when $B/H = 2.0$. The trend is the same for the bending model.

Including water compressibility and fluid-boundary interaction, a forced vibration analysis is carried out in the frequency domain, and the dam response to all three components of a harmonic ground motion is obtained.

Examining the crest acceleration transfer functions, it is deduced that:

1) When water compressibility is neglected, the hydrodynamic effects are equivalent to an added mass and added load which reduce the resonant frequencies of the system and increase the resonant amplitudes.
2) When water compressibility is considered, the added mass and added load vary with excitation frequency the same way the hydrodynamic pressures do.
3) Under the assumption of rigid boundaries, the response to longitudinal ground motion can be very large at excitation frequencies equal to the resonant frequencies of the reservoir.

The responses to transverse and vertical motions are unbounded at those frequencies. These very large or unbounded responses are reduced significantly when the boundaries are assumed flexible.

4) The transverse component contributes a very small amount to the crest acceleration response, as compared to the longitudinal component contribution. The vertical component contributes a fair amount.

5) A decrease in B/H increases the resonant frequencies of the system and alters the resonant amplitudes.

Acceleration, displacement and hydrodynamic pressure responses to earthquake ground motions are obtained through the use of the Fourier Integral and a special Fast Fourier Transform algorithm. Based on the results of the example of Chapter V, in which the N-S, E-W and vertical components of the Pacoima dam accelerogram records are used as the longitudinal, transverse and vertical components of the ground motion applied to the dam, and with compressibility of water and flexibility of the reservoir boundaries considered, it is observed that:

1) For longitudinal ground motion, a decrease in B/H from 5.0 to 2.0, and from 5.0 to 1.0, reduces the peak crest acceleration by 20% and 42%, respectively, and reduces the peak crest displacement by 47% and 82%, respectively. This indicates that the two-dimensional analysis, currently used by designers,

could greatly overestimate the response, if used for dams with relatively small lengths.

2) Depending on B/H, the peak crest acceleration due to vertical ground motion is about 20 → 35% of that due to longitudinal motion. The vertical motion produces a peak crest displacement in the range of 40 → 55% of what the longitudinal motion produces. This indicates that both components are of comparable level of importance.

3) The transverse component of ground motion produces, at quarter-span, peak crest acceleration and displacement which are less than 8% of what the longitudinal motion produces at mid-span. This indicates that the effect of the antisymmetrical modes is insignificant.

4) For a strong ground shaking such as the Pacoima Dam record (1.17g peak acceleration), cavitation of water occurs on the upstream face of the dam, at mid-span.

Local variations in the spectral content of a given earthquake may cause significant variations in the peak response due to earthquake excitation when the parameters of the dam are varied. Likewise, different earthquakes may result in different response behaviors of a given dam. Although the previous observations are based on results for a particular dam and a single earthquake, it is believed that the trends in the response would generally be the same for other earthquakes.

To summarize the most important conclusions:

1) The two dimensional solution, currently used for the analysis of gravity dams, would err considerably if applied to a dam whose length is less than four to five times its height. In such cases, a three dimensional model must be used, and this could result in substantial savings in the dam cost.
2) The antisymmetrical modes have little effect on the dam response, and the contribution of the transverse component of ground motion can be neglected without introducing a considerable error.
3) The level of importance of the vertical component of ground motion is comparable to that of the longitudinal component, and should be included in the analysis of dam responses to earthquake ground motion.
4) The possibility of water cavitation taking place at the upstream face, when the dam is subject to severe ground shaking, has been established.

As areas of further study, the generalization of the method of analysis to dams of variable thickness, modeled by a combined shear-bending theory, is straightforward. The model could also be improved to account for interaction between the dam and foundation. Further work is needed to investigate the stress response as well as the damage on the upstream face of the dam due to cavitation.

It is hoped that this study contributes to a better understanding of the dynamic behavior of gravity dams, and will help engineers to achieve a safer and more economical design of such important structures.

## NOTATION

The letter symbols are defined where they are first introduced in the text, and they are summarized herein in alphabetical order.

| | |
|---|---|
| $A$ | Maximum amplitude of dam motion, Eq. 2.8. |
| $\bar{A}$ | Normalized crest acceleration, Eq. 3.28. |
| $A_j\left(\frac{z}{H}\right)$ | Functions defined by Eq. 2.36. |
| $A_{ij}$ | Coefficients defined by Eq. 3.12. |
| $A_n$ | Coefficients defined by Eq. 5.14. |
| $AM$ | Added mass term, Eq. 3.69. |
| $a_g$ | Amplitude of ground acceleration. |
| $a_i$ | Coefficients defined by Eq. 3.16. |
| $a_m$ | Coefficients defined by Eq. 3.7a. |
| $B$ | Length of dam. |
| $B_j\left(\frac{Y}{B}\right)$ | Functions defined by Eq. 2.65. |
| $B_m$ | Coefficients defined by Eq. 5.15. |
| $b_j$ | Modal participation factors, Eq. 3.43. |
| $b_m$ | Coefficients defined by Eq. 3.7a. |
| $[C]$ | Damping matrix. |
| $c$ | Velocity of sound in the fluid, Eq. 2.1. |
| $c_i, \bar{c}_i$ | Constant coefficients, Eqs. 2.5 and 2.6, respectively. |
| $c_j$ | Coefficients defined by Eq. 2.65. |
| $c_m$ | Coefficients defined by Eq. 3.19. |

| | |
|---|---|
| $D$ | Domain occupied by the water in the reservoir. |
| $d$ | Thickness of dam. |
| $\bar{d}$ | Normalized dam thickness, d/H. |
| $d_e$ | Average thickness of element e. |
| $d_j$ | Coefficients defined by Eq. 2.36. |
| $d_m$ | Coefficients defined by Eq. 3.19. |
| $E$ | Modulus of elasticity of dam material. |
| $\{E\}$ | Vector of generalized coordinate displacements, Eq. 4.5. |
| $\bar{E}$ | $E/(1-\nu^2)$ |
| $e$ | Element number in the finite element mesh. |
| $e_j$ | Coefficients or generalized coordinate displacements, Eq. 4.4. |
| $\{F^I\}$ | Inertia load vector, Eq. 4.15. |
| $\{F^{(m)}\},\{f^{(m)}\}_e$ | Vectors defined by Eqs. 3.71 and 3.70, respectively. |
| $\{F^x\},\{F^y\},\{F^z\}$ | Added load vectors for ground motions in x, y and z directions, Eqs. 4.15, 4.21 and 4.25, respectively. |
| $f_j$ | Coefficient defined by Eq.3.42. |
| $f_j^I$ | Elements of $\{F^I\}$, Eq. 4.17. |
| $f_j^x$, $f_j^y$, $f_j^z$ | Elements of $\{F^x\}$, $\{F^y\}$ and $\{F^z\}$, Eqs. 4.18, 4.22 and 4.25, respectively. |
| $G$ | Shear modulus of dam material. |
| $g$ | Acceleration of gravity. |
| $H$ | Height of dam. |

| | |
|---|---|
| $\bar{H}$ | Normalized water depth, $H_\ell/H$. |
| $H_\ell$ | Depth of water in the reservoir. |
| $H_0^1$, $H_{00}^2$ | Spaces of variational functions. |
| $H_\beta^{(1)}$, $H_\beta^{(2)}$ | Hankel's functions of order $\beta$, Eq. 2.69. |
| $h_e$ | Length of element e. |
| $I_m$, $I_n$ | Integrals defined by Eqs. 3.38 (or 5.70) and 5.27, respectively. |
| $I_{m0}$, $I_{mn}$, $I_{m0}^i$, $I_{mn}^i$ | Integrals defined by Eqs. 2.16, 2.47, 3.15 and 4.9, respectively. |
| $I_\beta$ | Modified Bessel's function of order $\beta$ of the first kind, Eq. 2.67. |
| $i$ | $\sqrt{-1}$, Eq. 2.5 |
| $J_{m0}$, $J_{mn}$, $J_{m0}^j$, $\bar{J}_{m0}^j$ | Integrals defined by Eqs. 2.20, 2.50 and 4.23, respectively. |
| $J_\beta$ | Bessel's function of order $\beta$ of the first kind, Eq. 2.68. |
| $K_\beta$ | Modified Bessel's function of order $\beta$ of the second kind, Eq. 2.67. |
| $[K]$, $[K_d]$ | Dam stiffness matrix, Eqs. 3.76 and 3.66, respectively. |
| $[K^*]$ | Generalized stiffness matrix, Eq. 3.11. |
| $[K_d]_e$ | Element stiffness matrix, Eq. 3.67. |
| $k$ | Bulk modulus of elasticity of the fluid. |
| $\{L\}$, $\{L^{(1)}\}$, $\{L^{(2)}\}$ | Vectors defined by Eqs. 3.108, 3.105 and 3.107. |
| $\{\ell^{(1)}\}_e$ | Vector defined by Eq. 3.106. |

| | |
|---|---|
| $[M], [M_d], [M_\ell]$ | Total mass, dam mass and added mass matrices, Eqs. 3.76, 3.63 and 3.73, respectively. |
| $[M^*]$ | Generalized mass matrix, Eq. 3.111. |
| $[M_d]_e$ | Element mass matrix, Eq. 3.61. |
| $m_0, m_n$ | Constants defined by Eq. 2.15 and 2.46, respectively. |
| N | Number of degrees of freedom. |
| NH | Total number of finite elements |
| NW | Number of elements below water surface. |
| $\{N(\bar{z})\}$ | Vector of interpolation functions, Eq. 3.58. |
| $P_d, P_s$ | Total hydrodynamic and hydrostatic forces, respectively. |
| $\bar{P}$ | Normalized hydrodynamic force, $P_d/P_s$, Eq. 3.39. |
| $\{P_{eff}\}$ | Effective force vector, Eq. 3.108. |
| $p, p_s$ | Hydrodynamic and hydrostatic pressures, respectively. |
| $\bar{p}$ | Normalized hydrodynamic pressure, $p/p_s$, Eq. 3.37. |
| $p_{gx}, p_{gy}, p_{gz}$ | Hydrodynamic pressures due to x, y and z components of ground motion, Eqs. 2.25, 2.59 and 2.30, respectively. |
| $\{Q\}$ | Constant vector, Eq. 3.64. |
| q | Damping coefficient, Eq. 5.4. |
| $\{q\}_e$ | Constant vector, Eq. 3.57. |
| R | Radius of tank, intake tower or arch dam. |
| $\{R(t)\}$ | Overall nodal displacement vector, Eq. 3.64. |
| r | Radial coordinate of the cylindrical coordinate system. |

| | |
|---|---|
| $\{r(t)\}_e$ | Vector of nodal displacements, Eq. 3.57. |
| $\{S(\bar{z})\}$ | Vector of interpolation functions, Eq. 3.97. |
| $T(t)$ | Separation of variable function, Eq. 2.4. |
| $t$ | Time, Eq. 2.1. |
| $U(\xi), U^{I}(\xi), U^{II}(\xi)$ | Dam deformations, Eqs. 3.26, 3.29 and 3.30, respectively. |
| $U_j(t)$ | Functions given by Eq. 3.44. |
| $u$ | Dam displacement. |
| $u_i(t)$ | Generalized nodal coordinates, Eq. 3.40. |
| $u_g, v_g, w_g$ | Components of ground motion in the x, y and z directions, Eqs. 2.22, 2.54 and 2.27, respectively. |
| $\bar{u}_g, \bar{v}_g, \bar{w}_g$ | Amplitudes of the components of ground motion, Eqs. 2.22, 2.54 and 2.27, respectively. |
| $u_\ell, v_\ell, w_\ell$ | Water particle displacements in the x, y and z directions, respectively. |
| $u^e, v^e$ | u and v when expressed in local coordinates. |
| $u_i^e, v_i^e$ | Elements of vectors $\{r(t)\}_e$ and $\{q\}_e$, respectively. |
| $V$ | Constant defined by Eq. 5.8. |
| $v(z)$ | Variational function. |
| $W$ | Constant defined by Eq. 5.11. |
| $X(x), Y(y), Z(z)$ | Separation of variables functions, Eq. 2.4. |
| $Y_i\left(\frac{Y}{B}\right)$ | Deformation shapes, Eqs. 2.64 and 2.65. |
| $Y_n\left(\frac{Y}{B}\right)$ | Functions defined by Eq. 5.6. |

$Y_\beta$ Bessel;s function of order $\beta$ of the second kind, Eq. 2.68.

$Y_j(t)$ Elements of vector $\{Y(t)\}$, Eq. 3.115.

$\{Y(t)\}$ Vector of modal amplitudes, Eq. 3.110.

$Z_j\left(\frac{z}{H}\right)$ Deformation shapes, Eqs. 2.64 and 2.65.

$Z_m\left(\frac{z}{H}\right)$ Functions defined by Eq. 5.9.

$x,y,z$ Cartesian coordinates, Eq. 2.5.

$\bar{z}$ Local z-coordinate.

$\alpha$ Coefficient defined by Eq. 3.5.

$\alpha_i$ Coefficients defined by Eq. 2.65.

$\alpha_r$ Reflection coefficient, Eq. 5.4.

$\beta$ Separation constant, Eq. 2.5, also shear angle, Eq. 3.90.

$\beta_n$ Coefficients defined by Eq. 2.45.

$\gamma_j$ Coefficients defined by Eq. 2.36.

$\gamma_m$ Coefficients defined by Eq. 3.74.

$\delta,\bar{\delta}$ Separation constants, Eqs. 2.5 and 2.6, respectively.

$\delta_{m0},\bar{\delta}_{m0}$ Coefficients defined by Eq. 2.15.

$\delta_{mn},\bar{\delta}_{mn}$ Coefficients defined by Eq. 2.46.

$\varepsilon_n$ Coefficients defined by Eq. 2.45.

$\zeta_j$ Modal damping.

$\eta$ Separation constant, Eq. 2.5.

$\eta_m$ Coefficients defined by Eq. 2.14.

| | |
|---|---|
| $\theta$ | Circumferential coordinate of the cylindrical coordinate system. |
| $\theta_0$ | Central angle of arch dam. |
| $K$ | Constant defined by Eq. 3.102. |
| $\lambda_m$ | Coefficient defined by Eq. 3.7b or Eq. 3.19. |
| $\mu$ | Separation constant, Eq. 2.7. |
| $\mu_{mn}$ | Coefficients defined by Eq. 2.51. |
| $\nu$ | Poisson's ratio of dam material. |
| $\xi, \bar{\xi}$ | Normalized z-coordinates, Eq. 3.5. |
| $\rho, \rho_\ell$ | Mass density of the dam material and the fluid. |
| $\bar{\rho}$ | Normalized mass density, $\rho/\rho_\ell$. |
| $\sigma$ | Coefficient defined by Eq. 3.19. |
| $\tau$ | Separation constant, Eq. 2.4. |
| $[\Phi]$ | Matrix of modal displacement vectors, Eq. 3.110. |
| $\phi$ | Slope of deflection, Eq. 3.90. |
| $\phi^e$ | $\phi$ expressed in local coordinates. |
| $\phi_i^e$ | Constants defined in Eq. 3.97. |
| $\{\phi\}$ | Vector of displacement amplitudes, Eq. 3.77. |
| $\Psi\left(\frac{Y}{B}, \frac{Z}{H}\right)$ | Vibrational shapes, Eq. 2.63. |
| $\Psi_j$ | Admissible functions, Eq. 4.4. |
| $\varphi\left(\frac{Z}{H}\right), \varphi\left(\frac{Y}{B}, \frac{Z}{H}\right)$ | Deformation shapes of the dam, Eqs. 2.8 and 2.37, respectively. |
| $\varphi(\xi), \varphi^I(\xi), \varphi^{II}(\xi)$ | Dam deformations, Eqs. 3.3, 3.6 (or 3.20) and 3.8 (or 3.21), respectively. |

| | |
|---|---|
| $\Omega(z)$ | Variational function. |
| $\Omega^e$ | $\Omega$ expressed in local coordinates. |
| $\Omega_i^e$ | Constants defined in Eq. 3.97. |
| $\omega$ | Circular frequency of vibration. |
| $\bar{\omega}$ | Normalized frequency $\omega/\omega_1^r$. |
| $\omega_i$ | Natural frequencies of the dam. |
| $\omega_i^r, \omega_{ij}^r$ | Natural frequencies of the reservoir, Eqs. 2.17 and 2.48, respectively. |
| $(\omega_1^r)_f$ | Fundamental frequency of the full reservoir. |
| $\nabla^2$ | Laplace operator, Eq. 2.1. |
| $\nabla^4$ | Operator defined by Eq. 4.12. |
| $(\dot{})$ | Differentiation w.r.t. time. |
| $(')$ | Differentiation w.r.t. argument. |

## REFERENCES

[1] Westergaard, H.M., "Water Pressures on Dams During Earthquakes," Transactions, ASCE, Vol. 98, 1933, pp. 418-433.

[2] Brahtz, H.A., and Heilbron, C.H., discussion of "Water Pressures on Dams During Earthquakes," by H.M. Westergaard, Transactions, ASCE, Vol. 98, 1933, pp. 452-460.

[3] Hoskins, L.M., and Jacobsen, L.S., "Water Pressure in a Tank Caused by a Simulated Earthquake," Bulletin, Seismological Society of America, Vol. 24, No. 1, Jan. 1934, pp. 1-32.

[4] Bustamante, J.I., Rosenblueth, E., Herrera, I., and Flores, A., "Presíon Hidrodinámica en Presas y Depósitos," Boletín Sociedad Mexicana de Ingeniería Sísmica, Vol. 1, No. 2, Oct. 1963.

[5] Kotsubo, S., "Dynamic Water Pressure on Dams Due to Irregular Earthquakes," Memoirs Faculty of Engineering, Kyushu University, Fukuoka, Japan, Vol. 18, No. 4, 1959, pp. 119-129.

[6] Chopra, A.K., "Hydrodynamic Pressures on Dams During Earthquakes," Journal of the Engineering Mechanics Division, ASCE, Vol. 93, No. EM6, Proc. Paper 5695, Dec. 1967, pp. 205-223.

[7] Zangar, C.N., "Hydrodynamic Pressures on Dams Due to Horizontal Earthquake Effects," Engineering Monograph No. 11, U.S. Bureau of Reclamation, May 1952.

[8] Chwang, A.T., "Hydrodynamic Pressures on Sloping Dams During Earthquakes. Part 2. Exact Theory," Journal of Fluid Mechanics, Vol. 87, Part 2, 1978, pp. 343-348.

[9] Chopra, A.K., "Reservoir - Dam Interaction During Earthquakes," Bulletin, Seismological Society of America, Vol. 57, No. 4, Aug. 1967, pp. 675-687.

[10] Selby, A., and Severn, R.T., "An Experimental Assessment of the Added Mass of Plates Vibrating in Water," International Journal of Earthquake Engineering and Structural Dynamics, Vol. 1, No. 2, Oct-Dec. 1972, pp. 189-200.

[11] Mermel, T.W., Register of Dams in the United States, McGraw-Hill Book Company, New York, 1959.

[12] Werner, P.W., and Sundquist, K.J., "On Hydrodynamic Earthquake Effects," Transactions, American Geophysical Union, Vol. 30, No. 5, Oct. 1949, pp. 636-657.

[13] McLachlan, N.W., Bessel Functions for Engineers, 1st edition, Vol. 1, Oxford University Press, Oxford, Great Britain, 1934.

[14] Fischer, D., "Dynamic Fluid Effects in Liquid-Filled Flexible Cylindrical Tanks," International Journal of Earthquake Engineering and Structural Dynamics, Vol. 7, No. 6, Nov.-Dec. 1979, pp. 587-601.

[15] Jacobsen, L.S., "Impulsive Hydrodynamics of Fluid Inside a Cylindrical Tank and of Fluid Surrounding a Cylindrical Pier," Bulletin, Seismological Society of America, Vol. 39, No. 3, July 1949, pp. 189-204.

[16] Veletsos, A.S., and Yang, J.Y., "Dynamics of Fixed-Base Liquid-Storage Tanks," Proc., U.S. - Japan Seminar on Earthquake Engineering Research with Emphasis on Lifeline Systems, Tokyo, Japan, Nov. 1976, pp. 317-341.

[17] Liaw, C-Y., and Chopra, A.K., "Dynamics of Towers Surrounded by Water," International Journal for Earthquake Engineering and Structural Dynamics, Vol. 3, No. 1, July-Sept. 1974, pp. 33-49.

[18] Goto, H. and Toki, K., "Vibrational Characteristics and Aseismic Design of Submerged Bridge Piers," Proc., Fourth World Conference on Earthquake Engineering, Vol. II, New Zealand, 1965, pp. 107-125.

[19] Chandrasekaran, A.R., Saini, S.S., and Malhotra, M.M., "Hydrodynamic Pressure on Circular Cylindrical Cantilever Structures Surrounded by Water," Fourth Symposium on Earthquake Engineering, Roorkee, India, Nov. 1970, pp. 161-171.

[20] Kotsubo, S., "External Forces on Arch Dams During Earthquakes," Memoirs Faculty of Engineering, Kyushu University, Fukuoka, Japan, Vol. 20, No. 4, 1961, pp. 327-366.

[21] Porter, C.S., and Chopra, A.K., "Dynamic Response of Simple Arch Dams Including Hydrodynamic Interaction," Earthquake Engineering Research Center, University of California, Berkeley, Report No. EERC 80-17, July 1980.

[22] Chopra, A.K., "Earthquake Behavior of Reservoir-Dam Systems," Journal of the Engineering Mechanics Division, ASCE, Vol. 94, No. EM6, Proc. Paper 6297, Dec. 1968, pp. 1475-1500.

[23] Chopra, A.K., "Earthquake Response of Concrete Gravity Dams," Journal of the Engineering Mechanics Division, ASCE, Vol. 96, No. EM4, Proc. Paper 7485, Aug. 1970, pp. 443-454.

[24] Chakrabarti, P. and Chopra, A.K., "Earthquake Response of Gravity Dams Including Reservoir Interaction Effects," Earthquake Engineering Research Center, University of California, Berkeley, Report No. EERC 72-6, Dec. 1972.

[25] Chakrabarti, P. and Chopra, A.K., "Earthquake Analysis of Gravity Dams Including Hydrodynamic Interaction," International Journal for Earthquake Engineering and Structural Dynamics, ASCE Vol. 100, No. ST6, Proc. Paper 10616, June 1974, pp. 1211-1224.

[26] Chakrabarti, P. and Chopra, A.K., "Hydrodynamic Effects in Earthquake Response of Gravity Dams," Journal of the Structural Division, ASCE, Vol. 100, No. ST6, Proc. Paper 10616, June 1974, pp. 1211-1224.

[27] Finn, W.D.L. and Varoglu, P., "Forced Vibrations of a Plate-Reservoir System," Civil Engineering Soil Mechanics Series, No. 22, University of British Columbia, Vancouver, Canada, 1971.

[28] Finn, W.D.L. and Varoglu, P., "A Study of Dynamic Interaction in a Plate-Reservoir System," Paper Presented at the 5th European Conference on Earthquake Engineering, Istanbul, Turkey, 1975.

[29] Finn, W.D.L. and Varoglu, P., "Dynamics of Gravity Dam-Reservoir Systems," Computers and Structures, Vol. 3, 1973, pp. 913-924.

[30] Merchant, H.C., "Mode Superposition Methods Applied to Linear Mechanical Systems Under Earthquake Type Excitation," Ph.D. Thesis, California Institute of Technology, Pasadena, California, 1961.

[31] Clough, R.W., "Analysis of Structural Vibrations and Dynamic Response," Japan - U.S. Seminar on Matrix Methods of Structural Analysis and Design. Tokyo, Japan, Aug, 25-30, 1969.

[32] Meirovitch, L., Elements of Vibration Analysis, McGraw-Hill Book Company, 1975, pp. 65-68.

[33] Trifunac, M.D., "Analyses of Strong Motion Earthquake Accelerograms, Response Spectra, Vol. III," Earthquake Engineering Research Laboratory, California Institute of Technology, Pasadena, Report No. EERL 72-80, Aug. 1972.

[34] Timoshenko, S., Young, D.H., and Weaver, W., Vibration Problems in Engineering, 4th edition, John Wiley & Sons, New York, 1974.

[35] Anderson, R.A., "Flexural Vibrations in Uniform Beams According to the Timoshenko Theory," Transactions, ASME, Vol. 75, 1953, pp. 504-510.

[36] Miklowitz, J., "Flexural Wave Solutions of Coupled Equations Representing the More Exact Theory of Bending," Transactions, ASME, Vol. 75, 1953, pp. APM 511-514.

[37] Wilson, E.L., and R.W. Clough, "Dynamic Response by Step-by-Step Matrix Analysis," Proceedings, Symposium on the Use of Computers in Civil Engineering, Lisbon, Portugal, 1962.

[38] Meirovitch, L., Analytical Methods in Vibrations, The Macmillan Company, 1967, pp. 211-235.

[39] Meirovitch, L., Analytical Methods in Vibrations, The Macmillan Company, 1967, pp 308-312.

[40] Rea, D., Liaw, C.Y. and Chopra, A.K., "Dynamic Properties of Pine Flat Dam," Earthquake Engineering Research Center, University of California, Berkeley, Report No. EERC 72-7, Dec. 1972.

[41] Hall, J.F., "An FFT Algorithm for Structural Dynamics," accepted for publication in the International Journal for Earthquake Engineering and Structural Dynamics.

[42] Hall, J.F., and Chopra, A.K., "Dynamic Response of Embankment, Concrete-Gravity and Arch Dams Including Hydrodynamic Interaction," Earthquake Engineering Research Center, University of California, Berkeley, Report No. EERC 80-39, Oct. 1980.

[43] Haroun, M.A., University of California, Irvine, Personal Communication.

[44] Hudson, D.E., Trifunac, M.D. and Brady, A.G., Strong Motion Earthquake Accelerograms, Response Spectra, Vol. III, Part C, Earthquake Engineering Research Laboratory, Report No. EERL 73-81, California Institute of Technology, Pasadena, California, May 1973.